

Seismic Structure and Seismicity of Villarrica Volcano (Southern Central Chile)

Dissertation
zur Erlangung des Doktorgrades
der Mathematisch-Naturwissenschaftlichen Fakultät
der Christian-Albrechts-Universität zu Kiel

vorgelegt von

Cindy Nathalie Mora Stock

Kiel, 2015

Seismic Structure and Seismicity of Villarrica Volcano (Southern Central Chile)

Dissertation
zur Erlangung des Doktorgrades
der Mathematisch-Naturwissenschaftlichen Fakultät
der Christian-Albrechts-Universität zu Kiel

vorgelegt von

Cindy Nathalie Mora Stock

This Doctoral Thesis was supported financially between Dec. 2010 and Aug. 2014 by CONICYT Becas Chile - DAAD N°72110106.

Kiel, 2015

Referent: Prof. Dr. W. Rabbel
Koreferent: Prof. Dr. I. Grevemeyer
Tag der muendlichen Pruefung: 16.10.2015

Zum Druck genehmigt: Kiel, 16.10.2015

Der Dekan
gez.

Dedicated to those who fell in my absence
My family: Pedro Mora M. and Sata
My friends: Sandra and Naya

Acknowledgements

First and foremost I would like to express my sincere gratitude to my Advisor Professor Dr. Wolfgang Rabbel. Since the very beginning he supported me in this journey. His guidance, advices, patience, and reassurance gave me the necessary impulse to keep me going when strengths were lowering. I am sincerely and most deeply acknowledged for your words in the precise moment.

I am very grateful to have in my Commission PD. Dr. Ingo Grevemeyer, PD. Dr. Thor Hansteen, and Prof. Thomas Meier. In my time in Kiel, I have had the opportunity to meet such great researchers, and I am looking forward to continue collaborating in forthcoming projects. I want to thank Ingo for agreeing to review this work, and for improving it with his comments. Also, I would like to thank Thor for his good disposition and research cooperation throughout this journey. Thank you, Prof. Meier for your constant discussion about seismic topics and for agreeing to chair my Thesis Commission.

My sincere gratitude goes to the Chilean government along with the German governments through the DAAD institution, for their funding CONICYT Becas Chile - DAAD N°72110106 to pursue my studies in Germany.

Colleagues and co-authors I would not left behind. I want to thank Martin for his invaluable help, support, computational assistance, and fieldwork fun during my studies. Stefan for copious discussions and for complementing the research in Villarrica volcano through his topic of study. Colleagues at the IfG: Tina and Claudia for their patience with my German language; Laura, Denis, Julia, Felix and many more for the times we share a coffee, words of support, or just a smile :)

Many thanks to my friends in Chile, my support group, my chosen family. There is not enough space nor words to express how thankful I am for the talks, gifts, and time shared in my visits. Particularly, I am very much obliged to Cristián for being my cornerstone through all this years, even at 16 000 km away, in good times and in bad times.

My family in Kiel, without you all these year would have been as Kiel's weather. Brothers in arms: Lulu, Allein, Neus, Silvia, David, Odín. Thank you for sharing the perish of being a PhD student. The rest of the Spanish-speaking group, Santi, Adri, Antía, Concha, Pablo, Angélica; the non-Spanish-speaking, Agnieska, Torben, Ana; and the Costarican group, Silvia, Wendy, Ivonne y la tropa. Thank you for making living in Kiel a delicious adventure! To the small piece of Chile in Kiel: Jö, Susana, Javi, Mario y Vicky, Pame. Only those abroad know how much we miss our land and our Andes.

Not everything in life are studies. I am very much obliged to Katja and Asdis from the Kieler TB, for becoming my friends and allow me to take part of such wonderful group of trainers and gymnasts. Thank you for encouraging me and help me with the German language, and most importantly, for allowing me to share my soul through one of my passions. Thank you RSG-Ladies! For they gave joy and taught me not only to smile again: Vanessa, Maria S., Lauri, Ana, Emi, Maria B., Daisy, Rita, Johanna, Eli... you are just a few of the most dearest to me.

Last but not least, I want to thank my family. Pedro, Wely and Tata for you support and patience through these years. Tatita, this thesis is to you. To my Sata, for countless hours of fun and joy. To my mother, for you are the light through my eyes.

Abstract

Subduction zones are naturally linked to volcanism through the ascension of fluids from the subducted crust and the build of magmatic arc and mountain ranges. Chile is one of the most seismically active countries with an earthquake of magnitude ≥ 8 almost every ten years. It also hosts more than a hundred active volcanoes along the Central, Southern and Austral Volcanic Zone. Villarrica volcano is one of the most active volcanoes in the Southern Volcanic Zone with an average of ~ 10 years between eruptions. Great earthquakes at subduction zones can strongly modify dynamic and static stress surrounding the magma chamber of volcanoes located hundreds of kilometers away from the rupture zone, influencing the fluid behavior and, depending on the state of the system, triggering a volcanic eruption.

The Maule earthquake (Mw8.8, 2010) released the energy accumulated in the Concepción - Constitución seismic gap since the last event in 1835. The 450 km-long rupture advanced from south to north until north of Santiago (33°S). The earthquake revived the NW-SE crustal 40 km-long Pichilemu fault ($\sim 34.5^\circ\text{S}$) with two of the largest aftershocks ($\sim \text{Mw}7$) in the series presenting normal fault mechanisms. Two patches, in front of Lebu and Constitución, of high pre-seismic locking coincide with the areas of larger coseismic slip (> 10 m), and hypocenters of strong aftershocks.

According to historical records, the last earthquake in the region in 1835 enhanced the volcanic activity of volcanoes north of the epicenter area. The Valdivia earthquake, with the rupture zone starting just south of the Concepción earthquake, triggered the eruption of the Cordón Caulle just hours after the M9.5 shock. Given the similarities for the Maule earthquake, Villarrica and Llaima volcanoes were particularly monitored to verify potential influence in their behavior.

Villarrica is an open-vent seismically active volcano, with constant degassing through a movable lava lake at its crater. Llaima, on the other hand, contrastingly, is a close vent volcano, with fewer seismic activity and lower degassing rates. Based on temporary networks continuous records and the catalogue from the Volcanic Observatory of the Southern Andes (OVDAS), long period, tremor and volcano – tectonic time series were analyzed.

One month before the mainshock, Villarrica presented a strong increase in the seismic activity related to fluids which decayed sharply just before the earthquake. After the Maule earthquake, peaks in the amount of tremor and long period events, accompanied with synchronic peaks in degassing activity were observed. This activity is consistent with an augmented movement of fluids inside the volcanic system. For Llaima, the long period and tremor activity that was high in rate before the Maule event, decreased sharply after the event. On the contrary, VT activity increased notoriously directly after the event. This activity is interpreted as a fragile response to tectonic readjustment. The increased LP, tremor, and degassing activity prior to the event are interpreted as an increase in the inflow of magma supply. Calculation of pressure change reveal values two orders of magnitude lower than the ones observed for Valdivia earthquake. In combination, results indicate that Maule earthquake affected in some way the dynamic of these two volcanoes, but pressure changes and a non-critical condition for both volcanoes, resulted in insufficient conditions to trigger and eruption.

Five years after the Maule earthquake, in March 2015, Villarrica volcano presented a moderate (VEI 2) strombolian eruption. Lava fountains up to 1.5 km high, and an ash eruptive column that reached 11.5 km in the atmosphere, raised the alarms of governmental hazard monitoring institutions. To improve these mitigation plans, to achieve a better understanding of the processes that trigger volcanic eruptions,

and the behaviour of the volcanic system, the first model for the inner structure of the Villarrica volcano prior to this eruption was calculated.

A straight-ray inversion of P-wave arrival of local volcano tectonic earthquakes was performed with a dense temporal network of 50 stations at and around the volcano. Hipocenters indicate a main feeding conduit between 3 and 5 km depth consistent with the Liquiñe – Ofqui fault zone. One main shallow (1 to 4 km depth) low velocity zone of ~ 5 km diameter in the NNW direction below the crater is observed linked to this feeding source. Two conduit-like low velocity structures are observed in strong connection to Los Nevados and Challupén pyroclastic flows (ENE and S of the crater), and are interpreted as the remnants of those conduits. High velocity regions are consistent with consolidated products of previous caldera collapses to the east and below the present crater. To the west of the edifice, high velocity regions wrapping the low velocity zones are interpreted as consolidated products and crustal rock. Checker Board tests supports the resolution of this inversion, and Bootstrap model calculations provide statistical truthfulness to the data selected.

These results are expected to provide insight about the behaviour of the open and closed vent systems by classifying volcanic signals and their variation through time, particularly before and after a great subduction earthquake. Particularly for Villarrica volcano, these results provide a first approach to its inner velocity structure. This is particularly relevant for monitoring agencies, not only for improving models for locating seismicity, but also to understand better the processes in the volcanic plumbing system.

In conclusion, this study presents the first tomography of the Villarrica volcano along with the studies of time series before and after the Maule earthquake. As such, this thesis provides a detailed study of the processes that influence volcanic activity and the structures where this activity occurs. From this work, the knowledge that the scientific community has about the integral inner structure and working processes of Villarrica and similar volcanoes is advanced.

Zusammenfassung

Vulkanismus über Subduktionszonen geht zurück auf den Aufstieg von Fluiden aus der subduzierten Lithosphäre, der ursächlich ist für die Entstehung des magmatischen Bogens und der Gebirgskette. Chile ist eines der seismologisch aktivsten Länder der Erde, in dem nahezu alle 10 Jahre ein Erdbeben der Größenordnung $M_w \geq 8$ auftritt. Mehr als hundert aktive Vulkane breiten sich entlang der sogenannten Zentralen, Südlichen und Australen vulkanischen Zone aus. Der Villarrica bricht als einer der aktivsten Vulkane im südlichen Teil im Durchschnitt etwa alle 10 Jahre aus. Große Erdbeben in Subduktionszonen können die dynamischen und statischen Spannungszustände in der Umgebung von Magmakammern stark verändernd, selbst wenn diese sich in hunderten Kilometern Entfernung von der eigentlichen Bruchzone befinden. Je nach Zustand des Systems kann dies das Fluidverhalten beeinflussen und dadurch sogar einen Vulkanausbruch auslösen.

Das Maule-Erdbeben (M_w 8.8, 2010) gab die gesamte Energie frei, die sich seit dem letzten Ereignis im Jahr 1835 in der dortigen seismischen Lücke (Concepción - Constitución) angestaut hatte. Der 450 km lange Bruch breitete sich von Süden nach Norden bis nördlich von Santiago (33°S) aus. Das Erdbeben aktivierte die NW-SO verlaufende, 40 km lange krustale Pichilemu-Verwerfung ($34,5^\circ\text{S}$), was zwei der größten Nachbeben ($M7$ mit Abschiebungscharakteristik) zur Folge hatte. Zwei kleinere Gebiete bei Lebu und Constitución mit besonders niedriger Seismizität bis zum Zeitpunkt des Maule-Bebens fallen nun genau mit Bereichen zusammen, in denen ein großer koseismischer Versatz (≥ 10 m) und die Hypozentren von starken Nachbeben beobachtet wurden.

Historischen Aufzeichnungen zufolge führte das letzte Erdbeben in der Region im Jahr 1835 zu einer erhöhten Vulkanaktivität nördlich des Epizentrums. Das Valdivia-Erdbeben, dessen Bruchzone nur etwas südlich des Epizentrums des Concepción-Erdbebens beginnt, löste den Ausbruch des Cordón Caulle einige Stunden nach dem $M9.5$ -Beben aus. Aus diesem Grund wurden die Vulkane Villarica und Llaima während des Maule-Bebens verstärkt überwacht, um mögliche seismologische Einflüsse analysieren zu können.

Villarica ist ein seismisch aktiver Vulkan, der über einen ortsveränderlichen Lavasee in seinem Krater stetig Gase freisetzt ('open-vent'-Vulkan). Im Gegensatz dazu ist Llaima ein 'closed-vent'-Vulkan mit geringerer seismischer Aktivität und niedrigerer Entgasungsrate. Mithilfe von Daten aus temporären seismologischen Netzwerken und dem Erdbebenkatalog des vulkanischen Observatoriums der Südanden (OVDAS) wurden langperiodische (LP), Tremor- und vulkanotektonische (VT) Daten ausgewertet.

Einen Monat vor dem Maule-Beben zeigte der Villarrica eine starke Zunahme der mit dem Magmaaufstieg in Verbindung gebrachten seismischen Aktivität, die genau vor dem Beben plötzlich wieder zurückging. Direkt nach dem Hauptbeben wurde dann eine Häufung der Tremor- und langperiodischen Ereignisse beobachtet, was mit zeitgleichen Höchstwerten der Entgasung korrelierte. Diese allgemeine Aktivitätszunahme kann auf eine vermehrte Bewegung der Fluide im Innern des vulkanischen Systems zurückgeführt werden. Beim Vulkan Llaima hingegen nahm die Häufigkeit der langperiodischen und Tremoreignisse unmittelbar nach dem Maule-Beben sehr stark ab. Im Gegensatz dazu erhöhte sich die VT-Aktivität direkt nach dem Beben deutlich. Letzteres wird als Bruchverhalten aufgrund tektonisch induzierter Spannungsveränderungen interpretiert. Die erhöhte LP-, Tremor- und Entgasungsaktivität vor dem Beben wird mit einem erhöhten Magmazufuss in Zusammenhang gebracht.

Die innerhalb des vulkanischen Systems auftretenden Druckschwankungen für das Maule-Erdbeben

sind Berechnungen zufolge zwei Größenordnungen niedriger als die entsprechenden Werte für das Valdivia-Erdbeben. Zusammengefasst deuten die Ergebnisse darauf hin, dass das Maule-Beben die Dynamik der beiden Vulkane zwar beeinflusst hat, jedoch aufgrund der geringeren Druckänderungen und des unkritischen Zustands beider Vulkane keine Eruption ausgelöst wurde.

Fünf Jahre nach dem Maule-Erdbeben im März 2015 gab es am Villarrica-Vulkan einen strombolianischen Ausbruch mittlerer Intensität (VEI 2). Aufgrund von Lavafontänen bis in 1.5 km Höhe und einer 11.5 km hohen Aschewolke wurde die höchste Alarmstufe eine erhöhte Alarmstufe von der staatlichen Gefahrenüberwachung ausgerufen. Um die vulkanische Risikoanalyse zu verbessern sowie ein genaueres Verständnis für die mit der Eruption einhergehenden Vorgänge innerhalb des vulkanischen Systems zu erlangen, wurde ein seismisches Geschwindigkeitsmodell berechnet, das den inneren Aufbau des Vulkans Villarrica beschreibt.

Mithilfe eines dichten seismischen Netzwerks, bestehend aus 50 rund um den Vulkan temporär aufgebauten Stationen, wurde eine „straight-ray“-Inversion von P-Wellen lokaler vulkanotektonischer Beben durchgeführt. Die Lage der Hypozentren weist auf einen Hauptzufuhrkanal in drei bis fünf Kilometer Tiefe hin, der mit der Liquine – Ofqui-Störungszone zusammenfällt. Oberhalb dieses Kanals zeigen die Modelle in 1-4 km Tiefe eine Niedrig-Geschwindigkeitszone mit etwa 5 km Durchmesser in nordnordwestlicher Richtung unter dem Krater. Zwei kanalartige Niedriggeschwindigkeitsstrukturen werden als Förderschloten für die pyroklastischen Ablagerungen von Los Nevados und Challupén (ONO und S des Kraters) interpretiert. Bereiche höherer Geschwindigkeiten decken sich mit konsolidierten Ablagerungen eines früheren Kaldera-Einsturzes östlich und unterhalb des heutigen Kraters. Im westlichen Teil umlagern Bereiche höherer Geschwindigkeit solche mit niedrigerer Geschwindigkeit und werden als konsolidiertes Material und Krustengestein interpretiert. Die Auflösung und Robustheit des finalen Modells wird durch Checkerboard-Tests und Bootstrap-Modellrechnungen nachgewiesen.

Die Ergebnisse geben einen Einblick in die Vorgänge innerhalb von als „open-vent“ und „closed-vent“ klassifizierten vulkanischen Systemen, indem vulkanische Signale und deren zeitliche Änderungen vor und nach einem großen Subduktions-Beben analysiert werden. Für den Vulkan Villarrica wird ein tomographisches P-Wellen Geschwindigkeitsmodell präsentiert, mit dem die Seismizität in diesem Gebiet genauer lokalisiert werden kann und welches dazu beiträgt, die Prozesse im vulkanischen Schlot im Zusammenhang mit einem Ausbruch besser zu verstehen, was insbesondere für die vulkanische Gefahrenüberwachung und Risikoanalyse von besonderer Bedeutung ist.

Diese Arbeit präsentiert also die erste Tomographie des Vulkans Villarrica sowie eine Auswertung seismologischer Daten vor und nach dem Maule-Erdbeben. In diesem Rahmen liefert sie eine detaillierte Studie der Vorgänge, die die vulkanische Aktivität beeinflussen und identifiziert die Strukturen, wo diese auftreten. Die Arbeit leistet somit einen wichtigen Beitrag zum Verständnis des wesentlichen inneren Aufbaus und der aktiven Prozesse des Vulkans Villarrica und vergleichbarer Vulkansysteme.

Resumen

Las zonas de subducción están naturalmente ligadas al volcanismo mediante el ascenso de fluidos desde la corteza subductada y la construcción del arco magmático y las cadenas montañosas. Chile, con un evento de magnitud ≥ 8 cada aproximadamente 10 años, es uno de los países más activos sísmicamente. Es también uno de los más activos volcánicamente, con más de 100 volcanes activos a lo largo de las zonas volcánicas centro, sur y austral. El volcán Villarica es uno de los más activos en la zona volcánica del sur, con un promedio de 10 años entre cada erupción. Los grandes terremotos en este tipo de zonas pueden modificar fuertemente los stresses dinámico y estático que rodean las cámaras magmáticas de volcanes ubicados a cientos de kilómetros de la zona de ruptura, influenciando el desarrollo de burbujas y el movimiento de fluidos y, dependiendo del estado del sistema, desatar una erupción volcánica.

El terremoto del Maule ($M_w 8.8$, 2010) liberó la energía sísmica acumulada en la laguna sísmica de Concepción - Constitución desde el último evento en 1835. La ruptura de 450 km de largo avanzó de sur a norte llegando hasta el norte de Santiago (33°S). El sismo reactivó la falla Pichilemu, una estructura cortical de dirección NW-SE y 40 km de largo, con dos de las réplicas más importantes ($\sim M_w 7$) de la serie, que presentaron mecanismo de fallamiento normal. Dos zonas de alto bloqueo pre-sísmico, una frente a Lebu y la otra frente a Constitución, coinciden con las zonas de mayor deslizamiento co-sísmico (> 10 m) y con los hipocentros de las réplicas fuertes.

De acuerdo a registros históricos, el último sismo en la región en 1835, acentuó la actividad volcánica en la región al norte del área epicentral. El terremoto de Valdivia, cuya zona de ruptura comenzó al sur de la del terremoto de Concepción, gatilló la erupción del complejo Cordón Caulle solo horas después del evento de magnitud $M_w 9.5$. Dadas las similitudes con el terremoto del Maule, los volcanes Villarica y Llaima fueron particularmente monitoreados para verificar una posible influencia en sus comportamientos.

Villarica es un volcán de conducto abierto sísmicamente activo, con desgasificación constante través del lago de lava en su cráter. Llaima, por otro lado, es un volcán de conducto cerrado, con menor actividad sísmica y valores de desgasificación más bajos que Villarica. Se analizaron la serie de tiempo de eventos de largo período, tremor volcánico y sismos volcano-tectónicos de los registros continuos de una red temporal y del catálogo del Observatorio Volcánico de los Andes del Sur (OVDAS).

En el mes previo al terremoto, el volcán Villarica presentó un importante aumento en la cantidad de eventos relacionados a movimiento de fluidos, la cual decayó rápidamente justo antes del evento principal. Después del terremoto, se observaron picos de actividad de eventos LP y tremor acompañados de picos de desgasificación sincrónica con ellos. Este tipo de actividad es consistente con un aumento en el movimiento de fluidos dentro del sistema. En el volcán Llaima, los eventos LP y tremors venían presentaban un alto número antes del terremoto, y decreció notoriamente después. Por el contrario, la actividad volcano-tectónica aumentó notoriamente después del terremoto. Esto es interpretado como una respuesta tectónica frágil de reajuste del sistema. El incremento en la actividad de LPs, tremor y desgasificación antes del terremoto, son interpretadas como la entrada de un suministro de magma.

Cálculos en los cambios de presión revelan valores dos órdenes de magnitud menor que los observados en el terremoto de Valdivia. En conjunto, estos resultados indican que si bien el terremoto del Maule afectó de cierta manera la dinámica de ambos volcanes, los cambios de presión y el estado no-crítico de ambos volcanes fueron insuficientes para gatillar una erupción.

Cinco años después del terremoto del Maule, el volcán Villarrica presentó una erupción estromboliana moderada (VEI 2) en Marzo, 2015. La alarma de las instituciones de emergencia gubernamentales fue elevada al momento de la erupción. Las fuentes de lava alcanzaron los 1.5 km de altura, y la columna de cenizas llegó hasta los 11.5 km en la atmósfera. Para mejorar los planes de mitigación de riesgo, adquirir un mejor conocimiento de los procesos que gatillan erupciones volcánicas, y el comportamiento del sistema volcánico es que se generó el primer modelo de estructura interna de Villarrica.

Se realizó la inversión de tiempos de llegada de ondas P con rayos rectos para eventos VT localizados dentro de una red temporal de 50 estaciones instalada alrededor y sobre el volcán. Los hipocentros de los eventos indican un conducto alimentador entre los 3 y 5 km de profundidad, consistente con la dirección y ubicación de la zona de falla Liquiñe – Ofqui. Se observa una zona principal de baja velocidad somera (1 a 4 km de profundidad) de unos ~ 5 km de diámetro en dirección NNW bajo el cráter, la cual está ligada a este conducto alimentador. Dos estructuras similares a conductos de baja velocidad se observan fuertemente ligadas los flujos piroclásticos en superficie Los Nevados and Challupén (ENE y S del cráter), y son interpretados como conductos remanentes de dichas erupciones. Las zonas de alta velocidad hacia el este y debajo del cráter actual son interpretadas como productos consolidados de los previos colapsos de caldera. Las zonas al oeste del edificio, son interpretadas como productos consolidados y rocas de la corteza, ya que se encuentran bordeando la zona de baja velocidad principal. La inversión de tests sintéticos (Checker Board) da soporte a la resolución del modelo, y los cálculos del modelo Bootstrap proporcionan credibilidad estadística de los datos.

Estos resultados se esperan proporcionen información acerca del comportamiento de sistemas volcánicos abiertos y cerrados mediante la clasificación de señales sísmicas volcánicas y sus variaciones en el tiempo, en particular bajo la influencia de un gran evento de subducción. De manera particular para el volcán Villarrica, estos resultados entregan una primera aproximación a la estructura de velocidades interna del edificio volcánico. Esto es particularmente relevante para las agencias de monitoreo, no solo para mejorar los modelos de localización de la sismicidad, sino también para comprender de mejor manera los procesos en los conductos internos del sistema.

En conclusión, este estudio presenta, la primera tomografía del volcán Villarrica en conjunto con estudios de las series de tiempo previas y posteriores al terremoto del Maule. Como tal, esta tesis provee un estudio detallado de los procesos que influyen la actividad volcánica y las estructuras donde ésta ocurre. Con este trabajo, se ve enriquecido el conocimiento que tiene la comunidad científica acerca de la estructura y procesos del volcán Villarrica y similares.

Contents

Acknowledgements	vii
Abstract	ix
Zusammenfassung	xi
Resumen	xiii
List of Figures	xxvi
List of Tables	xxvii
1 Introduction	1
1.1 SFB 574 Project	1
1.1.1 Background	2
1.1.2 Objectives and Description of Subproject A2 related to this Work	2
1.1.3 Multiparameter surveillance of the Llaima and Villarrica volcanoes (Southern Chile): The near real-time approach	4
1.1.3.1 Objectives of the PaM project	5
1.2 Objectives	6
1.3 Outline	7
1.4 Seismic Signals at Volcanoes	7

2	Maule Mw 8.8 earthquake: a seismological review	11
2.1	Introduction	12
2.2	Geotectonic Setting of Chile	12
2.3	Geotectonic Setting of Epicentral Region and Historical Seismicity	14
2.3.1	Geotectonic Setting of the Concepción-Constitución seismic gap	14
2.3.2	Historical Seismicity	15
2.4	The Maule M8.8 earthquake	17
2.4.1	Description	17
2.4.2	Foreshocks	21
2.4.3	Aftershocks	25
2.5	Concluding Remarks	27
3	Comparison of Seismic Activity for Llaima and Villarrica Volcanoes prior to and after the Maule 2010 Earthquake	31
3.1	Introduction	32
3.2	Previous observations of volcanic eruptions triggered by great earthquakes	32
3.3	Geotectonic Context	34
3.4	Llaima and Villarrica Volcanoes	34
3.5	Volcanic Events Database	36
3.6	Methodology	38
3.7	Results	40
3.7.1	Villarrica Volcano	40
3.7.1.1	Long Period and Tremor events	40
3.7.1.2	Volcano Tectonic events	40
3.7.1.3	Other types of events	41

3.7.2	Llaima Volcano	42
3.7.2.1	Long Period and Tremor events	42
3.7.2.2	Volcano Tectonic events	43
3.7.2.3	Other types of events	43
3.8	Discussion	43
3.9	Conclusion	47
4	Inner Structure of the Villarrica Volcano derived from Local Tomography using Volcano Tectonic Events	49
4.1	Introduction	50
4.2	Geological Setting	51
4.3	Methods	52
4.3.1	Dense Temporary Volcanic Network	52
4.3.2	Records and First Velocity Model	52
4.3.3	Event Location and Selection	53
4.3.4	P-wave Tomography	55
4.3.5	Focal Plane Solutions	55
4.3.6	Checker-Board Test	55
4.4	Results	57
4.4.1	Medium Velocity from Delay in Arrival Times from Teleseismic Events and Wadati Diagrams	57
4.4.2	Earthquake Database	58
4.4.3	Tomography	58
4.4.4	Focal Plane Solutions	61
4.5	Discussion	67
4.5.1	Methodological Errors and Robustness	67

CONTENTS

4.5.2	Comparison of the First Velocity Model	67
4.5.3	Interpretation of Seismicity and Tomography	68
4.5.4	Other Studies at Villarrica Volcano	69
4.5.5	Comparison with Tomography Studies at other Volcanic Edifices	71
4.5.6	Proposed Inner Structure Model for Villarrica Volcano	71
4.6	Conclusions	72
5	Conclusions	75
	Bibliography	79
A	Appendix from Chapter “Comparison of Seismic Activity for Llaima and Villarrica Volcanoes prior to and after the Maule 2010 Earthquake”	93
A.1	SFB Catalogue Construction	93
A.2	Removal of aftershock sequence from time series	95
A.3	Activity in other volcanoes	95
B	Appendix from Chapter “Inner Structure of the Villarrica Volcano derived from Local Tomography using Volcano Tectonic Events”	97
B.1	Bootstrap Method	97
B.2	Polarities	99
B.3	Ray Bendings	100
B.4	Supplementary Material	101
B.4.1	Results	101
B.4.1.1	Horizontal Slices	101
B.4.1.2	Vertical Profiles East - West	110
B.4.1.3	Vertical Profiles North - South	116
B.4.2	Checker Board Test	123

CONTENTS

B.4.2.1	Horizontal slices	123
B.4.2.2	Vertical Profiles East - West	128
B.4.2.3	Vertical Profiles North - South	131
B.4.3	Bootstrap Results	135
B.4.3.1	Horizontal Slices	135
B.4.3.2	Vertical Profiles	142
	Eidesstattliche Erklärung	149
	Curriculum Vitae	151

List of Figures

1.1	Schematic overview of the processes studied by the SFB 574 project, and detailed areas of study for Themes A, B and C.	3
2.1	General geotectonic setting of Chile	13
2.2	Historical seismicity (magnitude over 7) for the Chilean trench between 32°S and 40°S, from XVI century	15
2.3	Record from Short-Period Station for the Maule earthquake	18
2.4	Locked zones prior to the Maule earthquake and slip contour lines	20
2.5	Seismic activity between 1st January 1990 and 26th February 2010 ($M \geq 3$) retrieved from NEIC, USGS	22
2.6	Histograms per year for events $M \geq 3$ and $M \geq 5$ between 1st January 1990 and 26th February 2010	23
2.7	Foreshock activity between 1st June 2009 and the 26th February 2010	24
2.8	Aftershock activity from 27th February 2010 until January 2011	26
2.9	Histogram of aftershocks until January 2011	27
2.10	Number of events per magnitude retrieved by U.S. Geological Survey and Chilean National Seismological Survey	27
2.11	Gutenberg-Richter scale for aftershocks from 27th February, 2010 until 31st January, 2011	28
2.12	Focal mechanisms for aftershocks with magnitude above 6, retrieved from NEIC (USGS)	29
3.1	Geotectonic setting of Chile and location of Llaima and Villarrica volcanoes	35
3.2	Station networks for Llaima and Villarrica, from SFB 574 project and OVDAS	38

LIST OF FIGURES

3.3	Time series of seismic events at Villarrica volcano (0.8 - 2.4 Hz) triggered in the continuous records of the SFB seismic network	39
3.4	Time series of seismic events at LLaima volcano (0.8 - 2.4 Hz) triggered in the continuous records of the SFB seismic network	39
3.5	Time series of seismic events at Villarrica volcano from Dec. 2009 to May 2011 based on OVDAS catalogue	41
3.6	Time series of seismic events at Llaima volcano from Dec. 2009 to May 2011 based on OVDAS catalogue	42
3.7	Weekly relative change in degassing activity at Villarrica volcano (Apr. 2009 - Jul. 2010)	44
3.8	Hipocenters for volcano-tectonic events at Llaima and Villarrica	45
3.9	Pressure change at 8.75 km depth as a response to the Maule earthquake	46
4.1	Dense temporary volcanic network at Villarrica during March 2012	53
4.2	Example of records for a volcano tectonic event	54
4.3	Resolution of synthetic model (Checker-Board test)	56
4.4	Example of V_p/V_s ratios	57
4.5	Initial velocity model for earthquake location at Villarrica	58
4.6	Hypocenter before and after grid search relocation	59
4.7	Velocity variation results for horizontal slices	60
4.8	Velocity variation results for vertical East-West profiles	61
4.9	Velocity variation results for vertical North-South profiles	62
4.10	Absolute Velocity model results for horizontal slices	63
4.11	Absolute Velocity model results for vertical East-West profiles	64
4.12	Absolute Velocity model results for vertical North-South profiles	65
4.13	Focal mechanisms for some of the events used in the tomography	66
4.14	Conceptual model derived from variations in velocity	69
4.15	Schematic model (East-West) for the edifice and the uppermost part of the conduit	72

LIST OF FIGURES

A.1	Spectrogram for a volcanic event in Villarrica and Llaima volcano, and a regional event	94
B.1	Polarities from P wave arrival	99
B.2	Ray bending calculation	100
B.3	Results from inversion in horizontal slice at 2.5 km a.s.l.	101
B.4	Results from inversion in horizontal slice at 1.5 km a.s.l.	102
B.5	Results from inversion in horizontal slice at 0.5 km a.s.l.	103
B.6	Results from inversion in horizontal slice at 0.5 km b.s.l.	104
B.7	Results from inversion in horizontal slice at 1.5 km b.s.l.	105
B.8	Results from inversion in horizontal slice at 2.5 km b.s.l.	106
B.9	Results from inversion in horizontal slice at 3.5 km b.s.l.	107
B.10	Results from inversion in horizontal slice at 4.5 km b.s.l.	108
B.11	Results from inversion in horizontal slice at 5.5 km b.s.l.	109
B.12	Results from inversion in vertical E-W profile at -4.5 km (west).	110
B.13	Results from inversion in vertical E-W profile at -3.5 km (west).	111
B.14	Results from inversion in vertical E-W profile at -2.5 km (west).	111
B.15	Results from inversion in vertical E-W profile at -1.5 km (west).	112
B.16	Results from inversion in vertical E-W profile at -0.5 km (west).	112
B.17	Results from inversion in vertical E-W profile at 0.5 km (east).	113
B.18	Results from inversion in vertical E-W profile at 1.5 km (east).	113
B.19	Results from inversion in vertical E-W profile at 2.5 km (east).	114
B.20	Results from inversion in vertical E-W profile at 3.5 km (east).	114
B.21	Results from inversion in vertical E-W profile at 4.5 km (east).	115
B.22	Results from inversion in vertical N-S profile at 8.5 km (north).	116
B.23	Results from inversion in vertical N-S profile at 7.5 km (north).	117

LIST OF FIGURES

B.24 Results from inversion in vertical N-S profile at 6.5 km (north). 117

B.25 Results from inversion in vertical N-S profile at 5.5 km (north). 118

B.26 Results from inversion in vertical N-S profile at 4.5 km (north). 118

B.27 Results from inversion in vertical N-S profile at 3.5 km (north). 119

B.28 Results from inversion in vertical N-S profile at 2.5 km (north). 119

B.29 Results from inversion in vertical N-S profile at 1.5 km (north). 120

B.30 Results from inversion in vertical N-S profile at 0.5 km (north). 120

B.31 Results from inversion in vertical N-S profile at -0.5 km (south). 121

B.32 Results from inversion in vertical N-S profile at -1.5 km (south). 121

B.33 Results from inversion in vertical N-S profile at -2.5 km (south). 122

B.34 Results from inversion in vertical N-S profile at -3.5 km (south). 122

B.35 Results from Synthetic inversion in horizontal slice at 1.5 km a.s.l. 123

B.36 Results from Synthetic inversion in horizontal slice at 0.5 km a.s.l. 124

B.37 Results from Synthetic inversion in horizontal slice at 0.5 km b.s.l. 124

B.38 Results from Synthetic inversion in horizontal slice at 1.5 km b.s.l. 125

B.39 Results from Synthetic inversion in horizontal slice at 2.5 km b.s.l. 125

B.40 Results from Synthetic inversion in horizontal slice at 3.5 km b.s.l. 126

B.41 Results from Synthetic inversion in horizontal slice at 4.5 km b.s.l. 126

B.42 Results from Synthetic inversion in horizontal slice at 5.5 km b.s.l. 127

B.43 Results from Synthetic inversion in vertical E-W profile at -4.5 km (west). 128

B.44 Results from Synthetic inversion in vertical E-W profile at -3.5 km (west). 128

B.45 Results from Synthetic inversion in vertical E-W profile at -2.5 km (west). 128

B.46 Results from Synthetic inversion in vertical E-W profile at -1.5 km (west). 129

B.47 Results from Synthetic inversion in vertical E-W profile at -0.5 km (west). 129

LIST OF FIGURES

B.48 Results from Synthetic inversion in vertical E-W profile at 0.5 km (east).	129
B.49 Results from Synthetic inversion in vertical E-W profile at 1.5 km (east).	129
B.50 Results from Synthetic inversion in vertical E-W profile at 2.5 km (east).	130
B.51 Results from Synthetic inversion in vertical E-W profile at 3.5 km (east).	130
B.52 Results from Synthetic inversion in vertical E-W profile at 4.5 km (east).	130
B.53 Results from Synthetic inversion in vertical N-S profile at 8.5 km (north).	131
B.54 Results from Synthetic inversion in vertical N-S profile at 7.5 km (north).	131
B.55 Results from Synthetic inversion in vertical N-S profile at 6.5 km (north).	131
B.56 Results from Synthetic inversion in vertical N-S profile at 5.5 km (north).	132
B.57 Results from Synthetic inversion in vertical N-S profile at 4.5 km (north).	132
B.58 Results from Synthetic inversion in vertical N-S profile at 3.5 km (north).	132
B.59 Results from Synthetic inversion in vertical N-S profile at 2.5 km (north).	132
B.60 Results from Synthetic inversion in vertical N-S profile at 1.5 km (north).	133
B.61 Results from Synthetic inversion in vertical N-S profile at 0.5 km (north).	133
B.62 Results from Synthetic inversion in vertical N-S profile at -0.5 km (south).	133
B.63 Results from Synthetic inversion in vertical N-S profile at -1.5 km (south).	133
B.64 Results from Synthetic inversion in vertical N-S profile at -2.5 km (south).	134
B.65 Results from Synthetic inversion in vertical N-S profile at -3.5 km (south).	134
B.66 Results from Bootstrapped tomography in horizontal slice at 1.5 km b.s.l.	135
B.67 Results from Bootstrapped tomography in horizontal slice at 0.5 km a.s.l.	136
B.68 Results from Bootstrapped tomography in horizontal slice at 0.5 km b.s.l.	137
B.69 Results from Bootstrapped tomography in horizontal slice at 1.5 km b.s.l.	138
B.70 Results from Bootstrapped tomography in horizontal slice at 2.5 km b.s.l.	139
B.71 Results from Bootstrapped tomography in horizontal slice at 3.5 km b.s.l.	140

LIST OF FIGURES

B.72 Results from Bootstrapped tomography in horizontal slice at 4.5 km b.s.l. 141

B.73 Results from Bootstrapped tomography in vertical profile EW at -4.5 km (west) 142

B.74 Results from Bootstrapped tomography in vertical profile EW at -3.5 km (west) 143

B.75 Results from Bootstrapped tomography in vertical profile EW at -2.5 km (west) 143

B.76 Results from Bootstrapped tomography in vertical profile EW at -1.5 km (west) 144

B.77 Results from Bootstrapped tomography in vertical profile EW at -0.5 km (west) 144

B.78 Results from Bootstrapped tomography in vertical profile EW at 0.5 km (east) 145

B.79 Results from Bootstrapped tomography in vertical profile EW at 1.5 km (east) 145

B.80 Results from Bootstrapped tomography in vertical profile EW at 2.5 km (east) 146

B.81 Results from Bootstrapped tomography in vertical profile EW at 3.5 km (east) 146

B.82 Results from Bootstrapped tomography in vertical profile EW at 4.5 km (east) 147

List of Tables

4.1	Comparison of results of velocity values, and percentage of variation of velocities for single-run tomography, and the values from the average velocity of 100 runs of Bootstrapped Tomography.	67
4.2	Standard Deviation per cube (σ_i) and Central Deviation (σ_i/\bar{v}_i) values for bootstrapped tomography using 100 runs with 63% of the events of the main sample (38 events). . . .	67
A.1	Triggering parameters for the three bands studied	94
A.2	Values of fitting parameters for the band 0.8 - 2.4 Hz, for both Llaima and Villarrica volcanoes	95

Chapter 1

Introduction

Volcanoes are the natural link between the lithosphere and the atmosphere. They are a door for asthenosphere fluids and chemicals ascending through crust and expelling gases and lava to build and reshape volcanic edifices. And we see many cities in subduction zones that have evolved at the feet of volcanoes, coexisting with natural hazards such as great earthquakes and volcanic hazards such as eruptions, lahars, tephra fall-outs, and other volcanic products. Volcanoes help regulate the global temperature and albedo by injecting chemicals, like sulphur, into the atmosphere, influencing the creation of clouds and thus lowering the temperature of the Earth. Locally, volcanoes are great potential sources of geothermal energy, provide sites for tourism in some regions, and enrich the soil since after several years of eruptions, the ground is fertilized by rich chemicals from volcanic ashes.

Understanding the behavior, dynamics, and structures that compose the volcanic system not only enhances scientific knowledge, but helps researchers to provide insights to monitoring agencies and communities for improving their hazard mitigation programs.

This thesis is strongly linked to the study of one particular touristic and highly active volcano in Chile. In this work, I present the study of seismicity and other geophysical methods to provide insight into the velocity structure of the Villarrica volcano in southern Chile. Specifically, this study concentrates on the major hazards for a Chilean community: great subduction earthquakes (Magnitude ≥ 8), and volcanoes.

1.1 SFB 574 Project

This work is part of the Sonderforschungsbereich SFB 574 project, “Volatiles and Fluids in Subduction Zones,” specifically within the side project, “Multiparameter Surveillance of the Llaima and Villarrica volcanoes (Southern Chile): The near real-time approach” (from here on, the “PaM project”). The SFB 574 project studied the interaction cycle, processes, and control of volatiles and fluids in earthquakes, volcanic eruptions, and gases, and submarine fluid seeps in subduction zones; while the PaM project is focused on the integration of geochemical and geophysical data to increase understanding of the magmatic plumbing system, and the role of processes in influencing volcanic unrest.

1.1.1 Background

The subduction process of oceanic crust embodies the cycle of halogens, water, sulphur, and carbon dioxide that come as sediments from continental erosion and weathering, or from alterations of the oceanic crust in depth, and come back to the atmosphere and oceans through marine vents and degassing of lava and magma in volcanic edifices. Subduction rates, earthquakes, eruptions of magmas, and submarine fluid seeps are in some form controlled by this input of fluids and reflect this transport cycle.

Water, halogens, sulphur, and carbon dioxide enter the oceanic crust through small cracks, or as sediments from the continental slope. In the forearc region, small vents can return part of these products to the ocean and atmosphere, or they get stored in hydrate reservoirs. As depth, pressure and temperature increase in the subducted slab, the devolatilization of the crust brings water and gases into the asthenosphere. From there, fluids ascend to magmatic reservoirs under volcanic chains, and are then returned in part to the atmosphere through volcanic eruptions and magma degassing. This complex recycling process plays a part in the chemical evolution of the atmosphere, oceans, sediments, continental crust, and the long-term global climate.

The SFB 574 project aimed to understand the subduction process in both oceanic and continental settings from 2001 to 2007 in Costa Rica, and from 2008 to 2012 in Southern Chile. In order to understand the processes involved in the different parts of this cycle, the project was divided into three main groups, (A, B, and C), focused on very specific topics regarding this cycle, which, at the same time, were subdivided into smaller specific topics. Figure 1.1 shows a schematic model of the subduction processes and the topics of each of the Themes.

Theme A studied the structure and tectonics of the subduction zone, and particularly for this thesis, subproject A2 was projected to characterize the seismic activity of the subduction zone, provide better constraints on the structuring of the subducting slab and the overriding plate, determine fluid pathways, and provide clues to the links between seismic activity and volcanism with its related hazards.

Theme B studied the input of materials in the subduction zone and its output in the ocean, quantifying the amount of relevant gases involved in global climate, such as methane, which is released in submarine cold water springs, and the influence these gases have on the activity of micro-organisms and environmental conditions.

Theme C studied the migration of fluids from the slab through the volcanic arc and back to the atmosphere to see whether the type, style, and rate of the subducting plate has relevance in the control of quantities or in the type of magma, the mechanism of return transportation, which gases are released to the atmosphere, and how they affect the climate.

1.1.2 Objectives and Description of Subproject A2 related to this Work

The subproject A2, “Geophysical search for links between earthquake and volcano hazard in south-central Chile,” inside the SFB 574 project, will benefit from the small scale work presented in this thesis. The project sought for better comprehension of the subduction processes since the subduction in south-central Chile is one of the best natural observatories in which to study it. This region was the stage of the greatest instrumentally registered earthquake, that occurred in 1960 (M9.5 Valdivia earthquake), and it

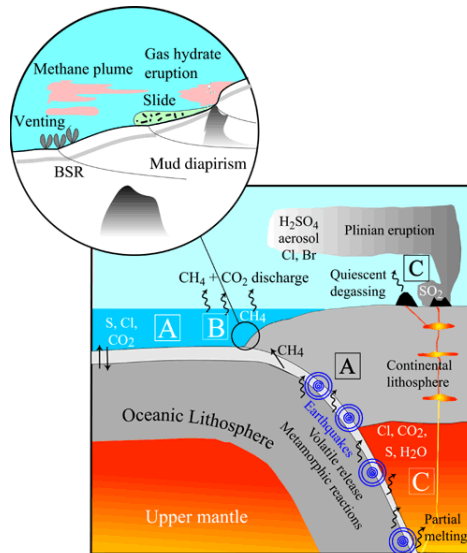


Figure 1.1: Schematic overview of the processes studied by the SFB 574 project, and detailed areas of study for Themes A, B, and C, as well as transportation and transformation of material in the subduction zones. Source: <https://sfb574.geomar.de/de/introduction.html>

houses one of the most active volcanoes in the Southern Volcanic Zone (SVZ). Seismicity and volcanism in south-central Chile are controlled by the input of sediments building the accretionary prism and going into the trench (Ranero et al., 2006; Contreras-Reyes et al., 2010), strain partitioning in the forearc due to the oblique convergence of the Nazca plate (Hoffmann-Rothe et al., 2006; Rosenau et al., 2006; Lavenu and Cembrano, 1999), and pre-Andean and deep crustal structures in the continental plate (Rapela and Pankhurst, 1992; Martin et al., 1999; Cembrano and Lara, 2009).

Among the objectives presented for this subproject, those that are most closely related to this study are:

- assessing the structure of the entire subduction system (including the oceanic slab and overriding plate), the locations of seismogenesis, of fluid release, and of magma production and storage
- characterizing the seismic activity, tectonic structure, fluid flow pathways, and thermal structure
- determining the links between seismic activity, volcanism, and related hazards

To reach these goals, the project installed a regional seismological network from the coastline to the back-arc of the region between 38.5°S and 40°S during the entire year of 2009. Gravity and magnetic measurements were carried out as well, with a focus on the arc to delineate fault structures and small-scale arc basins associated with the Villarrica volcano. Methods like receiver functions, characterization

of regional seismicity, and tomography provided insight into the crustal and deep seismic patterns, crustal thickness, slab geometry, and fluid pathways through the mantle.

In collaboration with Theme C, the “Multiparameter surveillance of the Llaima and Villarrica volcanoes (Southern Chile): The near real-time approach” was created in order to complement the study and knowledge of volcanic processes, especially of the relationship between volcano eruptions, degassing events, magma related seismicity, volcano surface deformation, and volume change.

1.1.3 Multiparameter surveillance of the Llaima and Villarrica volcanoes (Southern Chile): The near real-time approach

The main focus of this project is to contribute to the understanding of processes influencing the volcano behavior, in order to improve the natural hazard mitigation projects and early warning systems of two of the most active volcanoes in the Southern Volcanic Zone in Chile.

In the forecast of an upcoming eruption, or in the possible changes during an eruption, previous volcano-monitoring studies play a crucial part in providing a short-term scenario. Changes inside the magmatic system are observed as variations in geochemical and geophysical parameters which, when outside of the usual values, represent what we call “volcanic unrest”.

Seismic records and deformation signals (tilt-meters and GPS), along with gas concentration and flux measurement provided by DOAS and mini-DOAS (Differential Optical Absorption Spectroscopy) are the most common measurements in real-time volcano monitoring. In the past, these datasets have been studied independently due to differences in time resolution, particularly for gas measurements. But currently combined observation in a similar temporal resolution is possible, and many observatories are using this multi-parameter approach to recognize long- and short-term changes at volcanoes.

Large SO₂ fluxes in the fumarolic activity indicate the presence of magma during awakening episodes, and the rapid variations of these fluxes can provide information about the type (magmatic, tectonic, or hydrothermal) and style (passive degassing, strombolian, or vulcanian eruption) of the unrest. Rates of SO₂ degassing are controlled by variations in rates of magma supply, and permeability drops and rises due to cooling of the conduit, or after large eruptions or dome-collapse events, respectively (Saccorotti et al., 2015).

Seismicity at volcanoes is generated principally, but not only, by two sources of waves: a brittle response of the rock to changes in stress, whether in the magma chamber or a dike; and oscillations produced by fluid movement, magma or gases, inside the conduits or cracks. Different types of events precede an unrest episode, depending on the nature of the unrest. Magmatic and fluid intrusions through dikes generate brittle responses as the tip of the crack breaks, allowing the forward movement of the fluids. Pressure changes inside the magmatic chamber due to an increase in gas exsolution, magma withdrawal, or a new batch of magma intrusion, also generate a fragile response in the rock containing the reservoir. Low frequency events related to the movement of fluids are generated by the movement of magma, geothermal fluids, and gases through cracks or conduits. Tremors and explosions can overwhelm the record when an eruption is starting or is in course. A detailed description of the different volcano-seismic signals is presented in Section 1.4.

Geochemical and mechanical changes can be induced by variations in dynamic and static stresses due to the energy released in earthquakes at or near the volcano. Dynamic stress changes generated by the passing of waves can disturb the magma rapidly by stimulating bubble nucleation and bubble detachment, leading to an increase in the pressure inside the chamber. Changes in static stress in the crust favor the formation of cracks that allow magma and fluids to propagate, contributing to new pathways for degassing. Crack formation near geothermal areas or water sources can result in the entrance of water into shallow magmatic systems, possibly changing the degassing behavior or even inducing phreatomagmatic eruptions.

1.1.3.1 Objectives of the PaM project

The main objective of the “Multiparameter surveillance of the Llaima and Villarrica volcanoes (Southern Chile): The near real-time approach” is to increase knowledge of the combined processes responsible for the triggering of volcanic unrest; specifically, to understand the time scale and possible correlation between seismic activity, degassing rates, and chemical composition.

Among the specific objectives of the PaM project, those closely related to this thesis are:

- the determination of the role of magma supply rates, accumulation depths, volatile contents, and chemical composition, and variations of the tectonic situation in the behaviour and style of eruption;
- to increase the understanding of magma plumbing systems.

To accomplish the objectives for this project the first mini-DOAS station was installed in March, 2009 to scan the plume of the Villarrica volcano. It was followed by the installation of three permanent automated NOVAC-type Mini-DOAS UV-spectrometers in February, 2010 at Villarrica, and two others at the Llaima volcano. These stations were permanently donated to the Southern Andes Volcanic Observatory (OVDAS, acronym in Spanish) to improve degassing monitoring. The temporary seismological networks were installed in two stages. First, two small temporary networks of five stations each (three Short-Period stations, one Broad Band station, and one Ocean Bottom Seismometer) were installed at the Llaima and Villarrica volcanoes between December, 2009, and April, 2011. To improve the reception of volcanic signals, a dense temporary network of 75 Short-Period stations was installed only at Villarrica volcano during two full weeks in March, 2012. The choice of the Villarrica volcano was due to the higher level of seismicity at this volcano in comparison with Llaima. The goal is to enhance the knowledge of eruptive behavior and the dynamics of the Llaima and Villarrica volcanoes, to help strengthen specific Chilean volcanic hazard mitigation plans, and to provide insight into other plans for similar volcanoes.

The reason behind the selection of the Llaima and Villarrica volcanoes in southern Chile, besides the fact that they are the most active volcanoes in the Andean SVZ, is that they have distinctly different behavior in seismicity and degassing.

Villarrica is an open vent system with a constant lava lake of variable height inside the crater. The lava lake presents constant degassing and bubble bursting as seething magma or small lava fountains depending on the intensity of activity. It evidences little to no present-time ground deformation, although it is difficult to obtain deformation values through InSAR, for example, due to the large and permanent

glacier covering most of the east flank. Villarrica rarely presents an eruption of $VEI > 2$, with the historical exception of pyroclastic flows and ignimbrite forming eruptions. Since the eruption in 1984-85 (VEI 2), several smaller eruptions have been observed. The last eruption of the Villarrica volcano was in March, 2015, preceded by an increment in the seismic activity beginning in February of the same year. Lava fountains up to 1.5 km and an eruptive plume rising 6-8 km into the atmosphere were observed on the 3rd of March, as well as intense Strombolian activity, tephra fallout, and strong lahars in the main drainage associated with the volcano (Johnson and Palma, 2015).

Llaima has no open vent between volcanic eruptions, but presents moderate fumarolic activity. Seismic activity is scarce, and deformation rates are high with inflation-deflation processes associated with the accumulation of magma before the eruption and the consequent contraction after it (Bathke et al., 2011). Llaima eruptions occur in Strombolian, Hawaiian, and sometimes sub-Plinian types of activity, with VEI usually below 3. The last eruptive cycle from 2007-2009 presented activity of $2 \leq VEI \leq 3$, with the eruption on the 1st of January 2008, being the strongest one (VEI 3). The violent Strombolian eruption produced strong lava fountains, high levels of seismicity, and an eruptive column that reached 12.5 km at its highest point (Global Volcanism Program, 2013).

1.2 Objectives

The Villarrica volcano is one of the most active volcanoes in southern Chile; it is also the first volcano in the rank of hazards for Chile, which is the reason why it is the most monitored instrumentally by OVDAS in Temuco, Chile.

In order to improve awareness of volcanic eruptions and unrest episodes, it is important to combine information from historical eruptions and present-time behavior and structure. For the latter, volcano monitoring agencies obtain great benefit from knowing the dynamics of the volcano, its common seismic activity, and the structure and depth of possible reservoirs. Although Villarrica is one of the most studied volcanoes in the region, its relationship with the geological framework in which it is emplaced, and the processes influencing the unrest are still poorly understood, and its inner structure below the subsurface, beyond schematic profiles, is still unknown. The aim of this work is to study the volcano-tectonic and volcano-seismic features of the Villarrica volcano, particularly its inner velocity structure, in order to understand the processes influencing its behavior.

Specific objectives for this work are the following:

- to characterize and classify volcano-seismic signals to achieve a better understanding of the behavior of the volcano
- to verify crustal structures related to the emplacement of the Villarrica volcano
- to recognize variations in the type and quantity of activity regarding the great earthquake-volcano interactions
- to search for a correlation between seismic activity and degassing at the Villarrica volcano
- to provide insights into the inner velocity structure of the Villarrica volcano

1.3 Outline

This work presents three manuscripts, two of them already published, assessing different topics that resolve the objectives previously presented.

Chapter 1 introduces the framework on which these manuscripts and work were developed. It also includes a brief description of seismic volcanic signals, providing necessary background to the processes and characteristics of frequently mentioned events and abbreviations in the ensuing chapters.

In Chapter 2 the manuscript *Maule Mw 8.8 earthquake: a seismological review*, published in the book “The Chilean Earthquake and Tsunami 2010. A multidisciplinary study of Mw8.8, Maule” from WIT Press publishers, presents the general geological and tectonic setting of Chile, where the Villarrica volcano is located. Its focus is mainly on the Maule 2010 earthquake, historical seismicity of the region of study, and its extent.

Chapter 3 corresponds to the second paper *Comparison of seismic activity for Llaima and Villarrica volcanoes prior to and after the Maule 2010 earthquake*, published in the Special Issue from the SFB 574 project in the *International Journal of Earth Sciences*. It considers the behaviour and response of volcanoes facing the external forces generated by a great earthquake in the vicinity. In particular, the case of the Villarrica and Llaima volcanoes before the Maule earthquake, and their response to it in terms of seismic activity, are presented. Since degassing processes go hand in hand with long period activity, comparisons of the amounts of degassification are also presented to increase understanding of the dynamic processes associated with them.

In Chapter 4, the velocity structure of the Villarrica volcano derived from geophysical methods is presented. The inner velocity structure of the volcano, obtained through straight-ray local seismic tomography, is presented in the form of the manuscript, *Inner Structure of Villarrica Volcano derived from Local Tomography using Volcano Tectonic events*, to be submitted to the *Journal of Volcanology and Geothermal Research*.

Finally, Chapter 5 summarizes the main conclusions of these reports, and combines them into a comprehensive closure of the thesis. Future lines of work for increasing the knowledge and comprehension of volcanic dynamics and structures are presented.

1.4 Seismic Signals at Volcanoes

Earthquakes in volcanic regions serve as indicators of stress changes in the system, such as the intrusion of a magma dike, movements of geothermal fluids, and, most of the time, with a combination of different signals preceding an eruption.

There are four basic types of events commonly used and first described by Shimozuru (1972) and Minakami (1974). Lately, with the advance of seismology and instrumentation, these four types and others that have been found have been described extensively in the specific literature and reviews: Lahr et al. (1994); McNutt (1996); Chouet (1996); Wassermann (2012); Zobin (2003); McNutt (2000, 2005). Typically, the classification of volcanic events is done in terms of their frequency content. There are two

major groups: high frequency (HF) and low frequency (LF) events. The frequency content has a direct relation with the source of the seismicity. High frequency events are related to brittle response, cracks or explosions, while low frequency events are related to oscillations of fluids or path effects.

In this section, a brief description of the following types of events will be given:

- A-Type, Volcano Tectonic (VT) or High Frequency (HF)
- B-Type, Long Period (LP) or Low Frequency (LF)
- Very Long Period (VLP)
- Hybrid (HB)
- Volcanic Tremor (TR)
- Explosion

A-Type, Volcano Tectonic (VT) or High Frequency (HF)

Volcano tectonic events are brittle failure events caused by a slip in a fault similar to typical earthquakes in non-volcanic regions. VT events present clear impulsive P- and S- wave arrivals, but their coda is much shorter than common earthquakes, presenting smaller magnitudes. They occur with swarm-like behaviour, i.e. with no significant mainshock, but rather several events occurring in a short time and a concentrated space with similar magnitude, but sometimes presenting a few events of higher magnitude (Mogi, 1963). This results in large *b*-values and a great variety of focal mechanisms due to small cracks/faults and changes in stresses.

VT events can be found at different depth ranges in the crust, and have a broad frequency content with dominant frequencies of around 5-15 Hz. Events deeper than 2 km, often present frequencies higher than 5 Hz, and P- and S- clearly arrive. As for shallower events (depth < 2 km), frequency content shifts to a lower range (1-5 Hz), and the S- wave is not clear in the arrival (Wassermann, 2012). These events are mostly related to fragile responses on the front tip (compression) or sides (local extension) of the advancing dike in a magmatic intrusion; or to pressure changes in the surrounding rock of a magma chamber experiencing exsolution and bubble formation (increase), magma withdrawal, or cooling down (decrease).

Long Period Events

Long period events have a more harmonic component and a narrow band signal, with dominant frequencies of 1-5 Hz, but 2-3 Hz are more common. Their source is attributed to the interactions between fluids (magma, steam, bubbles, slugs) and the conduit through which they are passing, generating the oscillation of the walls. An increase in LP activity may indicate higher pressure in the magmatic or hydrothermal system, or an increase in the flow rate of fluids. LP events occur mostly at shallow depths (< 3 km) in volcanic areas, including geyser and geothermal reservoirs. Sometimes, but not very often, LP events are located very deep under the crust, presumably associated with the resupply of magma from

deeper reservoirs to shallower chambers. These are called Deep Long Period events (DLP) and have been found under the Fuji, Pinatubo, and Kilauea volcanoes, to name a few, at between 10 and 60 km depth (Kawakatsu and Yamamoto, 2007; White, 1996; Ukawa, 2005).

Associated with pressurized fluid, LP events show no S- wave, have emergent signal onset with transient characteristics, and are long-lived, lasting several seconds with a harmonic decaying coda. Typical S-P arrival time difference location is not possible, and other methods, such as amplitude distance curves and probabilistic location, must be used. A repetitive LP event suggests a non-destructive source process, and the frequency of resonance of the events can be used to reveal characteristics of the conduit or the fluid source (Richardson and Waite, 2013)

Very Long Period Events

Very Long Period events are also known as Very Low Frequency (VLF) or Ultra Low Frequency/Long Period (ULF, ULP) events. They have been observed due to the improvement in Broad Band instrumentation, as they have frequencies ranging between 0.1 to 0.001 Hz, below the Stromboli, Kilauea, Aso, Sakurajima, Mount Erebus and other volcanoes ((McNutt, 2002, and references therein)). Typically, VLP events present periods of 3-20 sec, have a fairly small amplitude, and are located at shallow depths (~ 1.5 km). The signal has been associated with the build-up of pressure before an eruption (inflation/deflation), but it has also been observed at erupting volcanoes. Other models associate the origin of the signal with a slug of magma, water, or gas passing through a constricting dike or sill in distinct pulses.

Hybrid Events

Hybrid events, or Multiphase events (MP), share characteristics of both high frequency and low frequency events, indicating a possible mixture in the processes generating the signals. A high frequency onset is visible, with clear P-wave and S wave arrivals, followed by an extended low frequency coda. They have short durations of a few seconds and have been found at shallow depths (< 4 km), but also at some deeper depths (5-9 km) in the Redoubt volcano, for example in Power et al. (1994). Initially, for studies performed in the Redoubt volcano, the source of the hybrid event was attributed to brittle failure and an ensuing excitation of fluid filled cracks surrounding the source (Power et al., 1994; Lahr et al., 1994). However, the following studies at Montserrat (White et al., 1998; Neuberg et al., 2000), Deception Island (Ibáñez et al., 2003) and St. Helens (Harrington and Brodsky, 2007), have shown that the low frequency and prolonged signal of the coda might be due more to a path effect rather than oscillation.

Volcanic Tremor

Tremors are an emergent sustained continuous vibration signal of long duration that can last from minutes to years at some volcanoes. They present no P- or S- wave arrivals, and may be generated by compressional waves or strong surface waves. A study of tremors at 107 volcanoes by McNutt (1992), showed that the frequency content of tremors ranges between 1 and 9 Hz, with some volcanoes presenting higher frequencies, and a mean frequency of 3.8 Hz.

Tremor activity has been observed at volcanoes during eruptions. The higher the activity at the volcano, the higher the amplitude of the tremor. In order to compare tremors at different volcanoes, the normalization called Reduce Displacement (RD) was created, similar to what is done with tectonic earthquakes. There are two formulations of RD based on the amplitude (A [cm] peak-to-peak) and wavelength (λ [cm]) of the signal, source - station distance (r [cm]) and seismograph magnification at the tremor frequency (M). Values observed by McNutt (1992) range between $\sim 0.01 \text{ cm}^2$ and $\sim 100.000 \text{ cm}^2$. RD is calculated as $RD = \frac{Ar}{2\sqrt{2}M}$ for Body waves, and as $RD = \frac{A\sqrt{\lambda}r}{2\sqrt{2}M}$ for Surface waves.

Two typical types of tremors are harmonic and spasmodic. Harmonic tremors are often consistent on a single frequency with different overtones, generated by the rapid flow of fluids through a constriction in the conduit. A Spasmodic tremor, or “banded” tremor, contains higher frequencies and a more pulsating signal of irregular amplitudes. Periods between the signals are often uniform, and records in helicorders have given the impression of bands (hence the term “banded”).

Explosions

Explosion signals have been seen accompanying eruptions at volcanoes. The source is still not very clear. It corresponds to high frequency arrivals from air-shock waves originated at the vent, probably as a sonic boom due to expanding gas accelerated at the exit of the vent. The energy released is partitioned as one part travels through the ground as seismic waves, and another part goes through the air as an acoustic wave. The air wave then couples back to the ground, and the signal is detected by the seismometer.

Chapter 2

Maule Mw 8.8 earthquake: a seismological review¹²

C. Mora-Stock and W. Rabbel

Abstract

Chile is one of the seismically most active countries in the world with an earthquake of magnitude 8 or larger ($M \geq 8$) occurring every ten years. The most recent 27th February 2010 ($M_w=8.8$) earthquake released the energy accumulated in the Concepción-Constitución seismic gap contained since the last earthquake, in 1835. The hypocentre ($36^\circ 17' 23''S$; $73^\circ 14' 20''W$) was located at the subduction interface of the Nazca plate under the South American plate, near the coasts of Talcahuano, at a depth of 30 km. The rupture area extended for approximately 450 km along the Pacific coast, from the Arauco Peninsula northwards to Pichilemu, and showed slip displacements up to ten meters. Hundreds of aftershocks have taken place in the rupture area, the largest and most remarkable of which was the Pichilemu $M=6.9$ earthquake on 11th March, 2010. The Maule earthquake has shown surprising seismic phenomena, such as the fact that no aftershocks over $M=7$ have occurred. Also, given the amount of energy released, some cities have experienced displacements of the order of meters caused by the re-accommodation of the South American plate, and some shores have been permanently uplifted. Studies of the aftershocks are being performed for a better understanding of the subduction processes and to improve the knowledge of earthquake-resistant construction.

¹The following is an authorized copy of the book chapter published in “The Chilean earthquake and Tsunami 2010. A multidisciplinary study of Mw8.8, Maule” from WIT Press. The original publication is available at <http://www.witpress.com/elibrary/wit-transactions-on-state-of-the-art-in-science-and-engineering/58/24003>.

²Please cite this book chapter as follows: C. Mora-Stock and W. Rabbel. Maule Mw 8.8 earthquake: a seismological review. L.A. Cárdenas-Jirón, ed. Pages 1 - 24. 2012.

2.1 Introduction

Chile is one of the seismically most active countries in the world, showing one event above magnitude 8 every 10 years, approximately. In historical times these events have been well documented (Darwin, 1845; Lomnitz, 1970; Comte and Pardo, 1991). Such large earthquakes occur in fractures along the mechanically stressed interface of the continental South American plate and the downgoing Nazca plate. Due to the relative movement between these two plates, the stress is released when a critical stress limit is exceeded, in a rupture of several hundred kilometers along the coast. When one of these sections has not presented a large earthquake for a certain span of time, it is called a “seismic gap”

The subduction zone along the Peru-Chile trench, between Arica and the Taitao Peninsula, is divided in several parts that had experienced least one $M \geq 8$ earthquake within the last 134 years (Barrientos, 2007; Madariaga, 1998; Melnick et al., 2009; Comte and Pardo, 1991; Ruegg et al., 2009). The different sections that break are separated, usually, by geological features such as ridges, peninsulas, or deep-reaching faults. These features are thought to act as barriers where the rupture may be terminated. The Arauco Peninsula is one of these important boundaries, located in between the rupture zones of the earthquakes of 1960 and 1835 (Melnick et al., 2009).

The earthquake of 27th February 2010 released the energy accumulated since last great subduction earthquake, in 1835 ($M_{8-8.5}$ (Darwin, 1845; Lomnitz, 1970; Campos et al., 2002)), in the Concepción-Constitución gap. In 1928, an earthquake affected the northern part, between Chanco and Constitución; and to the south, the events from 1960 and subsequent aftershocks, some of them with $M_w \geq 7$ in 1974-1975, affected the southern part of the Arauco Peninsula down to the Chile Triple Junction (Cifuentes, 1989). Although these events occurred near the gap, none of these events broke the section between the 36°S and 37.4°S (approximately between the cities of Pelluhue, near Cauquenes, from the north and Quiapo to the south). The earthquake of 1939, which destroyed the city of Chillán, was earlier considered as an interplate event (Kelleher, 1972) related to the Concepción-Constitución seismic gap, but works of Campos and Kausel (1990), Beck et al. (1998) and Campos et al. (2002) showed this was an oceanic intraplate event with a depth of 80-100 km. Then, even the epicentre was located in the middle of the gap, but inland, the seismic gap remained coupled.

2.2 Geotectonic Setting of Chile

Chile is located in the so-called “Ring of Fire” region, which corresponds to the subduction zones along the coasts of the Pacific Ocean. All along the west coast of South America, the subduction of oceanic plates under the continental South American plate generates a series of earthquakes, these being thrust earthquakes, the most destructive and important ones regarding their higher magnitude.

Chile has three well differentiated seismogenic zones (Barrientos, 2007): thrust earthquakes (0-50 km) of large magnitude at shallow depth along the coast, large earthquakes of intermediate depth (70-100 km) due to tensional and compressional forces in the subducted Nazca plate, and shallow seismicity (0-20 km) in the outer-rise, in the Andean regions of Central Chile, and in strike-slip faults in Southern Chile, such as the Magallanes-Fangnana and Liquiñe-Ofqui faults.

In Chile, earthquakes are caused by the interaction of the Nazca, Antarctic, Scotia and South Amer-

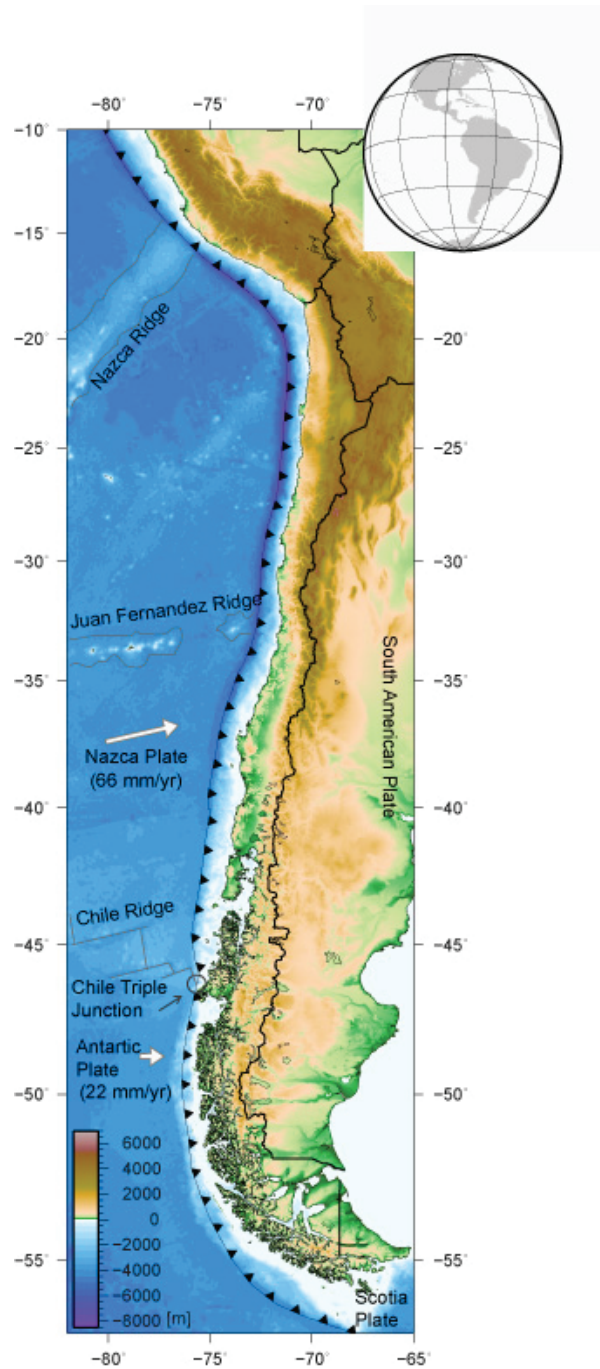


Figure 2.1: General geotectonic setting of Chile. Velocities of subduction for Nazca (66 mm/yr) and Antarctic (22 mm/yr) plates are denote as white arrows proportional to the velocity (Angermann et al., 1999). Black line with black triangles show the trench where Nazca plate meets South American plate, and the triangles indicate the direction of subduction. Gray lines roughly contour bathymetric features such as the Nazca ridge, Juan Fernandez ridge and Chile ridge (modified from Gutscher (2002)), Chile Triple Junction encircled in dark gray. Color scale for sea floor depth and altitude is presented. Mora, 2011

ican plates (Figure 2.1). Large thrust earthquakes along the coast from Arica (18°S) down to the Chile Triple Junction (46°S) near the Taitao Peninsula, are due to the subduction of Nazca plate under South American plate. The high rate of seismicity and large magnitude events are a consequence of the high rate of convergence. The Nazca plate approaches the South American plate at a velocity ranging between 6 and 9 cm per year (Angermann et al., 1999; Pardo-Casas and Molnar, 1987), being faster and closer to perpendicular to the trench in the northern part of Chile, and slower and more oblique near to the Triple Junction, where the Chile Ridge subducts the South American plate and the three plates, Nazca, Antarctic and South American, meet. South from the Triple Junction, the Antarctic plate subducts the South American plate at a much slower rate, ~ 2 cm per year De Mets et al. (1994) giving to this part of the country a much lower seismicity rate. Near 52°S and southwards, the Antarctic plate and Scotia plate interact in a diffuse convergence with a rate of 1,1 cm per year (Pelayo and Wiens, 1989). The boundary between Scotia plate and South American plate is the left-lateral strike-slip Magallanes-Fangnanao fault with a velocity of approximately 7 mm per year (Smalley et al., 2003).

2.3 Geotectonic Setting of Epicentral Region and Historical Seismicity

2.3.1 Geotectonic Setting of the Concepción-Constitución seismic gap

The epicentral region of the 27th February 2010 event is located in the Chile-Peru trench between the 35°S and 37°S, in the so-called Concepción-Constitución seismic gap Madariaga (1998), which is recognized as a transition zone between two distinctive seismic zones (Barrientos, 2007), highly active with shallow and deep events to the north and lower seismicity to the south. In the Arauco region, the Nazca plate has approximately 32 Ma and subducts under the South American plate at a rate of 68 mm/yr with an orientation 78°N, measured near the 36°S by Ruegg et al. (2009). The activity north of the 35°S is characterized by stress acting perpendicular to the trench, with intermediate and deep events along the subduction, and shallow crustal events in the Sierras Pampeanas region (33°S-35°S) (Barrientos, 2007). To the south of 38°S, few subduction-related events had occurred after the great M9.5 Valdivia earthquake in 1960. This scarce seismicity consisted of earthquakes with relatively small magnitudes ($M \leq 4.5$) located along the subduction under the Chiloé block, near volcanic centres and along crustal faults linked to the 1000km-long Liquiñe-Ofqui Fault (LOF) (Rosenau et al., 2006; Lange et al., 2007, 2008; Murdie et al., 1993; Tilmann et al., 2008). The LOF shows a strong parallel-to-the-trench motion at its beginning south from the Triple Junction, near 46°S, where the coastal sliver of crust (the Chiloé Block) is displaced northwards relative to the continent.

South of the epicentral region, between the 37°S and 39°S, the crustal seismicity is concentrated in the forearc on account of shortening and uprising of the Arauco Peninsula, and located along NNW-SSE and NW-SE faults, as the Lanahue (Haberland et al., 2006), Biobio and Gastre faults (Bohm et al., 2002). A horizontal (ca. 10°) plane of seismicity indicates the lower limit of the seismogenic zone near 40 km depth, and it is consistent with the arc segmentation bounded by the previously mentioned crustal faults, while intermediate depth events (60-155 km) might be associated to dewatering of the downgoing oceanic plate and related to changes in the mineral change phase processes (Bohm et al., 2002; Haberland et al., 2006).

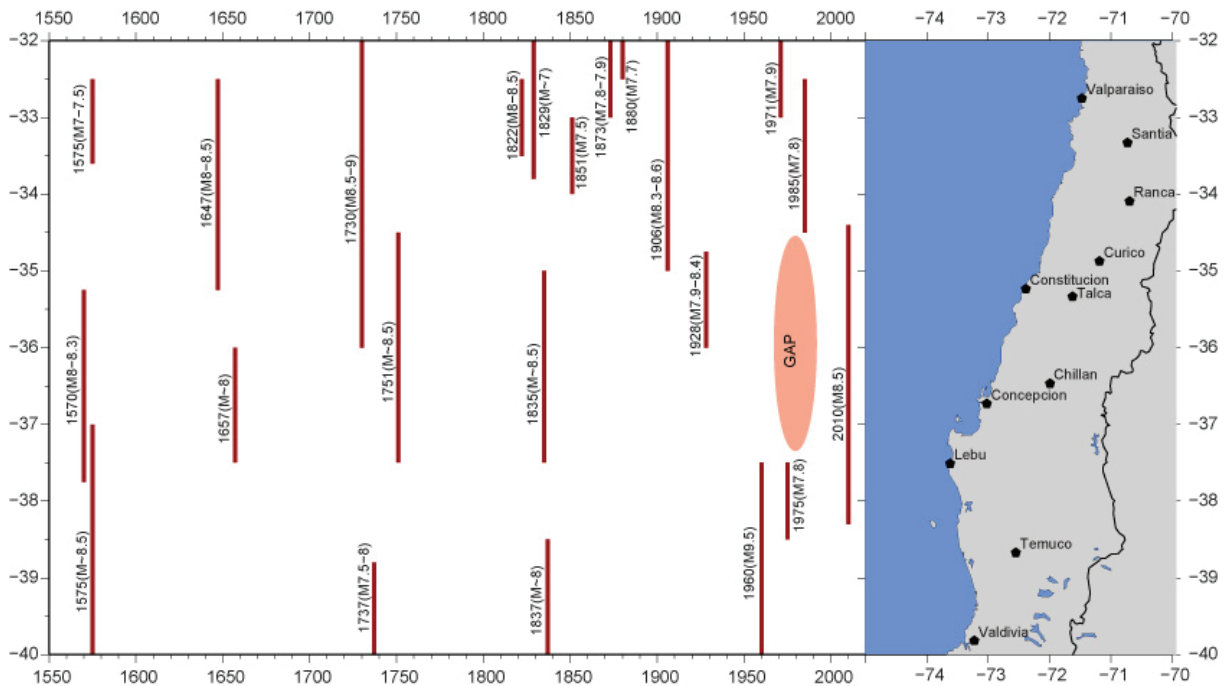


Figure 2.2: Historical seismicity (magnitude over 7) for the Chilean trench between 32°S and 40°S, from XVI century. Year and estimated or measured magnitude indicated above or under the inferred rupture length indicated as red lines. Inferred seismic gap indicated as an orange ellipse. Historical events, magnitudes and rupture areas compiled from Lomnitz (1970, 2004); Comte et al. (1986); Campos et al. (2002); Cifuentes (1989); Melnick et al. (2009). Modified from Melnick et al. (2009). Mora, 2011

2.3.2 Historical Seismicity

For the Chilean coasts, large and important earthquakes have been reported since the beginning of written history (Figure 2.2). Before the invention of seismological instruments and the surface-wave magnitude (M_s) around the year 1900 (Lomnitz, 2004), descriptions of damages were gathered together by naturalists like Darwin (Darwin, 1845) and later by the first “seismologist” in Chile, Count Fernand de Montessus de Ballore in the *Historia Sismica de los Andes Meridionales (1911-1916)*. Later, in 1957, seismicity catalogues for the Chilean earthquakes were generated thanks to the foundation of the Institute of Geophysics of the University of Chile (Lomnitz, 2004).

The region around the Concepción -Constitución seismic gap has been subjected to several great earthquakes. Lomnitz compiled the Chilean historical seismicity described by Montessus de Ballore, up to the 1960 Valdivia earthquake (Lomnitz, 1970, 2004). After this year, several authors completed the catalog with studies of different main earthquakes along the coasts of Chile (Comte et al., 1986; Campos et al., 2002; Cifuentes, 1989).

The first record of an event in the Concepción area dates from 1570, were a tsunamogenic event (M8) struck the city, originally situated where Penco is nowadays. The damage was likely to be as the 1835 earthquake in the same region (Lomnitz, 1970, 2004). A second great earthquake struck Concepción in 1657, with an estimated magnitude of $M \sim 8$, destroyed most the houses although the tsunami two hours

later took more lives than the earthquake itself. The damage extended north up to Chillán and probably was felt as far north as the Maule River and as far south as the Cautín River, according to the descriptions of Montessus de Ballore (Lomnitz, 1970, 2004). Almost a hundred years later, in 1751, another similar event (estimated magnitude M8.5) struck Concepción. Two large foreshocks announced the mainshock, on 23rd May, and the tsunami that came half an hour later was the greatest the city had undergone. The cities of Chillán and Talca were destroyed, Santiago showed some damage and the city of Concepción was moved inland to its present location after the large aftershock in June, 1751. The offshore islands showed permanent uplift and the tsunami caused damages along the Pacific coast, even in Japan and Callao (Peru) (Lomnitz, 1970, 2004).

The latest subduction event in the Concepción-Constitución seismic gap dates from 1835, and it was described by Charles Darwin in his memoirs on the Beagle voyage (Darwin, 1845). It lasted approximately two minutes and according to (Lomnitz, 1970) its magnitude was calculated to be in the range M8-8.5. The damage include the destruction of the cities of Concepción and Talcahuano, due to the earthquake and subsequent tsunami, but no damage was observed in Valdivia, where Darwin was at the time of the event. Also, he noted the permanent elevation of about three feet (0.914 m) of the land around the bay of Concepción, for which there was no evidence but the words of the inhabitants, although in the Santa Maria island, Fitz Roy found mussels still adhering to the rocks which indicated an elevation even larger, near ten feet (3.048 m) above the high-water mark (Darwin, 1845).

On 1st December 1928, a M8.4 Richter magnitude event (Lomnitz, 1970, 2004) ($M_s=8.1-8.2$ according to Beck et al. (1998) and Comte et al. (1986)) partially covered the area of the seismic gap, destroyed Talca and Constitución and damaged the coasts from Pichilemu to Cauquenes ($34,5^\circ\text{S} - 36^\circ\text{S}$) (Campos et al., 2002). The epicentre was estimated approximately 20 km to the west of Putú, possibly offshore, and caused a tsunami of about 1.5 m high in Constitución that destroyed the city of the epicentre (Lomnitz, 1970). No uplift was observed in Constitución, but about 10 miles to the north, in Putú, the waterline receded 200 meters (Lomnitz, 1970).

The Chillán event, on 25th January 1939, $M_s=8.3$ (Comte et al., 1986), took place directly in the seismic gap, but its epicentre was located inland. This was one of the most disastrous (ca. 28.000 casualties (Lomnitz, 2004)) earthquakes that Chile has experienced, where a large zone of complete destruction (intensities IX-X) was located on the Central Valley (Beck et al., 1998). Evidences show this event was an oceanic intraplate earthquake, with an estimated depth of 70 km determined by Gutenberg and Richter in 1941 (Campos et al., 2002). They recalculated that the fault was almost vertical and located at 80-100 km depth (Campos and Kausel, 1990; Beck et al., 1998). No tsunami or uplift was observed in the epicentral area, although the coastal range batholith was uplifted around five feet near the Central Valley margin, but with no visible connections with known geological structures (Lomnitz, 1970). Thus, the Concepción-Constitución seismic gap has been inactive since the large events in 1835.

The Concepción-Constitución seismic gap is delimited by other rupture areas of important events to the north and south of it, although the history of events and its recurrence vary at both extremes. To the north, between 32°S and 35°S , the recurrence of great earthquakes was between 72 and 92 years, counting the events of 1575, 1647, 1730, 1822, 1906 and 1985. All of them showed magnitudes above 8, and their epicentres were located in the Valparaíso region (Comte et al., 1986; Lomnitz, 2004). The M7-7.5 earthquake (Lomnitz, 1970, 2004) in 1575 has not been well documented, but its epicentre is thought to be located 100 km north from Santiago, possibly La Ligua (Lomnitz, 1970, 2004). The event of 1647, the Great Santiago Earthquake, lasted nearly 100 seconds and its magnitude has been estimated between 8 and 8.5 (Lomnitz, 1970, 2004), with its epicentre presumably located 50 miles from Santiago,

probably in the Andean range. The event of 1730 was probably the largest event in this zone (M8.5-9 (Lomnitz, 1970, 2004)) with a tsunami that reported damages along the Pacific coasts in Chile, from La Serena to Concepción, and in Callao and Japan (Lomnitz, 1970, 2004). The event in 1822 (M8-8.5) uplifted the coasts near Quintero and Valparaíso ca. 0.9-1.2 m (Comte et al., 1986), caused severe damages in Santiago and Valparaíso region, but no wooden houses were damaged, also the tsunami reported no damage (Lomnitz, 1970, 2004). Later, in 1906, two consecutive strikes separated by two minutes destroyed and burned down Valparaíso, it was felt from Tacna to Chiloé (M8.6) with an intensity VIII in Santiago (Lomnitz, 1970, 2004).

To the south of the seismic gap, the events with magnitude over or equal to 8 show a recurrence between 100 and 162 years, considering the events of 1575, 1737, 1837 and 1960 from Valdivia to the south. Among them the largest event ever recorded is the latest: Valdivia 1960 (M9.5). The first record of great events to the south of 38°S dates from 1575 in Valdivia region, where fissures were created during the mainshock and aftershocks and a highly destructive tsunami arrived during the first aftershock. The damage described by Montessus de Ballore (such as a bore in the Valdivia river where the bottom was visible) was very similar to that in the 1960 Valdivia earthquake. Thus an estimated magnitude of M8.5 is assigned to this event (Lomnitz, 1970, 2004). In 1737, an event with estimated magnitude of M7.5-8 destroyed Valdivia and the cities south in the Chiloé island. Not much is described but aftershocks were felt during the following five to ten years (Lomnitz, 1970, 2004). A hundred years later, in 1837, a large event had its epicentre offshore probably south of Valdivia. According to Montessus de Ballore, no tsunami was observed in the region but in the coasts of Japan, Samoa and Hawaii reports of damage seem to be related to this event (Lomnitz, 1970, 2004). The magnitude of this event has been estimated by Lomnitz (1970) to be at least 8. The latest event in the region was the greatest event ever recorded by seismological instruments, the Valdivia 1960 earthquake, with a moment magnitude of Mw=9.6 for the mainshock (Lomnitz, 2004). There were nine events in the previous 33 hours, starting on 21st May with an M8.3 event east of the Arauco Peninsula, near Concepción, followed by eight events, at least three of them with $M \geq 7-7.5$, of which epicenters migrated slowly towards the south. Fifteen minutes before the mainshock, a M7.8 stroke and later, the double-pulse great earthquake ruptured the zone from Valdivia down to the Taitao Peninsula, approximately 1000 km long (Cifuentes, 1989). The tsunami damaged ports in Japan, Juan Fernandez Island and most of the coast of southern Chile. As the rupture of the 1960 earthquake propagated southwards, the Concepción-Constitución seismic gap was not affected by this event. Thus delimitates the southern end of this gap, as the 1985 event delimitates the northern end.

2.4 The Maule M8.8 earthquake

2.4.1 Description

On the 27th February 2010 at 03:34 hours, local time in Chile (06:34 hrs UTC), an earthquake with moment magnitude (Mw) 8.8 had its epicentre off the coast of Cobquecura, between the cities of Concepción and Constitución. The hypocentre of the event was located at about 30 km depth in the interface between Nazca and South American plates, a subduction that runs along the entirely Chilean coasts. The rupture began, according to the Chilean National Seismological Service (SSN by its Spanish acronym), in 36° 17' 23" S and 73° 14' 20" W, but following estimates of international agencies (NEIC-USGS, GEOFON, EMSC), the location of the hypocentre has an uncertainty of 45 km in latitude, 45.5 km in longitude and 6 km in depth.

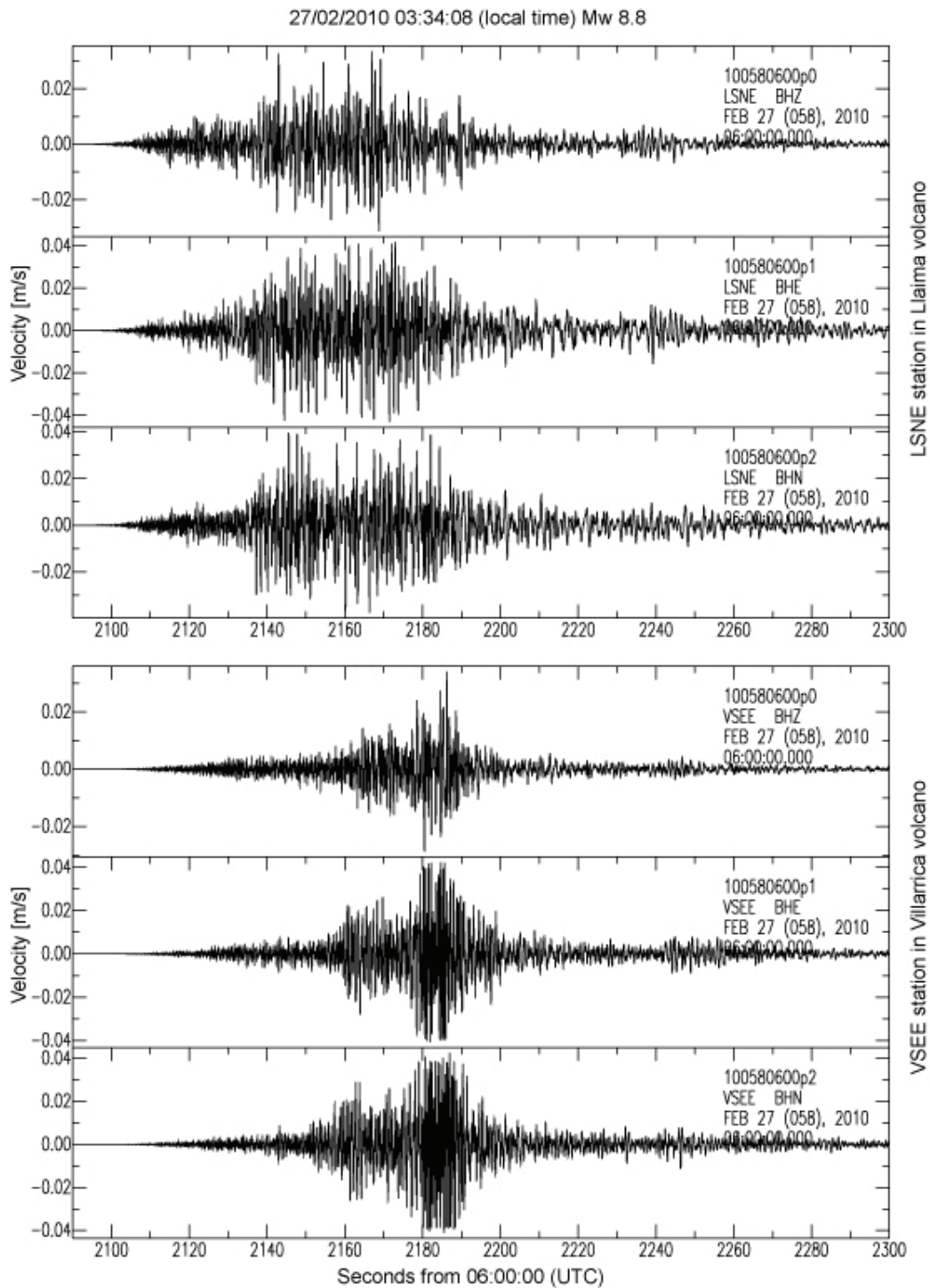


Figure 2.3: Vertical (top, BHZ), East-West (BHE, centre) and North-South (BHN, bottom) components recorded in two Short-Period stations at Llaima (LSNE) and Villarrica (VSEE) volcanoes, for the Maule earthquake, at 06:34 UTC time. Horizontal axis in seconds from 06:00:00 UTC, and vertical axis in velocity [m/s]. No filter was applied. Mora, 2011

The event lasted between 110 and 180 seconds (Barrientos, 2010; Madariaga et al., 2010; Saragoni et al., 2010) (Figure 2.3), in which the rupture started at the hypocentre and spread bilaterally (Lay et al., 2010) mostly northwards up to the latitude of Pichilemu (34.4S, 72.01W) and a few kilometers south from the Arauco Peninsula, near Tirúa (38.3S, 73.5W), comprising in total about 450 km long (Farías et al., 2010; Barrientos, 2010), and presented an average slip of about 10-12 m (Barrientos, 2010; Lorito et al., 2010).

The rupture propagated bilaterally, at approximately 2-2.6 km/s (Lay et al., 2010; Moreno et al., 2010; Lorito et al., 2010), mostly in the down-dip direction but with a dextral strike-slip component (Lay et al., 2010). Starting at the hypocentre, it extended updip to the south-west and to the north (Lay et al., 2010), in the direction of two highly locked zones described in different slip models (Sladen and Owen, 2010; Shao et al., 2010; Hayes, 2010; Moreno et al., 2010; Tong et al., 2010; Lorito et al., 2010).

Preliminary rupture models (Sladen and Owen, 2010; Shao et al., 2010; Hayes, 2010) coincide with later models (Moreno et al., 2010; Tong et al., 2010; Lorito et al., 2010) in two patches with significant slip, but have relatively lower maxima and differ on their location. Preliminary models used inversion of teleseismic data of body and surface waves, whilst later models reduce uncertainty by using also tsunami data, InSAR, GPS and/or land level changes. All models show two areas of high slip that can be correlated with previously highly locked zones (asperities) (Lorito et al., 2010; Moreno et al., 2010), separated about 200 km by a bridge of lower pre-stress (Moreno et al., 2010): one to the north of the epicentre, between 34°S and 36°S centered in the 35°S - 35.5°S, with a coseismic slip of 17-19 m (Moreno et al., 2010; Lorito et al., 2010); and a 130 km × 60 km patch to the south of the epicentre centered near 37.5°S with a lower coseismic slip of 9-10 m (Tong et al., 2010; Lorito et al., 2010) (Figure 2.4). Both maxima are located in the seismogenic zone, at about 16-40 km depth for the northern patch (Hayes, 2010; Shao et al., 2010; Lorito et al., 2010; Tong et al., 2010) and between 25-45 km depth (Hayes, 2010; Shao et al., 2010; Lorito et al., 2010) for the southern patch. For this last asperity, (Tong et al., 2010) found an almost linear decrease of the slip along-strike in the down-dip direction from 17 m at 18 km to almost no slip at 43-48 km depth, with a flattened decrease upon 30-35 km depth, which might be correlated with the depth of the continental Moho (Tong et al., 2010).

Most of the models establish the northern patch between 34°S and 36°S as stronger than the southern slip zone, except for the models presented by Shao et al. (2010) and Sladen and Owen (2010). These two models estimated at least 10 m of slip in the southern patch based on the inversion of SH waves (Shao et al., 2010) and teleseismic P waveforms, along with ground displacement measurements from some ISG stations (Sladen and Owen, 2010) and a similar model considering a 18° dip from the Global CMT (Ekström et al., 2012). However, these two models are stated to be preliminary and highly uncertain, therefore including interseismic and coseismic GPS data adds a constrain to posterior slip models. These later models (Moreno et al., 2010; Tong et al., 2010; Lorito et al., 2010) show the northern patch as the strongest, with an amount of slip of 17-19 m (Tong et al., 2010; Lorito et al., 2010), towards which the slip would have moved first with a velocity rupture of 2.0-2.5 km/s (Lay et al., 2010). Both northern and southern highly locked patches were ruptured, at least partially, in the past events from 1985 and 1960 (Shao et al., 2010). This is also supported with the distribution of aftershocks with magnitude $M \geq 5$ (Moreno et al., 2010), and of special relevance is the case of the aftershocks in the region of Pichilemu, which will be discussed later.

These asperities, of about 30 km each, are located close to cities where damage on buildings was observed, and also the highest peaks in acceleration were retrieve (Saragoni et al., 2010). The long period waves created in a Doppler effect due to the rupture going in the south direction, highly affected

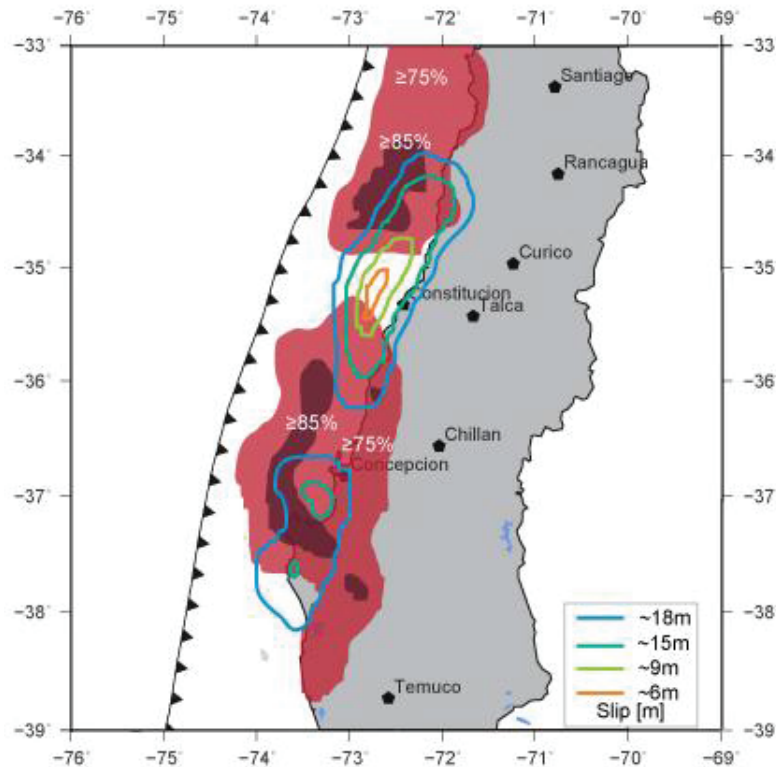


Figure 2.4: Highly locked zones prior to the Maule earthquake are shown in red (≥ 75) and dark red (≥ 85) obtained from Moreno et al. (2010). Color coded lines, roughly contour the slip distribution calculated by Lorito et al. (2010). Modified from Moreno et al. (2010); Lorito et al. (2010). Mora, 2011

high-rise concrete buildings in Santiago, as so did the soil amplification due to a sand layer in Concepción (Saragoni et al., 2010). There are 35 accelerographs established in buildings with and without isolation, at ground level, in which Peak Ground Acceleration (PGA) was registered at the time of the event. Values up to 0.928 g in the N-S component (in Angol, IX Region), 0.78 g in the E-W component (in Melipilla, Metropolitana Region) and 0.702 g in the vertical component (in Lolleo, V Region) were recorded, not taking into account a saturated accelerogram at Cauquenes, with PGA value of more than 1 g , which probably indicates that for this kind of earthquake, even 2 g of PGA can be expected (Saragoni et al., 2010).

This thrust event ruptured a zone previously known for its high degree of coupling (Beck et al., 1998; Ruegg et al., 2009). As a result of the work of Ruegg et al. (2009), where 41 GPS stations were installed in two surveys between 33°S and 38°S in the period 1996 - 2002, they concluded that the difference in the velocities fields found implies an accumulation of 30 mm/yr between the trench and the top of the Andes (approx. 200 km long), which would result in an earthquake of magnitude and rupture length very similar to the 27th February earthquake (Ruegg et al., 2009). Although the Maule earthquake coincides with the proposition from Ruegg et al. (2009), the average coseismic slip vector founded by Tong et al. (2010) is not parallel to the interseismic velocity vector, thus it would suggest a possible deficit in the strike-slip moment release of about $3.49 \times 10^{21}\text{ N}\cdot\text{m}$ (Tong et al., 2010) which may support the hypothesis from Lorito et al. (2010) that the Darwin gap remains unbroken, or at least part of it.

2.4.2 Foreshocks

During the years prior to the Mw8.8 Maule earthquake, there was a quiescence of seismicity in the region, which is characterized in the study from Xue et al. (2010), where two types of seismic gaps, or lack of certain types of seismic activity, are described in the region where the earthquake occurred. One is the “usual” seismic gap between two large events (in this case, $M \geq 8$) when the known recurrence time is passed by several years. This applies to the case of the 360 km long gap between the rupture zones from the 1960 and 1906 - 1985 events, where no event with magnitude higher than 8 had occurred (Xue et al., 2010). This was also pointed out in the work of Ruegg et al. (2009) but in terms of accumulated slip and the possible occurrence of a Mw8-8.5 event in the Concepción-Constitución gap. The other gap corresponds to a lack of moderate magnitude seismicity ($M \geq 5$) between April 2005 and the 26th February 2010, almost five-year period, in a region of about 780 km long south of 32°S , with only one event of Mw5.9 in November 2009 (Xue et al., 2010).

Events from January 1990 up to the 26th February 2010 (from here onwards, 2010* states the year 2010 comprising from 1st January 2010 until 26th February 2010 included), obtained from the National Earthquake Information Center (NEIC) catalogue (U.S.G.S., n.d.) with magnitudes $M \geq 3$, were plotted in groups of five years, except for the last 2005 - 2010* group which contain the events from January 2005 up to the day prior to the mainshock (Figure 2.5). A considerable difference in the amount of events is shown in the region north of 35°S - 34°S for all periods studied. Also it is noticeable a decrease in the number of events for the last period (2005 - 2010*), consistent with the study from Xue et al. (2010), but this decreasing is not restricted to the rupture area. In Figure 2.6, the events are separated into three areas: to the north of the rupture area (30°S - 34°S), the rupture area or gap section (34°S - 38.5°S) and south of the rupture area (38.5°S - 40°S). The average amount of events in the northern section is larger than in the other two areas, and decreases to the south. Also the southern section shows only one event with magnitude $M \geq 5$, and the northern section shows more events with these magnitudes than the gap section. After the year 2006, a decrease in the number of events per year is observable in the northern section and in the gap area, but it is difficult to state the same for the southern section due to the scarce seismicity.

Data from the National Seismological Centre (SSN, 2011) ($M \geq 2$, $\text{depth} \leq 70$ km) from June 2009 until 26th February 2010 shows little activity along the Chilean coasts, except for some cluster activity on the coasts of Valparaíso associated to the subduction of the Juan Fernandez ridge, a few events following the subduction towards north, and some crustal activity inland in Argentina. Near Concepción, a few events with depth less than 45 km occurred south of Lebu ($\sim 38^\circ\text{S}$) and on the coast in front of Concepción and Chillán (Figure 2.7.a). On the last three months prior to the mainshock, several events of magnitude $2 \leq M \leq 4$ in the coast of Valparaíso, where the Juan Fernandez ridge is subducting, are observed and some events in the epicentral area (Figure 2.7.b).

Quiescence prior to large events, as well as accompanying accelerating low-magnitude seismicity, has been broadly studied. Whether with real seismicity (Wardlaw et al., 1990; Taylor et al., 1991; Mignan and Di Giovambattista, 2008; Papadimitriou, 2008) or synthetic catalogues (Hainzl et al., 2000), studies have found a short-term increase in the seismicity of small magnitude ($M \leq 3$) events prior to a large earthquake in a zone that has previously showed a quiescence (activity below the average of background seismicity). This reduction in the seismic activity has been observed to last between months or years before the large mainshock, thus it could be used as an intermediate-term precursor for a large earthquake (Hainzl et al., 2000; Wardlaw et al., 1990), as well as foreshocks are usually considered but their activity

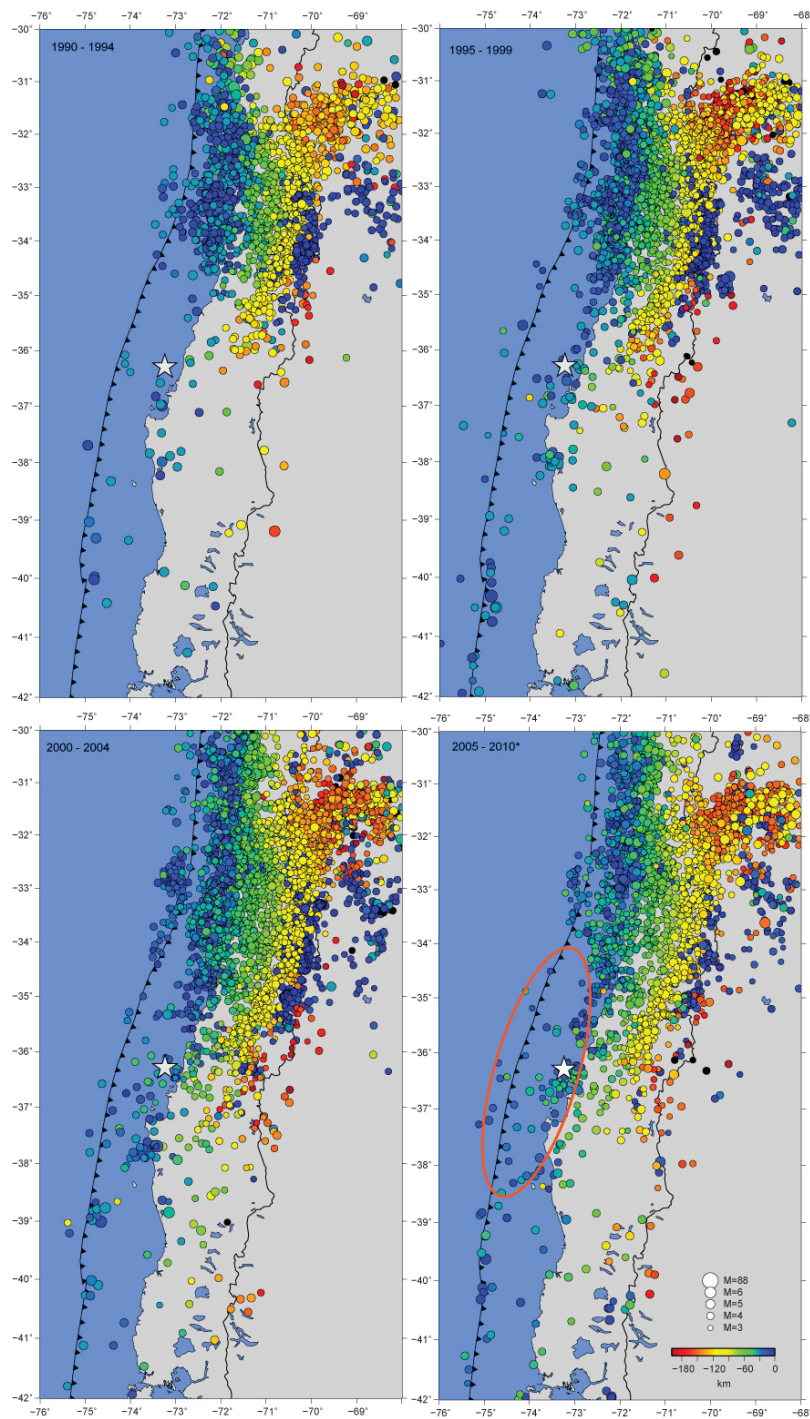


Figure 2.5: Events occurred between 1st January 1990 and 26th February 2010 with magnitude ≥ 3 retrieved from NEIC, USGS, plotted every five-years group. From left to right, from top to bottom: 1990 -1994, 1995 - 1999, 2000 - 2004, 2005 - 2010*. Diameter of the circle scaled according to its magnitude, and color coded according to its depth. Events in black have depths greater than 200 km. the orange ellipse shows the rupture area for the Maule earthquake for which the epicentre is shown as a white star. Mora, 2011

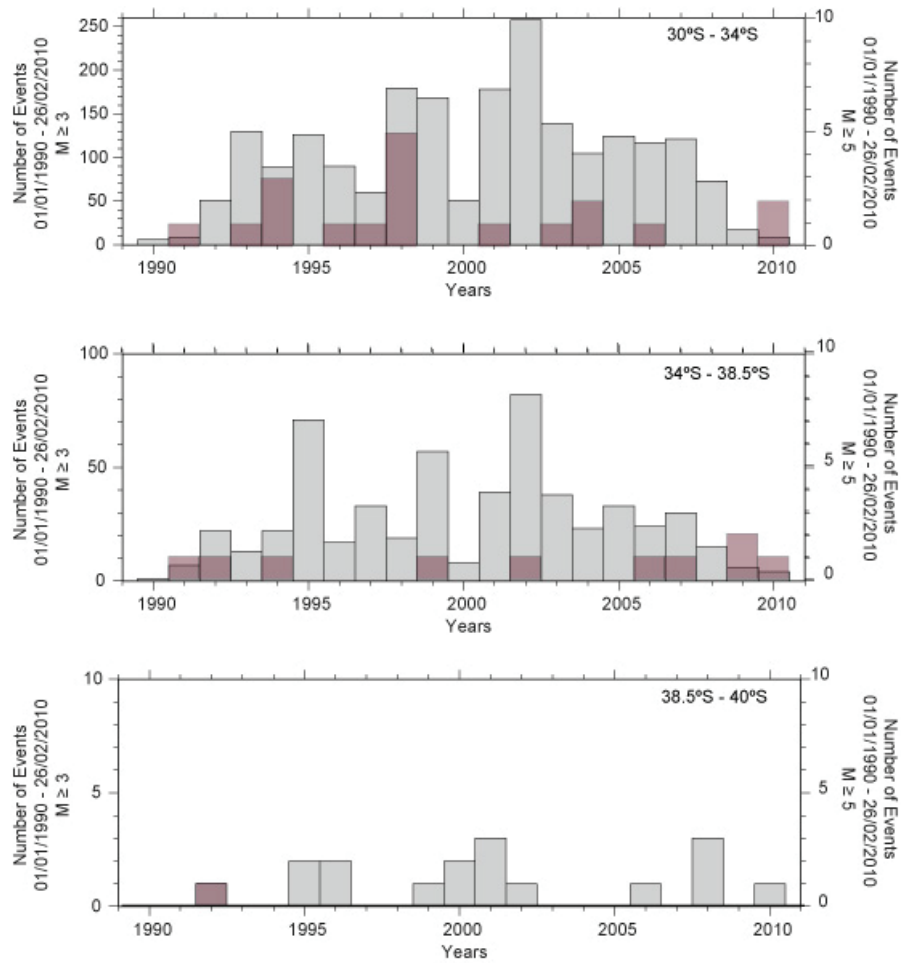


Figure 2.6: Number of events with magnitude $M \geq 3$ (gray bars, left axis) and $M \geq 5$ (purple bars, right axis) per year, between 1st January 1990 and 26th February 2010, separated into three zones as north of the rupture area ($30^\circ\text{S} - 34^\circ\text{S}$, top), rupture area ($34^\circ\text{S} - 38.5^\circ\text{S}$, center) and south of the rupture area ($38.5^\circ\text{S} - 40^\circ\text{S}$, bottom). Data retrieved from the NEIC, USGS. Mora, 2011

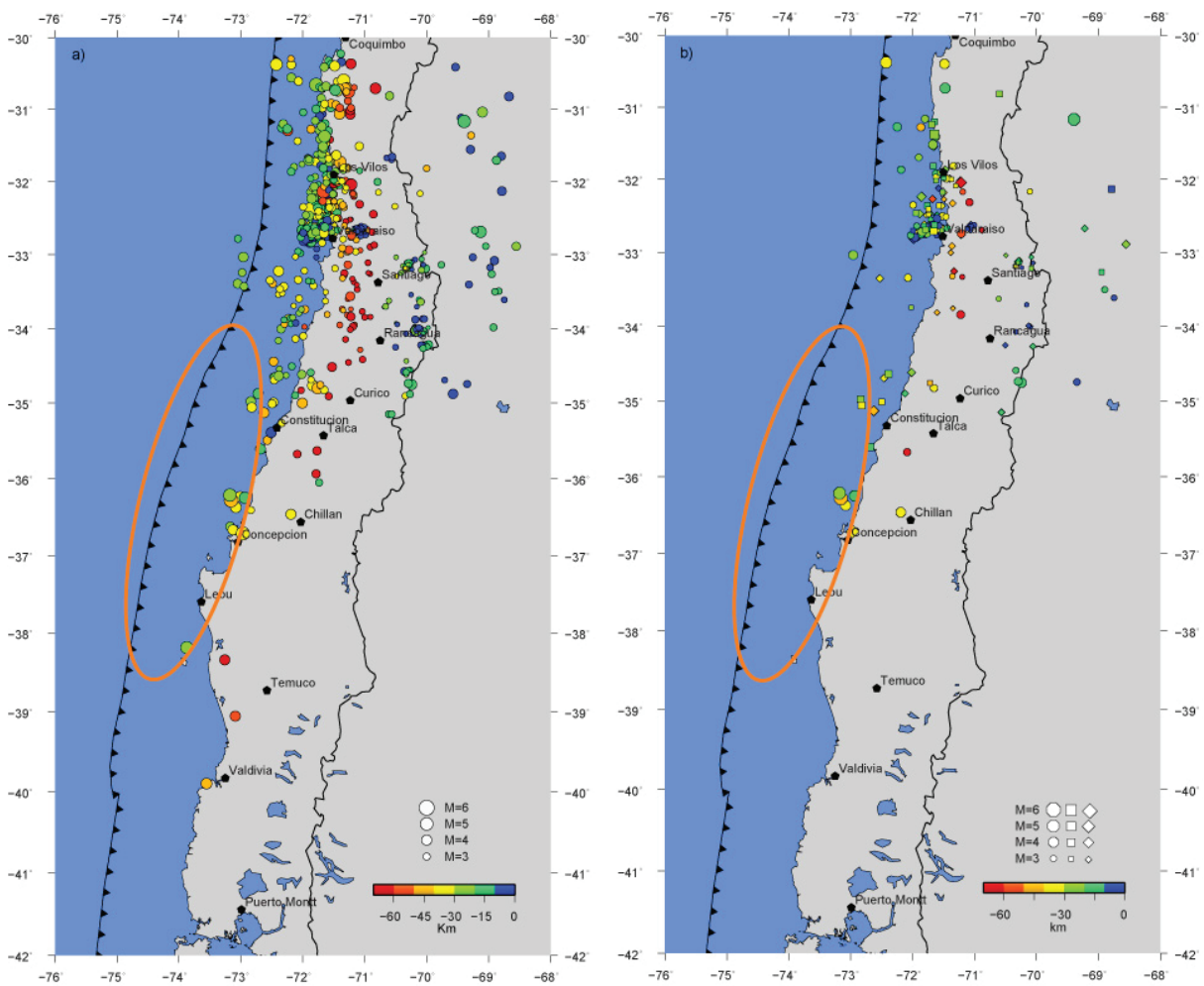


Figure 2.7: Left (a): Events from the SSN between 1st June 2009 and the 26th February 2010 ($M \geq 2$, depth ≤ 70 km). Right (b): Events from the three months prior to the mainshock, represented as diamonds (December, 2009), octagons (January, 2010) and diamonds (February, 2010) scaled according to its magnitude, and color coded according to its depth. Orange ellipse show the approximated rupture area. Mora, 2011

is not always observed. One theory for this relationship is that the longer and/or stronger the quiescence in time, more energy is accumulated in the interface, therefore the probability of a greater earthquake in the area increases (Hainzl et al., 2000). In many cases, this decrease in activity could be restricted to the future focal region, and it can also be accompanied by an increase in small magnitude events around the quiescent zone (Papadimitriou, 2008).

2.4.3 Aftershocks

Considering the events from the NEIC catalogue ($2.9 \leq M \leq 8.8$), from 27th February 2010 until 31st January 2011 and only events with depth above 70 km, the area of aftershocks is approximately 650-660 km long ((Xue et al., 2010), this study) ranging from 38.8°S latitude, where Temuco is located, to the coasts of Valparaíso, near 32.5°S. As the NEIC catalogue uses stations with teleseismic distances, several events show unreliable depths. In order to reassess the NEIC results, the events from the SSN catalogue were studied, too, under the same conditions (Figure 2.8).

Although all these events could be considered as aftershocks, because they occur after the mainshock, not all of them are directly related with the rupture of the fault. As Farías et al. (2010) postulate, the maximum rupture length extends for approximately 500 km between the 34°S and 38.5°S. Following (Farías et al., 2010), the events falling outside this range correspond to an accommodation of stress changes in neighbouring segments.

The aftershocks are distributed along the subduction zone, down to 180 km, but most of the events are located between 10 km to 60 km depth (Figure 2.8). These are directly related to the releasing of stress and re-accommodation of Nazca and South American plates. These events, down to 60 km denote the seismic coupling zone for the region between 33°S and 38°S. In plane view, the events are located between the trench and the coast of Chile and inland as far as 50-80 km, north from Constitución.

During the first month after the Maule earthquake (Figure 2.9, left), March 2010, the number of events per day showed a significant decay from more than 300 events/day to 20 events/day in the first week. These first events were retrieved by the USGS, since the SSN lost communication with several of its stations due to damage in the energy and communication issues after the great shock. After 10 days, the SSN retrieved the following aftershocks with a much lower threshold limit than USGS stations (Figure 2.10). This is due to the location of the network, since SSN is a local network and USGS uses teleseismic stations. The number of events per day is considerably lower after the first month (Figure 2.9, right) showing four events per day on average.

The catalogue is complete down to a magnitude 4 (Figure 2.11). Aftershocks of magnitude greater than seven were not observed. In Figure 2.12, events with magnitude above 5 are plotted (locations from NEIC (U.S.G.S., n.d.)) and focal mechanisms (Global CMT) (Ekström et al., 2012) are presented for events with magnitude above 6. The two patches of seismicity described by Moreno et al. (2010) are not so clearly identify, but events with $M \geq 6$ are more conclusive. In the area between Constitución and Temuco, focal mechanisms present clear compressive stress and inverse fault planes with a low dip angle, as for the area near Pichilemu, the events present normal focal mechanisms and higher magnitudes. These events are related to a NW-SE striking fault, in the area near the Pichilemu-Vichuquén fault, with approximately N35°W strike and 53° of dip according to the focal mechanism from Ekström et al. (2012). Its dimensions are approximately 40 km long and 20 km depth (Barrientos, 2010).

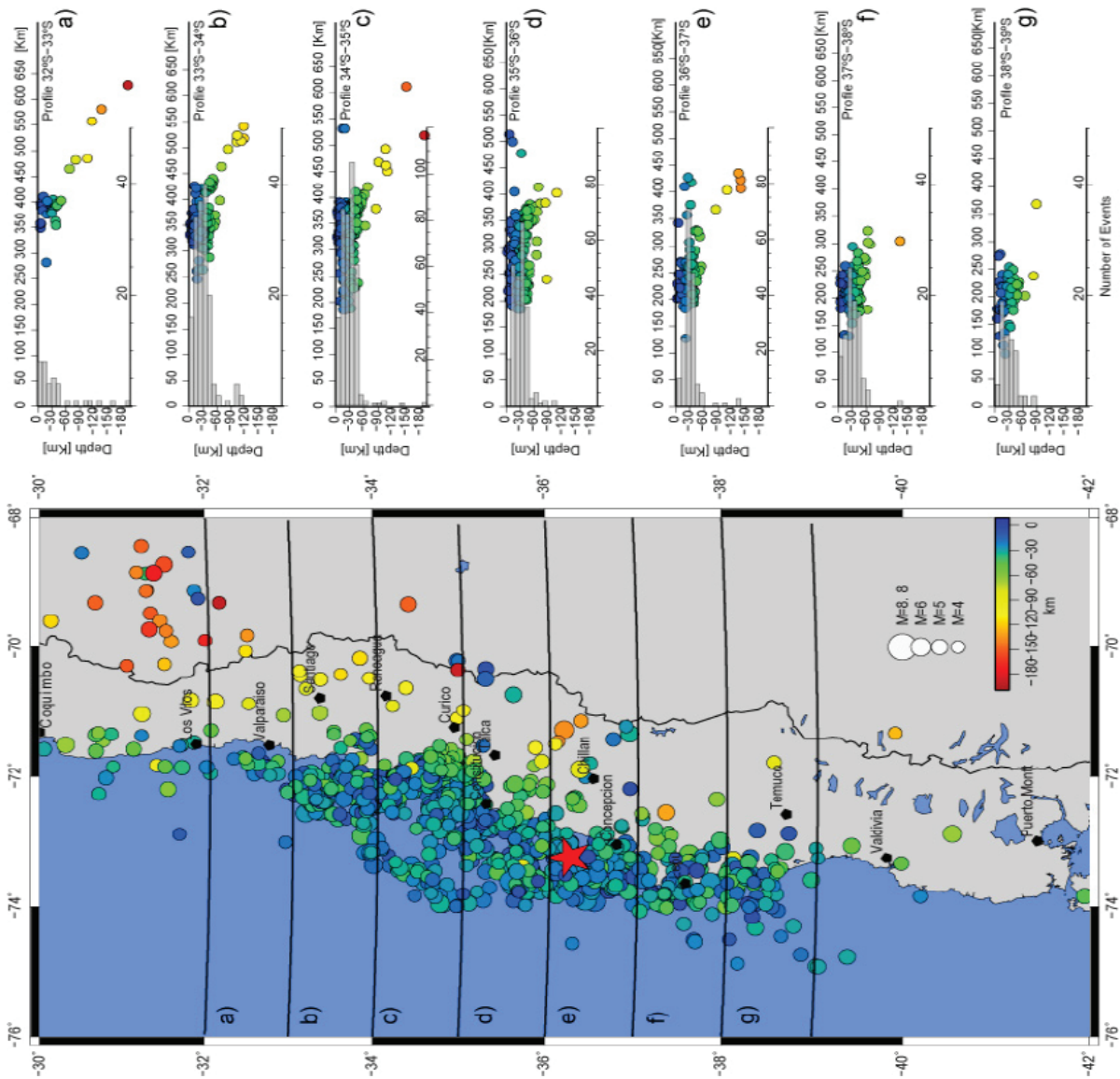


Figure 2.8: Left: Mainshock (red star) and aftershocks (color coded circles) from 27th February 2010 until January 2011 retrieve from Chilean National Seismological Survey (SSN). Color scale denotes the depth of the events and circle diameter denotes magnitude. Right: 1 degree in-depth profile from 32°S (a) to 39°S (g) for aftershocks in right figure to show the subduction of Nazca plate. Gray transparent bars indicate number of events per 10 km. Mora, 2011.

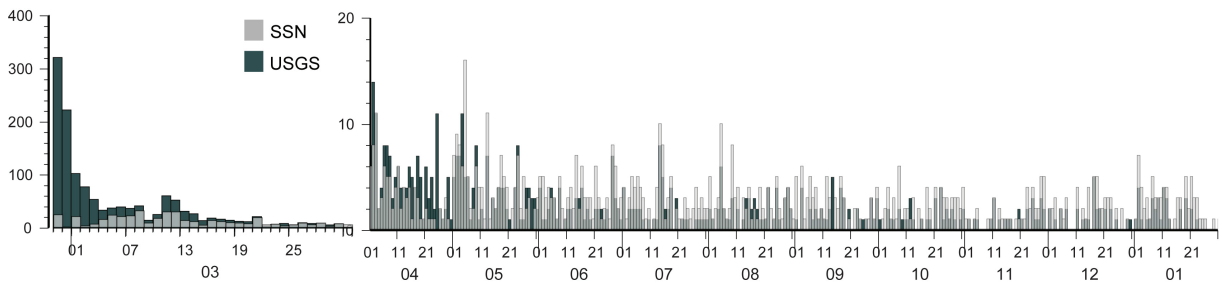


Figure 2.9: Histogram of aftershocks for March (left) and for April 2010 until January 2011 (right) for events retrieved by U.S. Geological Survey (dark gray) and Chilean National Seismological Survey (light gray). Months are denoted by numbers. Mora, 2011

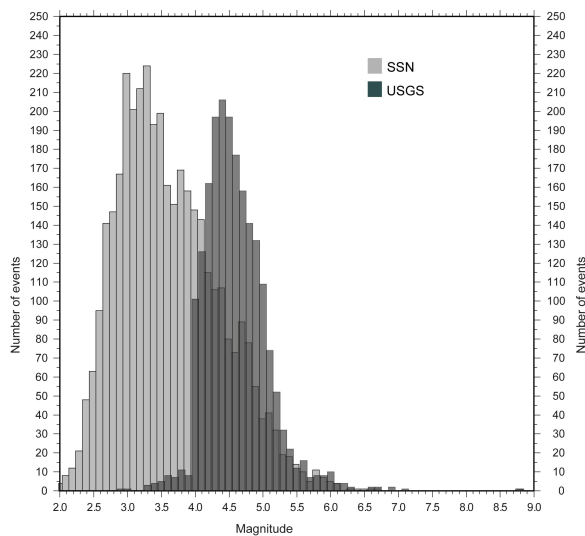


Figure 2.10: Number of events per magnitude retrieved by U.S. Geological Survey (dark gray) and Chilean National Seismological Survey (light gray). Mora, 2011

2.5 Concluding Remarks

The Maule earthquake occurred in an area of great accumulated slip, and ruptured towards another high slip area near Pichilemu. The distribution of aftershocks with magnitude over 6 coincides with these areas (figure 2.12) and might indicate a constitution in the interface of different asperities, linked by zones of low pre-seismic slip (Moreno et al., 2010). A number of events ($M \geq 5$) near 34°S showed normal faulting focal mechanisms and shallow depth, these are related to crustal normal faults instead of being a response from the interface between Nazca and South American plate. These events should also be considered as aftershocks since the stress release might have been triggered by the changes in the surroundings due to the large energy release from the Mw8.8 event. Some events in the following months after the Maule earthquake occurred in the area of rupture of the Valparaíso earthquake of 1985. This area regularly shows seismicity of moderate magnitude, therefore some authors, Farías et al. (2010) for example, consider these events as an accommodation response from Nazca plate due to the changes of stress at the northern end of the rupture zone, and not part of the rupture area of the Maule event.

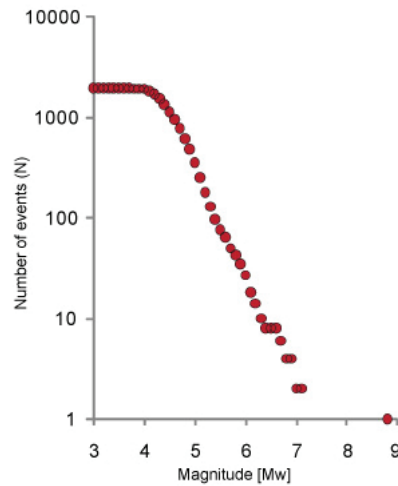


Figure 2.11: Gutenberg-Richter scale for aftershocks from 27th February, 2010 until 31st January, 2011.

In a highly active country, the seismic risk can be reduced by constructing better buildings and having better evacuation and response programs. With high-technology equipment, cartography maps and the help of historical seismicity catalogues, it is possible to determine areas prone to great earthquakes (Ruegg et al., 2009) and tsunami susceptible areas, and thus prepare inhabitants and buildings to face, in the best possible way, such tragedy. The possibility of predicting a great event, by determining the when, where and magnitude of it, is impossible to date, but at least it is possible to give a lower bound to rupture areas. However, by having a better understanding of the background seismicity and a constant monitoring of the coast and/or highly seismic areas, it is possible to recognize zones with lower activity that can be related to a quiescent zone possibly preparing for a large earthquake. Although quiescence has been observed in some cases, it has not been observed in others, therefore the lack of seismicity is neither a necessary nor sufficient condition for a large earthquake to occur.

The Maule earthquake in February 2010 proved that construction in Chile has been significantly improved since 1906. After the 1906 Valparaíso earthquake, Montessus de Ballore was hired as the director of the Instituto Sismológico de Chile (founded in 1908), which has worked in the improvement of the Seismic Chilean Code Nch 433 “Seismic Design of Buildings”. This code was created in 1931 and has had significant improvements and modifications in time. Buildings constructed following this code presented little damage after the Maule earthquake, and only three buildings in the affected area collapsed (one in Concepción, two in Santiago), other buildings were severely damaged but remained standing thus life of inhabitants was protected.

Projects should be undertaken to study also other known gaps, such as the northern gap from Mejillones, and southernmost Chile, in order to assess better emergency responses, in conjunction with government agencies.

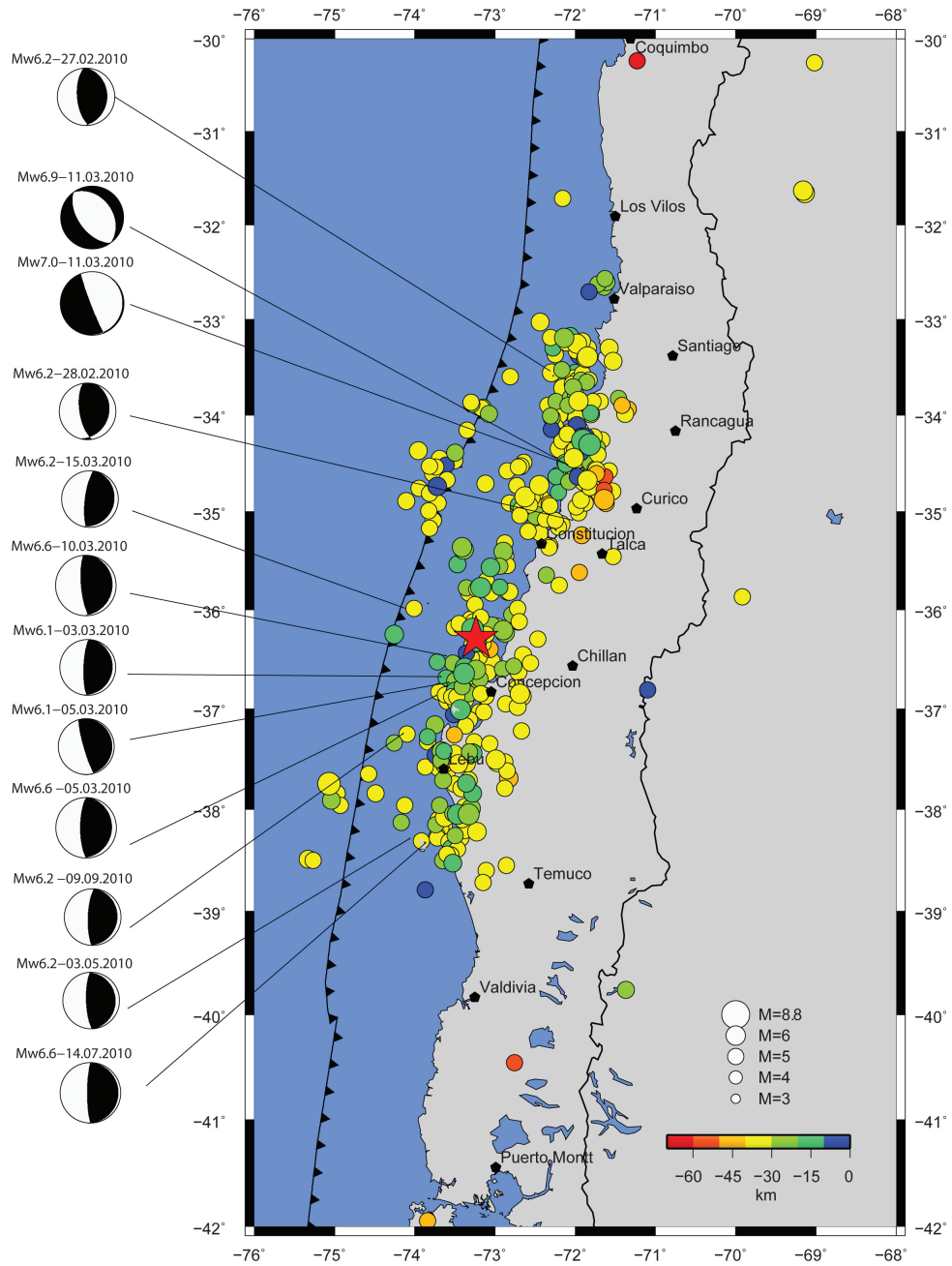


Figure 2.12: Focal mechanisms for aftershocks with magnitude above 6, retrieved from NEIC (USGS) (U.S.G.S., n.d.). Magnitude and date of the event provided. Only events with magnitude above 5 were plotted. Diameter of the circle denotes magnitude, and color scale for depth. Focal planes retrieved from Global CMT (Ekström et al., 2012). Mora, 2011

Acknowledgements

The first author acknowledges the Chilean National Council of Research, Science and Technology (CONICYT, acronym in Spanish) and the German Academic Exchange Service (DAAD, acronym in German) and their funding program BecasChile - DAAD for the grant that facilitates this research. She also thanks C. Bravo for his support and time in reviewing this paper.

Both authors acknowledge the SFB 574 “Volatiles and Fluids in Subduction Zones” for its funding. This publication is contribution no. 212 of the Sonderforschungsbereich 574 “Volatiles and Fluids in Subduction Zones” at Kiel University, Germany.

All figures were drawn using The Generic Mapping Tools (GMT, (Wessel and Smith, 1991, 1998)).

Chapter 3

Comparison of Seismic Activity for Llaima and Villarrica Volcanoes prior to and after the Maule 2010 Earthquake¹

Mora-Stock, C., Thorwart, M., Wunderlich, T., Bredemeyer, S., Hansteen, T., Rabbel, W.

Abstract

Llaima and Villarrica are two of the most active volcanoes in the Chilean Southern Volcanic Zone, and presently show contrasting types of activity. Llaima is a closed vent edifice with fumarolic activity, while Villarrica has an open vent with a lava lake, continuous degassing, and tremor activity. This study is focused on characterizing the relationships between volcanic and seismic activity in the months before and after the 2010 M8.8 Maule earthquake, which was located in NNW direction from the volcanoes. Time series for tremors, long period and volcano tectonic events were obtained from the catalogue of the Volcanic Observatory of the Southern Andes (OVDAS), and from the SFB 574 temporary volcanic network. An increase in the amount of tremor activity, long period events, and degassing rates was observed at Villarrica weeks before the mainshock, and continued at a high level also after it. This increase in activity is interpreted to be caused by enhanced magma influx at depth, and may be unrelated to the Maule event. In Llaima, an increase in the volcano tectonic activity was observed directly after the earthquake. The simultaneous post-earthquake activity at both volcanoes is consistent with a structural adjustment response. Since this enhanced activity lasted for more than a year, we suggest that it is related to a medium-term change in the static stress. Thus the Maule earthquake may have affected both volcanoes, but did not trigger eruptions, from which we assume that none of the volcanoes were in a critical state.

¹The following is the accepted pre-copyright editing version of the paper published in “Special Issue: Volatiles and Fluids in Subduction Zones” from the International Journal of Earth Sciences. The latest version of of this publication is available at <http://link.springer.com/article/10.1007/s00531-012-0840-x>. Please cite this paper as follows: C. Mora-Stock, M. Thorwart, T. Wunderlich, S. Bredemeyer, T. Hansteen and W. Rabbel. Comparison of seismic activity for Llaima and Villarrica volcanoes prior to and after the Maule 2010 earthquake, Vol. 103, Issue 7, Pages 2015 - 2028, 2014.

3.1 Introduction

The Ring of Fire, bordering the coast of the Pacific Ocean, is a highly active volcanic and tectonic zone, comprising chains of active volcanoes and great magnitude thrust earthquakes. These two phenomena are related to the subduction process. On the one hand, there is a geochemical link between the subducted slab and the volcanic arc on the overriding plate, located roughly 100 km inland parallel to the trench (Stern, 2004). This chemical link consists of mass transfer of slab derived material, like magma and fluids, to the arc. On the other hand, there is a physical link between subduction zone earthquakes and volcanic activity that has occasionally been observed directly in connection with great megathrust earthquakes (Alam and Kimura, 2004; Carr, 1977). Generally, the physical link can be understood in terms of stress transfer from the subducting plate interface into the overriding continent. Great megathrust earthquakes generate strong changes in the continental stress distribution that may affect the volcanic magma, fluid and volatile transport on a short term scale, from minutes to hours in the case of the dynamic stress (Hill et al., 2002).

The subject this article is to investigate if and how this physical link can be verified in the context of the recent Maule Mw8.8 2010 earthquake. To achieve this, changes in the volcano - seismic activity in two volcanoes during the months following the earthquake were analysed. The two volcanoes considered are Llaima and Villarrica, located at respectively ~ 300 and ~ 370 km distance from the epicentre of the Maule earthquake, two of the most active volcanoes of South America imposing a strong hazard on the urban and recreational centres nearby. Llaima and Villarrica were surveyed before and after the Maule earthquake with permanent seismic stations of the Volcanic Observatory of the Southern Andes (OVDAS) as well as with small aperture temporary seismic networks of the collaborative research project SFB 574 (University of Kiel and GEOMAR Research Centre, Germany). These data constitute the major basis of the present study. The results were compared to available qualitative observations from other Chilean volcanoes.

3.2 Previous observations of volcanic eruptions triggered by great earthquakes

Great earthquakes and large volcanic eruptions ultimately result from continent - scale tectonic processes (Linde and Sacks, 1998). However, their possible coupling can be investigated at both local and regional scales when volcanic eruptions follow or coincide with medium to shallow depth (0 - 100 km) seismicity in the area near the edifice (Alam and Kimura, 2004).

Many studies have focused on the time-and-space relation between great seismic events ($M \geq 8$) and the volcanic activity in edifices close to the epicentral area, generally of the order of hundreds of kilometres, in the days, months and even years following earthquakes (Carr, 1977; Barrientos, 1994; Linde and Sacks, 1998; Walter and Amelung, 2007). This complex interaction depends on several factors such as the magnitude of the earthquake and the distance to the epicentre (Carr, 1977). Also the dynamic and static deformations on the crust generated by body and surface waves may destabilize the volcanic edifice (Walter and Amelung, 2007). Finally, the initial state of the volcano, including the depth and compositions of magmas, is critical for its response to an earthquake (e.g. Linde and Sacks (1998)). In the study of Alam and Kimura (2004), a high correlation ($R = 0.99$) was found between eruptions and

post-eruptive earthquakes ($M \geq 7.6$), and between time and space ($R = -0.89$) regarding the start time of the eruption and the earthquake and the distance from the volcano to the epicentre. This finding is plausible since seismic activity can be triggered by volcanic activity due to crustal stresses generated by magma movements (Linde and Sacks, 1998) before or after a volcanic eruption.

Many earthquake - volcanic eruption relations have been studied, focusing on events with a magnitude over 9. Among them are the two eruptions of Talang volcano and Barren Island following the M9.3 Sumatra - Andaman earthquake in 2004 (Walter and Amelung, 2007), the eruption of Trident volcano two months after the Alaska M9.2 earthquake in 1964, and the awakening of the Redoubt volcano in 1966, after 64 years of quiescence (Walter and Amelung, 2007). After the Kamchatka earthquake in 1952 (M9.0), several volcanoes and calderas showed historic activity for the first time. Such is the case for the Karpinsky volcano, Tao Rusyr caldera and Bezymianny volcano which erupted one day, one week and three years after the mainshock, respectively. The Bezymianny volcano has been active since then (Walter and Amelung, 2007).

In Chile, a close temporal and spatial relationship was observed between the 1960 M9.5 earthquake and the eruption of the Puyehue - Cordón Caulle volcanic complex only 48 hours after the mainshock (Barrientos, 1994; Hill et al., 2002; Manga and Brodsky, 2006; Walter and Amelung, 2007). The volcanoes Calbuco and Villarrica erupted 8 months and ca. 3 years after the earthquake, respectively, and Planchón Peteroa and Tupungatito erupted coincidentally two months after the earthquake and re-erupted in the following two years (Walter and Amelung, 2007). Less well studied, but yet remarkable, are the eruptions prior to and after the great M8.5 (estimated) earthquake in Concepción described by Darwin on the 20th of February, 1835. At the time of this event, Michimahuida and Cerro Yanteles showed violent activity that lasted several months. The activity of these volcanoes may have been stimulated again by another shock in December 1835 (Darwin, 1845; Manga and Brodsky, 2006). Notably, Villarrica volcano was not affected by the shock (Darwin, 1845). Previously, Antuco volcano erupted two years before the earthquake, and Aconcagua and Osorno presented activity in January 1835 (Darwin, 1845).

These studies show that eruptions of more than one volcano over time periods of days to months after a great thrust earthquake are common (Darwin, 1845; Linde and Sacks, 1998; Hill et al., 2002; Walter and Amelung, 2007). The causal link appears to be in the dynamic and static deformation that earthquakes induce in the crust, in the magma reservoirs and volcanic edifice in a very wide radius around the rupture area of the earthquake (Linde and Sacks, 1998; Hill et al., 2002; Manga and Brodsky, 2006). The impulsive start or delay in the eruption relies on the eruptive stage of the volcano at the time of the earthquake (Linde and Sacks, 1998). It is necessary to distinguish between the effects of short term dynamic stress changes and intermediate to long term static stress changes. The dynamic stress change due to the passage of body and surface waves through the crust, can directly affect the edifice and its vicinity triggering a response in terms of minutes to hours. The static stress change contains both an instantaneous elastic portion and a viscoelastic part that is delayed due to relaxation, and it is capable of inducing an increase or decrease in the compressional stress around the magma chamber over months to years (Hill et al., 2002). As the amplitude of the static deformation decays with distance, volcanoes near the rupture could be affected by a contraction or expansion of the surrounding media. If the volcano is close to a critical state, an increase in the compressional stress could help the magmas move upwards to the surface, or alternatively, dynamically induced degassing could induce pressure build up and thus promote rupture at magma chamber roof levels (Barrientos, 1994; Hill et al., 2002). On the other hand, a decrease in the compressional stress may lead to a generation of additional melting with the consequent addition of volatiles as bubbles, overpressuring the magma and, finally, opening of the volcanic conduits (Hill et al., 2002; Manga and Brodsky, 2006).

During the Maule event on Feb. 27th 2010, an approximately 500 km long fault ruptured in the interface of the Nazca and South American plates. Nearly 15 months after the earthquake Cordón Caulle began its eruptive cycle that has lasted up to date. However, Llaima and Villarrica, which are much closer to the rupture area than Cordón Caulle, did not erupt after the earthquake. These two volcanoes have shown a very high level of activity during the past centuries and there is significant probability that these edifices present a $VEI \geq 2$ eruption in the next 20 to 50 years (Dzierma and Wehrmann, 2010)). Therefore, in the present study, the seismic activity of these two volcanoes is examined in order to investigate possible changes in the temporal seismic behaviour related to the Maule earthquake.

3.3 Geotectonic Context

The Andes are divided into several subduction related volcanic zones, following active segments and structural features, among other geological characteristics (Stern, 2004) Northern Volcanic Zone (NVZ) from 5°N to 2°S , Central Volcanic Zone (CVZ) from 14°S to 27°S , Southern Volcanic Zone (SVZ) from 33°S to 46°S , and Austral Volcanic Zone (AVZ) from 49°S to 55°S .

The Chilean SVZ is one of the most active sections with at least 60 potentially or historically active volcanoes and calderas (Stern, 2004). One of those volcanoes, Cordón Caulle, erupted approximately 15 months after the Maule earthquake reaching a VEI (Volcanic Explosivity Index) of 3, on June 4th, 2011 (Observatorio Volcánico de los Andes del Sur (OVDAS), 2011).

Like in 1960 and 1921, the activity was at first mistakenly attributed to the Puyehue volcano, but later observations lead to the Cordón Caulle fissure complex (Siebert and Simkin, 2002-).

The Peru-Chile Trench runs along the west coast of South America down to the Taitao Peninsula near 46°S , where it meets the Chile Triple Junction and the Antarctic plate (Figure 1). At this point in southern Chile both plates - Nazca and Antarctica - subduct under the continental South American plate at different rates and angles. The rapid subduction of the Nazca plate nowadays, determined from 6 to 9 cm/year (Angermann et al., 1999; Pardo-Casas and Molnar, 1987), is the cause for several great thrust earthquakes along the coast.

This applies to the recent Maule earthquake too. This $M_w 8.8$ earthquake lasted almost 2.5 minutes and ruptured 500 km along the interface of the Nazca and South American plates. The mainshock occurred at approximately 30 km depth beneath the coast of Cobquecura, a city between Concepción and Constitución ($36^{\circ} 17' 23''\text{S}$ and $73^{\circ} 14' 20''\text{W}$ according to the Chilean National Seismological Service, SSN in Spanish). It ruptured bilaterally to the north, up to $\sim 34^{\circ}\text{S}$ approximately, and southwards down to the 38.3°S latitude, south of the Arauco Peninsula (ellipse in Figure 3.1)(Lay et al., 2010; Farías et al., 2010; Moreno et al., 2010).

3.4 Llaima and Villarrica Volcanoes

Llaima and Villarrica each have shown approximately 50 eruptions in the past 400 years (Dzierma and Wehrmann, 2010; Siebert and Simkin, 2002-), making them the most active volcanoes in the SVZ. Both

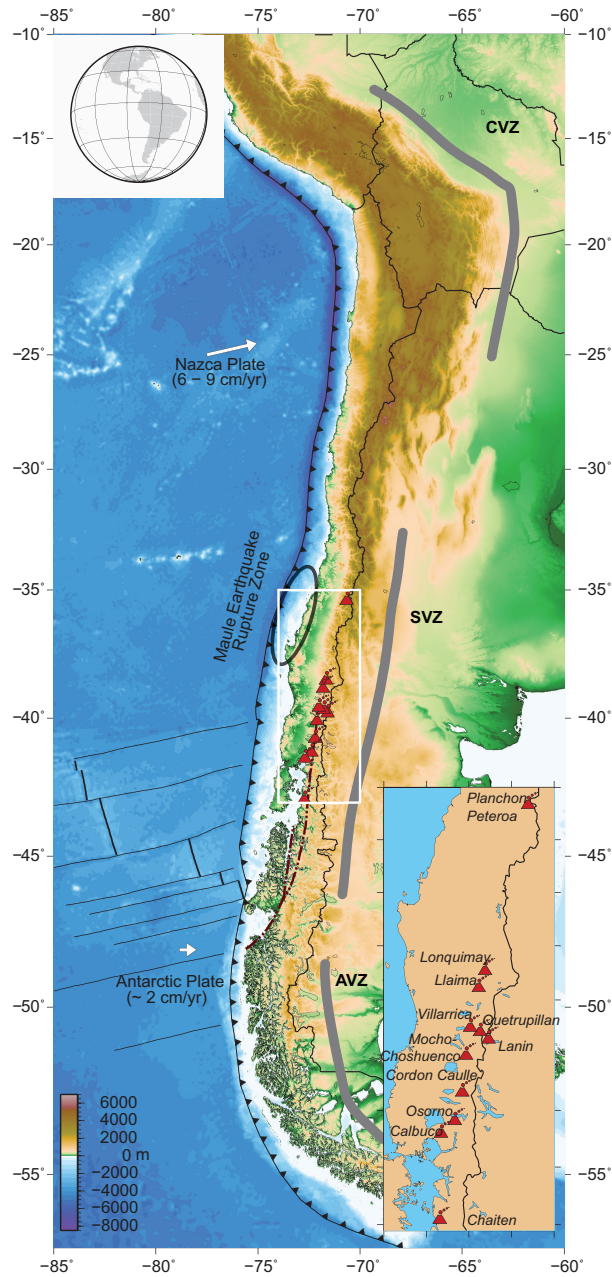


Figure 3.1: Geotectonic setting of Chile. Chile - Peru Trench marked as black line with triangles, pointing in the direction of subduction of both Nazca and Antarctic plates. Subduction rates are shown as white arrow, with size relative to velocity. Chile Ridge is shown as a black thick line, with accompanying fracture zones as thin lines. Dark gray ellipse denotes the rupture zone of the Maule M8.8 earthquake, last February 2010. Volcanic centres are shown as red triangles, with Llaima and Villarrica slightly bigger and darker, and Volcanic Zones (Central (CVZ), Southern (SVZ) and Austral (AVZ)) follow locations given by Stern (2004). White box denotes the zoomed area shown in the lower right corner with the names of the volcanoes identified in the text. Mocha Villarrica Fault Zone (MVFZ), Lanalhue fault (LAN) and Liquiñe - Ofqui Fault Zone (LOFZ) are depicted as grey dashed lines. Location of faults from Melnick and Echter (2006)

volcanoes are located along the lineaments of the N10°E trending Liquiñe - Ofqui Fault Zone (LOFZ), a 1000 km long strike slip fault that controls the location of volcanic edifices in southern Chile (Cembrano and Moreno, 1994; Cembrano et al., 1996; Cembrano and Lara, 2009).

Llaima volcano (38° 41' 33"S, 71° 43' 43"W, 3125 m.a.s.l.) is a basaltic to andesitic stratovolcano located almost 10 km west from the LOFZ (Dungan et al., 2008) that stands out due to its combination of explosive and effusive activity - such as the Holocene Curacautín Ignimbrite eruption at 13.5 ka BP (24 km³) which left a wide caldera (Lohmar et al., 2005; Dungan et al., 2008; Dzierma and Wehrmann, 2010). This very explosive period came to an end at 7.5 ka BP and continued with effusive activity and large plinian eruptions (Lohmar et al., 2005; Dzierma and Wehrmann, 2010). The recent 2008 eruption activity of Llaima lasted until mid 2009, presenting a central vent and radial fissure eruptions accompanied with lava flows and lahars, reaching a VEI of 4 (Siebert and Simkin, 2002-). Activity after the eruption has been characterized by constant and low seismic activity and fumarole degassing.

Villarrica volcano (39° 25' 14"S, 71° 56' 23"W, 2847 m.a.s.l.) is a large stratovolcano located at the northern end of the LOFZ, along a N60°W striking fault. It is located close to the Quetrupillán and Lanín volcanoes and includes more than 20 monogenetic cones that rise from the EW *écheleon* lineaments (Muñoz, 1983; Ortiz et al., 2003). Its formation started in the Mid - Late Pleistocene from several lava flows that produced the collapse of the elliptical caldera at 95 ka BP, and continued with frequent and effusive eruptions in the next 80 ka. Another caldera was formed at 14 ka BP (emission of the Licán Ignimbrite, ~10 km³ (Lohmar et al., 2006; Dzierma and Wehrmann, 2010)) and at 3.7 ka BP, a much smaller (~3 km³) Pucón Ignimbrite rejuvenated the edifice (Lohmar et al., 2006). After the last eruption in 1984-1985, the activity remained above the background level without a noticeable ending of the eruption cycle, and Villarrica has been showing continuous open-vent activity ever since (Ortiz et al., 2003; Calder et al., 2004). Current activity of Villarrica volcano is characterized by continuous degassing accompanied with constant tremor activity, and occasional mild strombolian eruptions (Calder et al., 2004). Nowadays, the ~200 m diameter summit crater hosts a 30 - 40 m diameter lava lake that changes its level according to the activity, varying between 100 and 150 m below the summit (Ortiz et al., 2003).

The most important hazards related to the eruption of these volcanoes are the spatters of lava and lava flows. These could cause secondary hazards such as forest fires, swollen rivers and lahars due to glacier ice melting (Ortiz et al., 2003; Dungan et al., 2008). This constitutes an important issue of hazard assessment and mitigation, since Llaima and Villarrica volcanoes lie near populated touristic cities. Llaima is 76 km distant from Temuco, capital of the Araucanía region, and close to other villages like Curacautín (32 km), Cherquenco (23 km) and Melipeuco (17 km). Villarrica is close to touristic centres such as Villarrica (28.5 km) and Pucón (16 km), and other minor villages such as Lican Ray (20 km) and Coñaripe (18 km).

3.5 Volcanic Events Database

This study is based on two data sources. One is the seismic catalogue provided by the OVDAS, which includes the number and type of events per day for each volcano, for the period 01.10.2009 - 27.05.2011 for Llaima and 09.10.2009 - 28.05.2011 for Villarrica (Gaps in the catalogue between days of recorded activity were assumed to be "no event" days). The OVDAS distinguished 8 types of events for each volcano,

determined visually by trained technicians. Most types of events are found at both volcanoes, notably, long period (LP), volcano - tectonic (VT), tremor (TR), hybrid (HB), ice quakes (IC), background (BG), and *bacha frecuencia* (low frequency) (BF). Some types of activity are exclusively occurring at one of the volcanoes, such is the case of *mariposa* events (butterfly in English)(SM) in Villarrica and *tornillo* (screw in English)(TO) in Llaima. These events are found only very rarely in each catalogue and will, therefore, not be considered in this study. Distinction between local volcano tectonic events and regional events is made considering the P-S wave time difference.

The catalogue is based on the events recorded at the stations run by OVDAS at both volcanoes. At Llaima volcano a variable network of 12 stations is composed by eight three - component Broad Band stations, between 2 and 19 km from the crater, one three - component Short Period station, and three one - component Short Period, between 1 and 11 km from the crater (Observatorio Volcánico del los Andes del Sur (OVDAS), 2010)). At the Villarrica volcano, a variable network is deployed, composed of three Broad Band stations, between 3 and 18 km from the crater, and one Short Period station located at the Volcanological Centre Villarrica at ca. 23 km from the crater (Observatorio Volcánico del los Andes del Sur (OVDAS), 2010).

The second catalogue (from here on referred to as “SFB catalogue”) was obtained from a temporary volcanic seismic network deployed between November 2008 and April 2011 as part of the SFB 574 project. Five stations were installed on and around the volcanic edifices, three Short Period stations, one Broad Band station and one Ocean Bottom Station (OBS) (Figure 3.2). The OBS was installed at a snow-covered place, where no solar panels could be installed, taking advantage of its long term stable clock and an extremely low battery power consumption. For the present study, data of the short period stations at both volcanoes were used. The catalogue was compiled directly from the continuous digital records by an STL/LTA trigger. It was applied to the frequency band between 0.8 and 2.4 Hz that contains the major energy of volcanic events such as LP, TR and some HB events. To avoid miscounting of triggered events, four stations from OVDAS were added to the list of stations, as well as some stations used in the regional network in the Villarrica region (Dzierma, Thorwart, Rabbel, Siegmund, Comte, Bataille, Iglesia and Prezzi, 2012; Dzierma, Rabbel, Thorwart, Koulakov, Wehrmann, Hoernle and Comte, 2012), and used to assure the number of stations required to count the trigger as an event. The automatic picks for LP events were exemplarily checked with manual picks founding a coherence of ~90%. A more detailed explanation on the methodology used to retrieve the SFB catalogue can be found in the Appendix A.1.

The SFB temporary network was deployed before the OVDAS network was fully operable. Therefore, although both networks are independent from each other, they are both complementary for this study.

Gas fluxes from Villarrica volcano were calculated from SO₂ measurements acquired using a permanent network of Mini-DOAS UV-spectrometers (Differential Optical Absorption Spectroscopy) that were installed as a cooperation between OVDAS and SFB 574 (Bredemeyer et al, in prep.). Further discussion of this data set, its evaluation and application is beyond the scope of this paper.

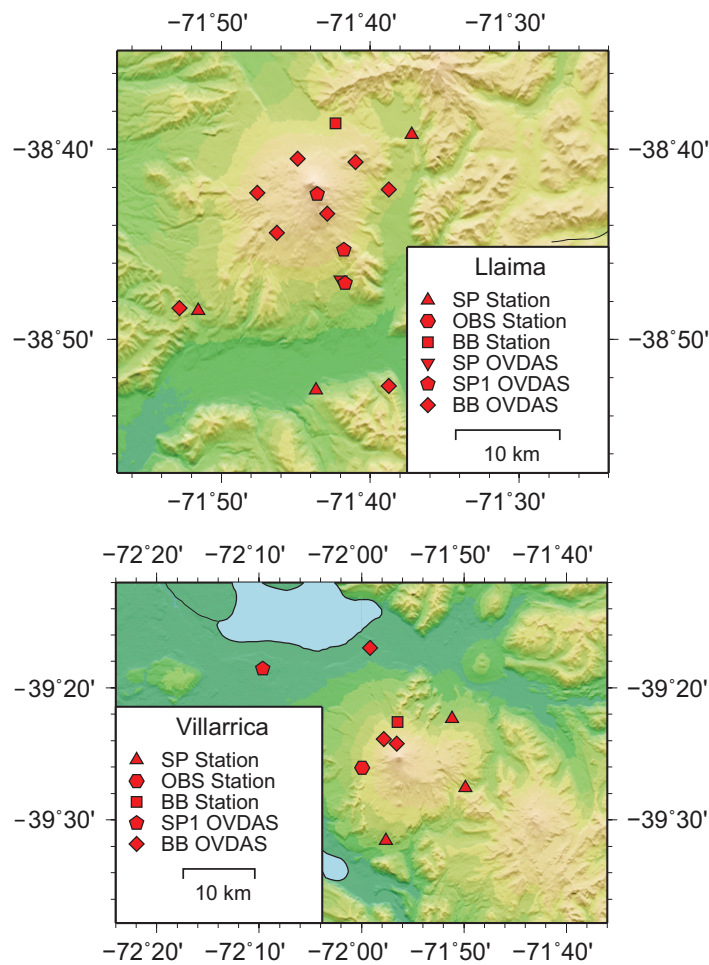


Figure 3.2: Station types and locations at Llaima (top) and Villarrica (bottom). Short Period (SP)stations shown as red triangles; Ocean Bottom Stations (OBS), as red hexagons; Broad Band (BB) stations, as red squares. Stations from OVDAS are depicted as red diamonds for Broad Band stations and inverted red triangles for three - component Short Period stations (SP) and red pentagons for one - component Short Period stations (SP1)

3.6 Methodology

The interpretation of the OVDAS catalogue was direct since it contained only volcanic events separated from tectonic events. Two time series were studied, the sum of Long Period and Tremor events and the Volcano - Tectonic events, ranging from from December 2009 to May 2011. They comprise almost three months before the mainshock of the Maule earthquake, and several months after to observe the level of seismicity free of aftershocks.

The automatically determined SFB catalogue contained initially all tectonic and volcanic events found by the trigger algorithm from November/December 2008 to April 2011. Therefore, the regional tectonic events, especially the high number of aftershocks of the Maule earthquake had to be removed before the analysis. A comparison of the records of Llaima and Villarrica for the time before the Maule earthquake showed that the number of regional tectonic events was negligible compared to the local

volcanic events.

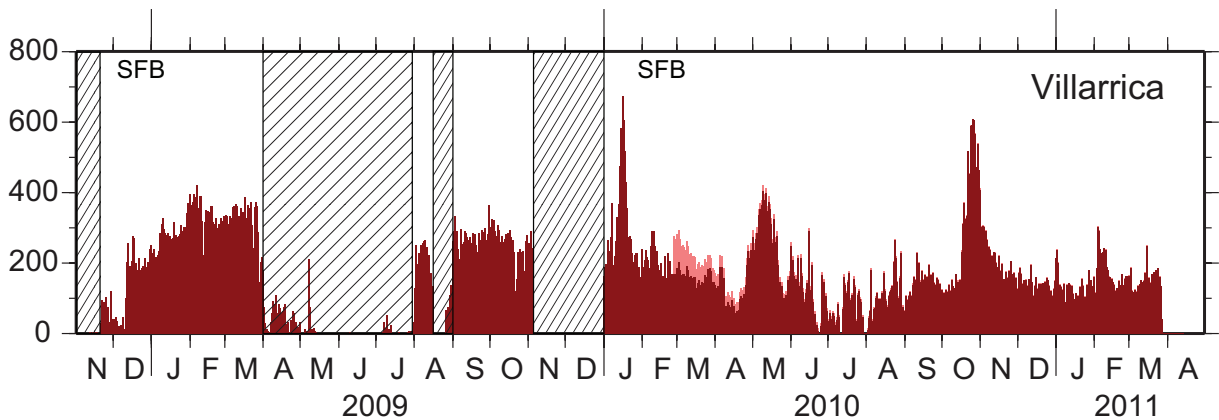


Figure 3.3: Time series of number of seismic events per day recorded at Villarrica volcano in the frequency band 0.8 - 2.4 Hz, triggered in the continuous records of the SFB seismic network with different configurations in 2009 and 2010. Original time series, including regional events and aftershocks of the 2010 Maule earthquake, are shown on the background in light red. Final time series are shown on the foreground in dark red. Dashed sections mark data gaps caused by poor or no station availability. Dashed black line marks February 27th, 2010, the day of the mainshock

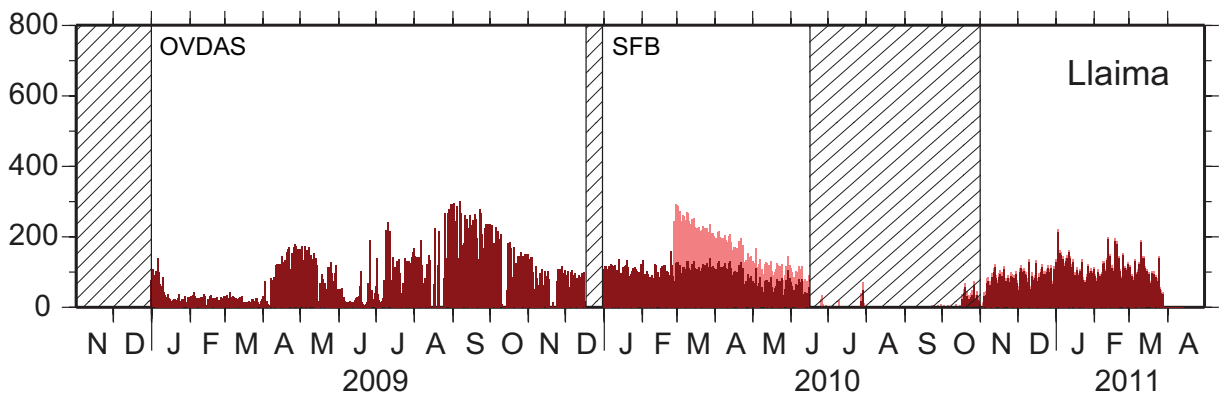


Figure 3.4: Time series of number of seismic events per day recorded at Llaima volcano in the frequency band 0.8 - 2.4 Hz, triggered in the continuous records of the SFB seismic network (data from January, 2010 and on) in collaboration with OVDAS seismic stations (data from January, 2009 until 17th December 2009). Original time series, including regional events and aftershocks of the 2010 Maule earthquake, are shown on the background in light red. Final time series are shown on the foreground in dark red. Dashed sections mark data gaps caused by poor or no station availability. Dashed black line marks February 27th, 2010, the day of the mainshock

In order to remove the aftershocks from the event statistics, the modified Omori's law was applied. The modified Omori's law describes the number of aftershocks as a function of time after the main shock, for example in the work of Lomnitz (1994). It is basically an exponential decay function with three free parameters that has to be adjusted to the actual earthquake sequence considered. For major earthquakes the decay of aftershock activity takes several months. Since here the interest is mainly in the short term changes of the volcanic seismicity, the number of aftershocks can be estimated by jointly fitting the modified Omori function and a continuous long term linear function to the data. For mathematical details on the calculation, refer to Appendix A.2.

In Figures 3.3 (for Villarrica) and 3.4 (for Llaima) the original time series and the reduced time series are shown. Gaps of poor or no data, occurred during winter time (April to August in southern hemisphere) since the power of the solar panels was not sufficient to record reliable data, as well as in November - December 2009 in Villarrica and part of December 2009 in Llaima, during fieldwork and new arrangement of the stations around the volcanoes.

3.7 Results

3.7.1 Villarrica Volcano

3.7.1.1 Long Period and Tremor events

The low frequency activity at Villarrica is characterized by peaks (Figure 3.3), reaching over 600 events/day in January 2010, before the Maule earthquake. After the earthquake, three other peaks stand out in May 2010, October - November 2010 and February 2011. In general, a constant background activity of ca. 200 events/day is recognizable during the year 2009, which is around 100 events/day lower during the year 2010. No prominent peaks of activity are observed during 2009, although their existence cannot be ruled out, since a large section is missing due to unreliable data. The influence of aftershocks on the total amount of events is not large, and the peak of activity during May 2010 remains after the subtraction of aftershocks.

The data from OVDAS is in accordance with the SFB catalogue regarding the amount of long period events and tremors at Villarrica volcano (Fig. 3.5a), although the background number of events is much lower. Here, the peaks observed are one during December 2009 reaching more than 200 events/day on the most active days, and a second phase starting in mid January with two peaks that stand out with 766 and 487 events/day respectively on January 16th and February 1st, and decaying almost exponentially after the Maule earthquake. On the first two days after the earthquake the number of events is zero, probably due to the impossibility of detecting visually the volcanic events in the overflowed record. After these days the activity remained on an average level of <50 events/day, except for certain limited peaks of activity. After the earthquake, three major peaks can be observed: one from May 5th to 20th, 2010 showing ~ 82 events/day on average, followed by six small bursts of ~ 50 events/day lasting only a few days each; a second one from mid of October until mid of November 2010 with ~ 106 events/day in average; and a third one in the first days of January 2011, with ~ 77 events/day.

3.7.1.2 Volcano Tectonic events

According to the OVDAS catalogue, a total of only 70 volcano tectonic events were detected in the considered period giving an average of almost one event per seven days (0,95) (Fig. 3.5b), with few exceptions of no more than 1 event/day and a maximum of 3 events/day. However, it is important to mention that only 5 isolated events, that is 7% of the total number of events, occurred before February 27th, 2010. This means that the average rate of volcano-tectonic events increased by a factor of >3 from the day of the Maule earthquake remaining at low level compared to LP and tremors.

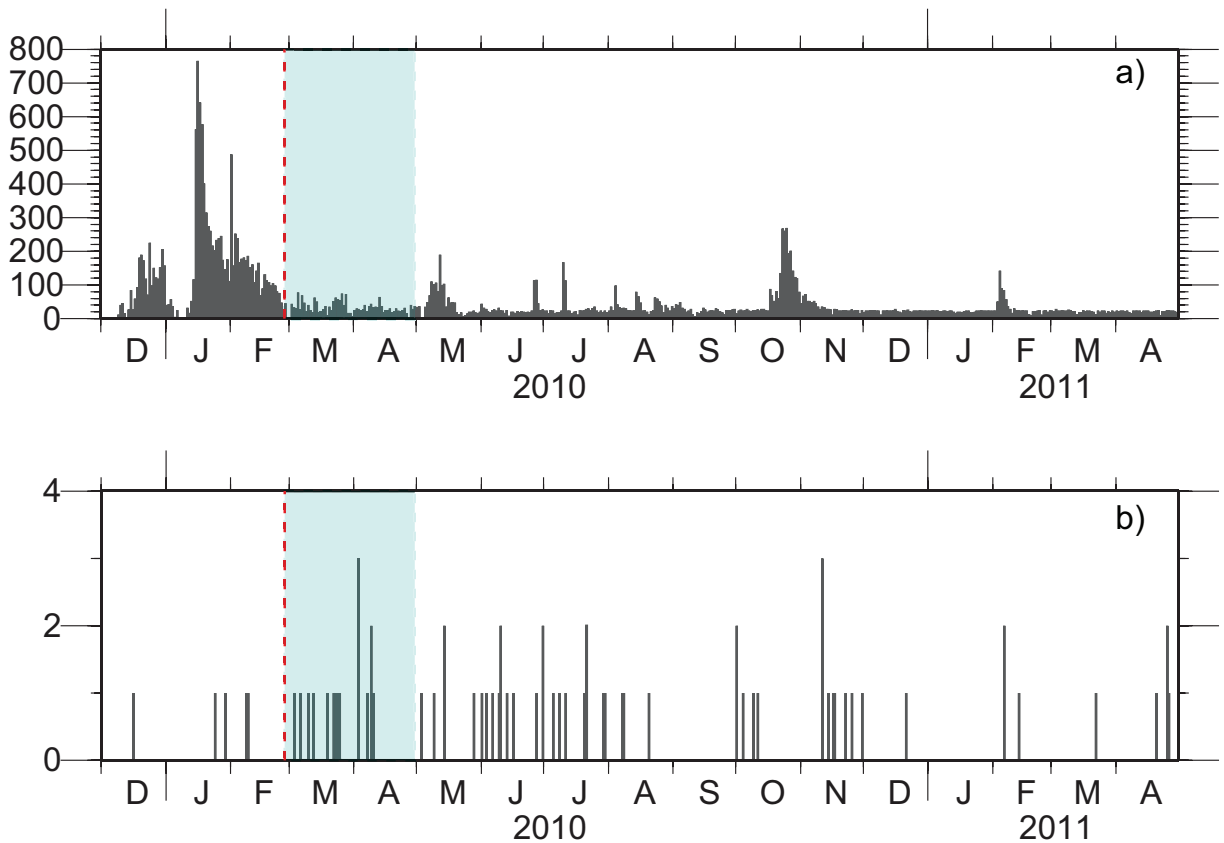


Figure 3.5: Time series of the number of seismic events per day of Villarrica volcano from December 2009 until end of May 2011 based on the OVDAS catalogue. From top to bottom: Long period plus tremor events (a) and volcano tectonic events (b). The red dashed line marks the 27th February, 2010, the day of the Mw8.8 Maule earthquake, and the light green covered area marks the months of higher aftershock activity

3.7.1.3 Other types of events

Only 14 hybrid events were reported in the OVDAS catalogue. Eleven events that occurred before the earthquake overlap in time with the first burst of activity of low period events, between December 3rd and 23rd, 2009. The other three events occurred on March 14th and two on March 23rd, 2010. Eight *bacha frecuencia* (BF) events were reported, seven before the earthquake and one after (March 8th, 2011). In addition, one ice quake on August 4th, 2010 was observed. Neither “butterfly” (SM) nor background (BG) events were reported.

3.7.2 Llaima Volcano

3.7.2.1 Long Period and Tremor events

According to the SFB catalogue, the activity of low frequency events for Llaima (Figure 3.4) is lower than for Villarrica. For Llaima, the continuous record of stations from OVDAS was used for the year 2009, and mainly stations from the SFB temporal volcanic network were used for the years 2010 - 2011. Peaks with higher activity are not observable, but rather longer periods of a higher number of events, as in April - May 2009 and August - November 2009. The influence of the aftershocks was considerably distinct, and after subtracting it, the volcanic activity was roughly constant in the time interval around the earthquake as far as the data is available.

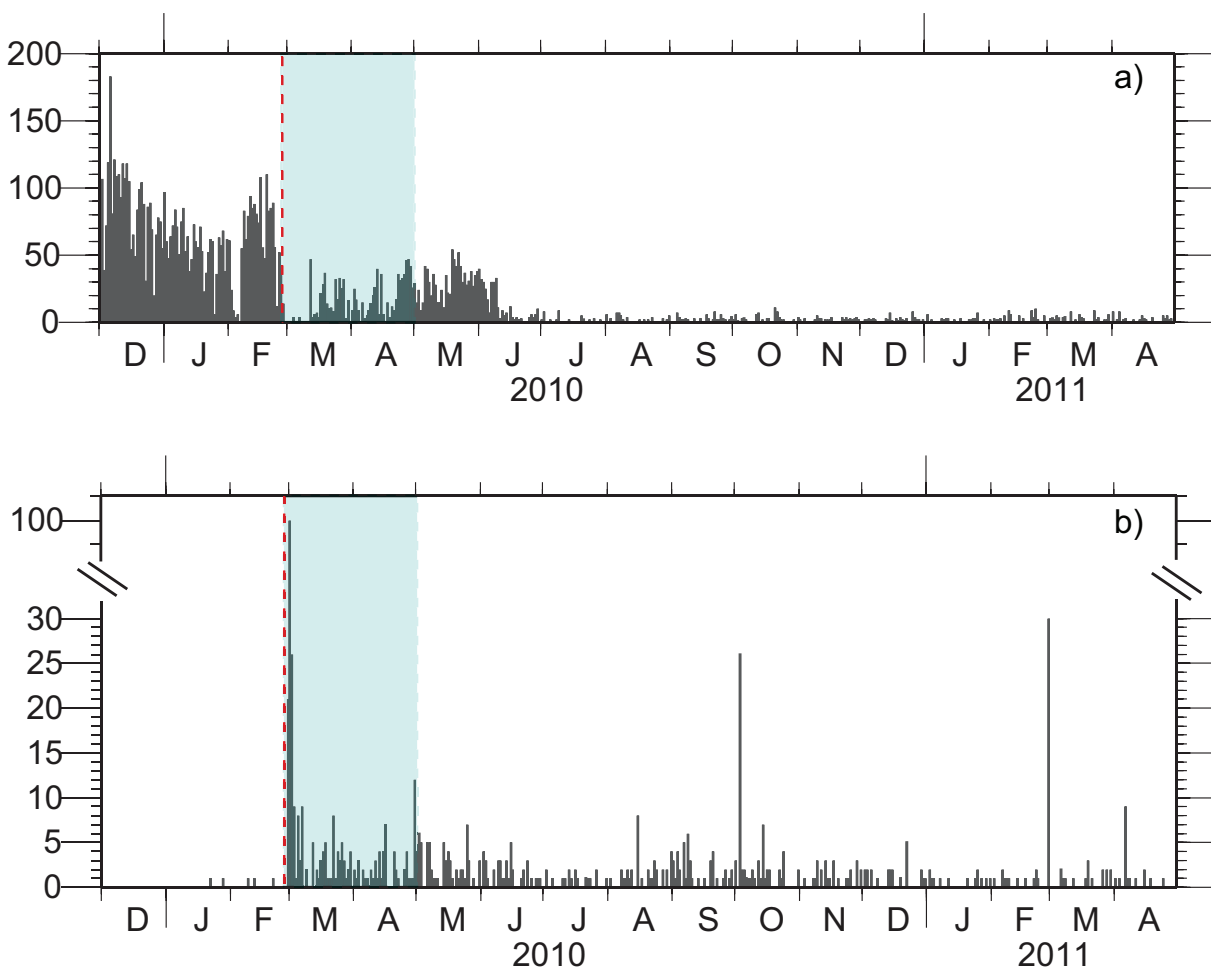


Figure 3.6: Time series of the number of seismic events per day of Llaima volcano from December 2009 until end of May 2011 based on the OVDAS catalogue. From top to bottom: Long period plus tremor events (a) and volcano tectonic events (b). The red dashed line marks the 27th February, 2010, the day of the Mw8.8 Maule earthquake, and the light green covered area marks the months of higher aftershock activity

The OVDAS record for Llaima volcano (Fig. 3.6a) starts with high activity on December 2009 with a maximum of 183 events/day on December 6th and 71 events on daily average. This average

decreases almost linearly afterwards and, after a sudden “gap” of four days, with less than 10 events/day, it rises again to an average of 69 events/day. The number of events per day decreases abruptly after the earthquake for about two weeks, probably due to technical problems or the inability of distinguishing volcanic events between the aftershocks, and maintained an average of ~ 21 events/day until June 10th, where the rate diminishes drastically to ~ 2 events/day on average.

There is an increase in the background activity due to the Maule aftershocks, which can be subtracted at the beginning of the sequence, directly after the mainshock, but it is rather difficult to identify aftershock activity several months after the mainshock. Certainly, this is the reason of the difference between Fig. 3.4 and Fig. 3.6 in November 2010 to February 2011, due to late high magnitude aftershocks, such as the Mw 7.2 event on January 2nd, the Mw 6.9 on February 11th and the Mw 6.7 on February 14th that could have activated the automatic trigger and therefore increased the counts.

3.7.2.2 Volcano Tectonic events

The change in the rate of volcano tectonic events in Llaima connected with the Maule mainshock is striking (Fig. 3.6b). Prior to the Maule earthquake, only five isolated events occurred since the beginning of the time series. Immediately after the mainshock, on 3 following days, 21, 100 and 26 VT events were observed, respectively, and from March 3rd, 2010 until the end of the period of the study, an average daily rate of ~ 2.5 VT events/day was observed, with a maximum of 56 events/day on March 28th 2011.

3.7.2.3 Other types of events

A small number of hybrid events occurred several weeks after the Maule earthquake with two pinpoint dates of activity on April 3rd and 4th with 32 events in these two days. Several ice quakes were recorded between March 24th and April, with a total of 162 events. Only 3 BF events and 1 TO event were recorded.

3.8 Discussion

Following the removal of the aftershocks' influence on the SFB catalogue (Figs. 3.3 and 3.4), Llaima volcano shows a relatively stable behaviour with no visible increase in activity for LP events, and for Villarrica volcano at least three peaks of activity are observed. In both cases, the total number of events presents little to no mismatch with the total amount of activity registered by OVDAS when Long Period and Tremor events are summed together. Judging by the graphic reading of the OVDAS catalogue, both volcanoes had a high activity of low - frequency events weeks to months before the earthquake which diminished after the main shock, and then continued for several months. At Villarrica volcano those phases of frequent long period events and increased tremor coincide with observations of enhanced degassing activity monitored at the surface of the volcano. A gradual increase of degassing and strombolian activity at the summit crater was observed well before the Maule earthquake (Figure 3.7), i.e. from December 2009 to February 2010. This phase of activity was interrupted by the Maule earthquake, which was followed by rapidly diminishing gas fluxes and ceasing lava lake activity. Three weeks after the main shock,

degassing fluxes and strombolian activity rose again to higher levels than before the earthquake.

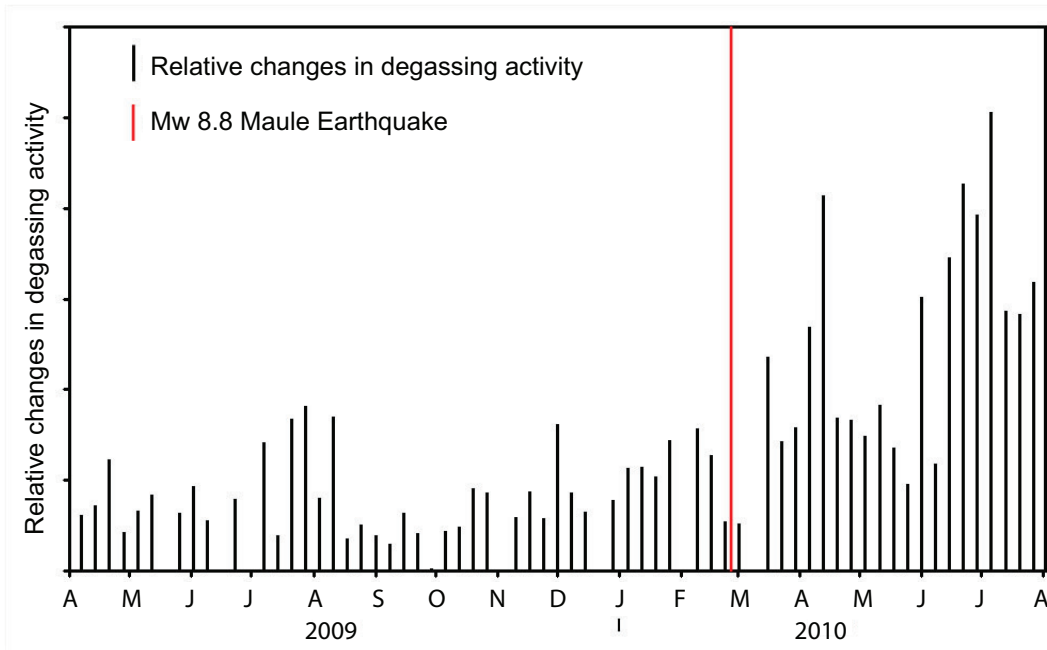


Figure 3.7: Weekly relative change in degassing activity at Villarrica volcano from April 2009 to July 2010. Red line marks the date of the Maule earthquake

Long period events are usually related to fluid movement as a response of the system to a sudden pressure transient and degassing (Chouet, 1996). Gas expelled through cracks that open and close accompanied by resonance as the gas moves through the conduit, or magma slugs ascending or passing through these conduits can produce such signals (Newhall, 2007). Long Period events and tremors could share a common source process, but differ in the duration, as they respond to a sustained pressure fluctuation (Chouet, 1996). Inferred origins for tremors involve the flow of magma or hydrothermal fluid through the cracks and conduits, creating a nonlinear oscillation or resonance, and the possible overlapping of successive events (Newhall, 2007). A less studied origin for tremors is the “subcooling boiling”, where bubbles generated by the boiling of groundwater at magma or gas depths implode (Leet, 1988).

At both volcanoes, the activity of these kinds of events is different. Llaima showed two stages of high activity, both before and after the mainshock. As for Villarrica, a sustained number of events both in daily average and time-integrated was observed after the earthquake. Evaluating the spectrograms for both types of events, tremors and long period differ only in the intensity of the energy spectrum.

Volcano tectonic events, on the other hand, correspond to a response on shear or tensile processes, brittle failure as a structural response to intrusion or withdrawal of fluids (Chouet, 1996). At Llaima volcano, the activity of this kind of event is highly peculiar, with an increase of the daily average directly after the Maule earthquake, and a peak in the number of events in the three following days after the mainshock. These VT events, some of them poorly constrained, have depths less than 12km and their locations are in recurrent zones near the city of Melipeuco and close to brittle zones such as branches from LOFZ (Fig. 3.8). Villarrica, however, does not show an increase in the average number of volcano tectonic events per day, but it shows an increase in the number of days that present events.

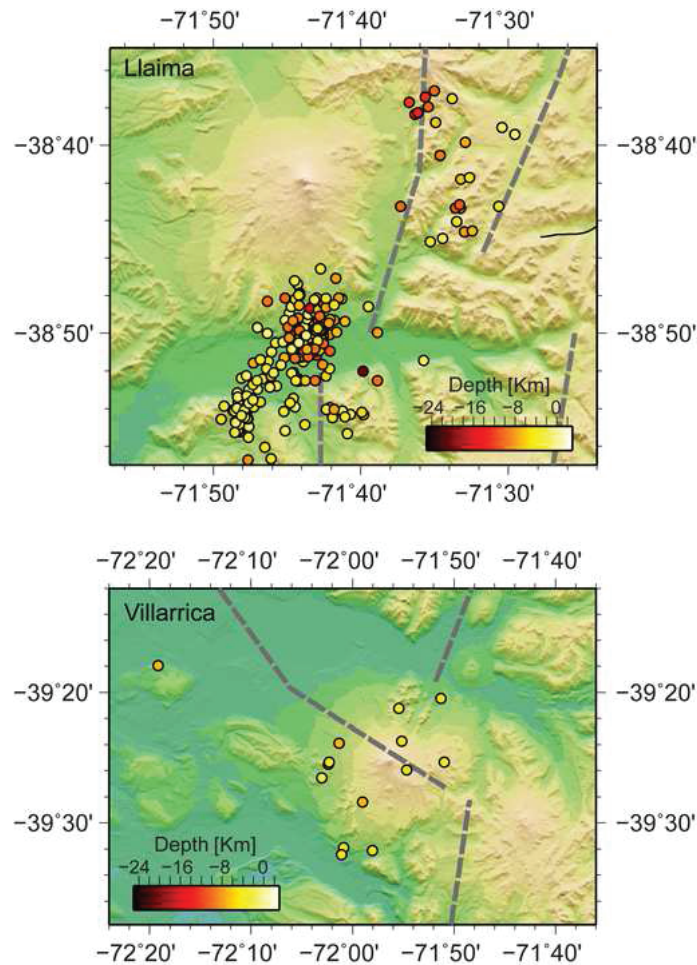


Figure 3.8: Location, given by OVDAS, of some of the volcano tectonic events in Llaima (top) and Villarrica (bottom). Color scale denotes depth. Grey dashed lines correspond to lineaments of LOFZ near Llaima and LOFZ, Lanalhue fault and MVFZ near Villarrica, given by Melnick and Echtler (2006).

Reactions of other volcanoes

It could be expected that other Chilean volcanoes located close to the rupture area presented some response to the earthquake. Lonquimay is one volcano north of Llaima for which OVDAS has reports. To the south of Villarrica, several others like Mocho - Choshuenco, Calbuco, Osorno, and the recently active Chai-tén and Cordón Caulle are also monitored.

Carr (1977) proposed a pattern of activity for volcanoes close to a subduction rupture zone prior to and after an earthquake: an initial precursory increase of activity, followed by a quiescent time before the mainshock and a rise in the activity again. This pattern would be dominated by the deformation that the convergent margin (static deformation) generates on the magma reservoirs, by raising, lowering and raising again its levels (Carr, 1977). For a volcano near a critical pressure state, this deformation and the dynamic deformation generated by the waves at the time of the earthquake could result in an eruption (Linde and Sacks, 1998). Also Eggert and Walter (2009) found a relation between earthquake - eruption sequences in terms of distance to the epicentre and days before and after the mainshock. In the

mentioned study, volcanoes with constant activity are less prone to erupt after a great earthquake than volcanoes without specific eruptive cycles. It has been observed that near field volcanoes usually present a silent period before an earthquake and more activity after it, which can vary from unrest to serious eruption, returning to a “normal” state after ~ 30 years (Eggert and Walter, 2009).

Most of the volcanoes mentioned previously presented some kind of activity before the earthquake, either on normal or low levels, except for Chaitén, which had higher activity corresponding to the end of its eruptive cycle in March 2010. For some of them it is impossible to recognize a real change in the behaviour, such as a quiet time before the Maule earthquake, since they were not previously monitored. For those with seismic stations installed before the Maule earthquake, the changes in the activity remained within the “normal” range. Detailed activity reports of these volcanoes can be found in Appendix A.3.

Contrast with 1960 M9.5 Valdivia earthquake

Pressure change due to the Maule earthquake (Figure 3.9) was calculated using a boundary element method based on Okada (1992). The fault geometry and slip distribution were taken from Delouis et al. (2010), and a crustal mean value of 30 GPa for both Lamé parameters was used. For the upper crust, at a depth where magma chambers typically lie (as e.g. 6-12 km for Llaima, according to Bathke et al. (2011)), the general result found is an extension towards inland, and compression on the west side of the coast (Figure 3.9). The values found are ~ -40 kPa for Llaima and ~ -5 kPa for Villarrica. For Nevados de Longaví volcano ($36^{\circ} 11' 35''\text{S}$, $71^{\circ} 9' 39''\text{W}$) which is closer to the middle point of the rupture zone, the pressure change is ~ 200 kPa.

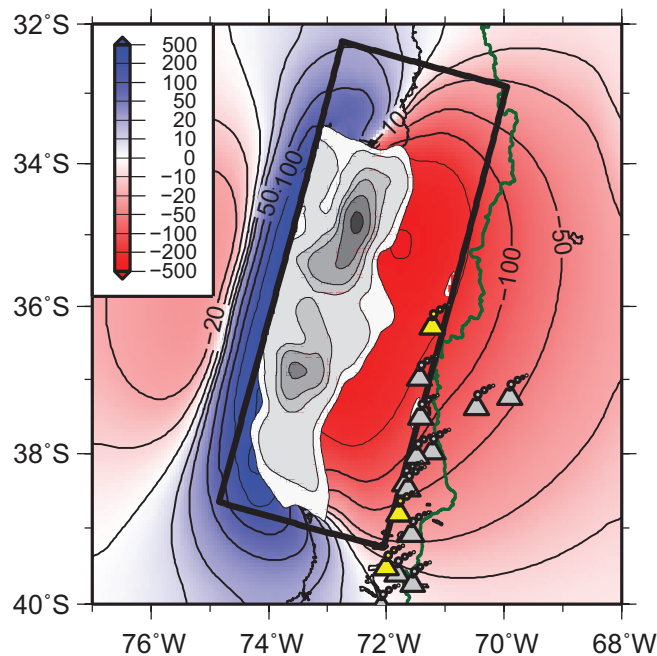


Figure 3.9: Pressure change at 8.75 km depth as a response to the Maule earthquake, from which its slip is shown as shades of gray, and black rectangle shows the fault plane used for calculations. Volcanic arc shown in gray, and Llaima, Villarrica and Nevados de Longaví emphasized in yellow. Blue and red color scale denotes positive and negative change in pressure, with units in kPa

These values are consistent with those in the study of Luttrell et al. (2011), where the coseismic shear stress change found ranges from -6 MPa to 17 MPa considering an average shear modulus of 40 GPa.

Also normal stresses were calculated on the Liquiñe - Ofqui Fault (N11°E trending) and Mocha - Villarrica Fault Zone (MVFZ) with a N299°E trending, coincident with the arrangement of the triad Villarrica - Lanín - Quetrupillán. On the LOFZ, Villarrica shows a compression of -10 kPa, while Llaima shows extension around 100 kPa. Since the southern rupture tip of the Maule earthquake is around 38.5°S, there is a nodal plane in the normal stress distribution between both volcanoes, hence, Llaima and the volcanoes north of it, show compression on the area around the LOFZ and Villarrica and volcanoes south of it, show extension. Similar phenomenon is shown for the MVFZ calculations, where Villarrica showed a value of 10 kPa (extension). Since only Villarrica is connected to this fault (in this study), effects on Llaima are not considered.

The same sort of changes in pressure and normal stress were calculated for the 1960 M9.5 earthquake using the slip model from Moreno et al. (2009), giving pressure changes between -1100 to -1200 kPa for Llaima and approximately -900 kPa for Villarrica. This can be correlated with a volume strain of $(5 - 10) \times 10^{-6}$ for Llaima and Villarrica, which are two orders of magnitude higher in comparison to those generated by the Maule M8.8 earthquake. The same is noticeable when calculating the normal stress in the LOFZ, which generated a 3000 kPa (3 MPa) stress in the area of Villarrica and between 2 to 3 MPa in the Llaima area. An extension ~ 1000 times higher than generated by the Maule earthquake could explain the increase in immediate activity of the volcanoes in the surroundings areas of the Valdivia 1960 rupture zone.

The usually accepted models relating volcanic eruptions after great earthquakes involve an increase in the compressive stress since it would force the magma to rise when the volcano is in a critical or near critical state (Barrientos, 1994; Hill et al., 2002). Also a sudden decay in the compressional stress would stimulate the bubble formation and unblocking of volcanic conduits, leading to an increase in the pressure while bubbles rise, allowing the magma to ascend from deep magma chambers (Barrientos, 1994; Hill et al., 2002).

Both volcanoes erupted years after the 1960 M9.5 earthquake in Valdivia (Villarrica in 1963, VEI 3, and Llaima in 1964, VEI 2). Since 1990, Llaima volcano has presented nearly 10 eruptions, the last one in 2007 - mid 2009, while Villarrica has presented at least 13 eruptions with VEI 1-2 since its change to open-vent behaviour in the eruption of 1984 - 1985. In comparison, Cordón Caulle volcano had only one eruption (VEI 1) in 1990 after the VEI 3 eruption in 1960. This could explain a closeness to a critical state in which Cordón Caulle was more prone to response, from months to years, to the large dimension static stress change in the surroundings of the rupture zone.

3.9 Conclusion

Despite the relative closeness of Villarrica and Llaima volcanoes to the rupture area of the M8.8 Maule earthquake, no dramatic change in the seismic behaviour was observed. There was a sustained activity of LP events and tremors in both volcanoes, related to the movement or activity of fluids (gas and/or magma) after the earthquake, which might have been induced by the sudden change of static stress around the reservoirs. This could also induce the structural adjustment response in Llaima and its vicinity, observed

in the sudden increase and sustained number of VT events after the earthquake and through the following months. For Villarrica, the co-variation of LP events and degassing rates strongly indicates increases in magma supply rates prior to the earthquake, and continued high rates of magma intrusion following the event.

No great eruption was generated, probably because both volcanoes were not in a critical state, as Cordón Caulle might have been, at the time of the event. Llaima had ended its previous eruptive phase in 2009, and erupted a few months before the earthquake. And Villarrica has shown permanent open vent degassing activity since 1985, including many VEI 1 events.

There has been a growing number of volcanoes presenting increased activity in southern Chile since the Maule earthquake. Even if they were not directly influenced by the imposed stress field changes, this activity could be related to movements of the LOFZ rather than to the earthquake itself. Finally, we underline that the Maule earthquake did affect in some way Llaima and Villarrica volcanoes, two of the most active volcanoes in southern Chile, but both edifices were not in a sufficiently critical state to generate a greater eruption.

Acknowledgements

Part of the data used in this publication was collected and provided by the Observatorio Volcánico de los Andes del Sur - Servicio Nacional de Geología y Minería (OVDAS - SERNAGEOMIN), and all authors acknowledge both institutions for their collaboration. All authors acknowledge the SFB 574 "Volatiles and Fluids in Subduction Zones" for its funding. The first author is grateful to the Chilean National Council of Research, Science and Technology (CONICYT, acronym in Spanish) and the German Academic Exchange Service (DAAD, acronym in German) and their funding program BecasChile - DAAD for the grant that facilitates this research. All authors acknowledge the GIPP of the GFZ Helmholtz - Zentrum Potsdam for providing the short period seismometers used for the SFB 574 project during the period November 2008 to April 2011. All authors appreciate the valuable comments and suggestions of two anonymous reviewers and the Topic Editor D. Völker that helped to improve this manuscript. All figures were drawn using the Generic Mapping Tools (GMT) software from Wessel et al. (2013). This is contribution number 238 to Sonderforschungsbereich 574 "Volatiles and Fluids in Subduction Zones" at Kiel University, funded by the German Research Foundation.

Chapter 4

Inner Structure of the Villarrica Volcano derived from Local Tomography using Volcano Tectonic Events¹

C. Mora-Stock, M. Thorwart, W. Rabbel

Abstract

We present the first model of the seismic structure of the Villarrica volcano (South central Chile). It refers to the state of the volcano in March 2012, 3 years before its eruption in March 2015. The model is based on a tomographic inversion of P-wave arrival times from local volcano-tectonic (VT) earthquakes recorded by a network of 50 short period stations. The hypocenters of the VT events are located between 2 and to 7 km b.s.l. at the transition between zones of low and high P-wave velocity zones found underneath the central part of the volcanic edifice. These locations are consistent with an extrapolated side-branch of the Liquiñe - Ofqui Fault, a major arc-parallel strike-slip fault of the Chilean subduction zone. The volcanic edifice shows an average P-wave velocity (V_p) of 4.5 km/s and V_p/V_s -ratios of 1.6 to 1.7. The maximum variation of V_p is of the order of $\pm 15\%$. Bootstrap tests showed that the standard deviation of the tomographic solutions is of the order of $\pm 3\%$. We find 3 pronounced low-velocity zones (LVZs) between 1 and 5 km depth that can be related to the presence of magma or magma-derived fluids: one LVZ of ~ 5 km diameter at 1 -2 km depth slightly NNW above the locus of seismicity, and two conduit-like LVZs reaching from ~ 5 km depth at the center to the well-known pyroclastic flows of Los Nevados and Challupén ENE and S of the crater. The latter LVZs can be interpreted as remnants of the related conduits. High-velocity anomalies found east and below the crater can be interpreted as consolidated volcanic rocks coinciding with two flanks of previously collapsed calderas.

¹The following is an up-to-date (to the time of writing) version of the paper “Inner Structure of the Villarrica Volcano derived from Local Tomography using Volcano Tectonic Events” to be submitted to Journal of Volcanic and Geothermal Research. As this is not a final version, please do not cite this paper without authorization.

4.1 Introduction

Villarrica volcano in southern Chile is one of the most active volcanoes in Southern Andes. It is located close to two highly touristic and populated cities, Villarrica and Pucón, and several other towns around its foot. Its last mayor eruption occurred in 1984-85, and its last eruptive cycle started in December 2014. One of the main strombolian pulses in this last cycle, on the 3rd March 2015, reached VEI (Volcanic Eruption Index) 2, and forced the evacuation of more than 3300 people living in the areas surrounding the edifice. Villarrica volcano is constantly monitored by the Volcanic Observatory of the Southern Andes (OVDAS - Acronym in Spanish) due to its hazards - mainly lahars and tephra fall outs - and constant seismicity.

At Villarrica Volcano most of the research has focused on degassing (Witter et al., 2004; Bredemeyer and Hansteen, 2014; Shinohara and Witter, 2005; Sawyer et al., 2011), volcanic products of recent and historical eruptions (Clavero and Moreno, 2004; Silva Parejas et al., 2010) as well as detailed historical eruptions (Casertano, 1963), and their geochemical composition regarding the tectonic emplacement (Cembrano and Lara, 2009). Studies on seismicity and infrasound are focused mainly on its characterization (Curilem et al., 2009; Ortiz et al., 2003; Tárraga et al., 2008; Ripepe et al., 2010; Goto and Johnson, 2011; Richardson et al., 2014; Richardson and Waite, 2013), its relationship with degassing (Calder et al., 2004; Palma et al., 2008) and its relationship with great subduction earthquakes (Watt et al., 2009; Mora-Stock et al., 2014; Bonali et al., 2013). A few studies have resolved some characteristics of the structure underneath the edifice with magnetotellurics and aerogravimetry (Muñoz et al., 1990; Brasse and Soyer, 2001; Delgado, 2012), but details are scarce, and the structure of the magma chambers and velocities inside the volcano are still unknown.

Some of the earliest reports of studies of volcanic structure using passive seismic appear in the review of Piermattei and Adams (1973) of the Kamchatka Volcano and the Kluchevskaya Group, and in Alaska. In 1977 Ellsworth and Koyanagi (1977) used the method of Aki et al. (1977) for seismic tomography to visualize the mantle and crustal structure beneath the volcanic region at Kilauea. Since then, different methods have been used to help in understanding magma chamber locations, geothermal spots, and velocity structure inside a volcano edifice. These methods include mostly passive source P-wave arrival as in local and regional tomography (Lees, 1992; Benz et al., 1996; Monteiller et al., 2005; Kuznetsov and Koulakov, 2014; Londoño and Sudo, 2003), but active sources (Wegler et al., 1999; Zandomenighi et al., 2013), and ambient noise tomography (Brenguier et al., 2007; Stankiewicz et al., 2010; Spica et al., 2015) among others that can also be found.

In this study we present a P-wave arrival-time inversion from volcano tectonic events located inside a temporary network of 50 stations encircling the Villarrica Volcano, used to perform a straight-rays body wave tomography of the edifice. In section 4.2, the geological setting and present characteristics of the Villarrica volcano are presented. A description of the network distribution, a pre-processing of the data, a summary of the methodology, the synthetic Checker-Board tests, and statistical method used are explained in section 4.3. Later in section 4.4, the results for location of seismicity, focal mechanisms, and tomography are shown. Finally we present in section 4.5 the statistical validation of our results. As well, due to the lack of detailed studies regarding the structure of the Villarrica Volcano, we present a comparison of our findings with other andesitic volcanoes and combine results of previous geophysical studies to obtain a schematic model starting from the crater rim to a depth of approximately 7 km. To round up, we present our main conclusion in section 4.6.

4.2 Geological Setting

Villarrica Volcano (39.42°S, 71.93°W, 2847 m above sea level -a.s.l.-) is an open-vent active compound basaltic-to-andesitic stratovolcano located at the westernmost end of the Villarrica - Lanín - Quetrupillán (VQL) lineament and its intersection with the Liquiñe - Ofqui Fault Zone (LOFZ) in southern Chile. The 1000 km-long LOFZ controls the emplacement of volcanic centers in the Andean Southern Volcanic Zone, either directly at NS-striking parallel branches, at the intersection with NE-SW concomitant faults, or at the intersection with pre-Andean NW-SE faults, as is the case for the Villarrica Volcano (Cembrano and Lara, 2009).

The origins of the Villarrica Volcano date from Middle - Upper Pleistocene to its first caldera formation at ~95 ka (Caldera 1; 6.5 km × 4.2 km ellipsoid). Subsequently, two other caldera eruptions have shaped the actual building. A collapse of the nested structure after the glaciation (ca. 14 ka) generated the Licán Ignimbrite (10 km³), producing the Caldera 2 roughly at the same place as Caldera 1, and marked the beginning of the effusive phase of activity of the volcano. A new stratocone was formed at the NW edge of the depression, which erupted at ca. 3.7 ka, generating the Pucón Ignimbrite (~ 5 km³) and leaving a small caldera with a diameter of about 2.2 km (Caldera 3) where the present cone is located (Clavero and Moreno, 2004). Two important adventitious volcanic centers surround the Villarrica Volcano: the Grupo Los Nevados to the ENE, with volcanic fissures, trending NE, and isolated craters to the NNE; and the Grupo Challupén to the S, with fissures trending S and SSW, and isolated craters to the SSE and SSW (Clavero and Moreno, 2004).

The present edifice holds a 200 m-diameter crater with a constant lava lake of about 30 - 60 m in diameter, visible when its depth is shallow, as its free surface that oscillates between 90 and 180 m below the crater rim. This lava lake has generated constant degassing since the end of the 1985 eruption, and presents mild strombolian activity when the level of seismic activity in the volcano increases. The top of the cone and the floor of the ancient caldera depression are filled with a 30,3 km² glacier that has an estimated water equivalent volume of 1,17 km³ (Rivera et al., 2015).

Historically, the Villarrica Volcano has presented about 50 eruptions in the last 400 years. Eruptions at Villarrica usually range between effusive to moderate explosions ($0 \leq \text{VEI} \leq 3$), generating hazardous lahars due to the spatters of lava that melt the snow coverage and parts of the glacier. The estimated likelihood for a future VEI 3 eruption at Villarrica in the next 100 years is of 20%, and of >90% for an eruption of $\text{VEI} \geq 2$ in the next 50 years (Dzierma and Wehrmann, 2010; Wehrmann and Dzierma, 2011).

Two and a half hour lahar and tephra fallouts were the principal hazard in its last eruption in March, 2015 (Johnson and Palma, 2015; SERNAGEOMIN, 2015a). A paroxysmal strombolian pulse at 03:08 AM (local time) on the 3rd of March was preceded by a sustained increase in seismic activity since February (yellow alert issued). The eruptive pulse lasted ~55 min and generated lava fountains of up to 1.5 km height, and a column of gas and ashes of 6-8 km into the atmosphere (Johnson and Palma, 2015; SERNAGEOMIN, 2015a). Activity slowly decreased after three days, but remained with LP activity above background levels at least until August, 2015 (SERNAGEOMIN, 2015b).

4.3 Methods

4.3.1 Dense Temporary Volcanic Network

A dense network of 75 DSS-Cube Short-Period stations was installed at and around the Villarrica Volcano from the 1st to 14th of March, 2012 (Figure 4.1). In total, 30 3-Component stations and 45 1-Component stations covered an area of approximately $68 \text{ km} \times 68 \text{ km}$. The average station spacing was 2.3 km inside the perimeter of the volcanic edifice, and 13 km outside this perimeter. Three arrays (AVW, ACV, ALN) of five stations each were installed at the west, north-northwest and east flanks of the edifice, respectively. The rest of the stations were installed at the crater rim (three stations at $\sim 2800 \text{ m}$, one station at 2400 m ; KRA), seven at ca. 1800 m (RIN), and 24 stations around the volcano mainly following the tourist path running at ca. 1500 m height, and 20 stations remain in the surroundings. A set of five stations (WES) was installed outside the radius of the volcanic edifice in order to record events without the direct influence of volcanic activity. The main region of focus for this study is shown in Figure 4.1.b.

4.3.2 Records and First Velocity Model

The continuous record from the two weeks was surveyed with an STA/LTA (Short Term Averaging/Long Term Averaging) trigger to obtain approximated arrival times for different events. Since the amplitude and envelope of local tectonic events differ from the onset of, for example, a long period event different thresholds were used. The complete records were separated into different catalogues for local tectonic events, volcano tectonic (VT) events, long period (LP) events, and teleseismic events. An example of a VT event can be seen in Figure 4.2.

Analysis of the STA/LTA trigger along the continuous records revealed 81 volcano tectonic events primarily located at SSW, SSE, and North of the crater, with clear P- and S-wave arrivals. Another 73 events were classified as “hybrid” events (HB) that presented high frequencies at the beginning of the signal, and a sharp and notorious S-wave at the crater stations, but a strong scattering, and lower frequency content than local tectonic events, as well as elongated coda on the stations along the volcanic edifice. Several long period events (LP) with main frequencies between 2-4 Hz were also observed, but not located.

Three sets of tectonic regional events can be distinguished: one coming from the southern end of the focal plane of the Maule earthquake (2010), with an S-P wave travel time difference of ca. 30 s or more; another closer group with an S-P wave travel time difference between 10 s and 20 s, probably attributed to subduction; and the last group with an S-P wave travel time difference of $<10 \text{ s}$ attributed to crustal activity.

To the best of our knowledge there was no detailed velocity model for Villarrica Volcano at the time of performing the location of events, and therefore it was decided that a first velocity model for the volcanic area had to be created. The record of an M6.1 event on 05.03.2012 (553.9 km depth; with epicenter in Santiago del Estero, Argentina) was used along with a cross-correlation method to obtain an average velocity around the edifice. To determine S-wave velocities, a V_p/V_s ratio was calculated from P- and S- wave arrivals of VT events with an S-P time difference of less than 5 seconds. With these values, the crustal velocity model from Bohm et al. (2002) and the ISSA2000 line (Lüth and Wigger,

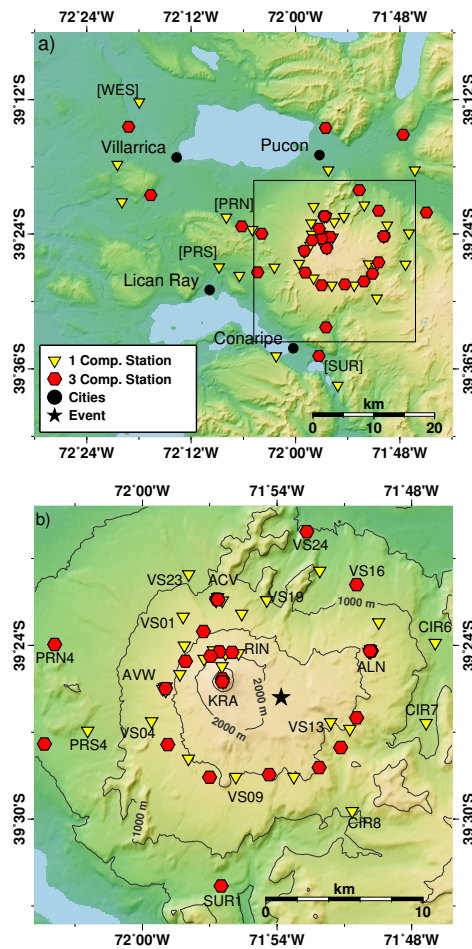


Figure 4.1: (a) Location of the 75 short period stations deployed at Villarrica Volcano during the first two weeks of March, 2012. Light gray inverted triangles show the locations of 1-Component short period stations, and dark gray hexagons show the locations of 3-Component short period stations. The major cities around the Villarrica Volcano are depicted as black circles. The black star shows the location for the waveforms of the event shown in Figure 2. The square inlet shows the area of study. (b) The zoomed area showing a detail of the three arrays (AVW, ACV, and ALN) of stations, as well as the KRA stations at the crater, the RIN stations at 1800 m.a.s.l., the stations around the tourist path numbered VSXX from 01 to 24 counter-clockwise (some of them shown for reference), and the stations in the surroundings of the volcanic edifice.

2003) were adjusted accordingly.

4.3.3 Event Location and Selection

With this first velocity model, 81 VT events were located using SEISAN (Havskov and Ottemoller, 1999) with picks for P-wave arrivals and S-waves when visible. A selection of “best events” was obtained following these criteria for each event: 1) clear signal and a fair amount of noise that did not distract from the arrival of a P-wave; 2) if possible, S-wave arrival time clear and visible; 3) readings in more than 20 stations; 4) stations present a 220° gap maximum; and 5) an RMS lower than 0.3 s. From this

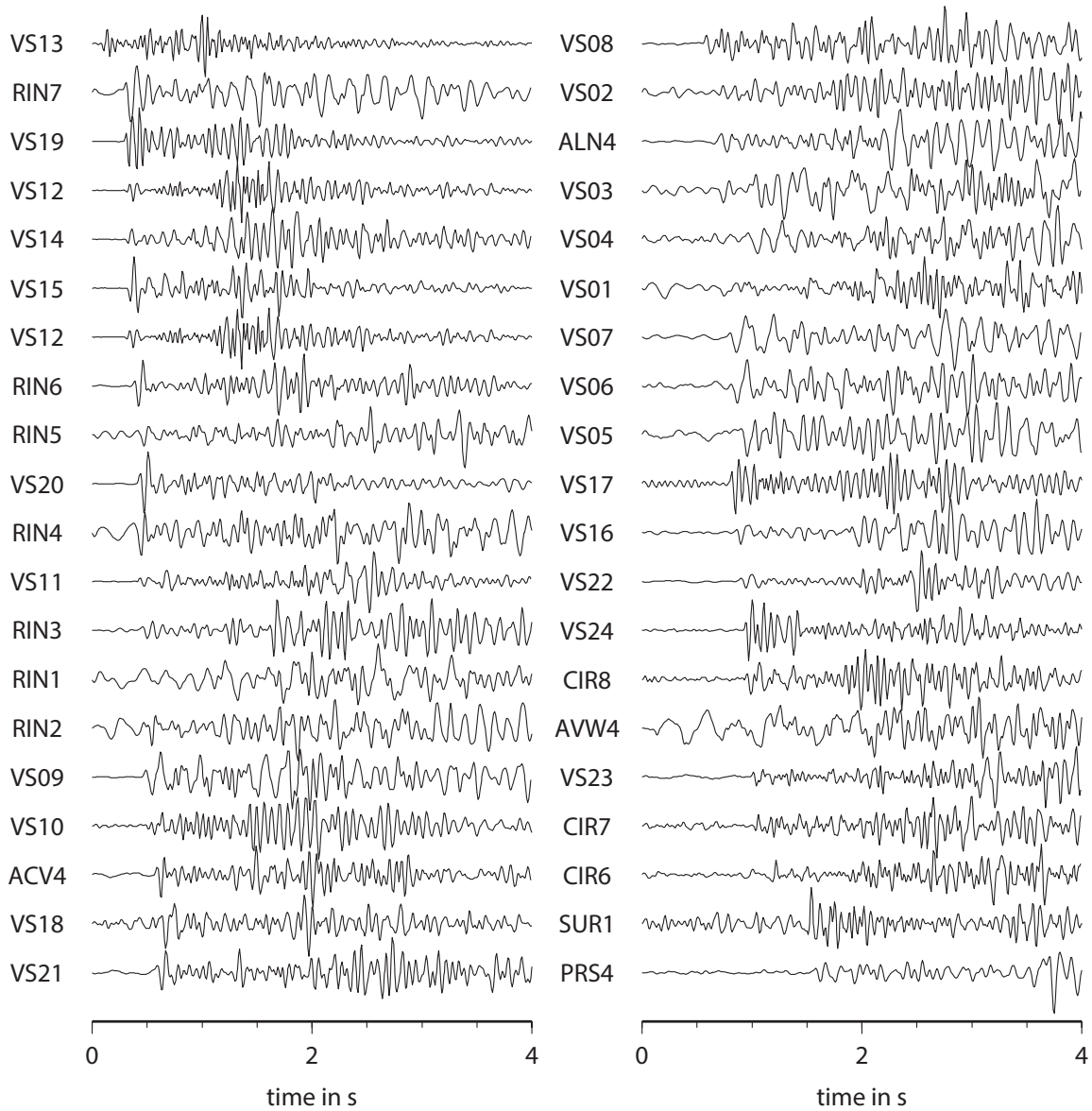


Figure 4.2: Example of records for a VT event on March 9, 2012 at 11:08:09 UTC, filtered between 0.1 - 10 Hz. The epicenter of the event is represented by a black star in Figure 4.1. The stations are arranged from top to bottom in order of wave arrival.

selection, 38 events remained and are the ones presented throughout this work.

Prior to the tomography, these 38 events were relocated using a grid search moving 0.2 km in each direction (x, y, z) and 0.2 s in origin time (t_0), with every 0.5 km/s variation in velocity between 3.0 - 7.0 km/s.

4.3.4 P-wave Tomography

To avoid artefacts from having a ray concentration towards the arrays, the station with the lowest residual from each array in each event was selected prior to running the model. Starting from a constant background velocity and the 38 hypocenters obtained from the grid search, a $25 \text{ km} \times 25 \text{ km} \times 10 \text{ km}$ model, constructed with blocks of 1 km length in every direction ($1 \text{ km} \times 1 \text{ km} \times 1 \text{ km}$), was resolved with straight-ray damped least-squares inversion in Python.

We found ray bending to be negligible due to small variations in velocity. Ray trajectory by computation of the 2D Eikonal equation can be seen in section B.3).

As result from the inversion, in each block the absolute velocity, as well as the percentage of velocity variation were calculated. For reliability the number of rays per block was also calculated. Using the Bootstrap method (see 4.5.1 and B.1 for detailed results and explanation), the bootstrapped tomography from hundred runs was obtained, and the Standard Deviation of the velocity per cube with respect to the mean cube velocity was calculated.

4.3.5 Focal Plane Solutions

Focal plane solutions were calculated reading P-wave polarities as input for the FocMec routine (Snoke et al., 1984; Snoke, 2003) in SEISAN. Given a certain angle of search, the program examines the family of planes solutions that fit the input provided in the focal sphere, and returns the solutions in written or graphic mode. For this study, a first search was obtained within a 20° search, and then refined between 10° and 5° search (2° when possible).

4.3.6 Checker-Board Test

As a robustness and resolution test for our method, a Checker-Board Test was performed using the same events as in the tomography, in a model with blocks of $3 \text{ km} \times 3 \text{ km} \times 3 \text{ km}$ with alternating velocities of 4 and 5 km/s. Different cube sizes were tested (0.5 km, 1 km, 2 km, 3 km and 5 km), and from visual inspection, 3 km was the minimum size that satisfactory resolved the synthetic model. Figure 4.3 shows an example of the resolution, which seems to resolve the edges of anomalies fairly well, with some smearing in regions where the ray coverage is not so dense. Anomalies are resolved better in terms of intensity in regions where seismic events are close.

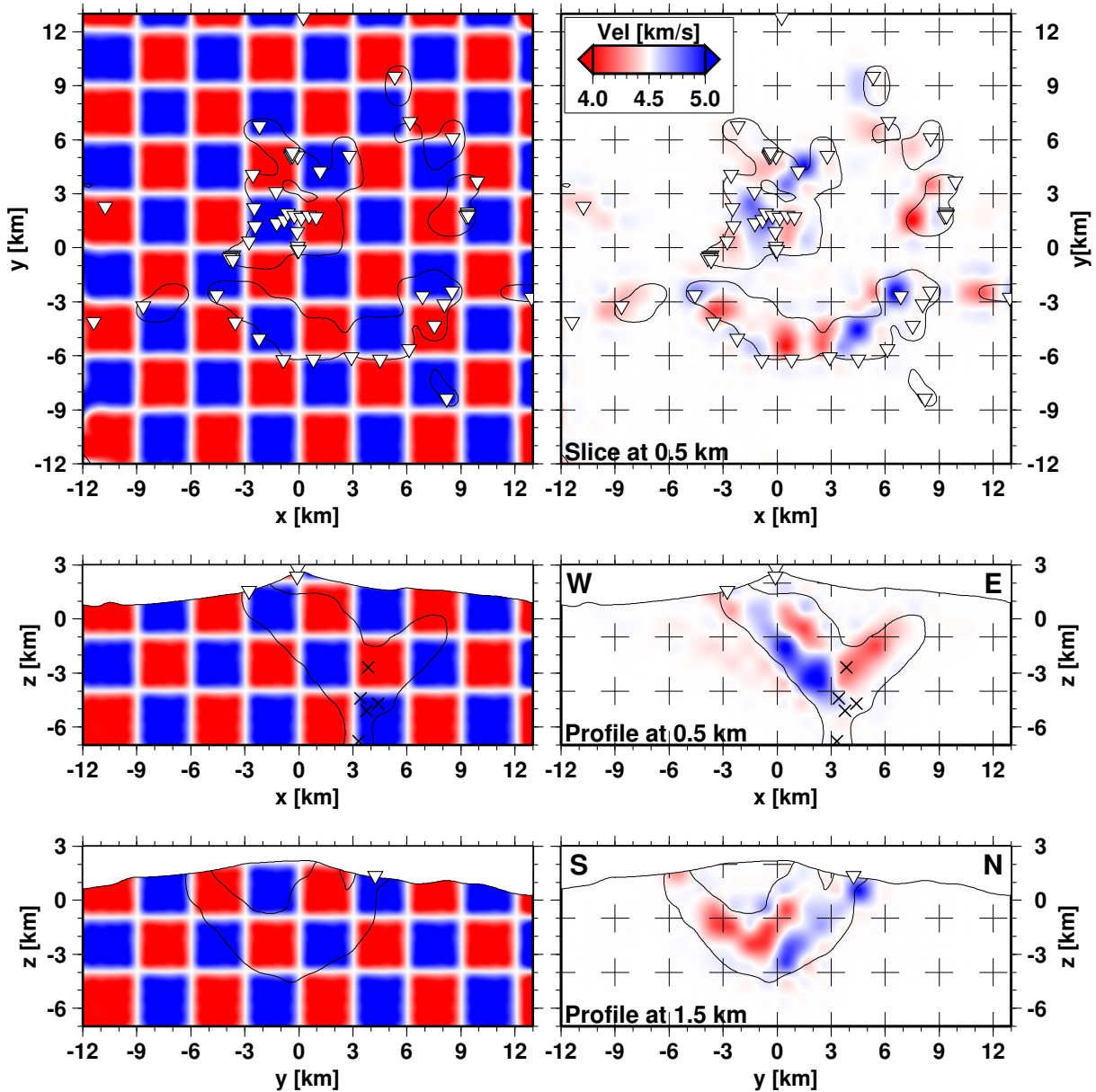


Figure 4.3: Resolution of synthetic model (Checker-Board test) with 3 km wide cubes with velocities of 4 km/s (red) and 5 km/s (blue), for 0.5 km above sea level (top), EW profile at 0.5 km east (middle), and NS profile at 1.5 km north (bottom). The thin black lines show the contour of the clipping mask in actual inversion results, showing only areas with more than 10 rays per cube. The white inverted triangles show station locations.

4.4 Results

4.4.1 Medium Velocity from Delay in Arrival Times from Teleseismic Events and Wadati Diagrams

A cross-correlation analysis was applied to the travel times of the regional events and a teleseismic event from Argentina to determine the average velocity structure of the volcano. The best model is a 6.5 km radius cylinder centered at the crater, with a constant velocity of 3.6 km/s inside the cylinder and 4.1 km/s for the surrounding area outside this radius.

Calculations of Wadati diagrams were performed using events with P- and S- waves picked, obtaining an average V_p/V_s ratio of 1.74 ± 0.19 . Examples of these Wadati plots are shown in Figure 4.4. With these values, the regional velocity model from Bohm et al. (2002) and the ISSA 2000 active lines (Lüth and Wigger, 2003) were adapted, leaving a top velocity of 3.6 km/s for the volcano edifice, and velocities between 4.9 and 6.7 km/s for the uppermost part of the continental crust. The model was not modified below 50 km (Figure 4.5).

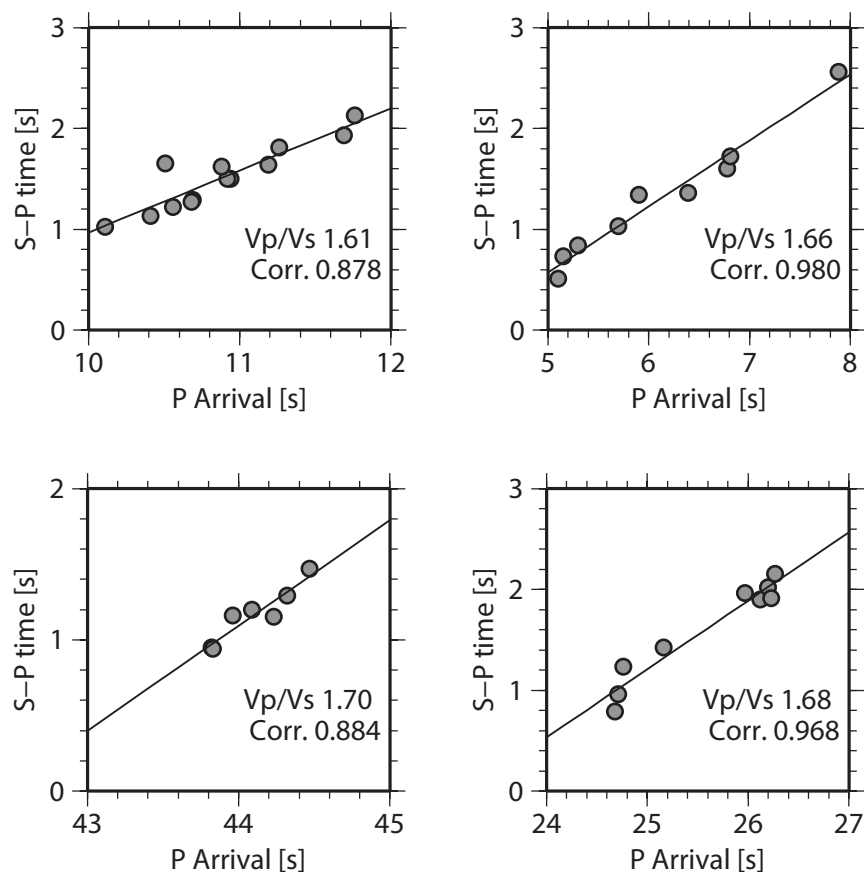


Figure 4.4: V_p/V_s ratios for four events from the final selection. P-arrival time is only referential.

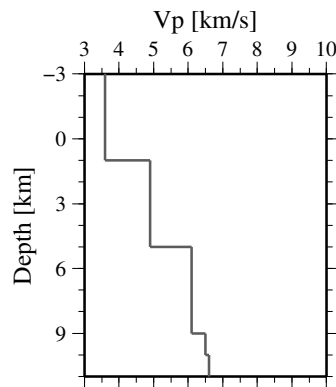


Figure 4.5: Initial velocity model adapted from Bohm et al. (2002) and Lüth and Wigger (2003) after obtaining a regional velocity through cross correlation of a magnitude M6.1 teleseismic event from Argentina.

4.4.2 Earthquake Database

After performance of STA/LTA trigger, and relocation using a grid search, the final locations of volcano tectonic events were focused between 1 and 7 km depth, with 33 of them forming an almost vertical NS trending volume between 2 and 5 km depth at approximately 4 km east of the crater. Only a few isolated events fell outside this volume in directions ESE, SSE, and ENE from the crater, at depths of 1-5 km, 2-7 km, and 7 km respectively (Figure 4.6).

4.4.3 Tomography

From the total volume studied, (25 km × 25 km × 10 km), the inversion provided resolution down to 5.5 km in depth and up to 1.5 km a.s.l. Horizontal (Figure 4.7) and vertical profiles (Figures 4.8 and 4.9) were portrayed at every one kilometer crossing the middle of the 1 km cubes. Given the ray distribution, most of the information of the tomography is visible between 1.5 km south and 7.5 km north of the crater, and between 4.5 km west and 3.5 km east of the crater. For future reference the model is centered at the crater; therefore all distances mentioned in the text, unless otherwise stated, are with respect to its following the distances from the profiles.

Variations in velocity percentage ($\Delta V/V$) go down to -7% and up to 9%. From the profiles and horizontal slides, two strong and one weak low velocity anomaly can be observed. The main low velocity region is a SE dipping structure that goes from 0.5 km to the east of the crater at 4 km depth, up to 1.5 km (1.8 km for the RIN stations) at 1.5 km NW of the crater. It is 3 km wide at its deepest part and it widens to ~6 km below the crater. A block of high velocity approximately 1 km wide is “floating” at this low velocity anomaly between -1 km and 1 km altitude. A less strong, pipe-like, low velocity anomaly runs for a bit less than 3 km, starting at close to 4 km depth at the locus of seismicity going towards the surface at Array Los Nevados (ALN). It has an average width of ~3 km and is obstructed by a high velocity wedge, 2 km wide, between 3.5 and 5.5 km west of the crater, to reappear as a strong anomaly at 0.5 km depth, 8.5 km west of the crater. A much weaker low velocity region can be observed at the southern flank of the volcano, between stations VS04 and VS11, ascending from a depth of 3 km and reaching up to a 0.5 km depth. Its easternmost part is slightly stronger, and has a width of ~2 km.

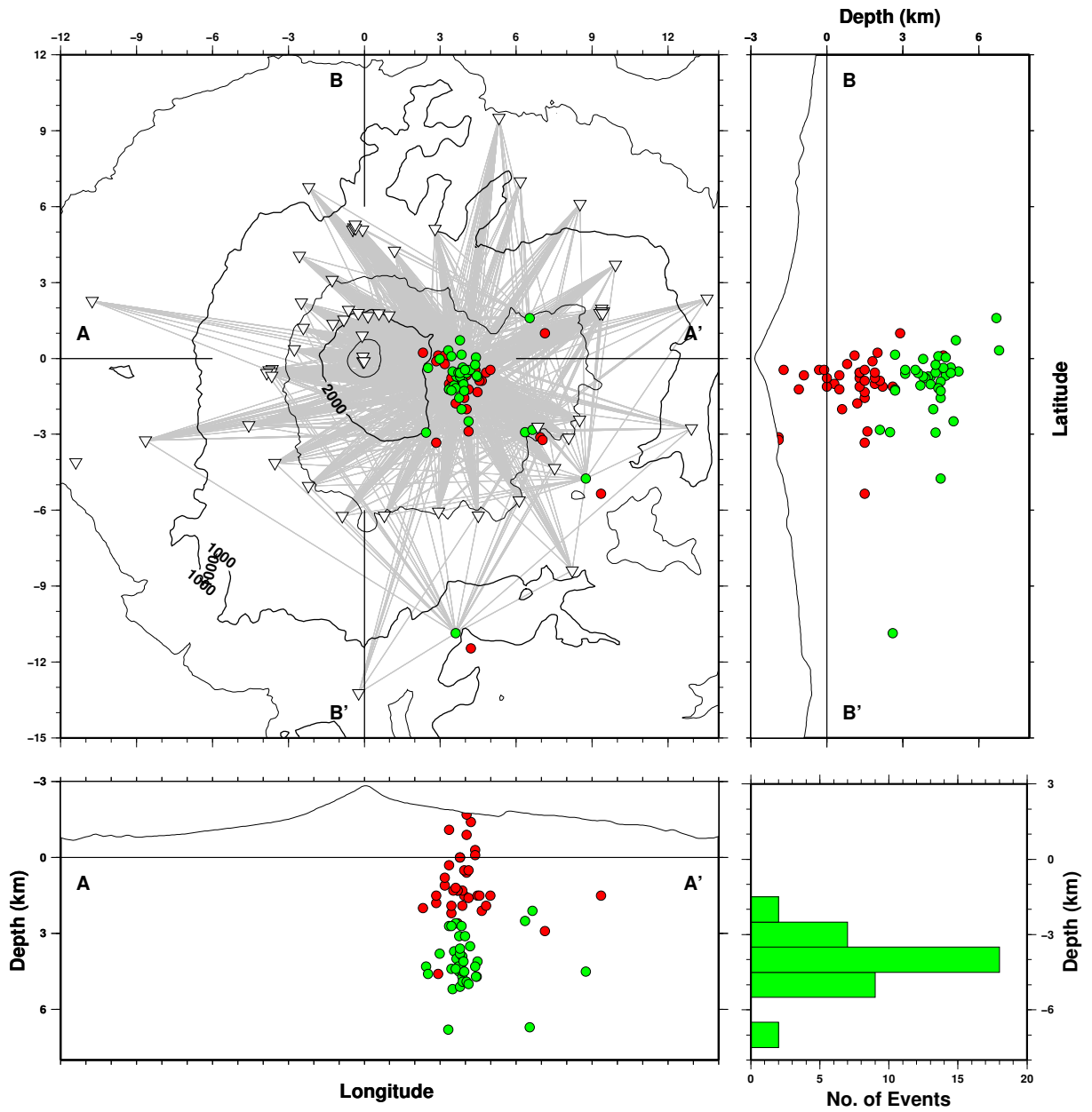


Figure 4.6: Location of the events in SEISAN (red circles) and after grid search (green circles). Raypaths from the final locations to the stations are marked as gray dotted lines.

Small patches of high velocity anomalies are observed surrounding the low velocity anomalies. Small patches are visible 4-6 km north of the crater at 0.5 km a.s.l. close to the ACV array, and between 6 to 9 km to the east of the crater, beneath stations VS13 to VS16. A much stronger higher velocity anomaly is observed underlying the main low velocity region at an angle of $\sim 45^\circ$ between 6-9 km west of the crater, starting at the locus of seismicity and reaching the surface at the west. One main high velocity anomaly is observed as a wedge-like structure starting at the cluster of seismicity and stretching towards the NE ascending up to 1 km a.s.l. at 7-8 km east of the crater. Its strongest intensity is located between 4.5 and 5.5 km east of the crater, and reaches an estimated maximum width of ~ 6 km to the ENE of the crater.

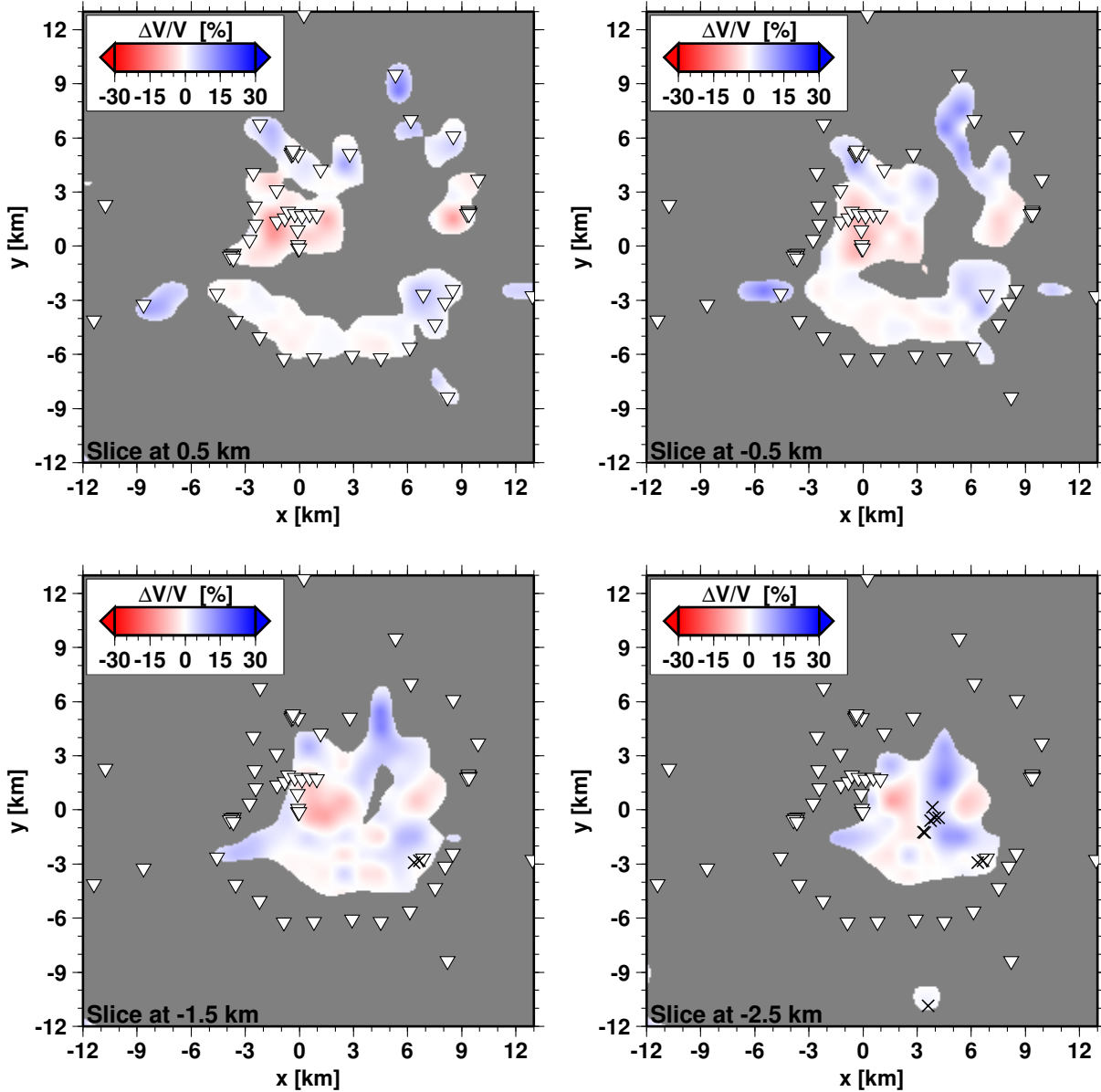


Figure 4.7: Velocity variation results for horizontal slices every kilometer, passing through the middle of the 1 km^3 cubes of the model. Positive is above sea level; negative is below sea level. Obscured areas represent cubes with less than 10 rays of information. For detailed information on the number of rays per cube, and standard deviations, see Section B.4.

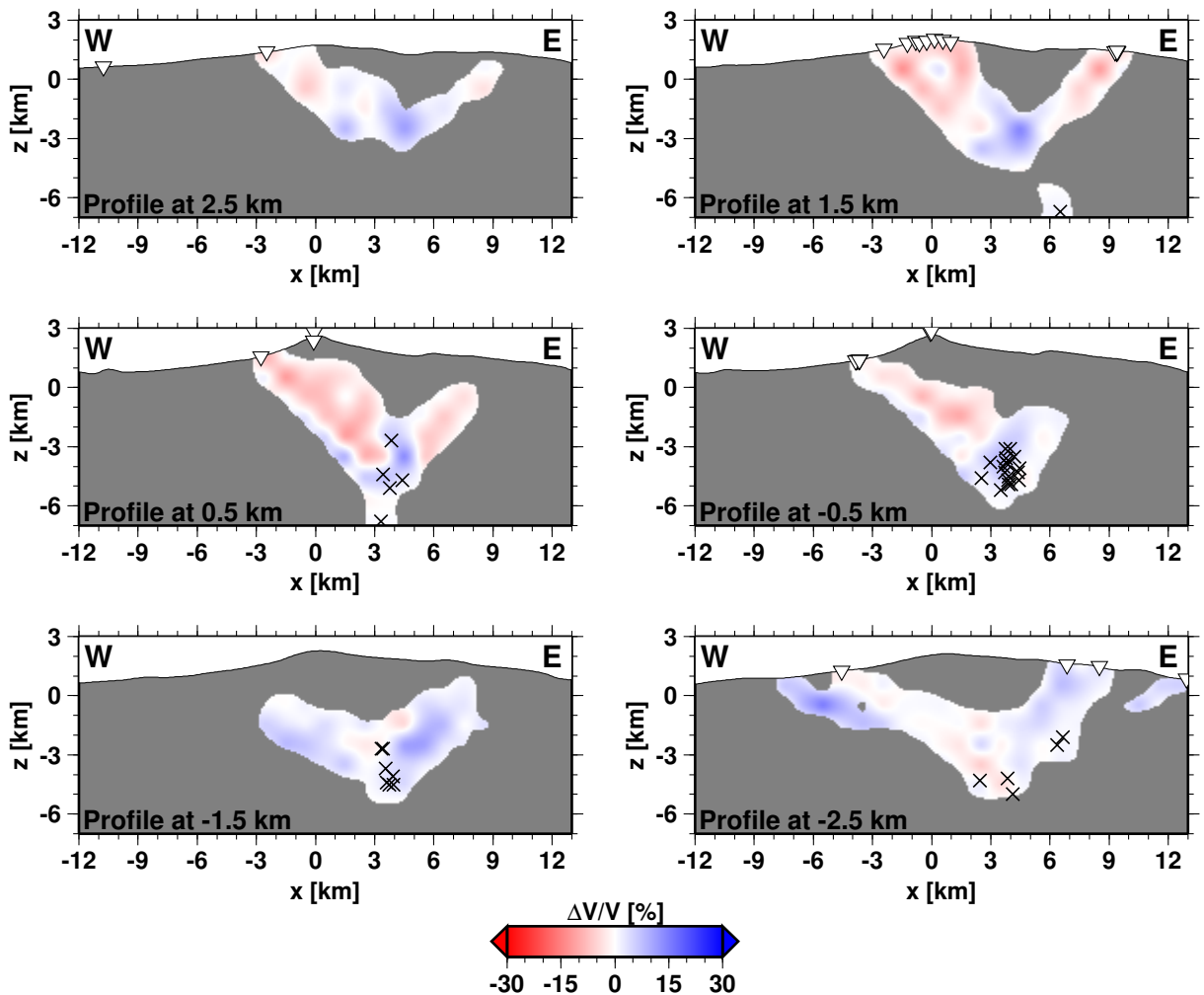


Figure 4.8: Velocity variation results for vertical East-West profiles every kilometer, passing through the middle of the 1 km³ cubes of the model. Positive are kilometers to the west of the crater; negative is those to the east. Obscured areas represent cubes with less than 10 rays of information. For detailed information on the number of rays per cube and standard deviations, see Section B.4

4.4.4 Focal Plane Solutions

A set of 15 focal plane solutions was obtained (Figure 4.13) with misfits of less than two polarities. On average, 66% of the P-wave arrivals read in the event were used in the construction of its focal mechanism. The highest error in the mechanism calculation is 12.5% for event 3 (see Figure B.1). Events deeper than 4 km show preferentially normal faulting mechanisms with strikes between 207° and 327°, with the exception of one sinistral strike slip mechanism with a strike of 300°. For events between 3 and 4 km depth, both normal and thrust faulting mechanisms with a visible strike slip component are observed, and one of the solution planes follows either the strike of the LOFZ, or the strike of the VQL lineament. Shallower events (above 3 km depth) show sinistral strike slip focal mechanisms with main planes roughly following the VQL lineament. One of these shallow events presents a thrust faulting mechanism with main solution planes in the strike of the LOFZ.

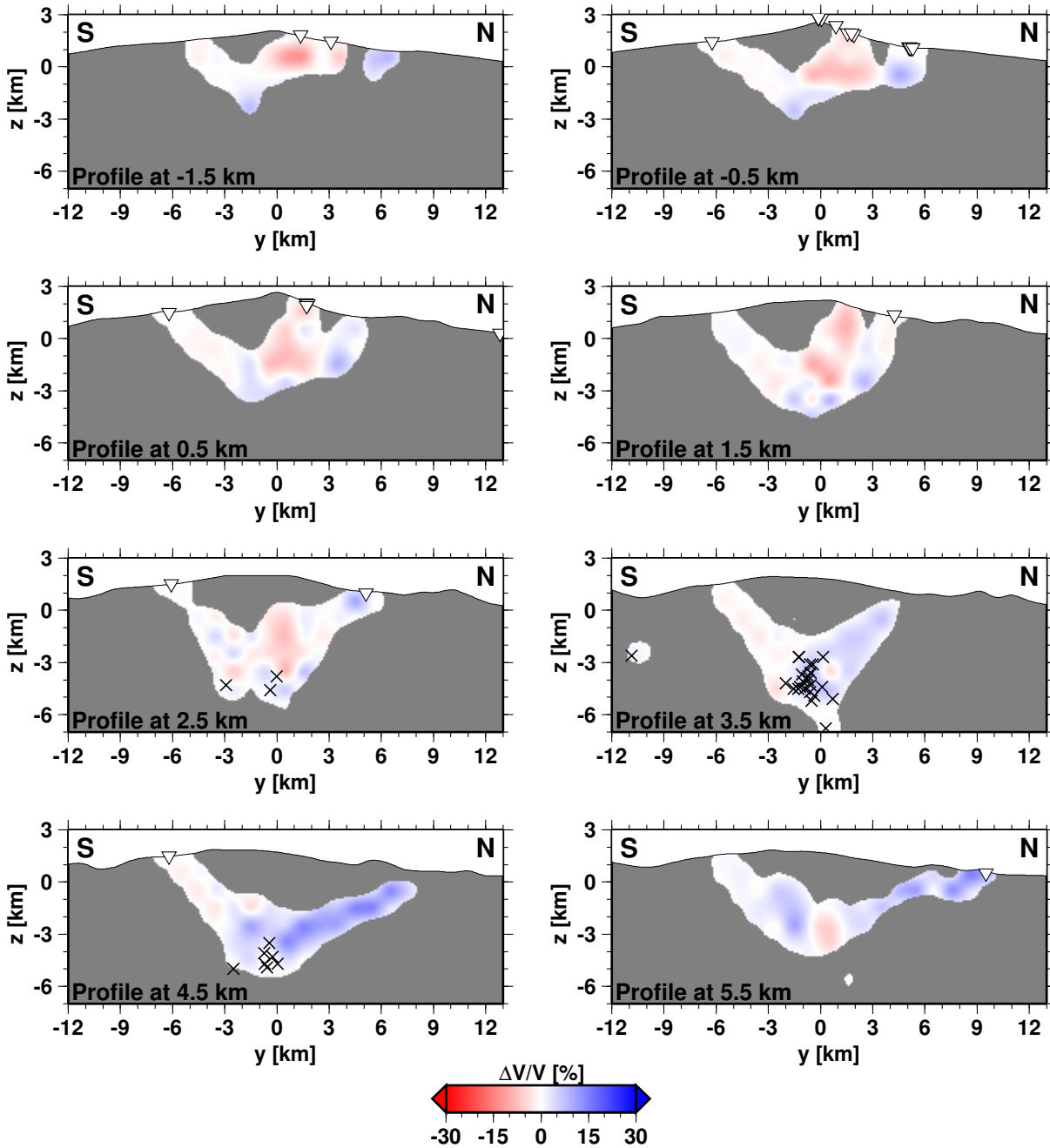


Figure 4.9: Velocity variation results for vertical North-South profiles every kilometer, passing through the middle of the 1 km³ cubes of the model. Positive is kilometers to the north of the crater; negative is those to the south. Obscured areas represent cubes with less than 10 rays of information. For detailed information on the number of rays per cube and standard deviations, see Section B.4

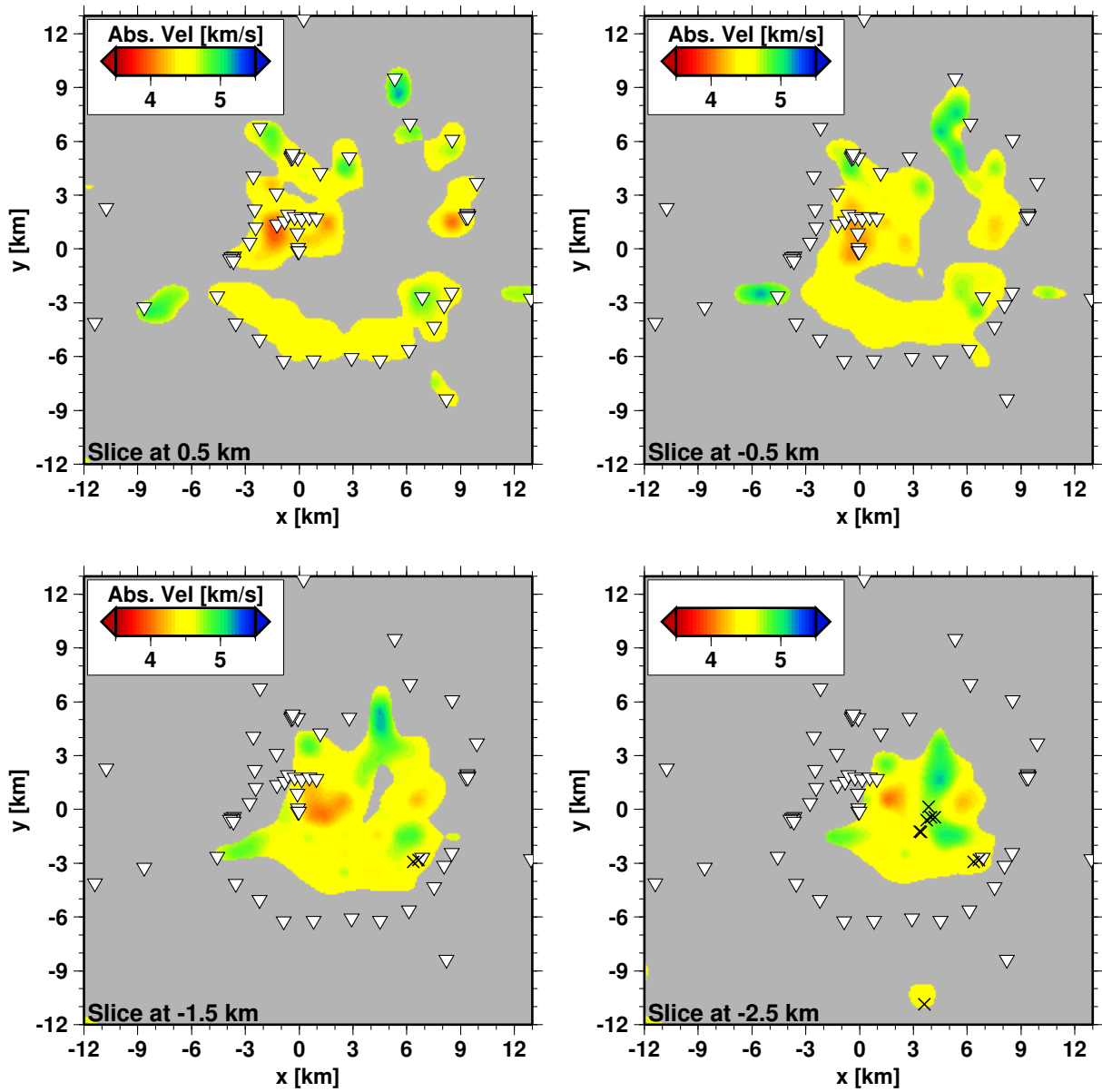


Figure 4.10: Absolute Velocity model results for horizontal slices every kilometer, passing through the middle of the 1 km³ cube of the model. Positive is above sea level; negative is below sea level. Obscured areas represent cubes with less than 10 rays of information. For detailed information on the number of rays per cube and standard deviations, see Section B.4.

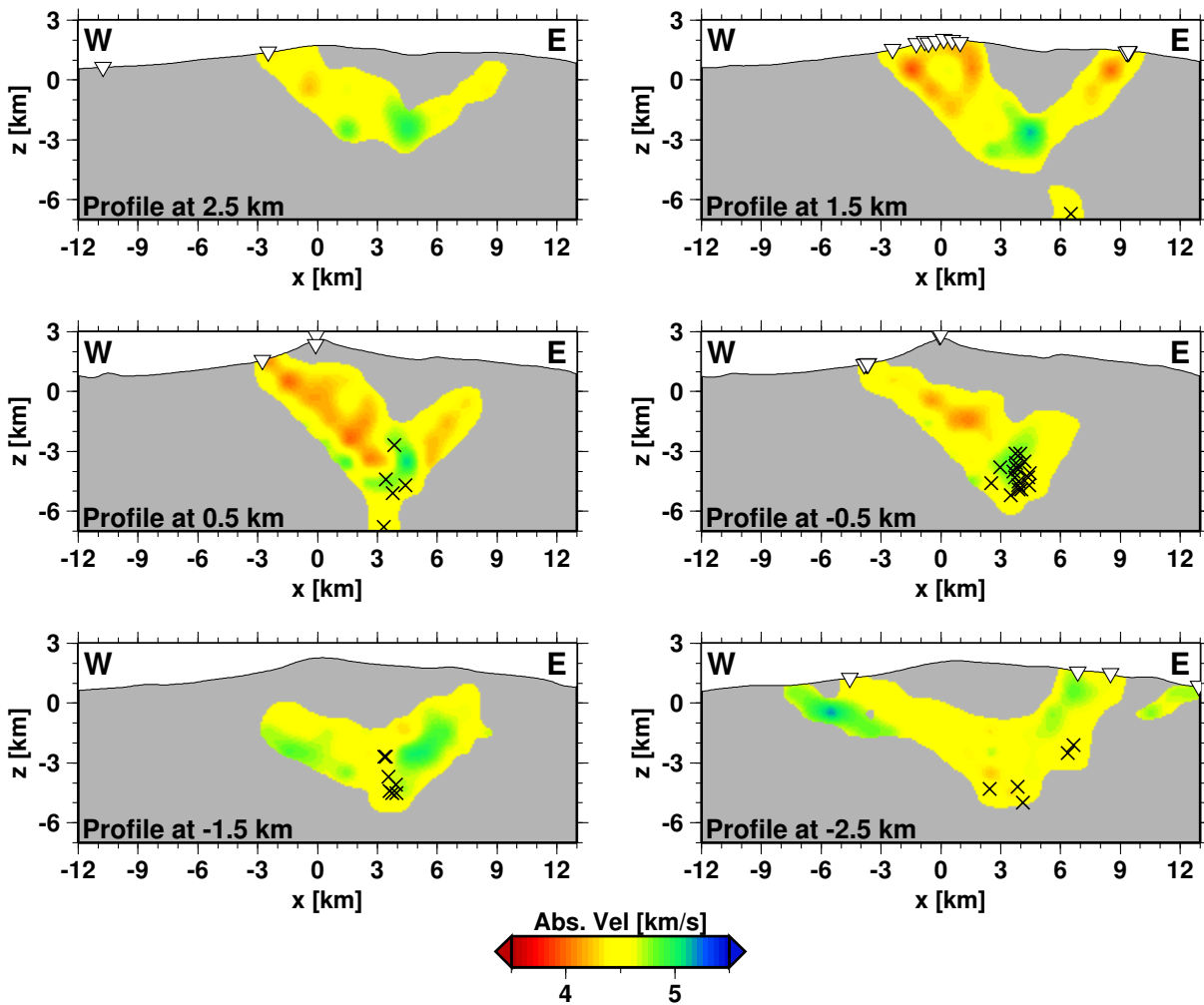


Figure 4.11: Absolute Velocity model results for vertical East-West profiles every kilometer, passing through the middle of the 1 km^3 cubes of the model. Positive are kilometers to the west of the crater; negative is those to the east. Obscured areas represent cubes with less than 10 rays of information. For detailed information on the number of rays per cube and standard deviations, see Section B.4

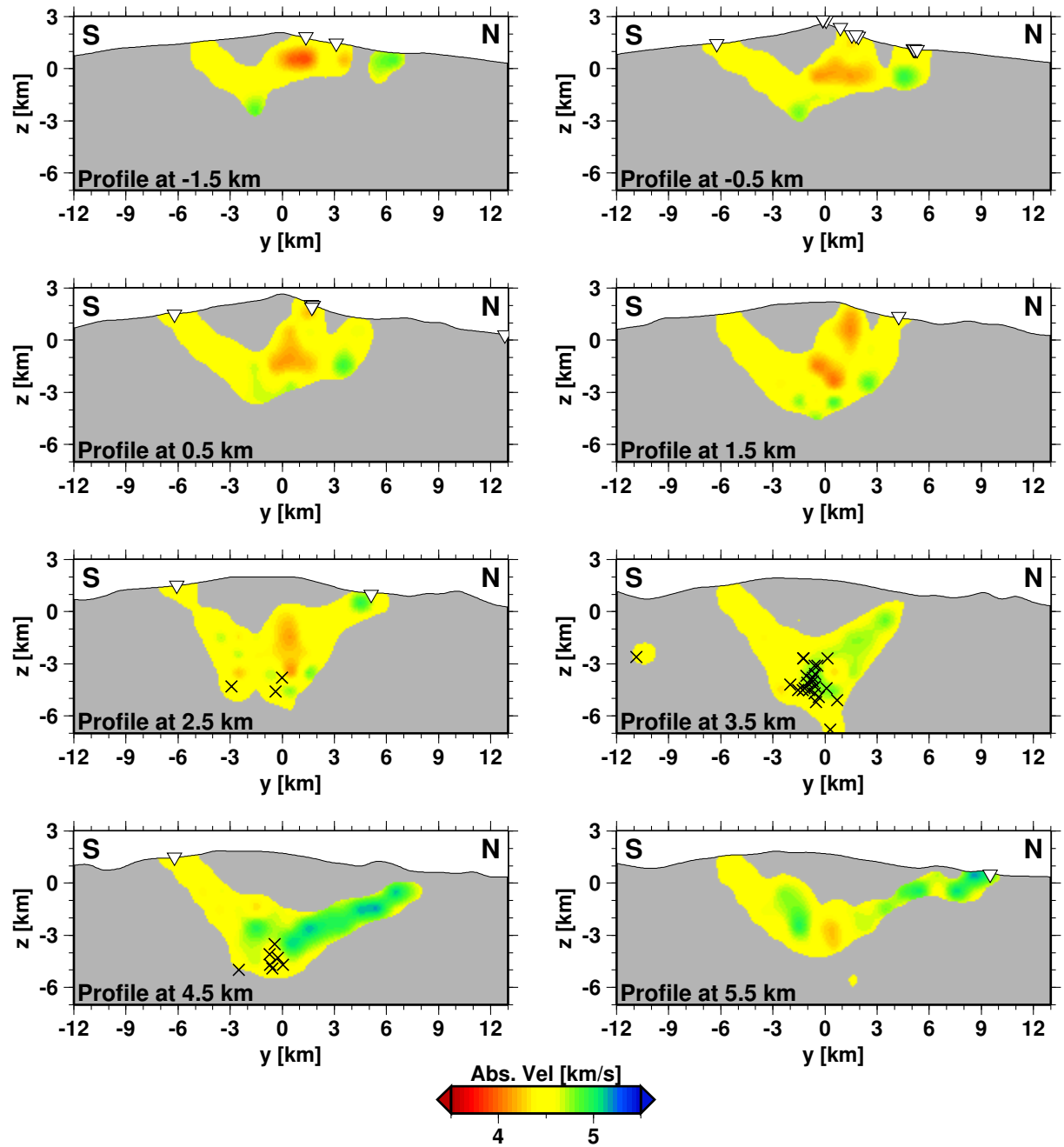


Figure 4.12: Absolute Velocity model results for vertical North-South profiles every kilometer, passing through the middle of the 1 km^3 cubes of the model. Positive is kilometers to the north of the crater; negative is those to the south. Obscured areas represent cubes with less than 10 rays of information. For detailed information on the number of rays per cube and standard deviations, see Section B.4

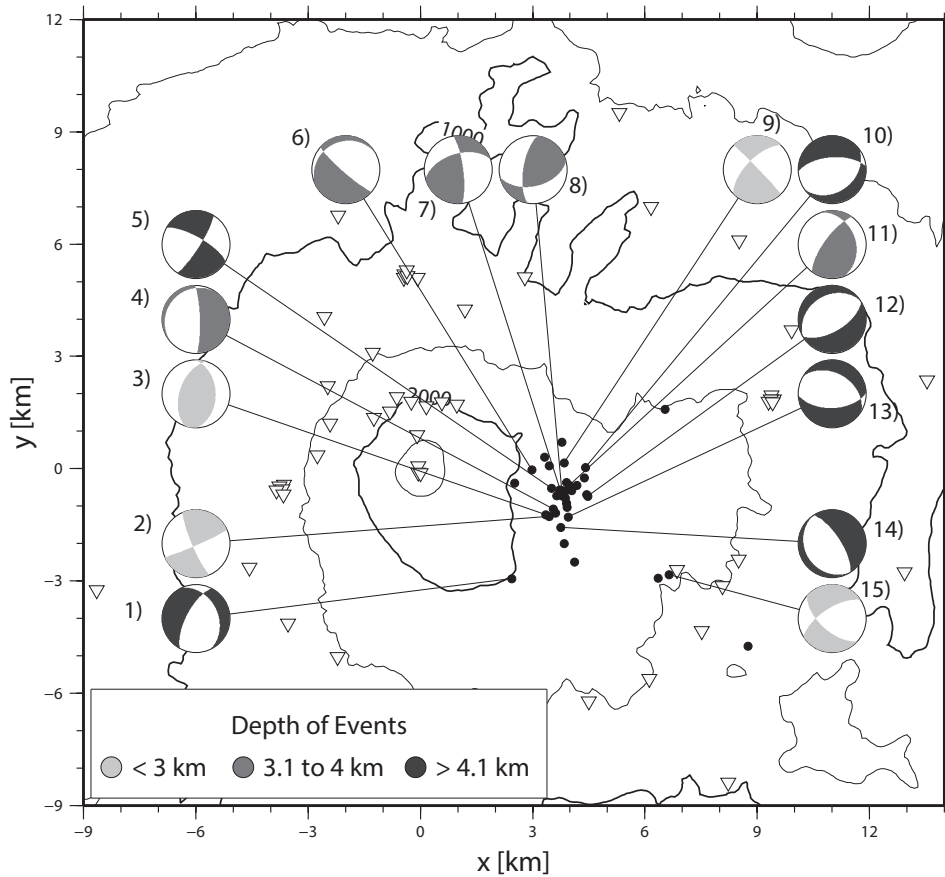


Figure 4.13: Focal mechanisms for some of the events used in the tomography. Compressional part is color coded according to depth: light gray for shallow events (less than 3 km depth), gray for events between 3 and 4 km depth, and darker gray for events deeper than 4.1 km depth. Focal plane solutions were obtained through P-wave polarity picking and the FocMec routine in Seisan. Polarities can be checked in Figure B.1 in Appendix B.2.

4.5 Discussion

4.5.1 Methodological Errors and Robustness

The Picking error for P- and S- waves is estimated to be around 0.05 s. The RMS residual of 0.16 s after performing the grid search drops to 0.13 s after performing the tomography.

We performed the Bootstrap Method (Efron, 1979) to estimate the standard errors of the model. The Bootstrap method consists in calculating a certain estimator for random subsamples of a population a large number of times. Usually the size of the subsample corresponds to the 63% of the population, which is the average number of distinct observations in each sample (Efron, 1983). A more detailed description of the method can be found in Appendix B.1.

In this study, we used subsamples corresponding to the 63% of the total population of 38 events, and ran the bootstrap 100 times for the sake of the time. The average velocities from the 100 runs using the Bootstrap Method are very similar to those found with the actual inversion (Table 4.1).

Table 4.1: Comparison of results of velocity values, and percentage of variation of velocities for single-run tomography, and the values from the average velocity of 100 runs of Bootstrapped Tomography.

	Single-Run Tomography	Bootstrapped Tomography
Min. Vel. [km/s]	3.93	3.97
Min. $\Delta V/V$ [%]	-13	-12
Max. Vel. [km/s]	5.17	5.18
Max. $\Delta V/V$ [%]	15	15

The standard deviation per cube (σ_i) was calculated with respect to the average velocity from 100 runs for that cube (\bar{v}_i). Since the standard deviation is zero when no rays are passing through the cube, the minimum and mean values in Table 4.2 consider only non-zero values. The maximum deviation in results is 7%, which corresponds to a standard deviation of 0.275 for a velocity of 4.19 km/s. The values shown in Table 4.2 indicate that the results are highly stable, which suggests that the data used is sufficient to obtain a good model of velocity structure.

Table 4.2: Standard Deviation per cube (σ_i) and Central Deviation (σ_i/\bar{v}_i) values for bootstrapped tomography using 100 runs with 63% of the events of the main sample (38 events).

	σ_i [km/s]	Central Deviation
min	0.008	0.002
max	0.275	0.066
mean	0.064	0.014

4.5.2 Comparison of the First Velocity Model

A reasonable velocity model is crucial for locating seismicity accurately. As there is no known velocity model in the literature for the Villarrica Volcano, authors have needed to create one according to their

requirements. Richardson and Waite (2013) tested five homogeneous velocity structures to validate synthetic LP seismograms in order to model the horizontal force source-time function responsible for the infrasonic signals at the top of the Villarrica Volcano. Constant values of 2400 m/s for V_p and 902 m/s for V_s were chosen after higher velocity models caused greater misfits in time differences at the stations, and lower velocities generated significantly contrasting mechanisms to those of the other models.

Velocity values near the summit of the edifice of other volcanoes are similar to the one suggested by Richardson and Waite (2013), such as 2.5-3.0 km/s for Popocatepetl (Berger et al., 2011), 2.7-3.4 km/s for Tunguragua (Molina et al., 2005), and 2.7-2.8 km/s for Redoubt (Benz et al., 1996). These studies show velocities closer to our first velocity model, in which values of V_p from the top of the edifice, and down to a depth of 5 km, range between 3.0 and 6.5 km/s (Lees, 1992; Kuznetsov and Koulakov, 2014; Berger et al., 2011; Molina et al., 2005) supporting the distribution from both the first velocity model and the background velocity for the running of the model.

4.5.3 Interpretation of Seismicity and Tomography

The main cluster of seismicity is focused at depths between 3 and 5 km, and extends 4 km in both the EW and NS directions. It clearly marks a NS strike in the EW profiles that is consistent with the LOFZ, as well as its location, as can be confirmed with a geological map (Moreno and Clavero, 2006). The few isolated events observed can be interpreted as other sources of shear movement most probably related either to the VQL lineament or to the LOFZ.

Focal mechanisms for events below 4 km show extension, which could indicate an opening for magma ascent, and thus mark a limit between two possible magma chamber locations. The events above 4 km have an inconsistent direction of strike in their focal mechanisms, showing mainly planes in the directions of LOFZ at depths between 3 and 4 km, but also in the direction of the VQL chain. This could be due to the swarm-like nature of the fragile volcano seismic activity, interpreted as changes in the stress due to the passing of fluids through small dikes connecting sources of magma. Villarrica Volcano is located at the intersection of the NS LOFZ with the NW-SE left-lateral strike slip inherited basement structure on which the VQL chain is superimposed. Then, even if the present stress regime were compressive at this site, the VQL chain would need supralithospheric stress to reactivate its activity (Cembrano and Lara, 2009), and the ascending magma could reactivate small faults in all directions in this highly fractured region.

One strong low velocity region going from the cluster of seismicity (4 km depth) and ascending in a NNW direction towards the crater has a maximum width of ~ 6 km at 0-1 km a.s.l. and can be interpreted as the possible location of a shallow magma chamber with its influence in the vicinity. It is shown as an inverted cone on the profiles, but this could be an effect from the ray paths. It most likely has an oblate ellipsoidal shape at its widest part below the crater, and is U-shaped at the shallowest parts, to the NNW of the crater.

For the pipe-like structures, the second strong low velocity region going NE from the cluster is interpreted as a remnant conduit/dike responsible for the surface features of Los Nevados' adventitious pyroclastic cones (>2600 AP). Geothermal activity in the vicinity (Termas Palguín) might indicate an extension of the conduit, or another branch that is not resolved with our distribution. The weaker low velocity region at the south part of the volcano coincides with the location on the surface of the Challupén

Group (also adventitious pyroclastic cones). Its variation is very small, and therefore no surface feature directly associated with this pipe-like structure is visible. It is therefore interpreted to be an aborted or consolidating conduit of that group.

The cylinder-like high velocity region, 2 km long and 1 km wide, surrounded by the wider low velocity region located beneath the crater, is explained as part of old amalgamated deposits from either the western edge of Caldera 1-2, or the chamber (or part of it) from Caldera 3 inside the molten magma of a present chamber, or fluids passing around it. This phenomenon has been observed at Kilauea Volcano by Rowan and Clayton (1993), and is a stable feature in other studies in Hawaii, interpreted as magmatic complexes where dense magma sets at a high pressure place surrounded by dikes that progressively expand with time. It can also be explained as old consolidated deposits in either a partially molten zone or in the presence of fluids or gases (Lees, 2007).

Three other small patches of high velocity anomaly observed to the north, west, and east of the crater are interpreted to be the surrounding crust or consolidated edifice walls. The patch at 4-6 km north of the crater is visible and has a high velocity inclusion in the void of the U-shaped cut of the magma chamber at 0.5 km a.s.l. On the surface, this feature is close to the location of the ACV array “Cuevas Volcánicas” which has the steepest descending path for lavas and other products. Similarly, the composition of the region between 6 to 9 km to the east of the crater, close to station VS13, is also consistent with lavas at the surface. The area to the west of the crater (6 to 9 km) shows a strong positive variation and a well-defined 45° angle towards the east, down to the locus of seismicity that wraps around the lower velocity region above.

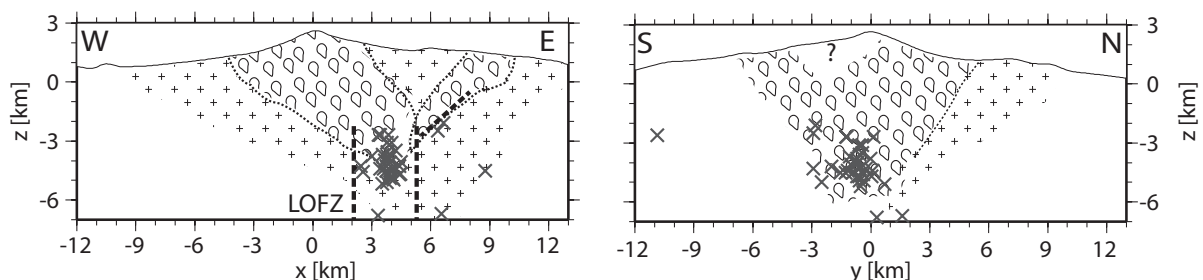


Figure 4.14: Conceptual model derived from variations in velocity, for the West-East profile (left) and North-South profile (right). Low velocity areas are demarcated with a blob pattern, while faster velocity areas are marked with a pattern of small crosses. Dotted lines mark limits between these areas. Bold dashed lines show the location of the LOFZ. Bold gray x's mark hypocenters. The zone demarcated by a question mark had no resolution.

4.5.4 Other Studies at Villarrica Volcano

Most of the research concerning the Villarrica Volcano is focused on past eruptions (Casertano, 1963; Clavero and Moreno, 2004; Silva Parejas et al., 2010) and degassing (Witter et al., 2004; Bredemeyer and Hansteen, 2014; Shinohara and Witter, 2005; Sawyer et al., 2011). While there are some interdisciplinary studies involving seismicity (Muñoz et al., 1990; Ortiz et al., 2003; Calder et al., 2004; Palma et al., 2008), there are only a few studies concerning the deeper structure of the crust in latitudes near the Villarrica Volcano (Muñoz et al., 1990; Brasse and Soyer, 2001; Delgado, 2012), and to the best of our knowledge, no seismic tomography studies.

Our results are in agreement with the low resistivity ($35 \Omega\text{-m}$) zone found at a depth between 2 and 4 km in the interdisciplinary magnetotelluric study of Muñoz et al. (1990), even though the authors considered it to be non-conclusive. The value found corresponds to igneous rocks of intermediate composition, which is consistent with the maximum intensity of the low velocity region and the depth at which our results show them to be. Pipe-like structures are also recognized to the east and south as small bodies accompanying a bigger isolated anomaly under Villarrica in the aeromagnetic study of Delgado (2012). A 20 km -diameter positive anomaly of 1500 nT under Villarrica was observed, following the NW-SE trend of the VQL lineament. The dimensions of this anomaly could be related to the ancient intrusive responsible for the generation of Caldera 1, which has been amalgamated with intrusions from more recent eruptions (Delgado, 2012), and thus generates a combined signal in which the size(s) of present magma chamber(s) cannot be differentiated. It is difficult to draw conclusions from the results found with gravity and magnetotellurics due to the small density contrast of near-surface magmas that are difficult to separate from background anomalies, and also because high temperature magmas present no magnetic contrast with respect to the country rock and/or generate a magnetically noisy region within which it is difficult to pinpoint anomalies (Marsh, 2015).

A model for reservoirs with 6 BB-stations around the volcano was proposed, after a study of the volcanic and regional seismicity performed between December 11, 2001 and January 23, 2002, in the seismotectonic study done by Hermosilla Pineda (2008). The model, which is based on the location of the seismicity, contains two lacoliths in a SW-NE direction of 8 and 12 km of lateral extension at 5 and 2 km depths, respectively under Los Nevados group. These lacoliths are thought to be connected through dikes on their west edges and, from them, to a feeding dike at a 6-7 km depth providing magma from the deeper reservoir. The largest lacolith reaches the Huelemolles Volcano, which is outside the boundaries of our inversion model. Our results agree with a structure that is about 2 km wide and is responsible for the extrusion of the Los Nevados group, but we can only account for a 7 km long structure and the direction of this shallower structure. A second structure below the one previously mentioned is not visible through our model.

Studies of LP events and infrasound done by Richardson and Waite (2013), Richardson et al. (2014) and Goto and Johnson (2011) describe different characteristics of the geometry of the uppermost part of the conduit. The crater rim is the antinode of a Bessel horn structure that is the conduit (Richardson et al., 2014) which produces the infrasound (Helmoltz resonance) in a cylindrical structure with a diameter of 65m that separates the spatter roof from the active lava lake roughly located between 23 and 31 m below, but its depth can reach as low as 220-370 m deep (Ripepe et al., 2010). This spatter roof would be the horizontal source force for LPs in an asymmetric lava lake with a subhorizontal structure (7°) oriented $N75^\circ E$, consistent with the roof and terrace shown in Palma et al. (2008).

This structure, that generates the LP, comprises a tetragonal volume of $600 \text{ m} \times 600 \text{ m}$ horizontally, and 525 m vertically (Richardson and Waite, 2013). The diameter of the conduit was mathematically estimated within $\sim 5 \text{ m}$ by Witter et al. (2004), while Ripepe et al. (2010) proposed it to be around 100 m wide. As for the length of it, Palma et al. (2008) suggest that bubbles can ascend freely within the edifice conduit with no bubble coalescence between the roof of the chamber and the entrance of the conduit, and that therefore the uppermost plumbing system would be a near-vertical cylindrical conduit of more than 2000 m. Given the altitude of the low velocity anomaly (approx 1800 m.a.s.l.) and its slight location to the north-east of the volcano, we concur on the near vertical characteristic, and hypothesize a (very) wide inverted funnel shape between the uppermost part of the magma chamber and the cylindrical conduit, allowing very little coalescence of bubbles, except where a batch of new volatile-rich magma enters.

4.5.5 Comparison with Tomography Studies at other Volcanic Edifices

Different volcanic regions have been studied lately using various tomography methods that have improved over time. In general, the characteristics of the volcanic structures found present similarities that are independent of the specific method used. P- wave Velocity variations, for example, range typically between $\pm 10\%$ (Redoubt (Benz et al., 1996), Krakatau (Jaxybulatov et al., 2011)) and in some rare cases up to $\pm 20\%$ (Popocatepetl (Berger et al., 2011; Kuznetsov and Koulakov, 2014), St. Helens (Lees, 1992)). Also, the location of shallow magma chambers depends on the geological setting of each volcano, ranging from 2 km to mid crustal depths, but tend to be between 2 and 7 km, and to have 1 to 5 km in diameter (Sibbett, 1988; Browne and Szramek, 2015). This is controlled mainly by lithospheric stress and the local stress regime.

For Nevado del Ruiz (Colombia), a basaltic-andesitic stratovolcano with similar characteristics to those of the Villarrica Volcano, Londoño and Sudo (2003) performed seismic tomography using more than 1500 regional and local events. Results showed a strong correlation with the surface geology and regional fault system, and were supported by previous experimental studies of rocks from the building. Velocities of ~ 6.5 km/s for the central part correspond to andesitic and basaltic lava flows with depths from 2 to 5 km, and a low region to the west of the volcano (< 4.1 km/s) consistent with pyroclastic rocks.

Lees (1992) found a small ($> 7\%$) low velocity area below the St. Helens crater that widens from a 1-2 km diameter with 1.5 to 3 km depth, to a 4-5 km diameter between 3 and 6 km deep. Below 6 km the low velocity changes to high velocity, which coincides with seismic activity, and continues down to 9 km where the next chamber begins. This high velocity anomaly was interpreted to be a plug capping the magma chamber beneath the 9 km depth.

4.5.6 Proposed Inner Structure Model for Villarrica Volcano

Results found in our study do not differ from those presented previously for St. Helens or Nevados del Ruiz. The shape of the shallow magma chambers varies between blobs of low velocity, and pipe-like structures, preferably below the crater, but not fixed there. From the locations of these “blobs” of low velocity, and their directionality we propose the following structures beneath the Villarrica Volcano (Figure 4.15):

Depth 3 - 5 km: Communicating conduit between a low velocity region and, possibly, a deeper one. The conduit follows the strike of the LOFZ, presents tensional stress allowing magma to ascend (below 4 km depth), and shows swarm-like stress behavior due to fracturing of small dikes. Located ~ 3 km SE of the actual crater, it most probably follows inherited structures from Caldera 1-2.

Depth 3 - 0 km: (1) Main lower velocity region that might indicate the location of a magma chamber extending in a NNW direction, and its influence on the surrounding area within a 6 km diameter. It is not resolvable in shape, but most probably is in the shape of a (very) wide inverted funnel between the uppermost part of the chamber and the cylindrical conduit, allowing very little coalescence of bubbles. (2) Lacoliths/conduit-like structures, of ca. 2 km width to the E and S the crater feeding the extrusions of pyroclastic groups Los Nevados and Challupén, respectively.

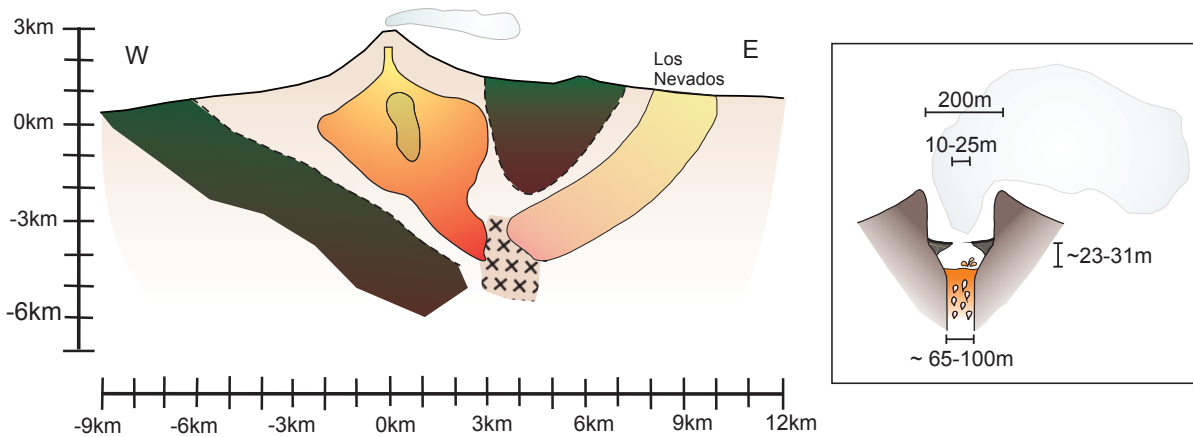


Figure 4.15: Schematic model derived from variations in velocity for the West-East profile (left), and from LP and infrasonic studies for the uppermost part of the conduit (right) according to Palma et al. (2008); Ripepe et al. (2010); Goto and Johnson (2011); Richardson and Waite (2013); Richardson et al. (2014). See Section 4.5.6 for details.

Altitude 0 - 1.8 km: Uppermost part of the inverted funnel-shaped region, containing probably amalgamated residual products of the Caldera 3 collapse.

Altitude 1.8 - ~2.3 km: Almost vertical hundred-meter wide conduit connecting the source of the low velocity region to the LP and resonance source of the volcano.

Altitude ~2.3 - 2.8 km: Horn shaped cylindrical conduit ten-meters wide, with a subhorizontal spatter roof and the free surface of the lava lake located roughly between 23 and 31 m below.

4.6 Conclusions

In this work, we presented a straight ray tomography using local volcano tectonic events from a dense temporary network encircling the Villarrica Volcano. We observe (1) volcano tectonic seismicity located between 2 and 5 km depth forming a NS striking vertical structure, consistent with the direction of the LOFZ. Focal mechanisms are consistent with a swarm like behaviour, with plane solutions following the strike of either LOFZ or VQL. Particularly, events below 4 km depth show extensional focal plane solutions, while shallower events (above 3 km depth) show strike-slip focal plane solutions. (2) We observed a NNW-SSE shallow low velocity region of at least 5 km in diameter starting above the region of VT seismicity. Its strongest intensity, between 1 to 2 km in depth, most probably indicates the location of a shallow magma chamber, and at lesser intensities, its influence on the surrounding rocks and conduit, as the anomaly reaches up to 1.5 km a.s.l. (3) Two lacolith/conduit-like low velocity structures connected to the feeding conduit were observed towards ENE and S directions, and are interpreted as remnants of dikes generating the previous pyroclastic flows of Los Nevados and Challupén, respectively. (4) High velocity regions to the west and north of the edifice underlie the main low velocity structure and conduits, respectively. The high velocity zone at the locus of seismic activity confirms a fragile highly-fractured zone of a magma-ascending path, probably inherited from a previous Caldera 1-2 edifice. (5) Location of anomalies is strongly supported by geologic features visible at the surface, and observed in depth

by previous geophysical studies. (6) A Checker-board test and Bootstrapped Tomography proved that selected strong quality data were stable and, although concentrated, able to resolve the uppermost part of the crust under the edifice up to a height of 1.8 km.

Acknowledgements

All the authors acknowledge the SFB 574 “Volatiles and Fluids in Subduction Zone” for its funding. C. Mora-Stock gratefully acknowledges the Chilean National Council of Research, Science and Technology (CONICYT, acronym in Spanish), and the German Academic Exchange Service (DAAD, acronym in German), and their funding program CONICYT Becas Chile N°72110106 for the grant that facilitated this research. All the authors acknowledge the GIPP of the GFZ Helmholtz-Zentrum Potsdam for providing the short period seismometers used for the SFB 574 project during March, 2012. Also to be acknowledged is the help of T. Wunderlich and E. Contreras in the field, and of D. Wilkens for the ray bending calculations. Figures and calculations were performed with the help of SEISAN, Python, and Generic Mapping Tools (GMT) software from Wessel et al. (2013). This is contribution number 278 to Sonderforschungsbereich 574 “Volatiles and Fluids in Subduction Zones” at Kiel University, funded by the German Research Foundation.

Chapter 5

Conclusions

In this thesis I have presented three scientific publications written within the main frame of the SFB 574 project and the multiparameter surveillance in the near-real time project. The main objective of these publications is to help in the understanding of the tectonics and seismicity of the Villarrica volcano, as well as to obtain the first inner velocity structure model of the edifice. Considering the great risk that earthquakes in subduction zones pose on populations, and the interactions in triggering volcanic activity, the behavior of the Villarrica volcano was studied in relation to the Mw 8.8 Maule earthquake.

The relation between great subduction earthquakes and the triggering of eruptions or increases in activity for nearby volcanoes, has been seen previously on the Chilean coast. Most remarkable examples in the region were in Concepción, in 1835, where volcanoes from Osorno to Yanteles presented activity directly after the earthquake; and in Valdivia, in 1960, where Cordón Caulle erupted just hours after the mainshock.

The Maule earthquake in 2010 closed the Darwin seismic gap that had existed since the last earthquake in 1835 along 450 km between 34°S and 38.5°S. The Mw 8.8 earthquake shows the great seismic and tsunami potential of the Nazca subduction zone below the South American plate. The area of rupture of the Maule earthquake reached from south of Santiago to south of the Lebu peninsula, although some aftershock activity was located as far as 33°S. Two areas of high slip, linked by areas of low pre-seismic slip, correspond to the two main asperities of the subducting slab in front of the coast of Constitución and Lebu, and represent the locus of Magnitude 6 aftershock seismicity.

Dynamic and static stresses play an important role in triggering volcanic activity, particularly when the edifice is in a critical state. Especially for the Villarrica and Llaima volcanoes, south of the rupture zone of the Maule earthquake, only a small change in the seismic and degassing activity was observed as long as one week before the event, and months after it.

For Villarrica, in particular, the increase in activity related to fluids prior to the earthquake, LP events and tremors, is consistent with a sudden change in the static stress around the magmatic chamber and conduits. This increased LP activity goes hand in hand with strong rates of degassing, meaning an increase in the magma supply rates at the time of the event. This heightened activity was interrupted by the earthquake, after which the LP and degassing activity declined along with the lava lake activity.

Calculations of changes in normal stress and pressure determined a small extension for the area of Villarrica. These calculations, along with the sequence of activity, can be interpreted as an opening of the conduits by these extensive forces generating a withdrawal of magma which decreases the movement or input through new conduits/paths, and a lowering in the height of the magma column at the conduit, diminishing or ceasing the lava lake activity — with the consequent low degassing rates. The effect lasted nearly three weeks, after which the activity of LP and tremors rose back to background values, and the degassing rates became higher than before the earthquake.

The small changes in stress along with the constant degassing and lava lake activity of Villarrica, plus several small (VEI=1) eruptions since the last eruption in 1984-85, left the system with sufficient released energy to keep it in a non-critical state before the Maule earthquake, and thus it did not respond with an immediate eruption.

How long in time the influence of a great earthquake on the possibility of triggering an eruption lasts is still unclear as seen in the literature. Most examples of eruptions take place between hours to days after the mainshock, but others might take several months to years. The last eruption of Villarrica volcano in March, 2015 might have been purely a coincidence five years after the February, 2010 earthquake. The details of the eruption and its previous activity are beyond the scope of this thesis.

The Villarrica volcano is emplaced at the westernmost part of the Villarrica-Lanín-Quetupillán lineament and the intersection with the NS striking Liquiñe - Ofqui fault. The VQL lineament is superimposed on the pre-Andean NW-SE basement-cutting structure Lanalhue fault, which is thought to have controlled the limits of rupture zones of previous events north and south of this structure (1835, 2010, and 1960 respectively) (Melnick et al., 2009). The volcano tectonic seismicity found with the network used for local seismic tomography follows the strike of the Liquiñe - Ofqui fault clearly, which is consistent with the main control that this structure poses in the emplacement of the volcanic edifice along the Southern Volcanic Zone.

The first straight-ray local tomography model obtained shows low velocity regions consistent with the location and influence of a main chamber structure, and feeding dikes/sills of the previous surface-visible pyroclastic flows Los Nevados and Challupén. All of the low velocity structures seem to connect at the locus of seismicity between 3 to 5 km depth, at 4 km east of the present crater. The main low velocity zone seems to have followed fractures that occurred in the western part of Caldera 1-2 and Caldera 3 events, and follows roughly the direction of the NW-SE structure. High velocity regions are consistent with basement rocks or crust, or consolidated products from caldera collapses, depending on their location at the volcano. A strong high velocity region can be observed wrapping the western part of the main low velocity region, as well as part of the north flank. A wedge-like structure separates the main low velocity region from the conduit-like structure to Los Nevados.

Results obtained in this work accomplish most of its objectives related to seismology and structure for the multiparameter surveillance project. Observations in the changing behavior before and after the Maule earthquake provide a better understanding of external processes influencing volcanic unrest, and the response dynamics of the volcano. A first visualization of the inner velocity structure of the Villarrica volcano contributes to the knowledge and understanding of the magmatic plumbing system, magma accumulation (at shallow) depths, and their relation to local crustal tectonic structures.

The SFB 574 observed the complete subduction zone in south-central Chile, while the A2 project focused strictly on the region between 39°S and 40°S. Although the area studied for this thesis is much

smaller, the study of the Maule earthquake collects information on the characterization of seismic activity in a subduction zone, and some crustal tectonic structures activated by the earthquake.

Through this compendium of manuscripts, I have provided insight into the seismicity of the Villarrica volcano, as well as the Llaima volcano, in a state, Chile, where an external process could have influenced volcanic unrest. Through the comparison and correlation of seismicity and degassing activity, the dynamic response for both volcanoes has been detailed, particularly in the case of a great earthquake occurring in the vicinity.

Most probably, one of the most valuable goals accomplished in this study was obtaining a first approximation of the inner structure of the Villarrica volcano, visible through seismic tomography. The configuration of crustal structures and principal tension direction visible in surface features are also evident in the distribution and direction of low velocity regions inside the volcano. To the best of my knowledge, this is the first seismic tomography that has been performed at the Villarrica volcano.

Future Work

Towards completing combined objectives of the multiparameter surveillance project, a more detailed characterization of the different types of seismic activity at the Villarrica volcano is expected. A real-time correlation between seismic activity and gas composition and flux data will provide insights into the nature of volcano dynamics. The location of long period and tremor sources, complemented with the tomography results, will provide information about the sections of the structures transporting fluids, the nature of the fluids that fill the structures, and possibly the geometry of the paths. Overall, a more comprehensive image of the structures and fluid pathways inside the volcano could be developed. As the method provided in this study is straight-ray local tomography, a more detailed imaging study could be considered adding local seismicity and/or combining the record with information of other stations around the volcano. A compound model is expected to be obtained by combining the deep-reaching tomography model for the subduction zone at 39.5°S retrieved by Dzierma, Rabbel, Thorwart, Koulakov, Wehrmann, Hoernle and Comte (2012) with the results of this study. With this combined model, the pathways of fluids from the dehydrating slab up to the volcano edifice could be observed in detail, increasing the knowledge of reservoir depths and their relation to deep-reaching structures.

The long-term relation between crustal structures and the geometry of the emplacement of volcanoes has been studied previously, as well as the short term relation between earthquake-magma chamber interaction either from dynamic and static stress changes due to great earthquakes, as seen in this study, or by the mechanisms by which the reservoirs transfer stress to the surrounding rock, and thus release it as earthquakes. However, the interaction between long-term structures controlling the emplacement of volcanic edifices and the short-term stress transfer due to chamber-to-fault or earthquake-to-chamber mechanisms is still not well understood. On a more tectonic focused theme, the Villarrica volcano poses a great scenario to study, at least on a small scale, the role of the crustal arrangement in the volcano dynamics of controlling the crustal seismicity around the volcano and its stress state. It is important to understand the interaction between the NW-SE inherited Mocha-Villarrica fault and the LOFZ that allows magma ascent even under the present compressive regime. This is expected to be determined by the characterization of volcanic long-period seismicity at Villarrica volcano, and the tectonic activity in the vicinity related to the crustal faults involved in the emplacement of the volcano: LOFZ, Mocha-

Villarrica, and Lanalhue.

The region around the Villarrica volcano is a highly populated area, with Villarrica and Pucón being two of the most touristic cities in its vicinity. The combination of these factors motivates the future project aim of increasing the understanding of the dynamics of the volcano and the location and structure of the magmatic reservoirs, in order to complement and aid in monitoring the volcano with consequent hazard-mitigation.

Bibliography

- Aki, K., Christoffersson, A. and Husebye, E. S. (1977), 'Determination of the three-dimensional seismic structure of the lithosphere', *Journal of Geophysical Research* **82**(2), 277–296. **URL:** <http://dx.doi.org/10.1029/JB082i002p00277>
- Alam, M. and Kimura, M. (2004), 'Statistical analysis of time-distance relationship between volcanic eruptions and great earthquakes in Japan', *Earth, Planets and Space* **56**, 179 – 192.
- Angermann, D., Klotz, J. and Reigber, C. (1999), 'Space-geodetic estimation of the Nazca-South America Euler vector', *Earth and Planetary Sciences Letters* **171**, 329 – 334.
- Barrientos, S. (1994), 'Large Thrust Earthquakes and Volcanic Eruptions', *Pure and Applied Geophysics* **142**(1), 225 – 237.
- Barrientos, S. (2007), *The Geology of Chile*, The Geological Society, chapter 10. Earthquakes in Chile, pp. 263–287.
- Barrientos, S. (2010), Informe Técnico Terremoto Cauquenes 27-Febrero-2010, Technical report, Servicio Sismológico Nacional. **URL:** http://sismologia.cl/links/Informe_Terremoto_Cauquenes.pdf
- Bathke, H., Shirzaei, M. and Walter, T. R. (2011), 'Inflation and deflation at the steep-sided Llaima stratovolcano (Chile) detected by using InSAR', *Geophysical Research Letters* **38**(10), L10304. **URL:** <http://dx.doi.org/10.1029/2011GL047168>
- Beck, S., Barrientos, S., Kausel, E. and Reyes, M. (1998), 'Source characteristics of historic earthquakes along the central Chile subduction zone', *Journal of South American Earth Sciences* **11**(2), 115–129.
- Benz, H., Chouet, B., P.B., Lahr, J., Page, R. and Hole, J. (1996), 'Three-dimensional P and S wave velocity structure of Redoubt Volcano, Alaska', *Journal of Geophysical Research* **101**(B4), 8111 – 8128.
- Berger, P., Got, J.-L., González, C. V. and Monteiller, V. (2011), 'Seismic tomography at Popocatepetl volcano, Mexico', *Journal of Volcanology and Geothermal Research* **200**(3–4), 234 – 244. **URL:** <http://www.sciencedirect.com/science/article/pii/S0377027311000035>
- Bohm, M., Lüth, S., Echtler, H., Asch, G., Bataille, K., Bruhn, C., Rietbrock, A. and Wigger, P. (2002), 'The Southern Andes between 36° and 40°S latitude: seismicity and average seismic velocities', *Tectonophysics* **356**(4), 275 – 289. **URL:** <http://www.sciencedirect.com/science/article/pii/S0040195102003992>
- Bonali, F., Tibaldi, A., Corazzato, C., Tormey, D. and Lara, L. (2013), 'Quantifying the effect of large earthquakes in promoting eruptions due to stress changes

BIBLIOGRAPHY

- on magma pathway: The Chile case', *Tectonophysics* **583**, 54 – 67. **URL:** <http://www.sciencedirect.com/science/article/pii/S0040195112006890>
- Brasse, H. and Soyer, W. (2001), 'A magnetotelluric study in the Southern Chilean Andes', *Geophysical Research Letters* **28**(19), 3757–3760.
- Bredemeyer, S. and Hansteen, T. (2014), 'Synchronous degassing patterns of the neighbouring volcanoes Llama and Villarrica in south-central Chile: the influence of tidal forces', *International Journal of Earth Sciences* **103**(7), 1999–2012.
- Brenguier, F., Shapiro, N., Campillo, M., Nercessian, A. and Ferrazzini, V. (2007), '3-D surface wave tomography of the Piton de la Fournaise volcano using seismic noise correlations', *Geophysical Research Letters* **34**, L02305.
- Browne, B. and Szramek, L. (2015), Chapter 9 - Rates of Magma Ascent and Storage, in H. Sigurdsson, ed., 'The Encyclopedia of Volcanoes (Second Edition)', second edition edn, Academic Press, Amsterdam, pp. 203 – 214. **URL:** <http://www.sciencedirect.com/science/article/pii/B9780123859389000092>
- Calder, E., Harris, A., Peña, P., Pilger, E., Flynn, L. P., Fuentealba, G. and Moreno, H. (2004), 'Combined thermal and seismic analysis of the Villarrica volcano lava lake, Chile', *Revista Geologica de Chile* **31**(2), 259–272.
- Campos, J., Hatzfeld, D., Madariaga, R., Lopez, G., Kausel, E., Zollo, A., Iannacone, G., Fromm, R., Barrientos, S. and Lyon-Caen, H. (2002), 'A seismological study of the 1835 seismic gap in south-central Chile', *Physics of the Earth and Planetary Interiors* **132**(1–3), 177 – 195. Subduction Zone Structure and Megathrust Earthquakes. **URL:** <http://www.sciencedirect.com/science/article/pii/S0031920102000511>
- Campos, J. and Kausel, E. (1990), 'The large 1939 intraplate earthquake of Southern Chile.', *Seismological Research Letters* **61**.
- Carr, M. (1977), 'Volcanic Activity and Great Earthquakes at Convergent Plate Margins', *Science* **197**(4304), 655 – 657.
- Casertano, L. (1963), 'General characteristics of active andean volcanoes and a summary of their activities during recent centuries', *Bulletin of the Seismological Society of America* **53**(6), 1415–1433. **URL:** <http://www.bssaonline.org/content/53/6/1415.abstract>
- Cembrano, J., Hervé, F. and Lavenue, A. (1996), 'The Liquine-Ofqui fault zone: a long-lived intra-arc fault system in southern Chile', *Tectonophysics* **259**, 55 – 66.
- Cembrano, J. and Lara, L. (2009), 'The link between volcanism and tectonics in the southern volcanic zone of the Chilean Andes: A review.', *Tectonophysics* **471** (1), 96 – 113.
- Cembrano, J. and Moreno, H. (1994), Geometría y naturaleza contrastante del volcanismo cuaternario entre los 38°S y 46°S: ¿Dominios compresionales y tensionales en un régimen transcurrente?, in 'Actas del 7mo Congreso Geológico Chileno, Universidad de Concepción', Vol. 1, pp. 240 – 244.
- Chouet, B. (1996), New Methods and Future Trends in Seismological Volcano Monitoring, in 'Monitoring and Mitigation of Volcano Hazards', Springer Berlin Heidelberg, pp. 23–97. **URL:** http://dx.doi.org/10.1007/978-3-642-80087-0_2
- Cifuentes, I. (1989), 'The 1960 Chilean earthquakes', *Journal of Geophysical Research* **94**, 665–680.

BIBLIOGRAPHY

- Clavero, J. and Moreno, H. (2004), Evolution of Villarrica Volcano, *in* L. Lara and J. Clavero, eds, 'Villarrica Volcano (39.5°S) Southern Andes, Chile. Boletín No. 61', Servicio Nacional de Geología y Minería.
- Comte, D., Eisenberg, A., Lorca, E., Pardo, M., Ponce, L., Saragoni, R., Singh, S. K. and G. Suárez (1986), 'The 1985 Central Chile Earthquake: A Repeat of Previous Great Earthquakes in the Region?', *Science* **233**, 449–453. **URL:** <http://www.jstor.org/stable/1697810>
- Comte, D. and Pardo, M. (1991), 'Reappraisal of Great Historical Earthquakes in the Northern Chile and Southern Peru Seismic Gaps', *Natural Hazards* **4**, 23–44.
- Contreras-Reyes, E., Flueh, E. R. and Grevemeyer, I. (2010), 'Tectonic control on sediment accretion and subduction off south central Chile: Implications for coseismic rupture processes of the 1960 and 2010 megathrust earthquakes', *Tectonics* **29**(6), n/a–n/a. **URL:** <http://dx.doi.org/10.1029/2010TC002734>
- Curilem, G., Vergara, J., Fuentealba, G., Acuña, G. and Chacón, M. (2009), 'Classification of seismic signals at Villarrica volcano (Chile) using neural networks and genetic algorithms', *Journal of Volcanology and Geothermal Research* **180**(1), 1–8.
- Darwin, C. (1845), *Journal of Researches into the Natural History and Geology of the countries visited during the voyage of H.M.S. Beagle around the world*, 2nd. edition edn. **URL:** <http://darwin-online.org.uk>
- De Mets, C., Gordon, R., Argus, D. and Stein, S. (1994), 'Effect of recent revisions to the geomagnetic reversal time scale on estimates of current plate motions', *Geophysical Research Letters* **21** (20), 2191–2194.
- Delgado, F. (2012), Estudio aeromagnético de la estructura interna de los volcanes Villarrica y Quetrupillán (Andes del Sur, Chile), *in* 'Congreso Geológico Chileno', Vol. 13, pp. 624 – 626. **URL:** http://biblioserver.sernageomin.cl/opac/DataFiles/14127_pp_624_626.pdf
- Delouis, B., Nocquet, J. M. and M., V. (2010), 'Slip distribution of the February 27, 2010 Mw = 8.8 Maule Earthquake, central Chile, from static and high-rate GPS, InSAR, and broadband teleseismic data', *Geophysical Research Letters* **37**, L17305.
- Dungan, M. A., Bouvet de Maisonneuve, C., Sellés, D., Naranjo, J. A., Moreno, H., Langmuir, C., Reubi, O., Goldstein, S., Jweda, J., Escrig, S., Bachmann, O. and Bourdon, B. (2008), Volcán Llaima (38.7°S, Chilean Southern Volcanic Zone): Insights into a dominantly mafic and hyperactive subduction-related magmatic system, *in* '7th International Symposium on Andean Geodynamics (ISAG 2008, Nice), Extended Abstracts'.
- Dzierma, Y., Rabbel, W., Thorwart, M., Koulakov, I., Wehrmann, H., Hoernle, K. and Comte, D. (2012), 'Seismic velocity structure of the slab and continental plate in the region of the 1960 Valdivia (Chile) slip maximum—insights into fluid release and plate coupling', *Earth and Planetary Science Letters* **331**, 164–176.
- Dzierma, Y., Thorwart, M., Rabbel, W., Siegmund, C., Comte, D., Bataille, K., Iglesia, P. and Prezzi, C. (2012), 'Seismicity near the slip maximum of the 1960 Mw 9.5 Valdivia earthquake (Chile): Plate interface lock and reactivation of the subducted Valdivia Fracture Zone', *Journal of Geophysical Research: Solid Earth (1978–2012)* **117**, B06312.

BIBLIOGRAPHY

- Dzierma, Y. and Wehrmann, H. (2010), 'Eruption time series statistically examined: Probabilities of future eruptions at Villarrica and Llaima Volcanoes, Southern Volcanic Zone, Chile', *Journal of Volcanology and Geothermal Research* **193**, 82 – 92.
- Efron, B. (1979), 'Bootstrap methods: Another look at the jackknife', *The Annals of Statistics* **7**(1), pp. 1–26. **URL:** <http://www.jstor.org/stable/2958830>
- Efron, B. (1983), 'Estimating the error rate of a prediction rule: Improvement on cross-validation', *Journal of the American Statistical Association* **78**(382), 316–331. **URL:** <http://www.tandfonline.com/doi/abs/10.1080/01621459.1983.10477973>
- Efron, B. and Tibshirani, R. (1997), 'Improvements on Cross-Validation: The .632+ Bootstrap Method', *Journal of the American Statistical Association* **92**(438), pp. 548–560. **URL:** <http://www.jstor.org/stable/2965703>
- Eggert, S. and Walter, T. R. (2009), 'Volcanic activity before and after large tectonic earthquakes: Observations and statistical significance', *Tectonophysics* **471**(1 - 2), 14 – 26. Understanding stress and deformation in active volcanoes. **URL:** <http://www.sciencedirect.com/science/article/pii/S0040195108004757>
- Ekström, G., Nettles, M. and Dziewonski, A. M. (2012), 'The global CMT project 2004-2010: Centroid-moment tensors for 13,017 earthquakes', *Physics of the Earth and Planetary Interiors* **200-201**, 1–9.
- Ellsworth, W. L. and Koyanagi, R. Y. (1977), 'Three-dimensional crust and mantle structure of Kilauea Volcano, Hawaii', *Journal of Geophysical Research* **82**(33), 5379–5394.
- Farías, M., Comte, D., Charrier, R., Martinod, J., David, C., Tassara, A., Tapia, F. and Fock, A. (2010), 'Crustal-scale structural architecture in central Chile based on seismicity and surface geology: Implications for andean mountain building', *Tectonics* **29**(3), n/a–n/a. **URL:** <http://dx.doi.org/10.1029/2009TC002480>
- Global Volcanism Program (2013), 'Volcanoes of the world, v. 4.4.0., Venzke, E (ed.)'. Last accessed: Sep. 2015. **URL:** <http://volcano.si.edu/volcano.cfm?vn=357110>
- Goto, A. and Johnson, J. B. (2011), 'Monotonic infrasound and Helmholtz resonance at Volcan Villarrica (Chile)', *Geophysical Research Letters* **38**, L06301.
- Gutscher, M. (2002), 'Andean subduction styles and their effect on thermal structure and interplate coupling', *Journal of South American Earth Sciences* **15**, 3–10.
- Haberland, C., Rietbrock, A., Lange, D., Bataille, K., and Hofmann, S. (2006), 'Interaction between fore-arc and oceanic plate at the south-central Chilean margin as seen in local seismic data', *Geophysical Research Letters* **33**, L23302.
- Hainzl, S., Zöller, G., Kurths, J. and Zschau, J. (2000), 'Seismic quiescence as an indicator for large earthquakes in a system of self-organized criticality', *Geophysical Research Letters* **27**(5), 597–600.
- Harrington, R. M. and Brodsky, E. E. (2007), 'Volcanic hybrid earthquakes that are brittle-failure events', *Geophysical Research Letters* **34**(6), n/a–n/a. L06308. **URL:** <http://dx.doi.org/10.1029/2006GL028714>
- Havskov, J. and Ottemoller, L. (1999), 'SeisAn Earthquake Analysis Software', *Seismological Research Letters* **70**(5), 532–534. **URL:** <http://srl.geoscienceworld.org/content/70/5/532.short>

BIBLIOGRAPHY

- Hayes, G. (2010), 'Finite Fault Model. Updated Result of the Feb 27, 2010 Mw 8.8 Maule, Chile Earthquake'. **URL:** http://earthquake.usgs.gov/earthquakes/eqinthenews/2010/us2010tfan/finite_fault.php
- Hermosilla Pineda, G. A. (2008), Características sismotectónicas del volcán Villarrica, Memoria para optar al título de Geólogo, Universidad de Concepción.
- Hill, D., Pollitz, F. and Newhall, C. (2002), 'Earthquake-volcano interactions', *Physics Today* **55**, 41 – 47.
- Hoffmann-Rothe, A., Kukowski, N., Dresen, G., Echtler, H., Oncken, O., Klotz, J., Scheuber, E. and Kellner, A. (2006), Oblique Convergence along the Chilean Margin: Partitioning, Margin-Parallel Faulting and Force Interaction at the Plate Interface, in O. Oncken, G. Chong, G. Franz, P. Giese, H.-J. Götze, V. A. Ramos, M. R. Strecker and P. Wigger, eds, 'The Andes', *Frontiers in Earth Sciences*, Springer Berlin Heidelberg, pp. 125–146.
- Ibáñez, J., Carmona, E., Almendros, J., Saccorotti, G., Del Pezzo, E., Abril, M. and Ortiz, R. (2003), 'The 1998–1999 seismic series at Deception Island volcano, Antarctica', *Journal of volcanology and geothermal research* **128**(1), 65–88.
- Jaxybulatov, K., Koulakov, I., von Seht, M. I., Klinge, K., Reichert, C., Dahren, B. and Troll, V. R. (2011), 'Evidence for high fluid/melt content beneath Krakatau volcano (Indonesia) from local earthquake tomography', *Journal of Volcanology and Geothermal Research* **206**(3–4), 96 – 105. **URL:** <http://www.sciencedirect.com/science/article/pii/S0377027311001752>
- Johnson, J. B. and Palma, J. L. (2015), 'Lahar infrasound associated with Volcán Villarrica's 3 March 2015 eruption', *Geophysical Research Letters* **42**, n/a–n/a. 2015GL065024. **URL:** <http://dx.doi.org/10.1002/2015GL065024>
- Kawakatsu, H. and Yamamoto, M. (2007), 4.13 - Volcano Seismology, in G. Schubert, ed., 'Treatise on Geophysics', Elsevier, Amsterdam, pp. 389 – 420. **URL:** <http://www.sciencedirect.com/science/article/pii/B9780444527486000730>
- Kelleher, J. (1972), 'Rupture Zones of Large South American Earthquakes and Some Predictions', *Journal of Geophysical Research* **77**(11), 2087–2102.
- Kuznetsov, P. and Koulakov, I. Y. (2014), 'The three-dimensional structure beneath the Popocatepetl volcano (Mexico) based on local earthquake seismic tomography', *Journal of Volcanology and Geothermal Research* **276**, 10 – 21. **URL:** <http://www.sciencedirect.com/science/article/pii/S037702731400064X>
- Lahr, J., Chouet, B., Stephens, C., Power, J. and Page, R. (1994), 'Earthquake classification, location, and error analysis in a volcanic environment: implications for the magmatic system of the 1989–1990 eruptions at Redoubt volcano, Alaska', *Journal of Volcanology and Geothermal Research* **62**(1–4), 137 – 151. The 1989-1990 Eruptions of Redoubt Volcano, Alaska. **URL:** <http://www.sciencedirect.com/science/article/pii/0377027394900310>
- Lange, D., Cembrano, J., Rietbrock, A., Haberland, C., Dahm, T. and Bataille, K. (2008), 'First seismic record for intra-arc strike-slip tectonics along the Liquiñe-ofqui fault zone at the obliquely convergent plate margin of the southern Andes', *Tectonophysics* **455**(1–4), 14–24.
- Lange, D., Rietbrock, A., Haberland, C., Bataille, K., Dahm, T., Tilmann, F. and Flüh, R. (2007), 'Seismicity and geometry of the south Chilean subduction zone (41.5°S–43.5°S): Implications for controlling parameters.', *Geophysical Research Letters* **34**, L06311.

BIBLIOGRAPHY

- Lavenu, A. and Cembrano, J. (1999), 'Compressional- and Transpressional-stress pattern for Pliocene and Quaternary brittle deformation in fore arc and intra-arc zones (Andes of Central and Southern Chile)', *Journal of Structural Geology* **21**, 1669–1691.
- Lay, T., Ammon, C. J., Kanamori, H., Koper, K. D., Sufri, O. and Hutko, A. R. (2010), 'Teleseismic inversion for rupture process of the 27 February 2010 Chile (Mw 8.8) earthquake', *Geophysical Research Letters* **37**, L13301.
- Lees, J. M. (1992), 'The magma system of Mount St. Helens: non-linear high-resolution P-wave tomography', *Journal of Volcanology and Geothermal Research* **53**(1–4), 103 – 116. **URL:** <http://www.sciencedirect.com/science/article/pii/037702739290077Q>
- Lees, J. M. (2007), 'Seismic tomography of magmatic systems', *Journal of Volcanology and Geothermal Research* **167**(1–4), 37 – 56. Large Silicic Magma Systems. **URL:** <http://www.sciencedirect.com/science/article/pii/S0377027307001965>
- Leet, R. (1988), 'Saturated and Subcooled Hydrothermal Boiling in Groundwater Flow Channels as a Source of Harmonic Tremor', *Journal of Geophysical Research* **93**(B5), 4835 – 4849.
- Linde, A. T. and Sacks, I. S. (1998), 'Triggering of volcanic eruptions', *Nature* **395**, 888–890. **URL:** <http://dx.doi.org/10.1038/27650>
- Lohmar, S., Parada, M. A., Robin, C., Gerbe, M., Deniel, C., Gourgaud, A., López, L. and Moreno, H. Naranjo, J. (2006), Origin of postglacial “mafic” ignimbrites at Llaima and Villarrica volcanoes (southern Andes, Chile): assimilation of plutonic rocks as one of the triggering factors?, in 'V South American Symposium on Isotope Geology'.
- Lohmar, S., Robin, C., Parada, M., Gourgaud, A., López-Escobar, L., Moreno, H. and Naranjo, J. (2005), The two major postglacial (13 - 14,000 BP) pyroclastic eruptions of Llaima and Villarrica volcanoes (Southern Andes) : A comparison., in '6th International Symposium on Andean Geodynamics (ISAG 2005, Barcelona), Extended Abstracts', pp. 442 – 445.
- Lomnitz, C. (1970), 'Major earthquakes and tsunamis in Chile during the period 1535 to 1955', *Journal International of Earth Sciences, Springer Berlin/Heidelberg* **59**(3), 938–960.
- Lomnitz, C. (1994), *Fundamentals of earthquake prediction*, John Wiley and Sons, Inc., New York.
- Lomnitz, C. (2004), 'Major Earthquakes of Chile: A Historical Survey, 1535-1960', *Seismological Research Letters* **75**(3), 368–378. **URL:** <http://srl.geoscienceworld.org/content/75/3/368.short>
- Londoño, J. M. and Sudo, Y. (2003), 'Velocity structure and a seismic model for Nevado del Ruiz Volcano (Colombia)', *Journal of Volcanology and Geothermal Research* **119**(1–4), 61 – 87. **URL:** <http://www.sciencedirect.com/science/article/pii/S0377027302003062>
- Lorito, S., Romano, F., Atzori, S., Tong, X., Avallone, A., McCloskey, J., Cocco, M., Boschi, E. and Piatanesi, A. (2010), 'Limited overlap between the seismic gap and coseismic slip of the great 2010 Chile earthquake', *Nature Geoscience* **4**, 173–177.
- Lüth, S. and Wigger, P. (2003), 'A crustal model along 39°S from a seismic refraction profile - ISSA 2000.', *Revista Geologica de Chile* **30**(1), 83 – 101.
- Luttrell, K., Tong, X., Sandwell, D., Brooks, B. and Bevis, M. (2011), 'Estimates os stress drop and crustal tectonic stress from the 27 February 2010 Maule, Chile, earthquake: Implications for fault strength', *Journal of Geophysical Research* **116**, B11401.

BIBLIOGRAPHY

- Madariaga, R. (1998), 'Sismicidad de Chile', *Fisica de la Tierra* **10**, 221–258.
- Madariaga, R., Métois, M., Vigny, C. and Campos, J. (2010), 'Central Chile finally breaks', *Science* **328**, 181–182.
- Manga, M. and Brodsky, E. (2006), 'Seismic Triggering of Eruptions in the Far Field: Volcanoes and Geysers', *Annual Review of Earth and Planetary Science* **34**, 263 – 91.
- Marsh, B. D. (2015), Chapter 8 - Magma Chambers, in H. Sigurdsson, ed., 'The Encyclopedia of Volcanoes (Second Edition)', second edition edn, Academic Press, Amsterdam, pp. 185 – 201. **URL:** <http://www.sciencedirect.com/science/article/pii/B9780123859389000080>
- Martin, M. W., Kato, T. T., Rodriguez, C., Godoy, E., Duhart, P., McDonough, M. and Campos, A. (1999), 'Evolution of the late Paleozoic accretionary complex and overlying forearc-magmatic arc, south central Chile (38°S–41°S): Constraints for the tectonic setting along the southwestern margin of Gondwana', *Tectonics* **18**(4), 582–605. **URL:** <http://dx.doi.org/10.1029/1999TC900021>
- McNutt, S. (1992), Volcanic tremor, in 'Encyclopedia of Earth System Science', Academic Press, pp. 417–425.
- McNutt, S. (1996), Seismic monitoring and eruption forecasting of volcanoes: A review of the state-of-the-art and case histories, in 'Monitoring and Mitigation of Volcano Hazards', Springer Berlin Heidelberg, pp. 99–146. **URL:** http://dx.doi.org/10.1007/978-3-642-80087-0_3
- McNutt, S. (2000), Volcanic seismicity, in H. Sigurdsson, B. Houghton, S. McNutt, H. Rymer and J. Stix, eds, 'Encyclopedia of Volcanoes', Academic Press, San Diego, CA, chapter 63, pp. 1015–1033.
- McNutt, S. (2005), 'A review of volcanic seismology', *Annual Reviews of Earth and Planetary Sciences* **33**, 461–491.
- McNutt, S. R. (2002), Volcano seismology and monitoring for eruptions, in P. C. J. William H.K. Lee, Hiroo Kanamori and C. Kisslinger, eds, 'International Handbook of Earthquake and Engineering Seismology', Vol. 81, Part A of *International Geophysics*, Academic Press, chapter 25, pp. 383 – V. **URL:** <http://www.sciencedirect.com/science/article/pii/S0074614202802285>
- Melnick, D., Bookhagen, B., Strecker, M. and Echtler, H. (2009), 'Segmentation of megathrust rupture zones from fore-arc deformation patterns over hundreds to millions of years, Arauco peninsula, Chile', *Journal of Geophysical Research* **114**, B01407.
- Melnick, D. and Echtler, H. (2006), Morphotectonic and Geologic Digital Map Compilations of the South-Central Andes (36°S - 42°S), in O. Oncken, G. Chong, G. Franz, P. Giese, H.-J. Götze, V. A. Ramos, M. R. Strecker and P. Wigger, eds, 'The Andes', *Frontiers in Earth Sciences*, Springer Berlin Heidelberg, pp. 565–568.
- Mignan, A. and Di Giovambattista, R. (2008), 'Relationship between accelerating seismicity and quiescence, two precursors to large earthquakes', *Geophysical Research Letters* **35**, L15306.
- Minakami, T. (1974), Chapter 1 - Seismology of Volcanoes in Japan, in G. L. CIVETTA, P. GASPARINI and A. RAPOLLA, eds, 'Physical Volcanology', Vol. 6 of *Developments in Solid Earth Geophysics*, Elsevier, pp. 1 – 27. **URL:** <http://www.sciencedirect.com/science/article/pii/B978044411419500073>

BIBLIOGRAPHY

- Mogi, K. (1963), 'Some discussions on aftershocks, foreshocks and earthquakes swarms: the fracture of a semi-infinite body caused by an inner stress origin and its relation to the earthquake phenomena (Third Paper).', *Bulletin of the Earthquake Research Institute* **41**, 615–658.
- Molina, I., Kumagai, H., Pennec, J.-L. L. and Hall, M. (2005), 'Three-dimensional P-wave velocity structure of Tungurahua Volcano, Ecuador', *Journal of Volcanology and Geothermal Research* **147**(1-2), 144 – 156. **URL:** <http://www.sciencedirect.com/science/article/pii/S0377027305001289>
- Monteiller, V., Got, J., Virieux, J. and Okubo, P. (2005), 'An efficient algorithm for double-difference tomography and location in heterogeneous media, with an application to the Kilauea volcano', *Journal of Geophysical Research: Solid Earth* **110**(B12), n/a.
- Mora-Stock, C., Thorwart, M., Wunderlich, T., Bredemeyer, S., Hansteen, T. and Rabbel, W. (2014), 'Comparison of seismic activity for Llaima and Villarrica volcanoes prior to and after the Maule 2010 earthquake', *International Journal of Earth Sciences* **103**(7), 2015–2028. **URL:** <http://dx.doi.org/10.1007/s00531-012-0840-x>
- Moreno, H. and Clavero, J. (2006), 'Mapa geológico del área del volcán Villarrica, Regiones de la Araucanía y de los Lagos (escala 1:50.000).', *Servicio Nacional de Geología y Minería* (No. 98), 35.
- Moreno, M., Rosenau, M. and Oncken, O. (2010), '2010 Maule earthquake slip correlates with pre-seismic locking of Andean subduction zone', *Nature* **467**, 198–202.
- Moreno, M. S., Bolte, J., Klotz, J. and Melnick, D. (2009), 'Impact of megathrust geometry on inversion of coseismic slip from geodetic data: Application to the 1960 Chile earthquake', *Geophysical Research Letters* **36**, L16310.
- Muñoz, M. (1983), 'Eruption Patterns of the Chilean Volcanoes Villarrica, Llaima, and Tupungatito', *Pure and Applied Geophysics* **121**, 835 – 852.
- Muñoz, M., Fournier, H., Mamani, M., Febrer, J., Borzotta, E. and Maidana, A. (1990), 'A comparative study of results obtained in magnetotelluric deep soundings in Villarrica active volcano zone (Chile) with gravity investigations, distribution of earthquake foci, heat flow empirical relationships, isotopic geochemistry $^{87}\text{Sr}/^{86}\text{Sr}$ and sb systematics', *Physics of the Earth and Planetary Interiors* **60**(1-4), 195–211.
- Murdie, E., Prior, D., Styles, P., Flint, S., Pearce, R. and Agar, S. (1993), 'Seismic responses to ridge-transform subduction: Chile Triple Junction', *Geology* **21**, 1095–1098.
- Neuberg, J., Luckett, R., Baptie, B. and Olsen, K. (2000), 'Models of tremor and low-frequency earthquake swarms on Montserrat', *Journal of Volcanology and Geothermal Research* **101**(1 -2), 83 – 104. **URL:** <http://www.sciencedirect.com/science/article/pii/S0377027300001694>
- Newhall, C. (2007), 4.12 - Volcanology 101 for Seismologists, in G. Schubert, ed., 'Treatise on Geophysics', Elsevier, Amsterdam, pp. 351 – 388. **URL:** <http://www.sciencedirect.com/science/article/pii/B9780444527486000729>
- Observatorio Volcánico de los Andes del Sur (OVDAS) (2011), Reporte Especial de Actividad Volcánica No 28, Región de Los Ríos, Complejo Volcánico Puyehue – Cordón Caulle, Technical report, Servicio Nacional de Geología y Minería (SERNAGEOMIN).

BIBLIOGRAPHY

- Observatorio Volcánico del los Andes del Sur (OVDAS) (2010), Informe mensual de actividad volcánica Región de La Araucanía (Volcanes: Llaima, Villarrica y Lonquimay) Junio 2010., Technical report, Servicio Nacional de Geología y Minería (SERNAGEOMIN).
- Okada, Y. (1992), 'Internal deformation due to shear and tensile faults in a half-space', *Bulletin of the Seismological Society of America* **82**(2), 1018–1040. **URL:** <http://www.bssaonline.org/content/82/2/1018.abstract>
- Ortiz, R., Moreno, H., García, A., Fuentealba, G., Astiz, M., Peña, P., Sánchez, N. and Tárrega, M. (2003), 'Villarrica volcano (Chile): characteristics of the volcanic tremor and forecasting of small explosions by means of a material failure method', *Journal of Volcanology and Geothermal Research* **128**(1-3), 247–259.
- Palma, J. L., Calder, E. S., Basualto, D., Blake, S. and Rothery, D. A. (2008), 'Correlations between SO₂ flux, seismicity, and outgassing activity at the open vent of Villarrica volcano, Chile', *Journal of Geophysical Research: Solid Earth* **113**(B10), n/a–n/a. **URL:** <http://dx.doi.org/10.1029/2008JB005577>
- Papadimitriou, P. (2008), 'Identification of seismic precursors before large earthquakes: Decelerating and accelerating seismic patterns', *Journal of Geophysical Research* **113**, B04306.
- Pardo-Casas, F. and Molnar, P. (1987), 'Relative motion of the Nazca (Farallón) and South American Plates since Late Cretaceous time', *Tectonics* **6**, 233–248.
- Pelayo, A. and Wiens, D. (1989), 'Seismotectonics and relative plate motions in the Scotia sea region', *Journal of Geophysical Research* **94**, 7293–7320.
- Perez, M. and Bancroft, J. (2000), 'Traveltime computation through isotropic media via the eikonal equation', *CREWES Research Reports* **12**. **URL:** <http://www.crewes.org/ForOurSponsors/ResearchReports/2000/2000-13.pdf>
- Piermattei, R. and Adams, W. (1973), 'Historical review of seismic studies on structure of volcanocs', *Annals of Geophysics* **26**(4), 525–559.
- Power, J. A., Lahr, J. C., Page, R. A., Chouet, B. A., Stephens, C. D., Harlow, D. H., Murray, T. L. and Davies, J. N. (1994), 'Seismic evolution of the 1989–1990 eruption sequence of Redoubt Volcano, Alaska', *Journal of Volcanology and Geothermal Research* **62**(1 - 4), 69 – 94. The 1989-1990 Eruptions of Redoubt Volcano, Alaska. **URL:** <http://www.sciencedirect.com/science/article/pii/0377027394900299>
- Ranero, C., von Huene, R., Weinrebe, W. and Reichert, C. (2006), Tectonic Processes along the Chile Convergent Margin, in O. Oncken, G. Chong, G. Franz, P. Giese, H.-J. Götze, V. A. Ramos, M. R. Strecker and P. Wigger, eds, 'The Andes', *Frontiers in Earth Sciences*, Springer Berlin Heidelberg, pp. 91–121. **URL:** http://dx.doi.org/10.1007/978-3-540-48684-8_5
- Rapela, C. W. and Pankhurst, R. J. (1992), 'The granites of northern Patagonia and the Gastre Fault System in relation to the break-up of Gondwana', *Geological Society, London, Special Publications* **68**(1), 209–220. **URL:** <http://sp.lyellcollection.org/content/68/1/209.abstract>
- Richardson, J. P. and Waite, G. P. (2013), 'Waveform inversion of shallow repetitive long period events at Villarrica Volcano, Chile', *Journal of Geophysical Research: Solid Earth* **118**(9), 4922–4936. **URL:** <http://dx.doi.org/10.1002/jgrb.50354>

BIBLIOGRAPHY

- Richardson, J. P., Waite, G. P. and Palma, J. L. (2014), 'Varying seismic-acoustic properties of the fluctuating lava lake at Villarrica volcano, Chile', *Journal of Geophysical Research: Solid Earth* **119**(7), 5560–5573. **URL:** <http://dx.doi.org/10.1002/2014JB011002>
- Ripepe, M., Marchetti, E., Bonadonna, C., Harris, A. J. L., Pioli, L. and Ulivieri, G. (2010), 'Monochromatic infrasonic tremor driven by persistent degassing and convection at Villarrica Volcano, Chile', *Geophysical Research Letters* **37**(15), n/a–n/a. **URL:** <http://dx.doi.org/10.1029/2010GL043516>
- Rivera, A., Zamora, R., Uribe, J., Wendt, A., Oberreuter, J., Cisternas, S., Gimeno, F. and Clavero, J. (2015), 'Recent changes in total ice volume on Volcán Villarrica, Southern Chile', *Natural Hazards* **75**(1), 33–55. **URL:** <http://dx.doi.org/10.1007/s11069-014-1306-1>
- Rosenau, M., Melnick, D. and Echtler, H. (2006), 'Kinematic constraints on intra-arc shear and strain partitioning in the southern Andes between 38°S and 42°S latitude', *Tectonics* **25** (4), TC4013.
- Rowan, L. R. and Clayton, R. W. (1993), 'The three-dimensional structure of Kilauea Volcano, Hawaii, from travel time tomography', *Journal of Geophysical Research: Solid Earth* **98**(B3), 4355–4375. **URL:** <http://dx.doi.org/10.1029/92JB02531>
- Ruegg, J., Rudloff, A., Vigny, C., Madariaga, R., de Chabalier, J. B., Campos, J., Kausel, E., Barrientos, S. and Dimitrov, D. (2009), 'Interseismic strain accumulation measured by GPS in the seismic gap between Constitución and Concepción in Chile', *Physics of the Earth and Planetary Interiors* **175**, 78–85.
- Saccorotti, G., Iguchi, M. and Aiuppa, A. (2015), Chapter 7 - In situ Volcano Monitoring: Present and Future, in J. F. S. Papale, ed., 'Volcanic Hazards, Risks and Disasters', Elsevier, Boston, pp. 169 – 202. **URL:** <http://www.sciencedirect.com/science/article/pii/B9780123964533000071>
- Saragoni, G. R., Lew, M., Naeim, F., Carpenter, L. D., Youssef, N. F., Rojas, F. and Schachter Adaros, M. (2010), 'Accelerographic measurements of the 27 February 2010 offshore Maule, Chile earthquake', *The Structural Design of Tall and Special Buildings* **19**, 866–875.
- Sawyer, G., Salerno, G., Blond, J. L., Martin, R., Spampinato, L., Roberts, T., Mather, T., Witt, M., Tsanev, V. and Oppenheimer, C. (2011), 'Gas and aerosol emissions from Villarrica volcano, Chile', *Journal of Volcanology and Geothermal Research* **203**(1–2), 62 – 75. **URL:** <http://www.sciencedirect.com/science/article/pii/S0377027311000850>
- SERNAGEOMIN (2015a), 'Informe de Resumen Crisis Volcán Villarrica Febrero-Marzo 2015'. Last accessed: August, 2015. **URL:** <http://www.sernageomin.cl/archivosVolcanes/informe-volcanvillarica.pdf>
- SERNAGEOMIN (2015b), 'Reporte de Actividad Volcánica (RAV) - REGIONES DE LA ARAUCANÍA - LOS RÍOS'. **URL:** http://www.sernageomin.cl/reportesVolcanes/20150818050613346RAV_Araucan%C3%ADa-Los_R%C3%ADos_Agosto_2015_vol_102%20%281%29.pdf
- Shao, G., Li, X., Liu, Q., Zhao, X., Yano, T. and Ji, C. (2010), 'Preliminary slip model of the Feb 27, 2010 Mw 8.9 Maule, Chile Earthquake'. Accessed Sep. 2015. **URL:** http://www.geol.ucsb.edu/faculty/ji/big_earthquakes/2010/02/27/chile_2_27.html
- Shimozuru, D. (1972), A seismological approach to the prediction of volcanic eruptions, in 'The Surveillance and prediction of volcanic activity', UNESCO, pp. 19–45.

BIBLIOGRAPHY

- Shinohara, H. and Witter, J. B. (2005), 'Volcanic gases emitted during mild Strombolian activity of Villarrica volcano, Chile', *Geophysical Research Letters* **32**(20), n/a–n/a. **URL:** <http://dx.doi.org/10.1029/2005GL024131>
- Sibbett, B. S. (1988), 'Size, depth and related structures of intrusions under stratovolcanoes and associated geothermal systems', *Earth-Science Reviews* **25**(4), 291 – 309. **URL:** <http://www.sciencedirect.com/science/article/pii/0012825288900700>
- Siebert, L. and Simkin, T. (2002-), 'Volcanoes of the World: an Illustrated Catalog of Holocene Volcanoes and their Eruptions'. Revised: October, 2011. **URL:** <http://www.volcano.si.edu/world/>
- Silva Parejas, C., Druitt, T., Robin, C., Moreno, H. and Naranjo, J. (2010), 'The Holocene Pucón eruption of Volcán Villarrica, Chile: deposit architecture and eruption chronology', *Bulletin of Volcanology* **72**(6), 677–692. **URL:** <http://dx.doi.org/10.1007/s00445-010-0348-9>
- Sladen, A. and Owen, S. (2010), 'Preliminary model combining teleseismic and GPS data 02/27/2010 (Mw 8.8), Chile'. **URL:** http://tectonics.caltech.edu/slip_history/2010_chile/prelim-gps.html
- Smalley, J. R., Kendrick, E., Bevis, M. G., Dalziel, I. W. D., Taylor, F., Lauria, E., Barriga, R., Cassasa, G., Olivero, E. and Piana, E. (2003), 'Geodetic determination of relative plate motion and crustal deformation across the Scotia-South America plate boundary in eastern Tierra del Fuego', *Geochemistry, Geophysics, Geosystems* **4**(9), 1070.
- Snoke, J. A. (2003), FOCMEC: FOcal MEchanism determinations, in W. Lee, H. Kanamori, P. Jennings and C. Kisslinger, eds, 'International Handbook of Earthquake and Engineering Seismology', Vol. 81, Part B of *International Geophysics*, Academic Press, chapter 85.12, pp. 1629–1630. **URL:** <http://www.geol.vt.edu/outreach/vtso/focmec/>
- Snoke, J., Munsey, J., Teague, A. G. and Bollinger, G. (1984), 'A program for focal mechanism determination by combined use of polarity and SV-P amplitude ratio data', *Earthquake notes* **55**(3), 15. **URL:** *ii*
- Spica, Z., Legrand, D., Iglesias, A., Walter, T. R., Heimann, S., Dahm, T., Froger, J.-L., Rémy, D., Bonvalot, S., West, M. and Pardo, M. (2015), 'Hydrothermal and magmatic reservoirs at Lazufre volcanic area, revealed by a high-resolution seismic noise tomography', *Earth and Planetary Science Letters* **421**, 27 – 38. **URL:** <http://www.sciencedirect.com/science/article/pii/S0012821X15001910>
- SSN (2011), 'Servicio Sismológico Nacional'. **URL:** <http://www.sismologia.cl>
- Stankiewicz, J., Ryberg, T., Haberland, C., Fauzi and Natawidjaja, D. (2010), 'Lake Toba volcano magma chamber imaged by ambient seismic noise tomography', *Geophysical Research Letters* **37**(17), n/a–n/a. L17306. **URL:** <http://dx.doi.org/10.1029/2010GL044211>
- Stern, C. (2004), 'Active Andean volcanism: its geologic and tectonic setting', *Andean Geology* **31**(2), 161–206.
- Tárraga, M., Carniel, R., Ortiz, R., García, A. and Moreno, H. (2008), 'A dynamical analysis of the seismic activity of Villarrica volcano (Chile) during september - october 2000', *Chaos, Solitons & Fractals* **37**(5), 1292–1299.
- Taylor, D. W., Snoke, J. A., Sacks, I. S. and Takanami, T. (1991), 'Seismic quiescence before the Urakawa-Oki earthquake', *Bulletin of the Seismological Society of America* **81**(4), 1255–1271.

BIBLIOGRAPHY

- Tilmann, F., Grevemeyer, I., Flueh, E. R., Dahm, T. and Gossler, J. (2008), 'Seismicity in the outer rise offshore southern Chile: Indication of fluid effects in crust and mantle', *Earth and Planetary Science Letters* **269**, 41–55.
- Tong, X., Sandwell, D., Luttrell, K., Brooks, B., Bevis, M., Shimada, M., Foster, J., Smalley Jr., R., Parra, H., Báez Soto, J. C., Blanco, M., Kendrick, E., Genrich, J. and Caccamise, D. J. (2010), 'The 2010 Maule, Chile earthquake: Downdip rupture limit revealed by space geodesy', *Geophysical Research Letters* **37**, L24311.
- Ukawa, M. (2005), 'Deep low-frequency earthquake swarm in the mid crust beneath Mount Fuji (Japan) in 2000 and 2001', *Bulletin of Volcanology* **68**(1), 47–56. **URL:** <http://dx.doi.org/10.1007/s00445-005-0419-5>
- U.S.G.S. (n.d.), 'U.S. Geological Survey'. **URL:** <http://earthquake.usgs.gov/earthquakes/>
- Utsu, T. (1969), 'Aftershocks and earthquake statistics(1) : Some parameters which characterize an aftershock sequence and their interrelations', *Journal of the Faculty of Science, Hokkaido University. Series 7, Geophysics* **3**(3), 129–195.
- Utsu, T. (1970), 'Aftershocks and earthquake statistics(2) : Further investigation of aftershocks and other earthquake sequences based on a new classification of earthquake sequences', *Journal of the Faculty of Science, Hokkaido University. Series 7, Geophysics* **3**(4), 197–266.
- Vidale, J. (1988), 'Finite-difference calculation of travel times', *Bulletin of the Seismological Society of America* **78**(6), 2062–2076. **URL:** <http://www.bssaonline.org/content/78/6/2062.abstract>
- Walter, T. and Amelung, F. (2007), 'Volcanic eruptions following $M \geq 9$ megathrust earthquakes: Implications for the Sumatra-Andaman volcanoes', *Geology* **35**, 539 – 542.
- Wardlaw, R., Frohlich, C. and Davis, S. D. (1990), 'Evaluation of precursory seismic quiescence in sixteen subduction zones using single-link cluster analysis', *Pure and Applied Geophysics* **134**, 57–78.
- Wassermann, J. (2012), Volcano seismology, in P. Bormann, ed., 'IASPEI New manual of seismological observatory practice 2 (NMSOP-2)', second edn, Vol. 13, Deutsches GeoForschungsZentrum GFZ, Potsdam, pp. 1 – 77.
- Watt, S. F., Pyle, D. M. and Mather, T. A. (2009), 'The influence of great earthquakes on volcanic eruption rate along the Chilean subduction zone', *Earth and Planetary Science Letters* **277**(3–4), 399 – 407. **URL:** <http://www.sciencedirect.com/science/article/pii/S0012821X08007115>
- Wegler, U., Lühr, B. G. and Ratdomopurbo, A. (1999), 'A repeatable seismic source for tomography at volcanoes', *Annals of Geophysics* **42**(3), 2037–416X. **URL:** <http://www.annalsofgeophysics.eu/index.php/annals/article/view/3736>
- Wehrmann, H. and Dzierma, Y. (2011), 'Applicability of statistical eruption analysis to the geological record of Villarrica and Lanín volcanoes, Southern Volcanic Zone, Chile', *Journal of Volcanology and Geothermal Research* **200**, 99–115.
- Wessel, P. and Smith, W. H. F. (1991), 'Free software helps map and display data', *EOS Trans. AGU* **72**, 441.

BIBLIOGRAPHY

- Wessel, P. and Smith, W. H. F. (1998), 'New, improved version of the Generic Mapping Tools released', *EOS, Transaction, American Geophysical Union* **79**, 579.
- Wessel, P., Smith, W. H. F., Scharroo, R., Luis, J. and Wobbe, F. (2013), 'Generic Mapping Tools: Improved Version Released', *Eos, Transactions American Geophysical Union* **94**(45), 409–410. **URL:** <http://dx.doi.org/10.1002/2013EO450001>
- White, R. A. (1996), 'Precursory deep long-period earthquakes at mount pinatubo: Spatio-temporal link to a basalt trigger', *Fire and Mud: Eruptions and Lahars of Mount Pinatubo, Philippines. Univ. Washington Press, Seattle* (-), 307–328.
- White, R. A., Miller, A. D., Lynch, L. and Power, J. (1998), 'Observations of hybrid seismic events at Soufriere Hills Volcano, Montserrat: July 1995 to September 1996', *Geophysical Research Letters* **25**(19), 3657–3660. **URL:** <http://dx.doi.org/10.1029/98GL02427>
- Witter, J. B., Kress, V. C., Delmelle, P. and Stix, J. (2004), 'Volatile degassing, petrology, and magma dynamics of the Villarrica Lava Lake, Southern Chile', *Journal of Volcanology and Geothermal Research* **134**(4), 303 – 337. **URL:** <http://www.sciencedirect.com/science/article/pii/S0377027304000630>
- Xue, Y., Liu, J. and Li, G. (2010), 'Characteristics of seismic activity before Chile MW8.8 earthquake in 2010', *Earthquake Science* **23**(4), 333–341.
- Zandomenighi, D., Aster, R., Kyle, P., Barclay, A., Chaput, J. and Knox, H. (2013), 'Internal structure of Erebus volcano, Antarctica imaged by high-resolution active-source seismic tomography and coda interferometry', *Journal of Geophysical Research: Solid Earth* **118**(3), 1067–1078. **URL:** <http://dx.doi.org/10.1002/jgrb.50073>
- Zobin, V. M. (2003), Introduction to volcanic seismology, in 'Developments in Volcanology', Vol. 6, Elsevier, pp. 1–290.

Appendix A

Appendix from Chapter “Comparison of Seismic Activity for Llaima and Villarrica Volcanoes prior to and after the Maule 2010 Earthquake”

A.1 SFB Catalogue Construction

Catalogue Construction

To retrieve a seismic activity catalogue of the volcanoes Villarrica and Llaima the following three steps was performed:

1. filtering in three bands,
2. automatic triggering and
3. network triggering.

Filtering

The data were filtered in the following frequency bands: (1) between 0.25 Hz and 0.5 Hz, (2) between 0.8 Hz and 2.4 Hz and (3) between 6 Hz and 12 Hz. While volcanic events such as LP, TR and some HB events have their main energy in the second band, local, regional and teleseismic events would also appear in the other frequency bands (see Figure A.1).

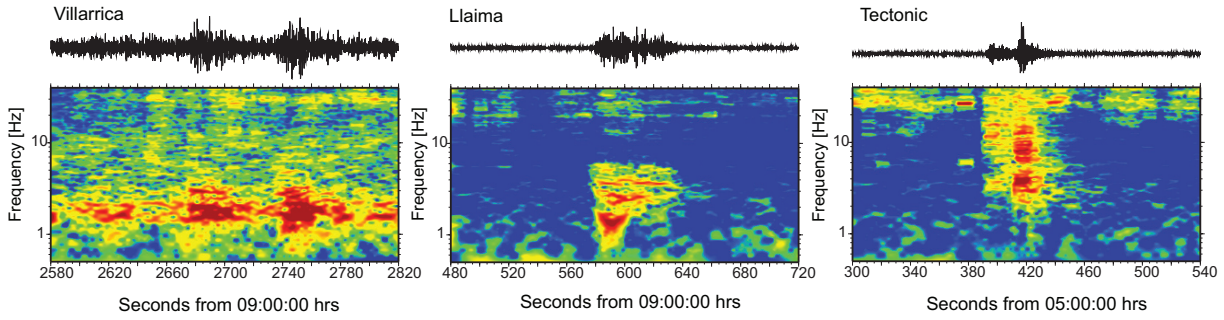


Figure A.1: Left: Spectrogram for a volcanic event in Villarrica volcano. Horizontal axis marks seconds from 09:00:00 (GMT) of January 17th, 2011. Center: Spectrogram for a volcanic event in Llaima volcano. Horizontal axis marks seconds from 09:00:00 (GMT) of January 17th, 2011. Right: Spectrogram for a tectonic regional event, for comparison of frequency band content. Horizontal axis marks seconds from 05:00:00 (GMT) of January 17th, 2011.

Automatic Triggering

The aim of an automatic triggering is to identify a sudden increase of the recorded seismic energy. The most common approach is the calculation of the ratio STA/LTA (Short-Term-Average/Long-Term-Average) of the seismic energy. A sudden increase of the seismic activity would affect the STA, increasing the ratio. When the ratio exceeds a threshold, the trigger is active and the time is stored. Once the event is finished or levels of energy are below the threshold, the ratio decreases again to normal values. The parameters of the triggering (Table A.1) were manually adjusted by visual inspection.

Table A.1: Triggering parameters for the three bands studied

Parameter	Band		
	0.25 - 0.5 Hz	0.8 - 2.4 Hz	6 - 12 Hz
STA length [s]	10	10	5
LTS length [s]	100	100	10
Trigger threshold	2	1.7	1.3
Detrigger threshold	1	1	1

Event Detection

A seismic event should be triggered on all seismic stations, while a random increase of seismic energy on one station should not be seen at the others. This random increases of energy could be generated by animal farming, human activity and/or nearby traffic. To distinguish between an event and a random increase, the times of the trigger are compared on several stations. Here only the Short Period stations were used because of consistency. If there are triggers on 2 or 3 stations within a time window, it is assumed to be a real seismic event. The time window had a length of 15 seconds due to travel time differences and time shift of the trigger onset caused by higher noise.

A.2 Removal of aftershock sequence from time series

The removal of the aftershock sequence from time series of seismic events was performed by fitting a combination of a linear trend and modified Omori's law to a relevant part of the time series. The modified Omori's law describes the rate of occurrence of aftershocks t days after the main shock (e.g. Lomnitz (1994)) and can be approximated for relatively short times by (Utsu, 1969, 1970):

$$\lambda(t) \approx \frac{\alpha}{(t + \beta)^p} \quad (\text{A.1})$$

where p varies between 1 and 2 (Lomnitz, 1994) and α and β are fitting parameters. To maintain the overall trend in the time series a combination of Omori's law and linear model was used to fit the data:

$$\lambda(t) = \begin{cases} c_0 + c_1 t & t < 0 \\ \frac{\alpha}{(t + \beta)^p} + c_0 + c_1 t & t \geq 0 \end{cases} \quad (\text{A.2})$$

$t = 0$ is the day of the main shock, that is, 27 February 2010. The fitting parameters α , β , p , c_0 , and c_1 (see values on Table A.2) were determined by minimizing the difference between the observed time series and eq.A.2 in a least-squares sense. The parameter p was constrained to be between 1 and 2 following Lomnitz (1994). After that, the Omori part (equation A.1) was calculated separately and subtracted from the time series.

Table A.2: Values of fitting parameters for the band 0.8 - 2.4 Hz, for both Llaima and Villarrica volcanoes

	α	β	p	c_0	c_1
Llaima	1,3E+06	86	2	109	0,2
Villarrica	2,08E+06	43	2	179	-1,6

A.3 Activity in other volcanoes

Here we describe the activity presented by other volcanoes prior to or after the earthquake, according to the reports from OVDAS.

Lonquimay and Planchón Peteroa

The station at Lonquimay volcano, deployed in May 2010, recorded since August 2010 VT activity situated between 8 and 16 km away from the volcano, possibly related to the Liquiñe - Ofqui Fault. On Planchón Peteroa volcano, a station was installed after a white fumarole was observed during August 2010. In September, a continuous tremor was accompanying the fumarole, which presented an intermittent change from white to gray (ashes). The tremor lasted until February 2011, and was combined with VT and LP events. On April 18th, 2011 the volcano started its eruptive process, throwing ashes in the near radius ($leq 10$ km), as a continuation of its previous process started in September 2010.

Mocho - Choshuenco, Calbuco and Osorno

Mocho - Choshuenco volcano presented some activity (approx. 20 VT events) in November 2009. After the earthquake, in March 2010, an increase in activity (463 events between VT and LP) was observed, but still remained under normal levels. Most of the attention was on the Chaitén volcano that had began its eruptive cycle in May 2008, and continued until March 2010 (Siebert and Simkin, 2002-). Osorno volcano showed LP activity in May, 2009 which decreased in January, 2010, and some VT events starting in July 2009. Activity was stated as “normal” in May, 2010. Calbuco presented some activity in 2009, but related to Chaitén, and most of the time the stations were malfunctioning.

Cordón Caulle

Cordón Caulle volcano, which erupted at the beginning of June 2011, was presenting a normal to low VT activity in June - July 2009, and two VT events/day on average, with magnitudes $0.5 \leq M \leq 3.2$. From November 2009 to January 2010 the data states as “not reliable” due to technical problems with the station (less than 6 events in a complete month). In August and November 2010, a significant increase in activity was observed (125 VT/month and 122 VT/month, respectively). The number of events per month raised to ca. 40 VT/month and very few LP events (less than three) on the following months were reported. On April 26th, 2011, a column of gas started to flow out of the volcano accompanied by a swarm of Hybrid and LP events. On June 2nd, 2011 the OVDAS declares the eruption after a total of 25 events/hour.

Appendix B

Appendix from Chapter “Inner Structure of the Villarrica Volcano derived from Local Tomography using Volcano Tectonic Events”

B.1 Bootstrap Method

The Bootstrap Method was introduced by Efron (1979) as an improvement of the Jackknife method, and it is generally used to improve statistical validity and accuracy. It includes the use of different data samples from an original larger sample set to compute statistics and to estimate the distribution of the original set without *a priori* knowledge. Only part of the original sample is used in each subsample with the average number of observations in each bootstrap sample being about $0.632 \times N$, where N is the total number of observations in the original sample (Efron, 1983; Efron and Tibshirani, 1997). This selection reduces data overlapping, and provides a more robust approximation of the true value of the estimator measured (in our case the velocities in each cube of the model).

Lets assume we have a main sample of N observations $x = (x_1, x_2, \dots, x_N)$ and we want to calculate a statistical parameter of arbitrary estimator $\hat{\theta} = s(x)$.

A random sample x_k^* of x will be $x_k^* = (x_1^*, x_2^*, \dots, x_m^*)$ where $m < N$, and typically m is around 63% of N . Each random subsample is identically distributed as the main sample, and thus the particular estimate to calculate can be computed for each of these bootstrap samples $\theta_k^* = s(x_k^*)$, a process which is named Bootstrapped replication.

Then $\theta_1^*, \theta_2^*, \dots, \theta_k^*$ is a random sample distribution of $\hat{\theta}$, and, with K sufficiently large, it can be used to determine statistical quantities of $\hat{\theta}$, in our case, $K = 100$ which is greater than $0.632N$ for $N = 38$.

The Bootstrap estimate for standard error (σ) of $\hat{\theta}$ will be given by

$$\sigma_k(\hat{\theta}) = \sqrt{\frac{\sum_{k=1}^K (\theta_k^* - \bar{\theta}^*)^2}{K-1}} \quad (\text{B.1})$$

with

$$\bar{\theta}^* = \frac{\sum_{k=1}^K \theta_k^*}{K}. \quad (\text{B.2})$$

In our case the original sample is $N = 38$ and each x_j is an event with $x_j = (x, y, z, t_o)$, and the estimator $\hat{\theta}$ is the velocity model V given by $V = (v_1, v_2, \dots, v_i, \dots, v_z)$ with z the total number of cubes in the model. Then $V_k^* = (v_{ik})$ with $i \in 1, 2, \dots, z$ the velocity model obtained for each subsample with v_{ik} the velocity for each cube i in the bootstrapped run k .

In our case, the velocity model retrieved from the Bootstrap is the average of the velocities found for every Bootstrapped tomography in each cube ($\hat{V}_i = \frac{\sum_{k=1}^K v_{ik}}{K}$). And thus the standard deviation per cube is given by

$$\sigma_i = \sqrt{\frac{\sum_{k=1}^K (v_{ik} - \bar{v}_i)^2}{K-1}} \quad (\text{B.3})$$

with

$$\bar{v}_i = \left(\frac{\sum_{i=1}^K v_{ik}}{K} \right) \quad (\text{B.4})$$

as the mean velocity per cube, and the Central Deviation (CD) is

$$CD = \frac{\sigma_i}{v_i}. \quad (\text{B.5})$$

B.2 Polarities

Polarities readings from P- wave arrival.

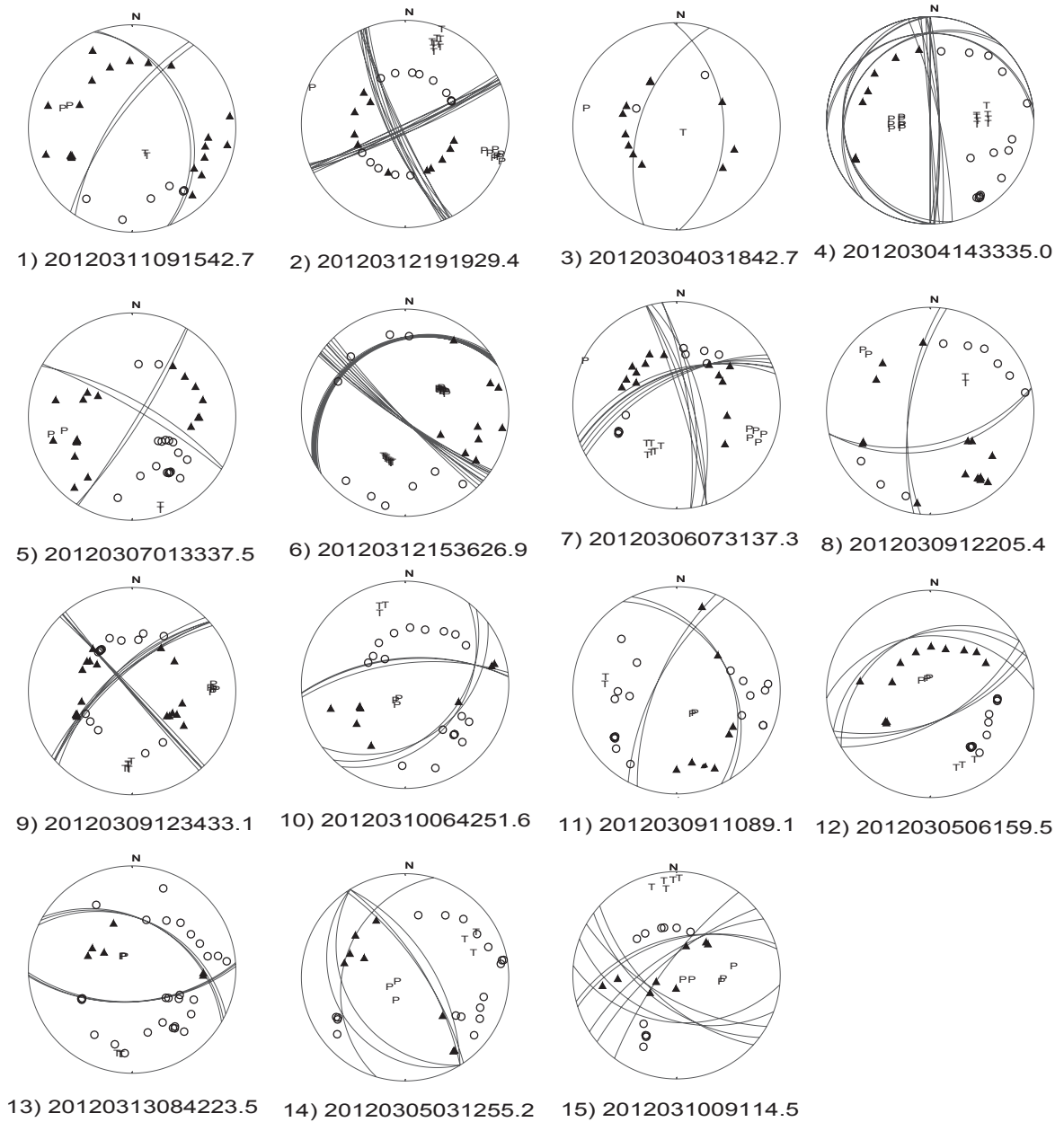


Figure B.1: Polarities from P wave arrival. Compression arrivals are represented as black triangles; dilation arrivals, as white open circles. Number under each focal mechanism shown for reference to the Figure 4.13.

B.3 Ray Bendings

Ray bending calculation were derived using Finite-Difference Eikonal-solving method from Vidale (1988) in the code originally based on the one from Marco Perez in Perez and Bancroft (2000) using traveltime gradient.

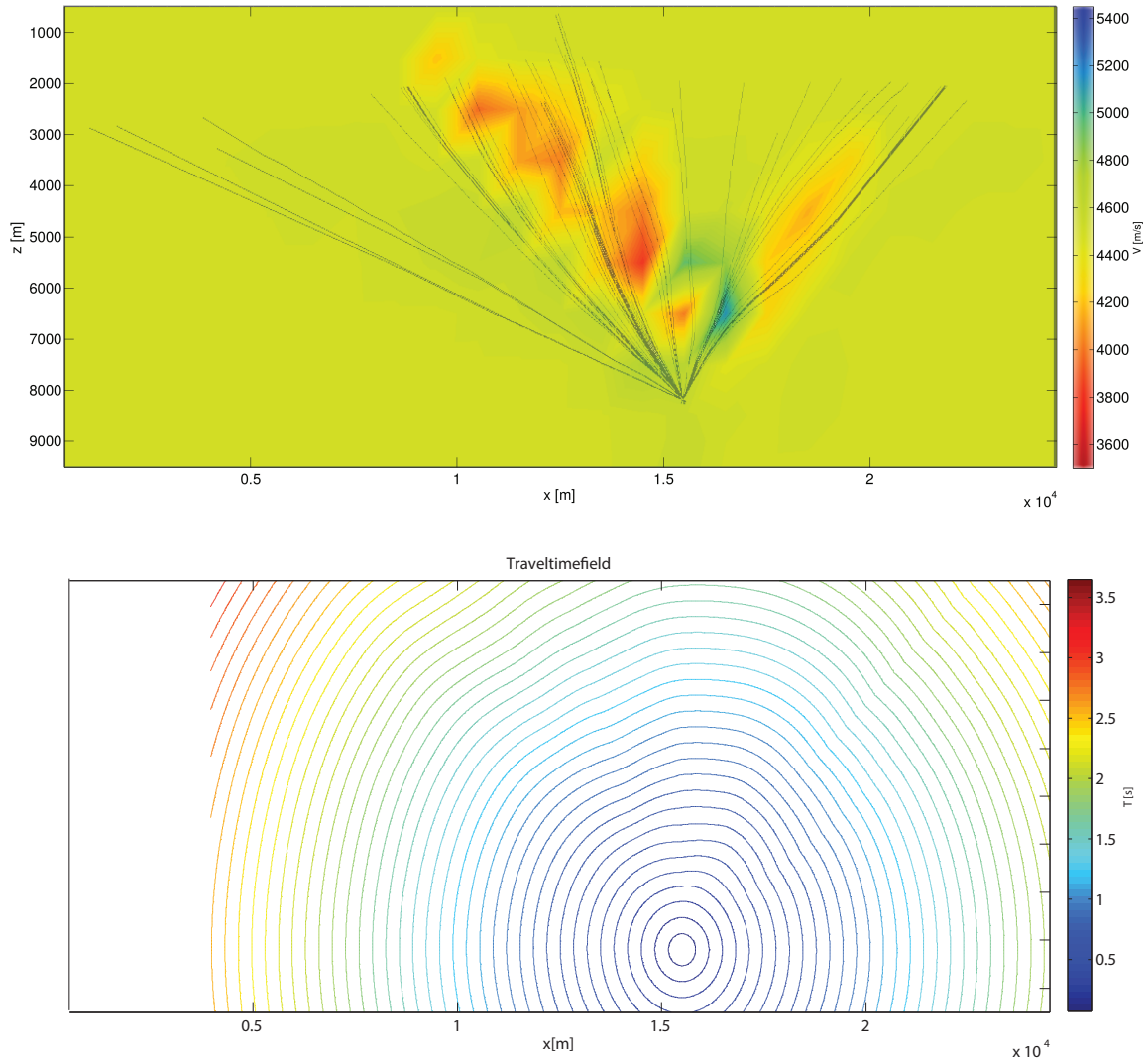


Figure B.2: Ray bending from the solution of Eikonal equation for a East-West profile.

B.4 Supplementary Material

B.4.1 Results

A detailed version of the results for each slice are shown in this appendix. Each figure shows final model of absolute velocity (bottom left), percentage of velocity variation (top left), number of rays per cube (bottom right), and standard deviation per cube (top right). Profiles are clipped, except “Number of Rays”, showing only the area for cubes with 10 or more rays passing through.

B.4.1.1 Horizontal Slices

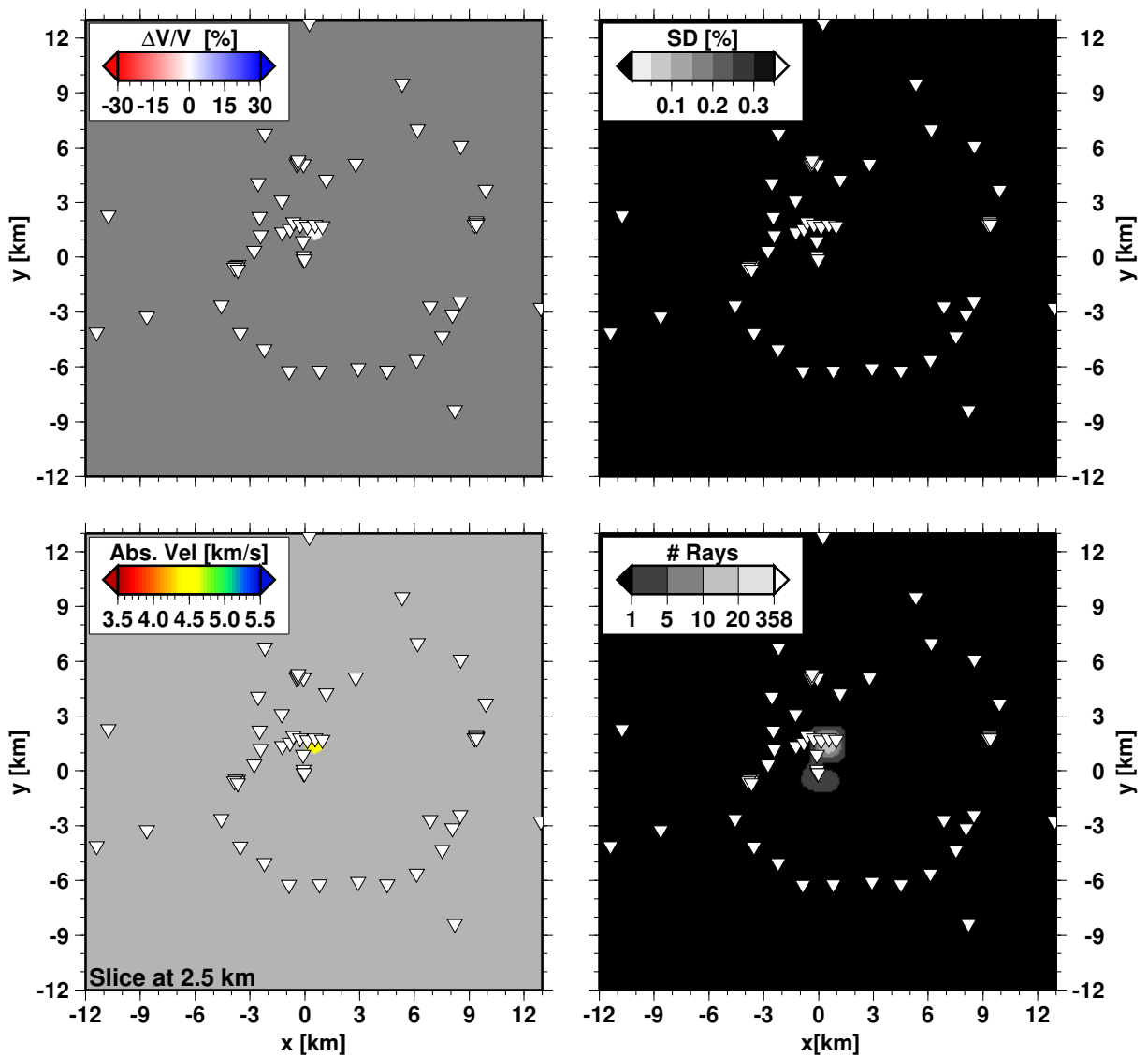


Figure B.3: Results from inversion in horizontal slice at 2.5 km a.s.l.

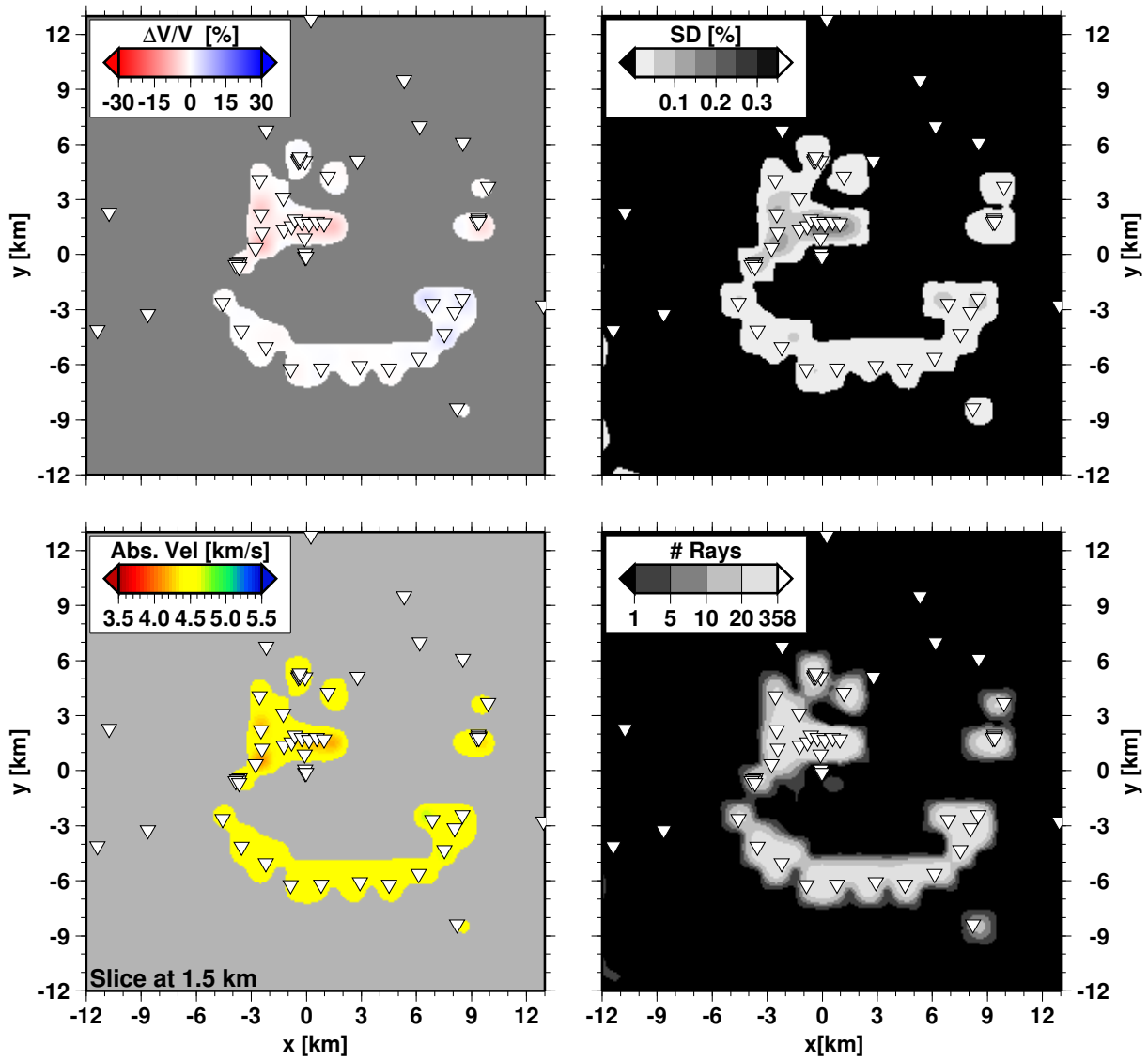


Figure B.4: Results from inversion in horizontal slice at 1.5 km a.s.l.

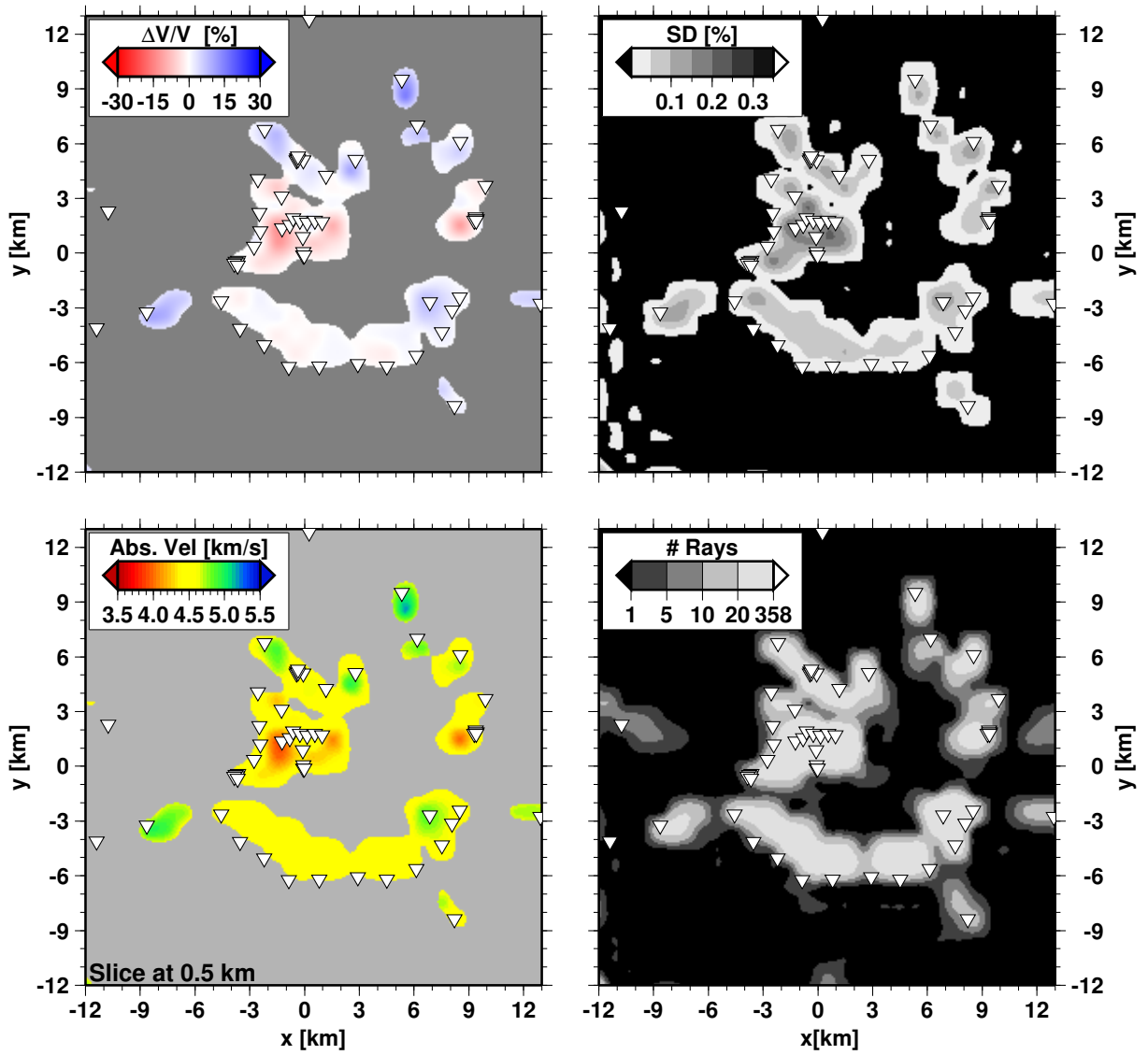


Figure B.5: Results from inversion in horizontal slice at 0.5 km a.s.l.

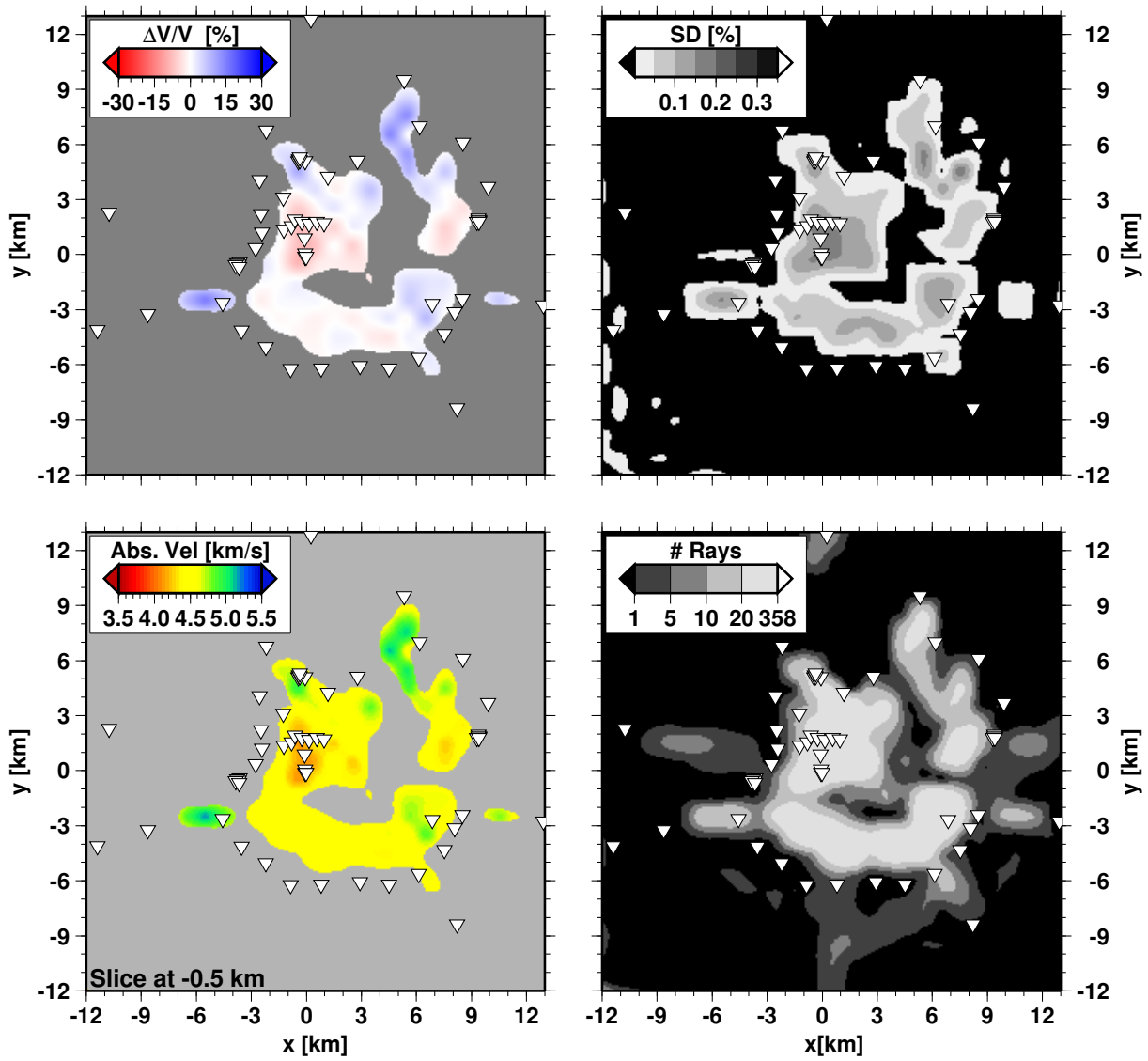


Figure B.6: Results from inversion in horizontal slice at 0.5 km b.s.l.

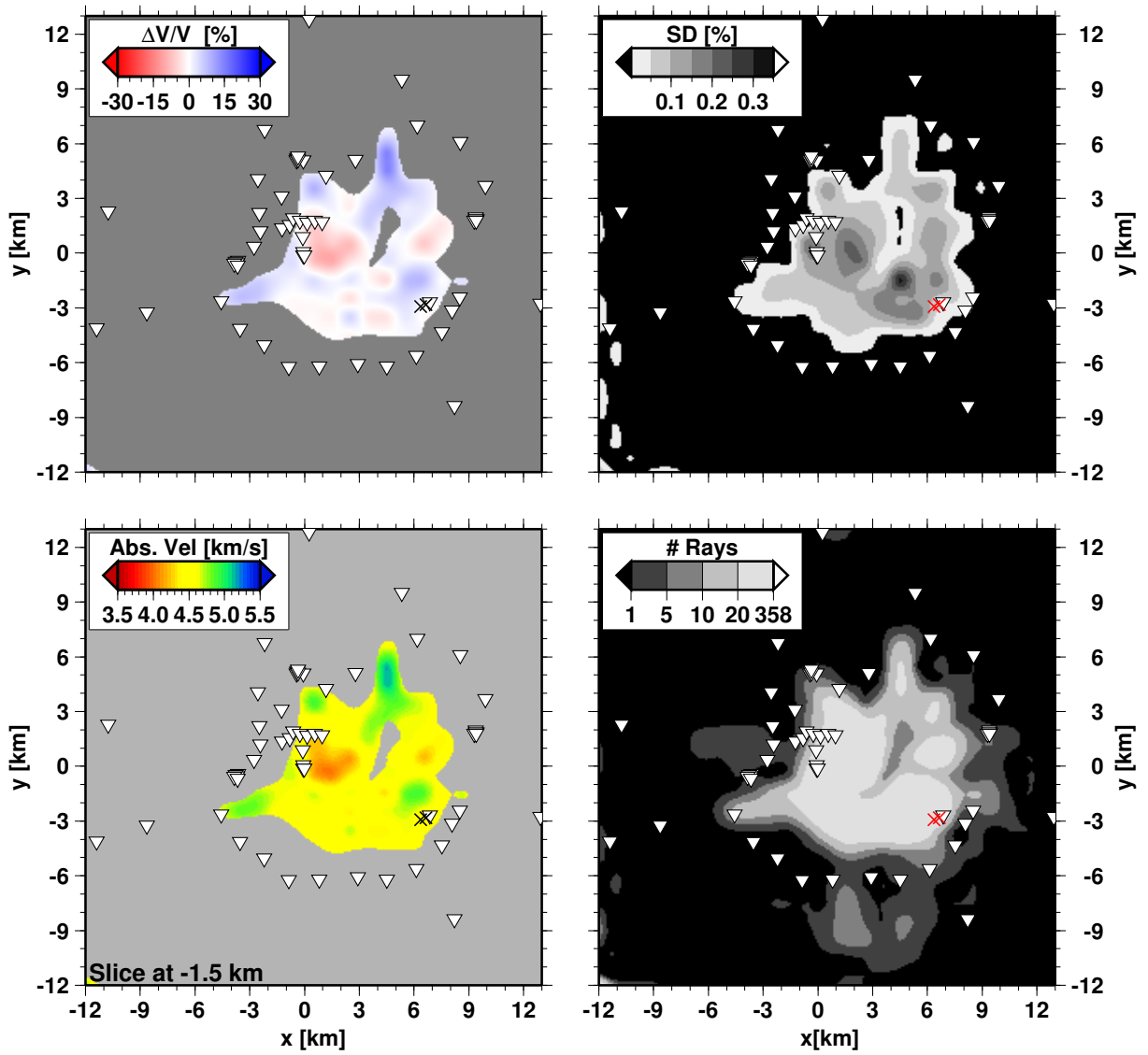


Figure B.7: Results from inversion in horizontal slice at 1.5 km b.s.l.

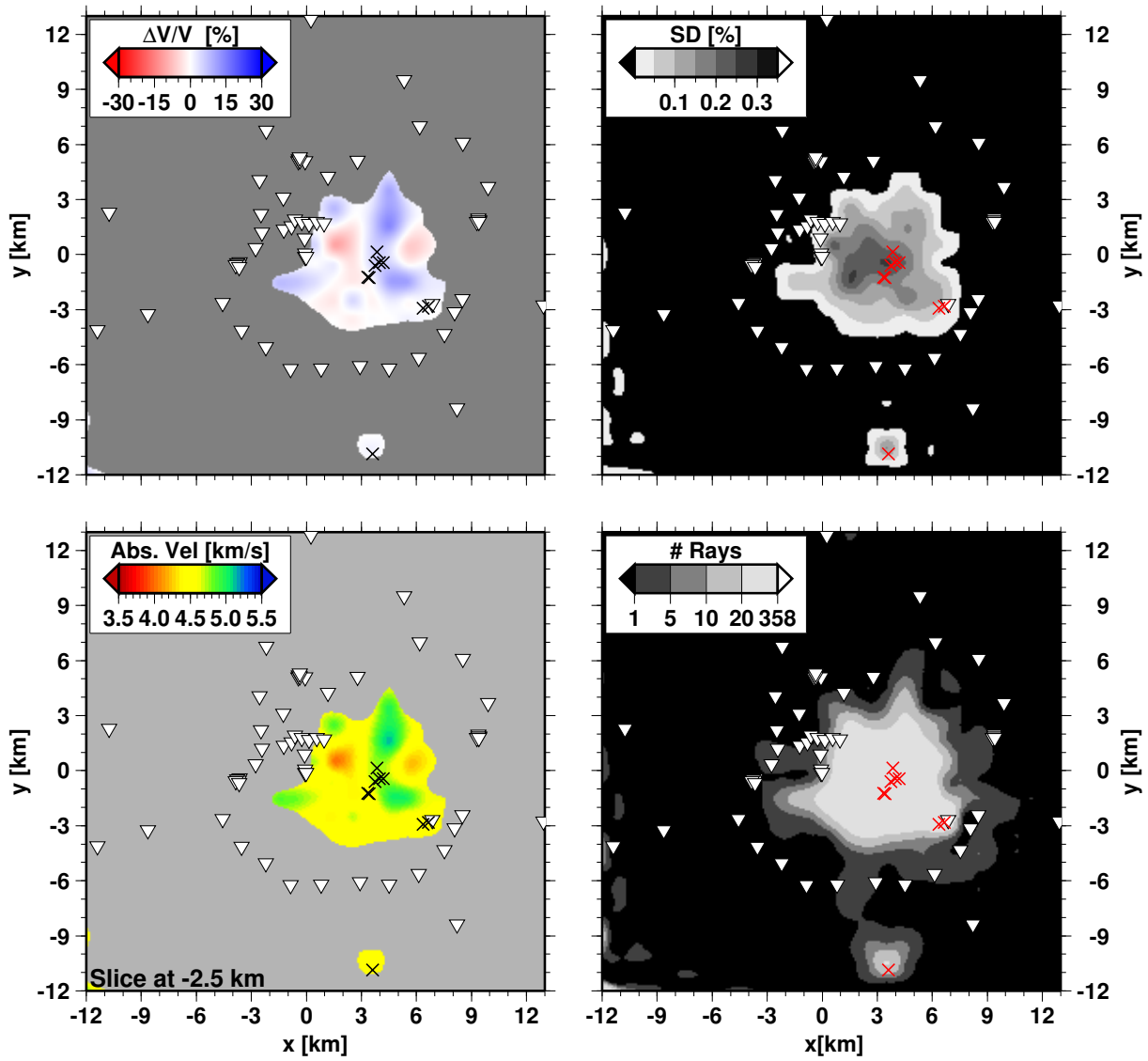


Figure B.8: Results from inversion in horizontal slice at 2.5 km b.s.l.

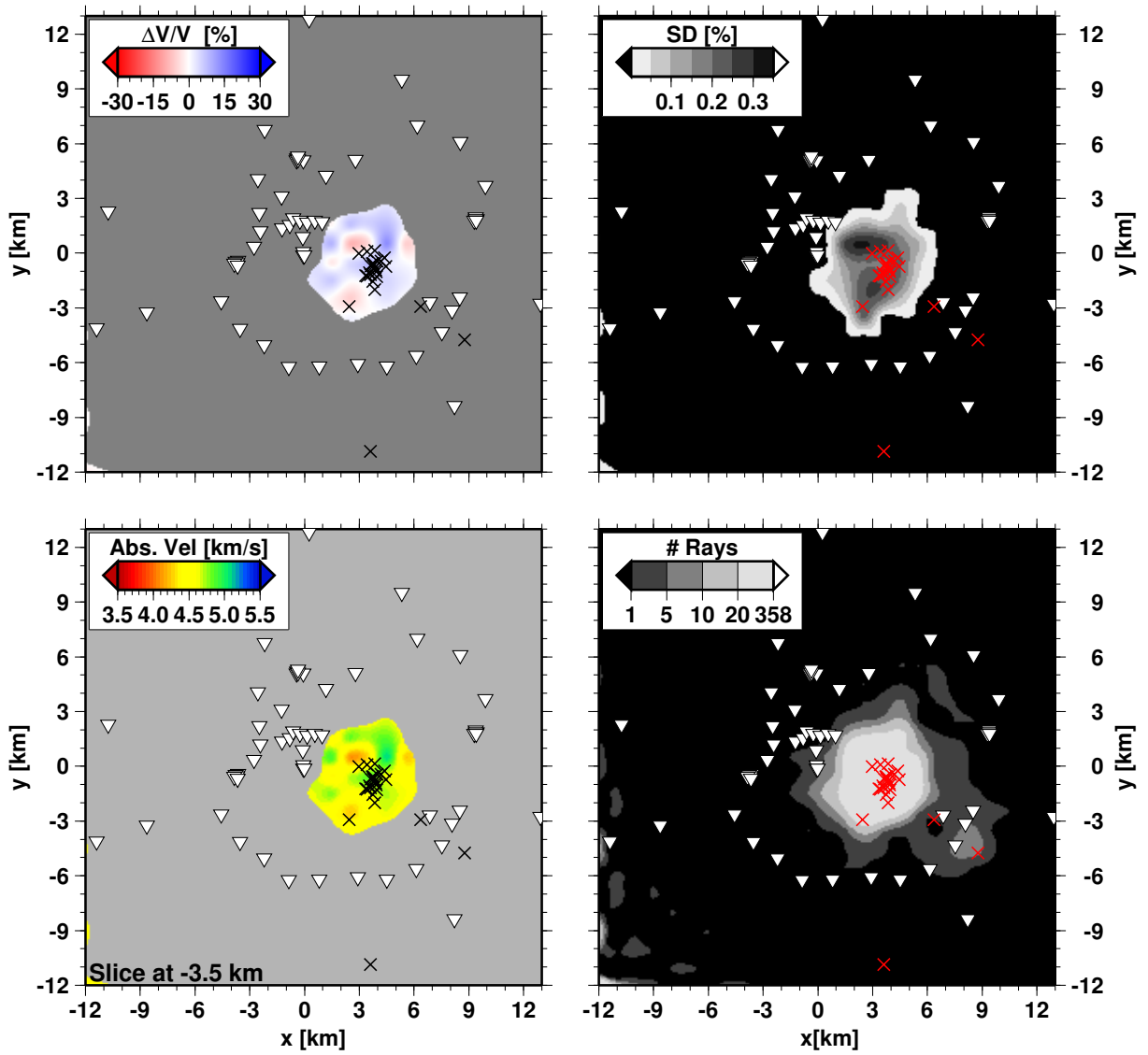


Figure B.9: Results from inversion in horizontal slice at 3.5 km b.s.l.

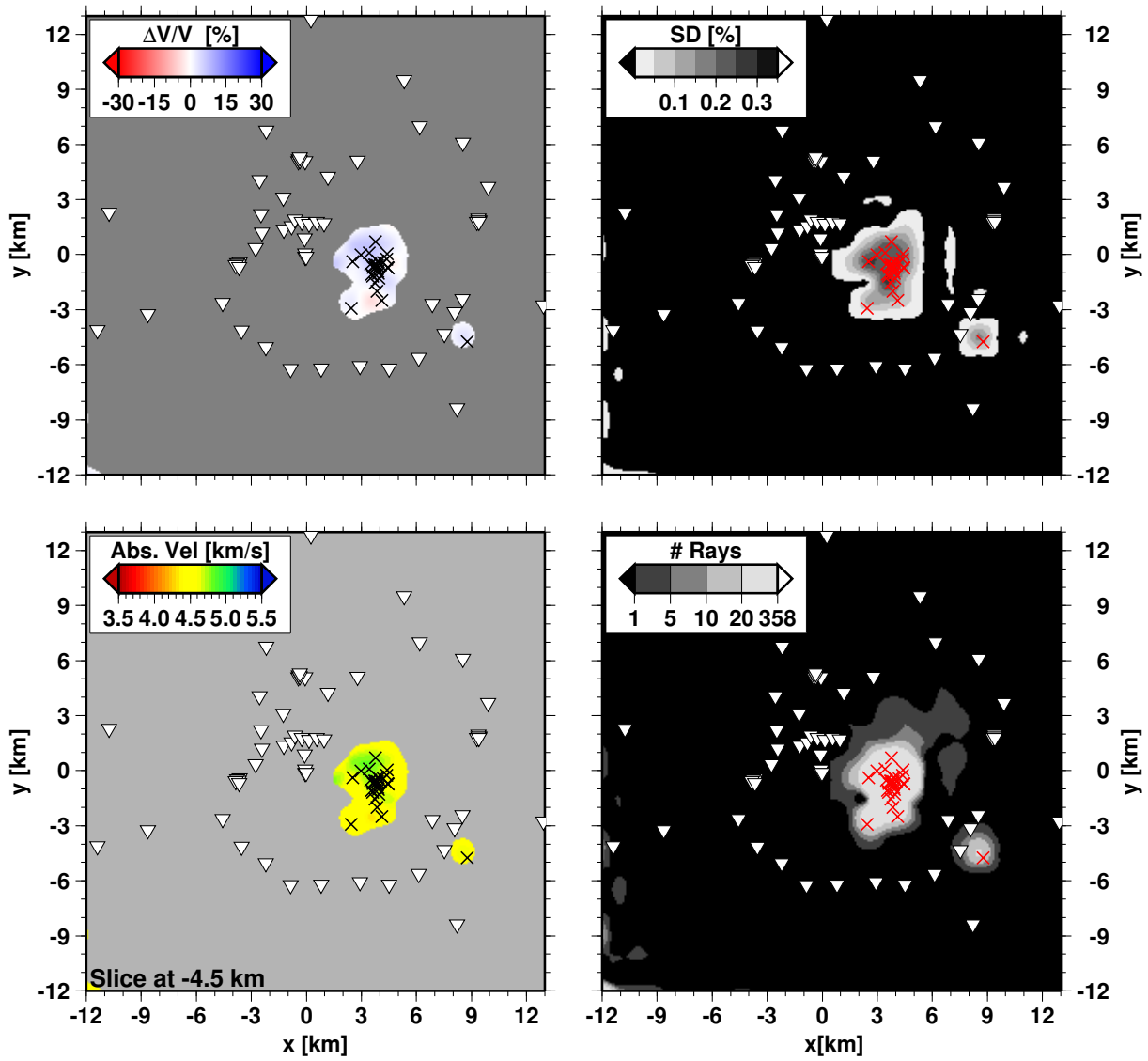


Figure B.10: Results from inversion in horizontal slice at 4.5 km b.s.l.

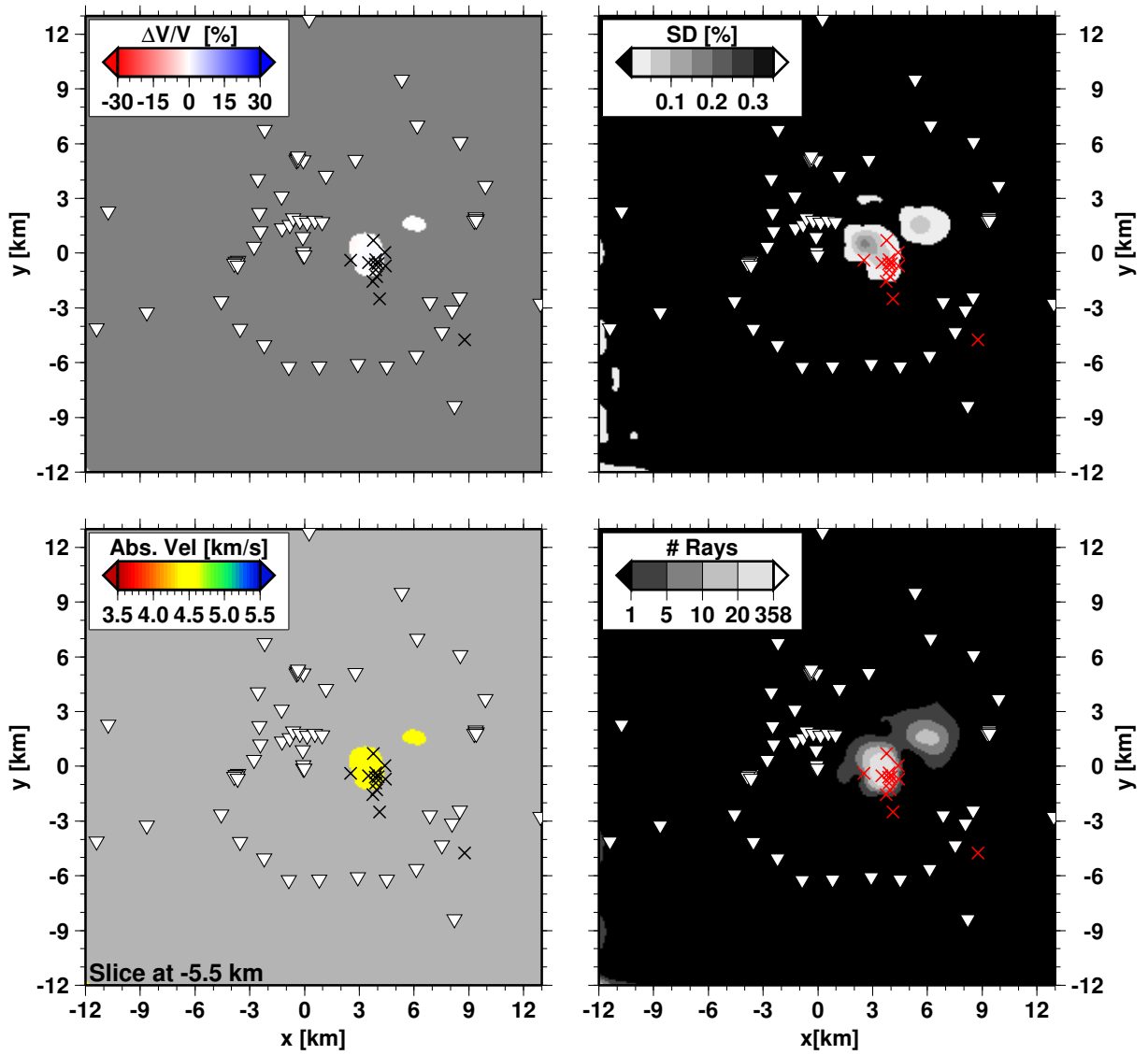


Figure B.11: Results from inversion in horizontal slice at 5.5 km b.s.l.

B.4.1.2 Vertical Profiles East - West

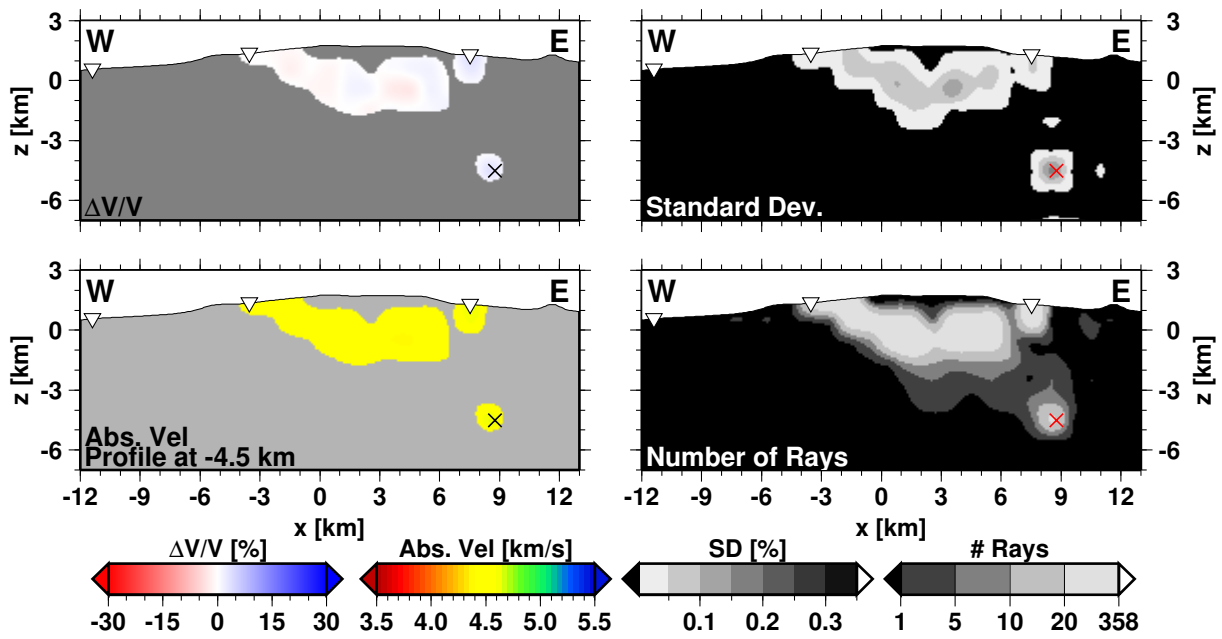


Figure B.12: Results from inversion in vertical E-W profile at -4.5 km (west).

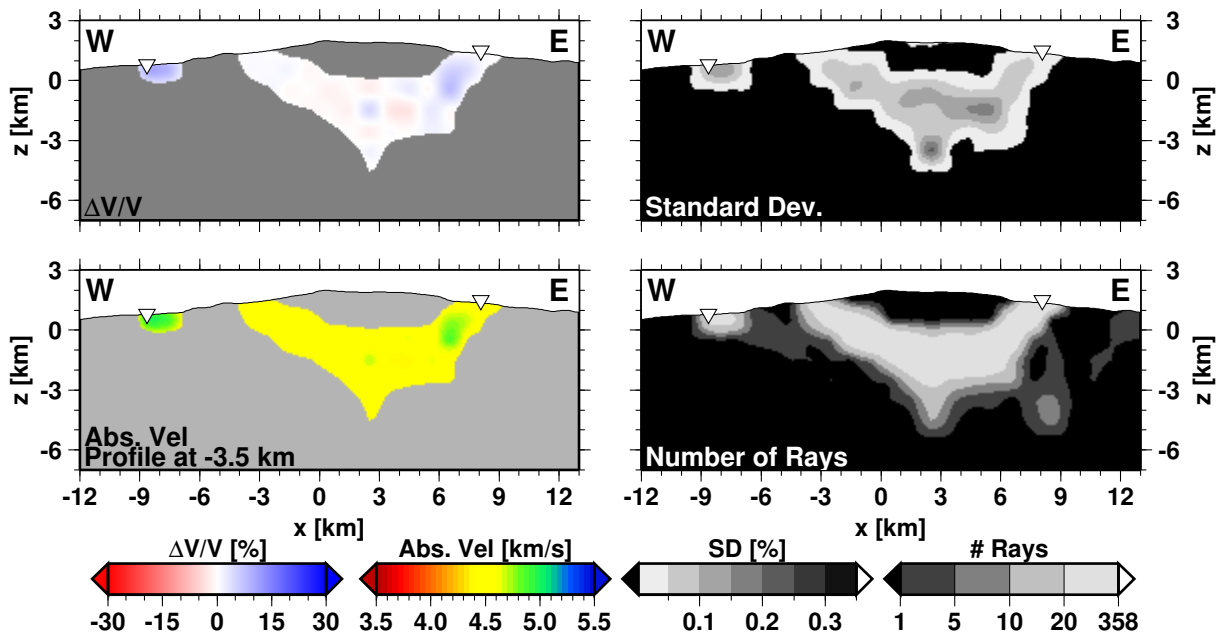


Figure B.13: Results from inversion in vertical E-W profile at -3.5 km (west).

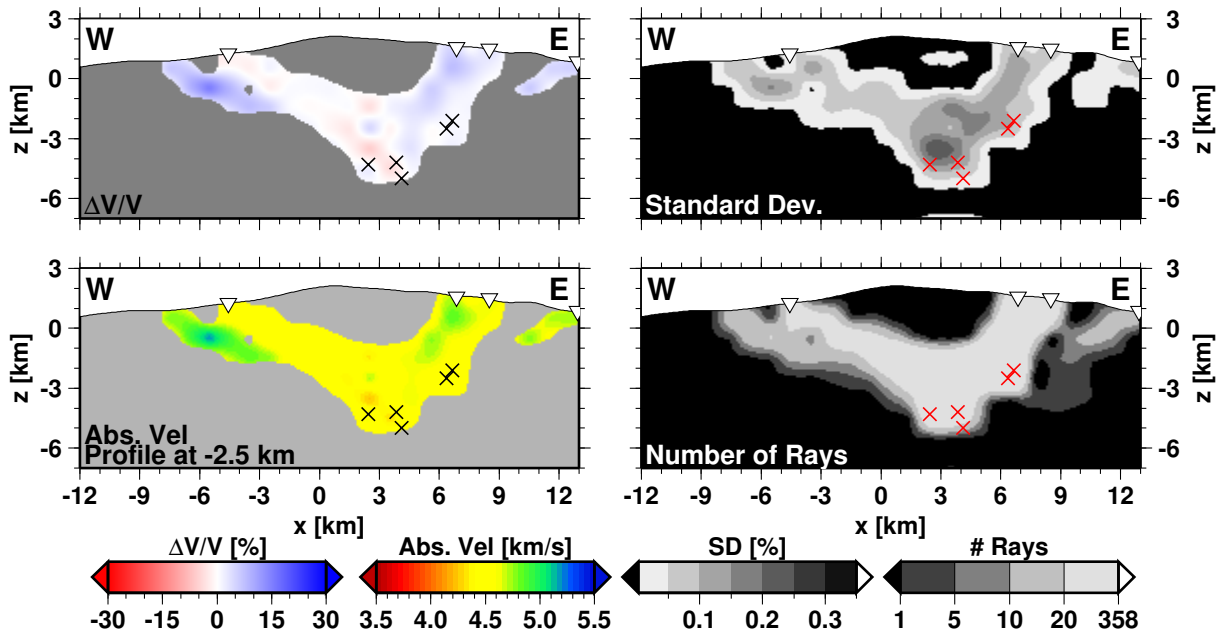


Figure B.14: Results from inversion in vertical E-W profile at -2.5 km (west).

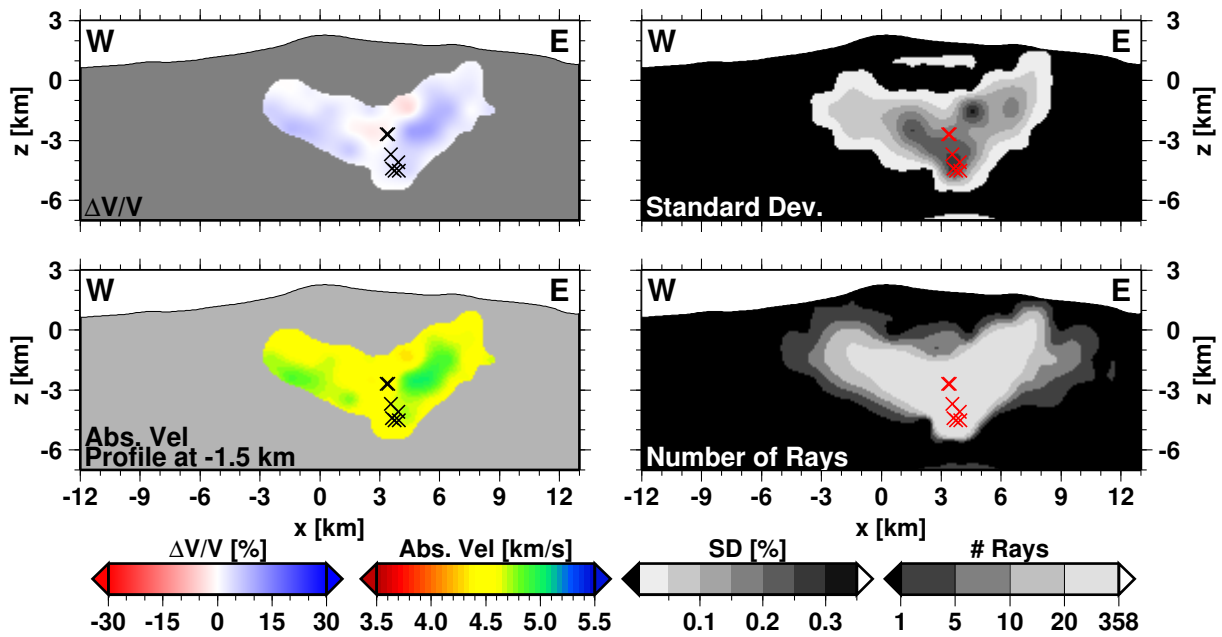


Figure B.15: Results from inversion in vertical E-W profile at -1.5 km (west).

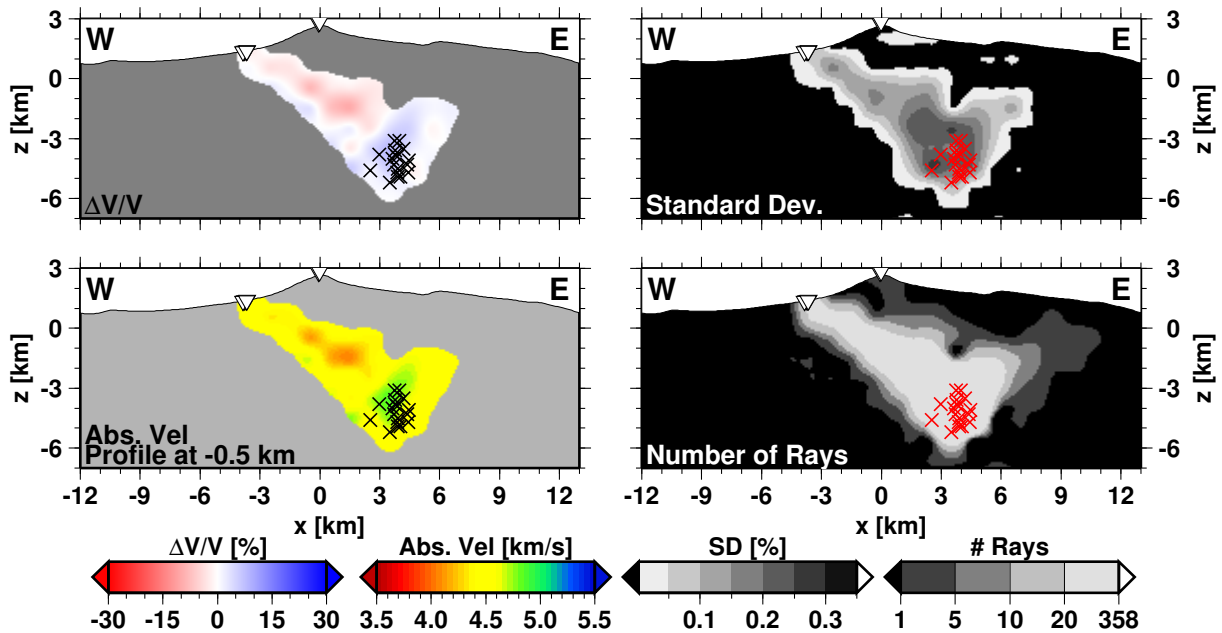


Figure B.16: Results from inversion in vertical E-W profile at -0.5 km (west).

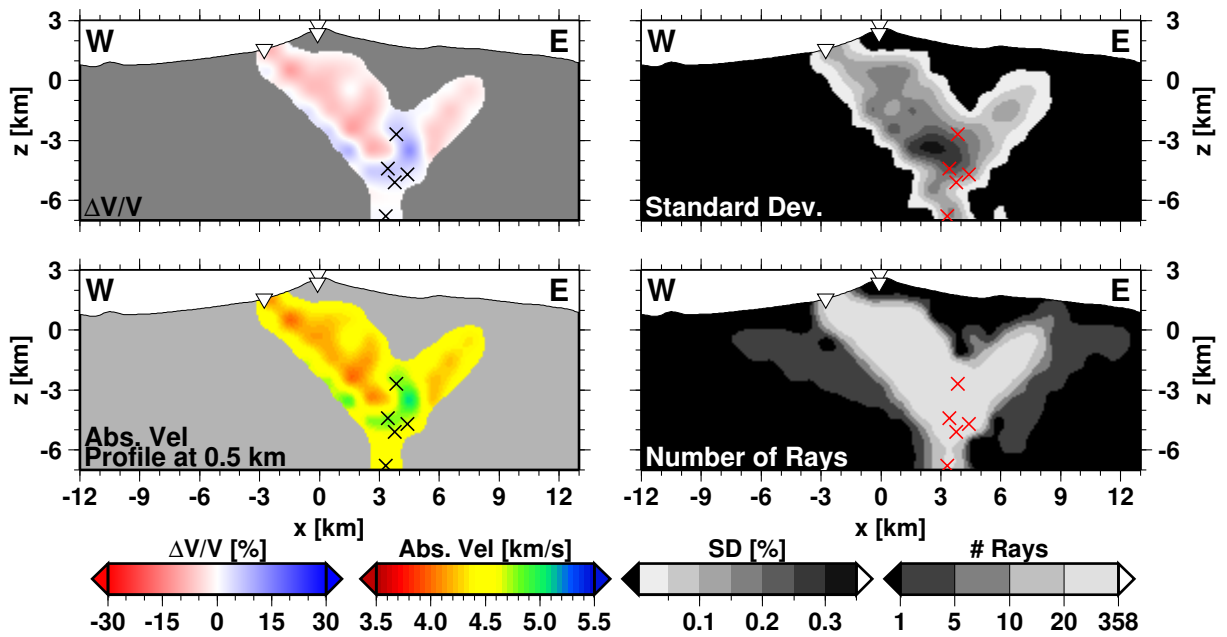


Figure B.17: Results from inversion in vertical E-W profile at 0.5 km (east).

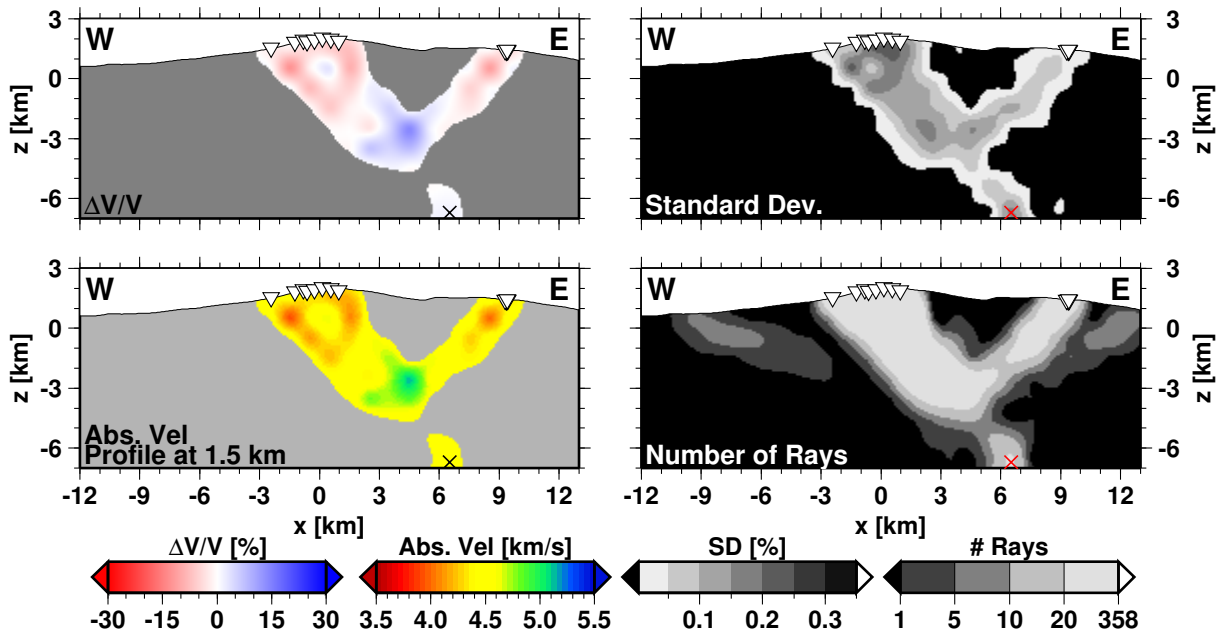


Figure B.18: Results from inversion in vertical E-W profile at 1.5 km (east).

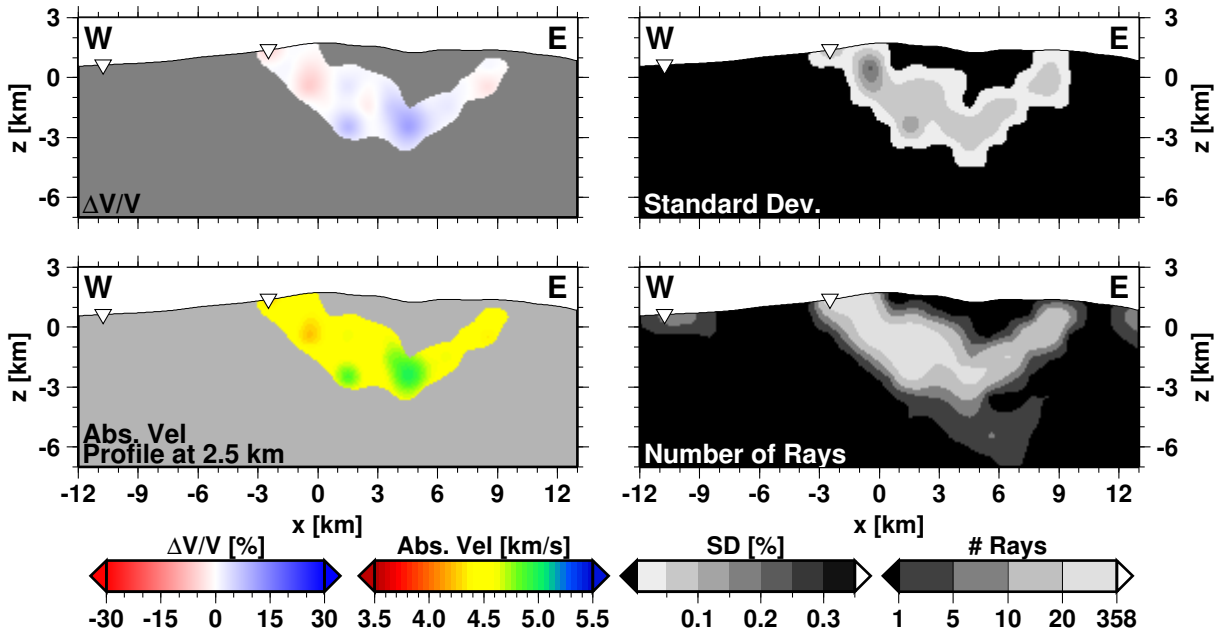


Figure B.19: Results from inversion in vertical E-W profile at 2.5 km (east).

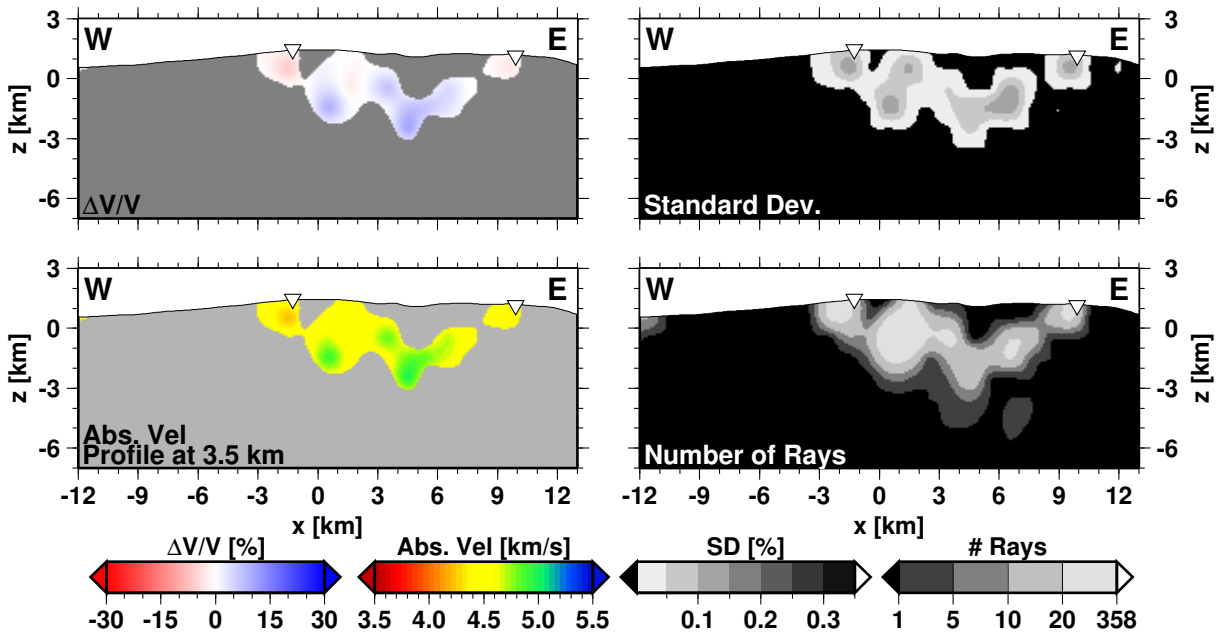


Figure B.20: Results from inversion in vertical E-W profile at 3.5 km (east).

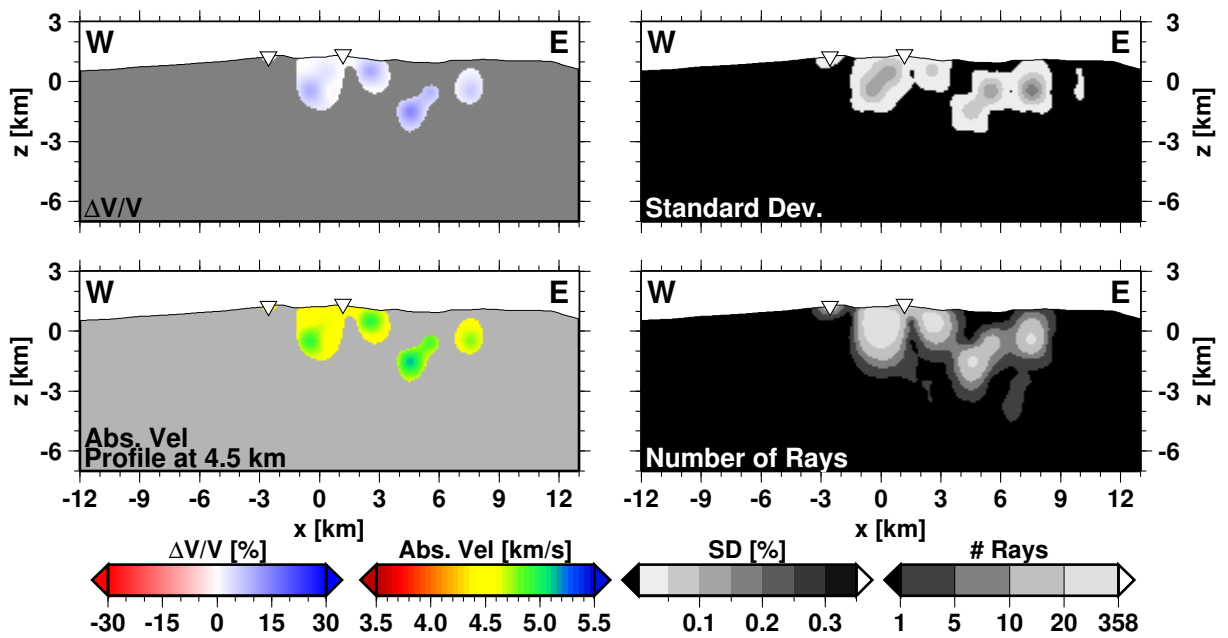


Figure B.21: Results from inversion in vertical E-W profile at 4.5 km (east).

B.4.1.3 Vertical Profiles North - South

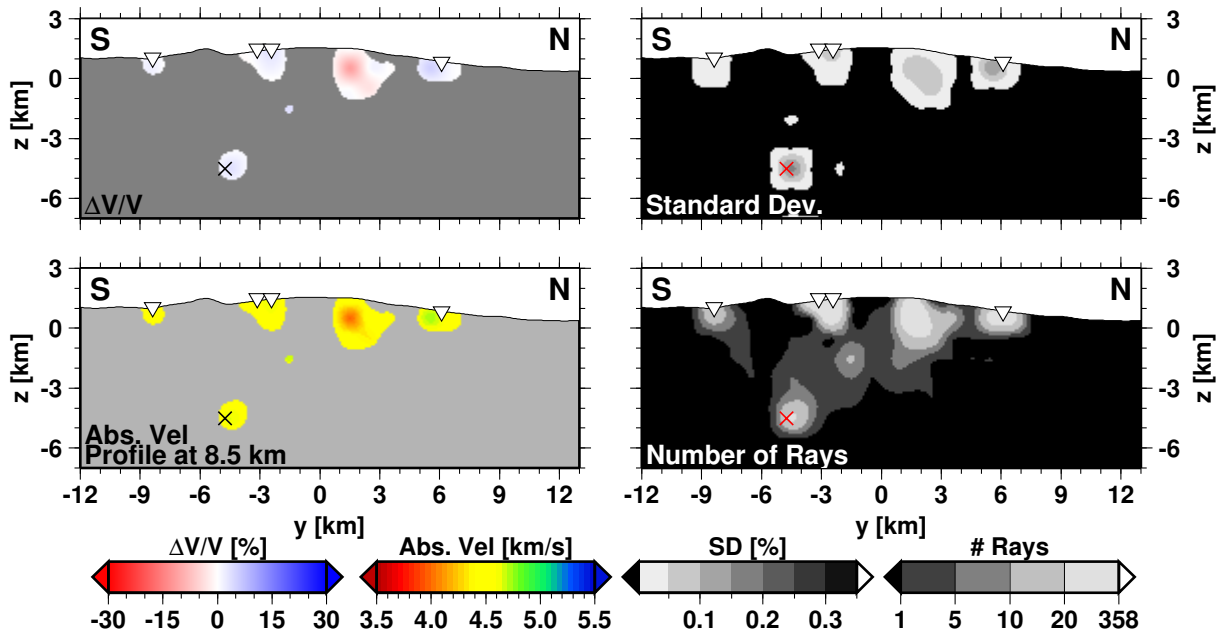


Figure B.22: Results from inversion in vertical N-S profile at 8.5 km (north).

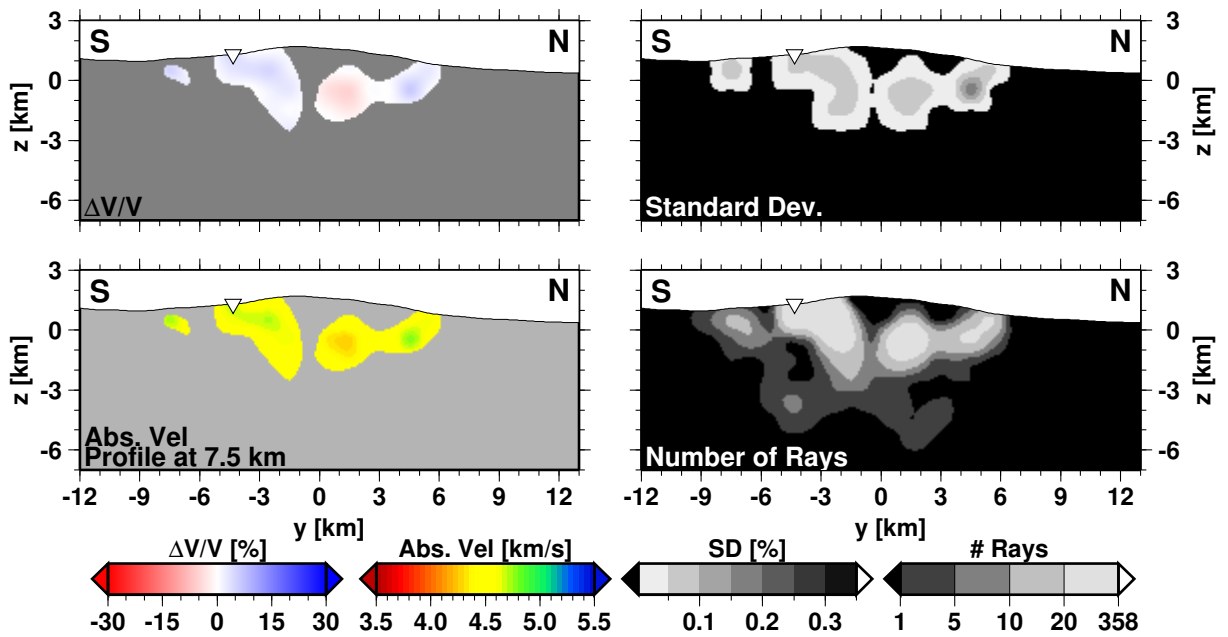


Figure B.23: Results from inversion in vertical N-S profile at 7.5 km (north).

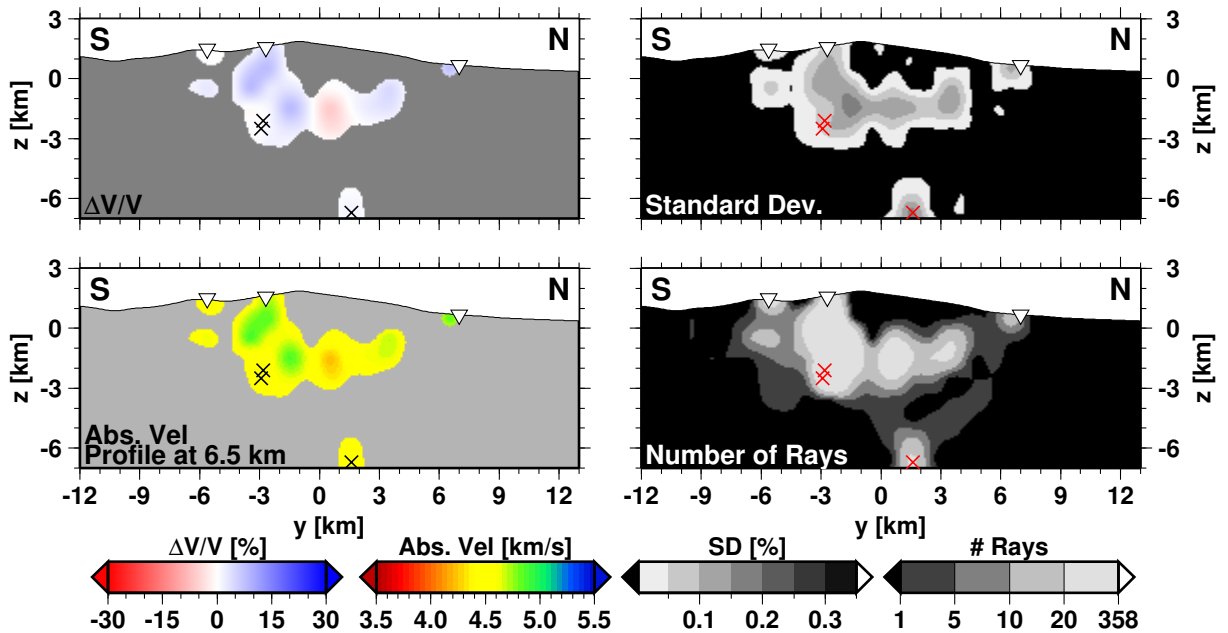


Figure B.24: Results from inversion in vertical N-S profile at 6.5 km (north).

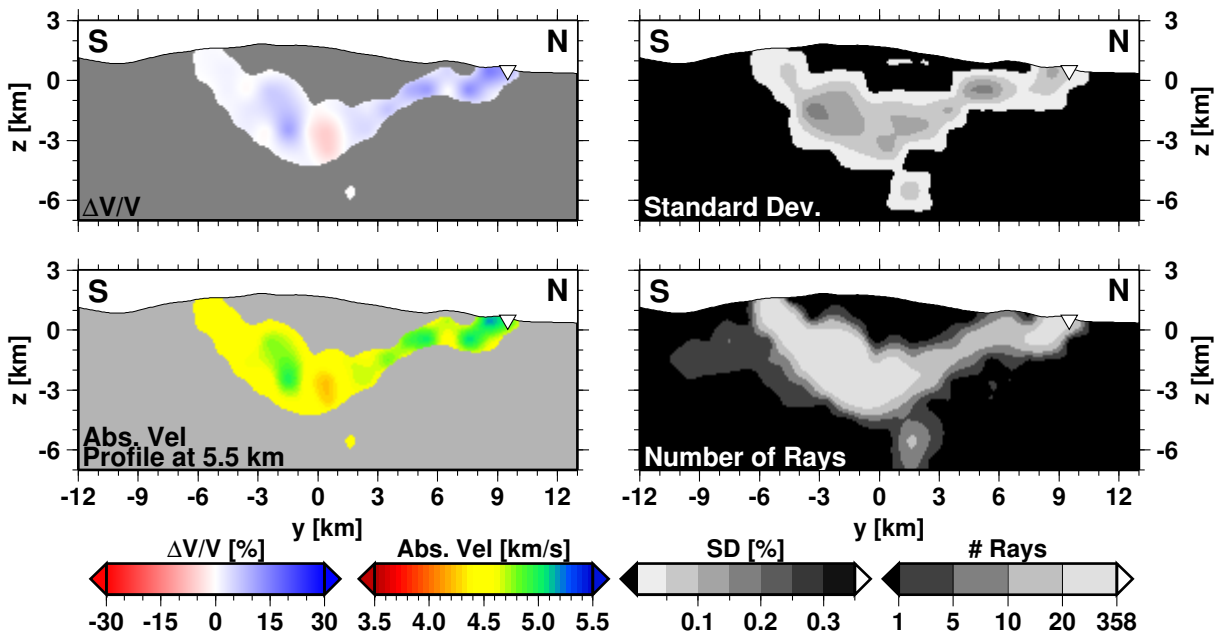


Figure B.25: Results from inversion in vertical N-S profile at 5.5 km (north).

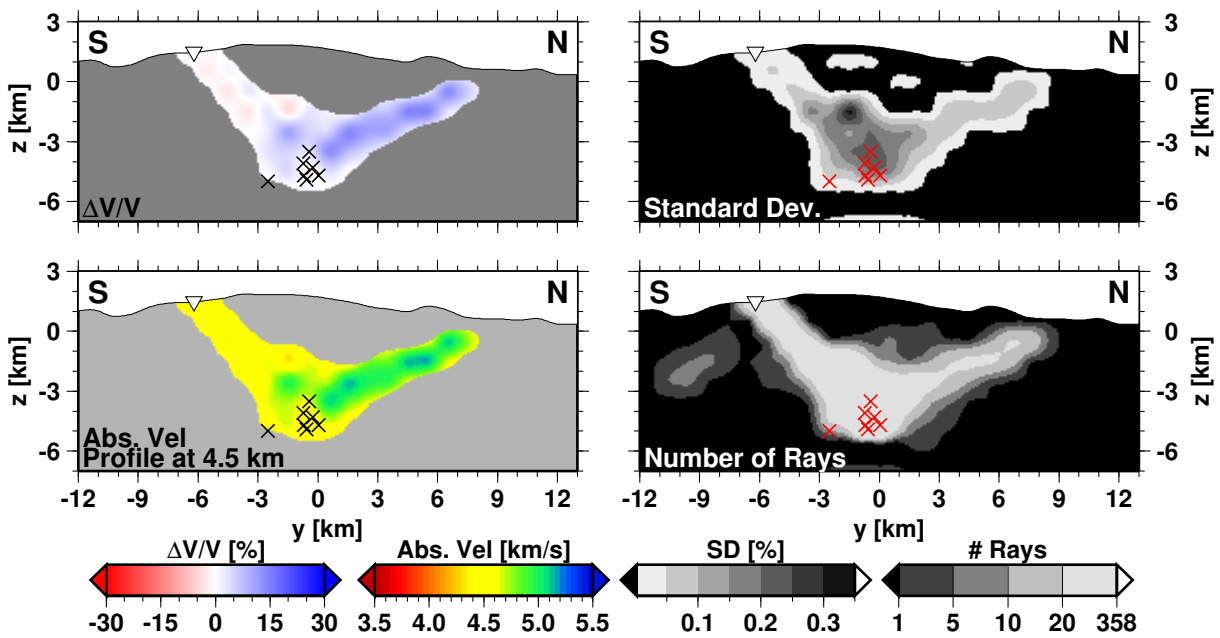


Figure B.26: Results from inversion in vertical N-S profile at 4.5 km (north).

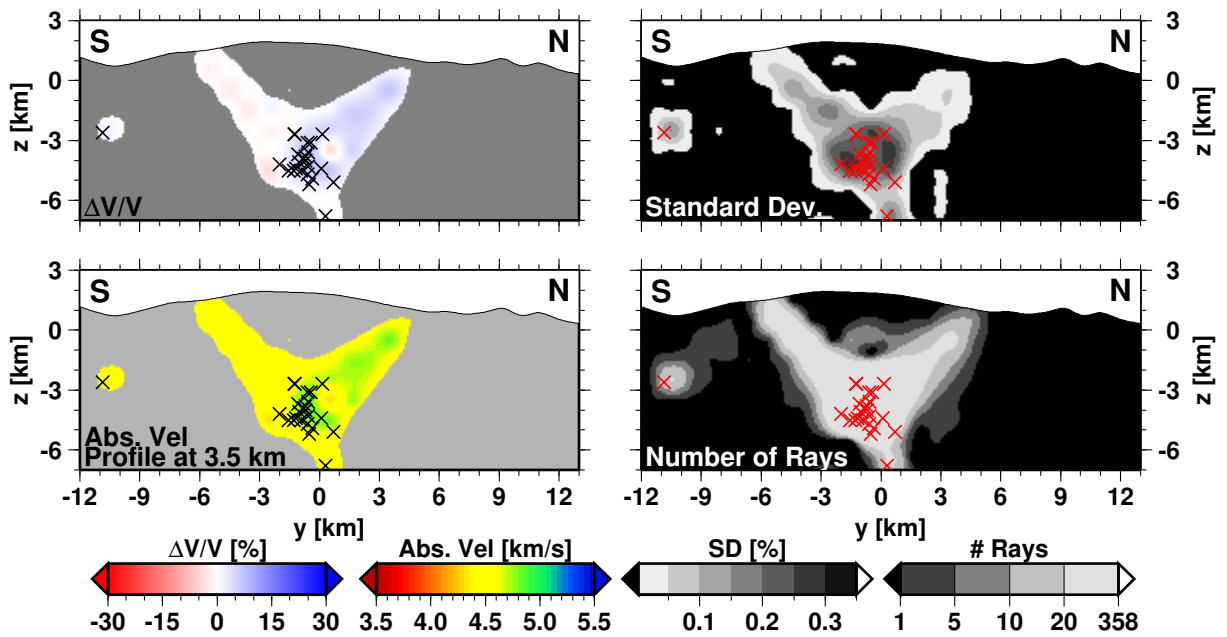


Figure B.27: Results from inversion in vertical N-S profile at 3.5 km (north).

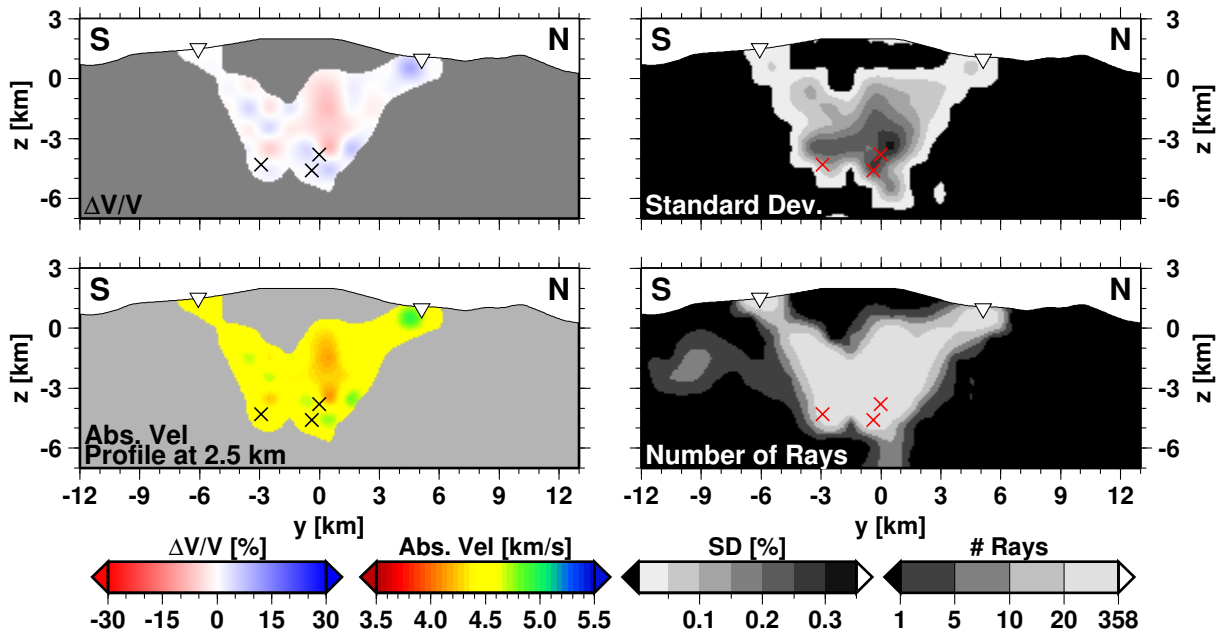


Figure B.28: Results from inversion in vertical N-S profile at 2.5 km (north).

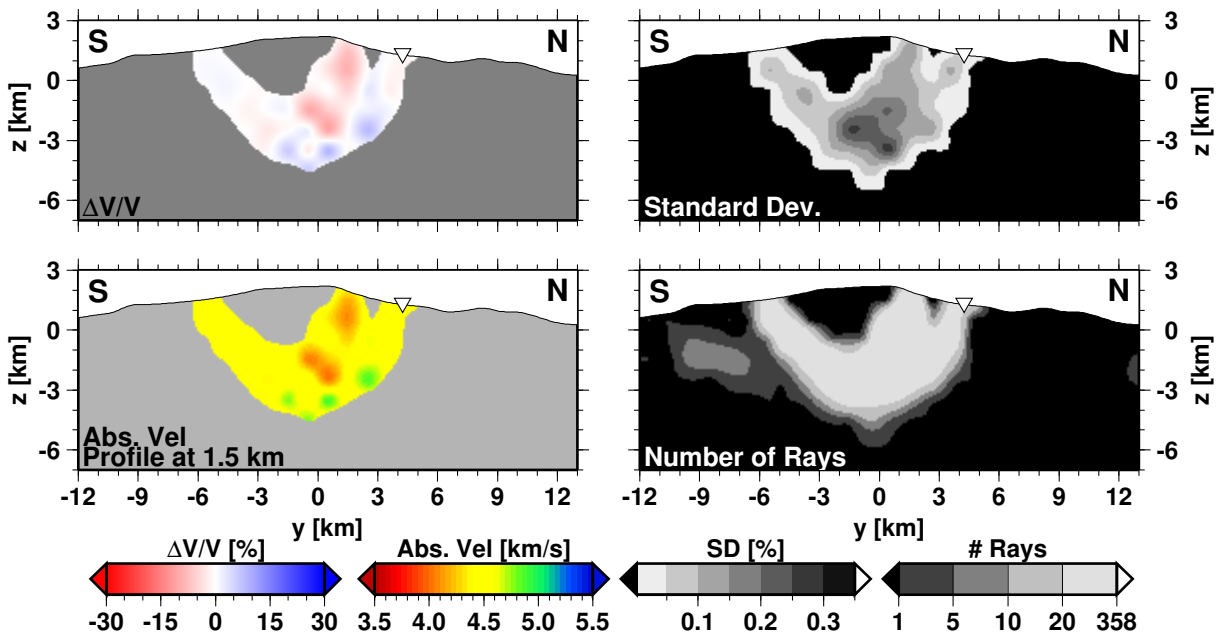


Figure B.29: Results from inversion in vertical N-S profile at 1.5 km (north).

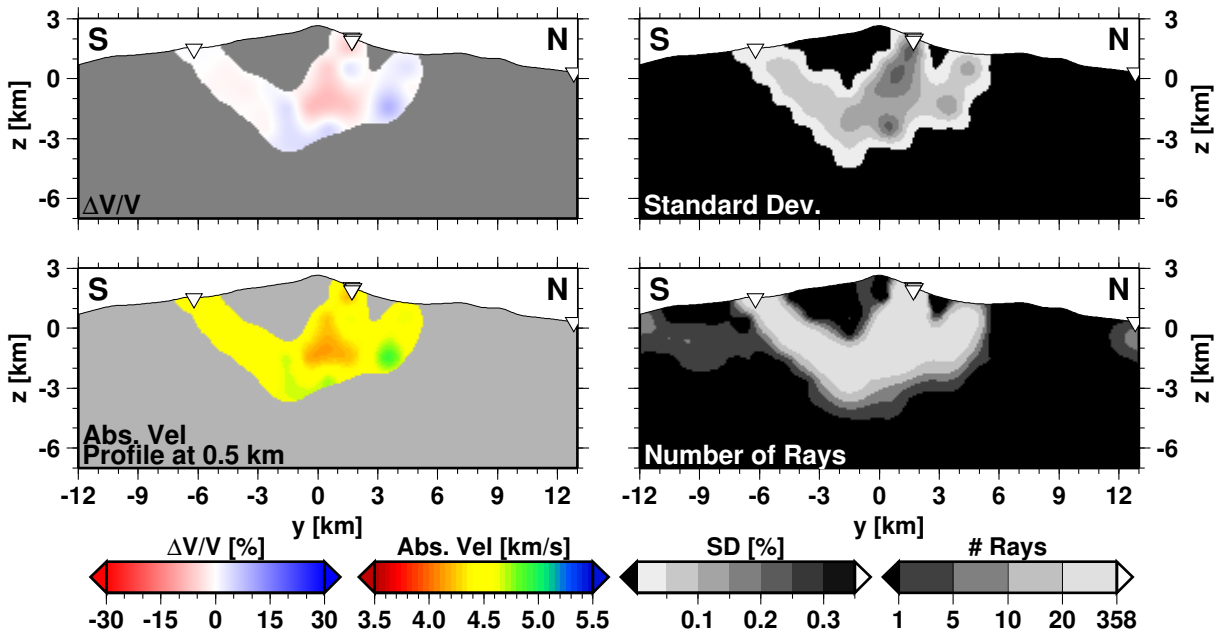


Figure B.30: Results from inversion in vertical N-S profile at 0.5 km (north).

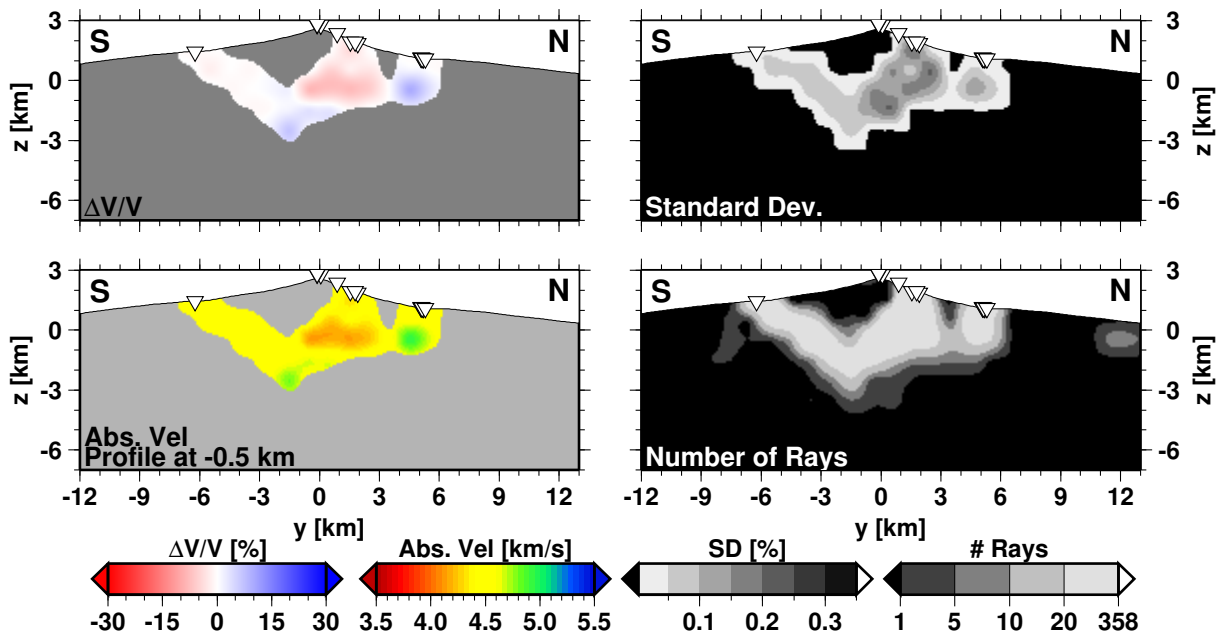


Figure B.31: Results from inversion in vertical N-S profile at -0.5 km (south).

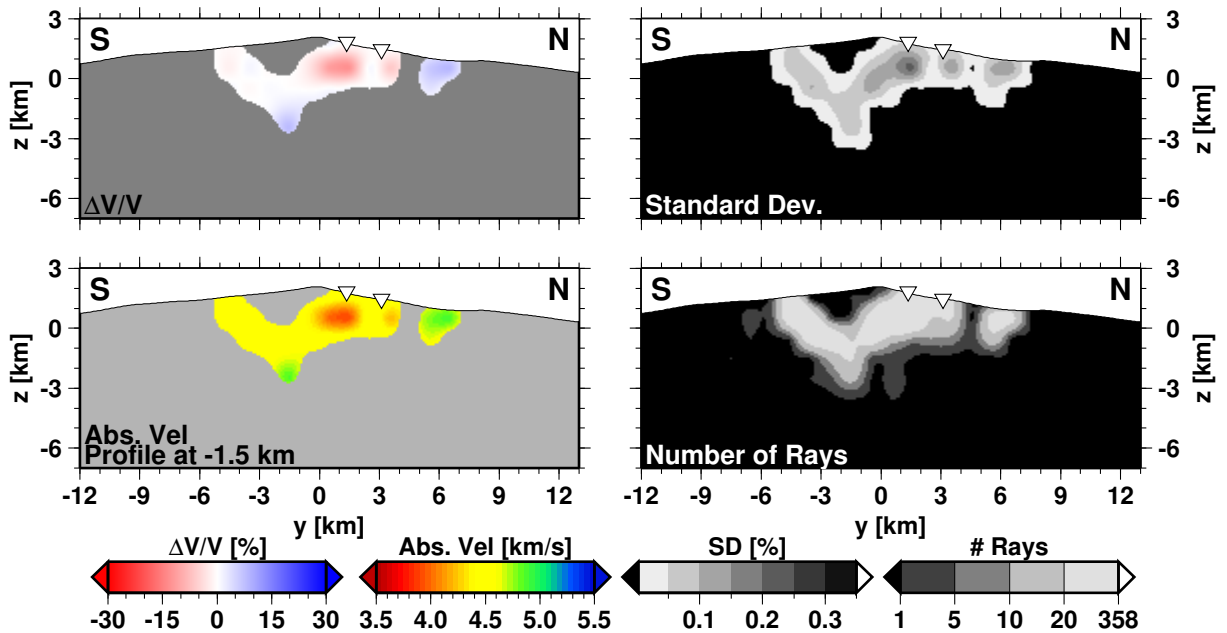


Figure B.32: Results from inversion in vertical N-S profile at -1.5 km (south).

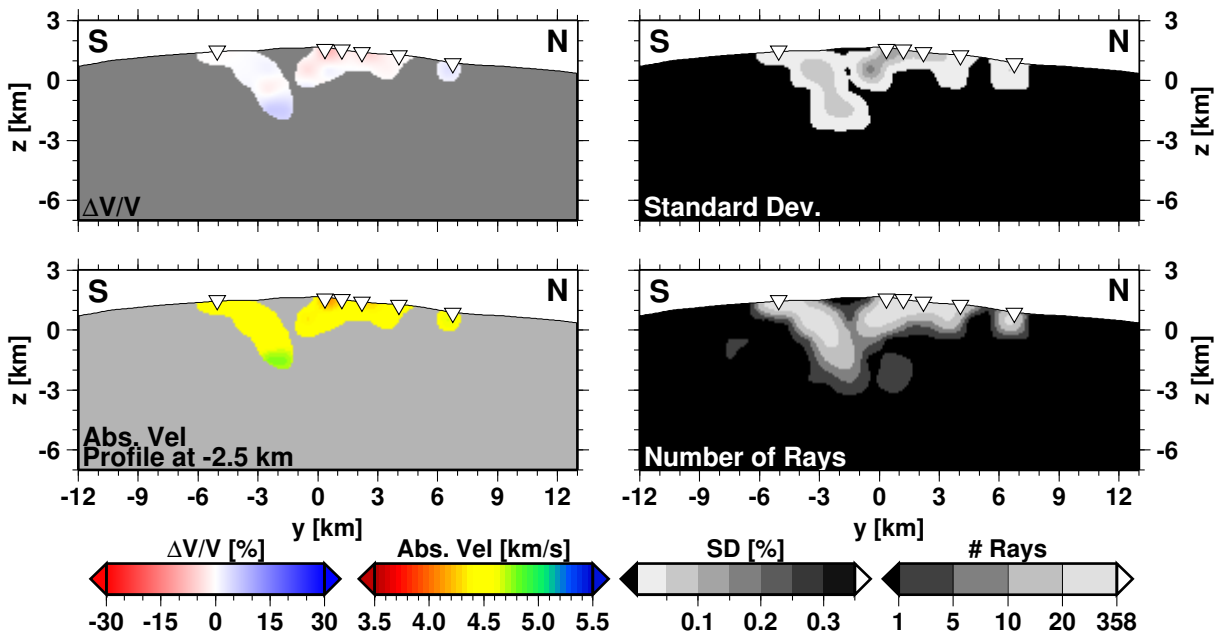


Figure B.33: Results from inversion in vertical N-S profile at -2.5 km (south).

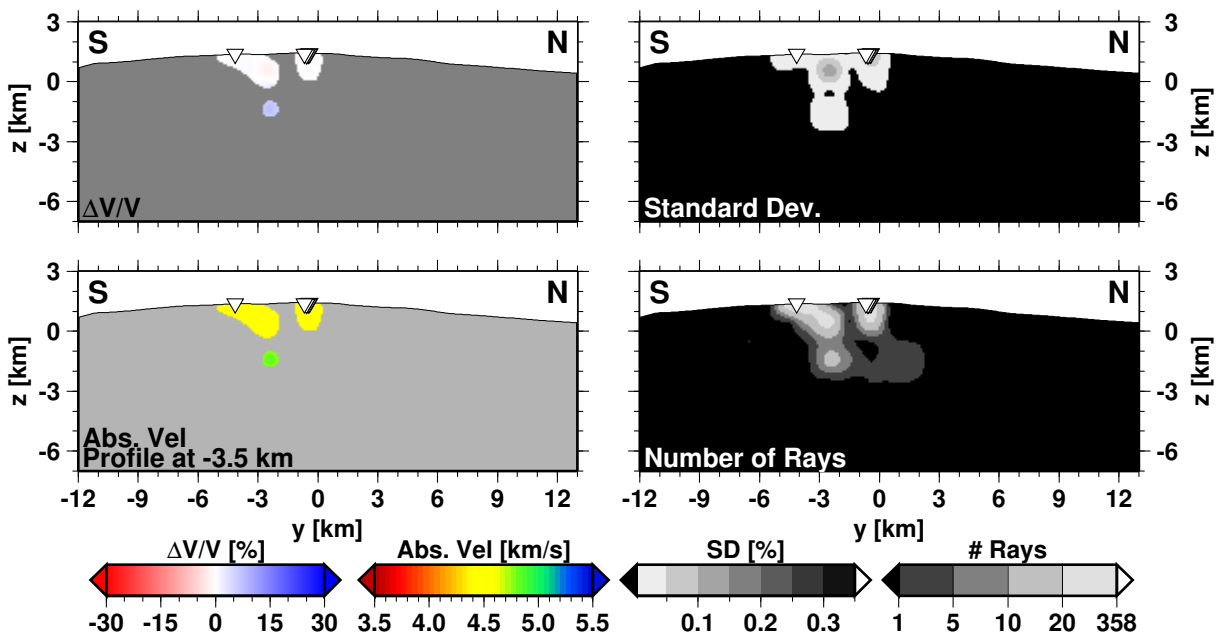


Figure B.34: Results from inversion in vertical N-S profile at -3.5 km (south).

B.4.2 Checker Board Test

Detailed figures for each slice of the Checker Board test are presented. All figures show to the left the original input velocity, and to the right the resolved inversion.

B.4.2.1 Horizontal slices

From top to bottom of the edifice.

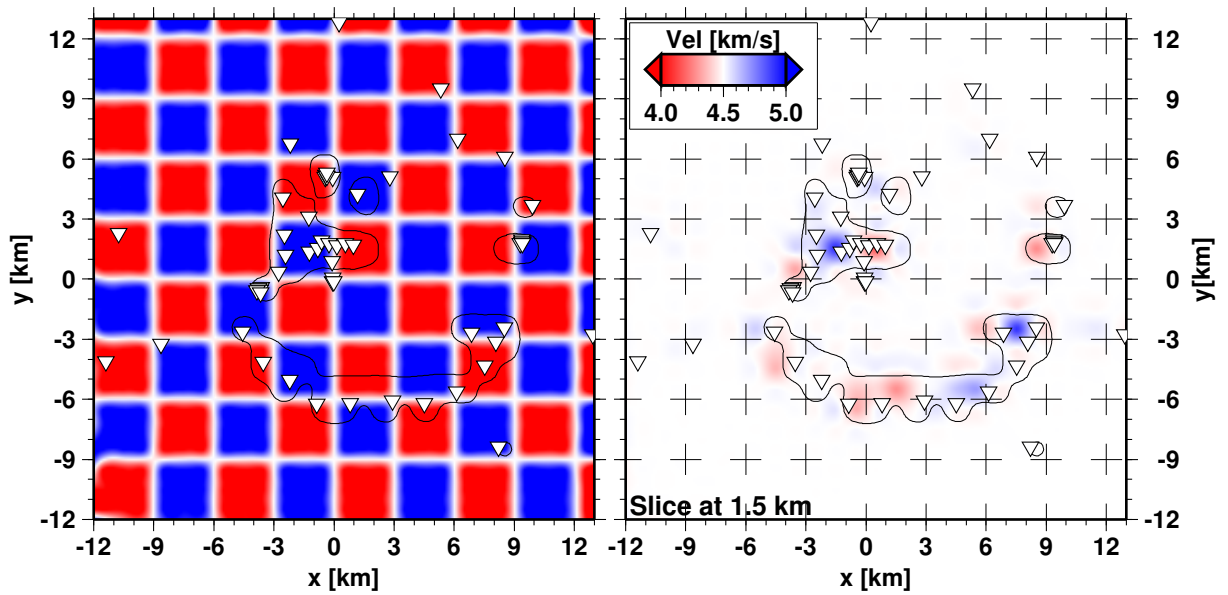


Figure B.35: Results from Synthetic inversion in horizontal slice at 1.5 km a.s.l.

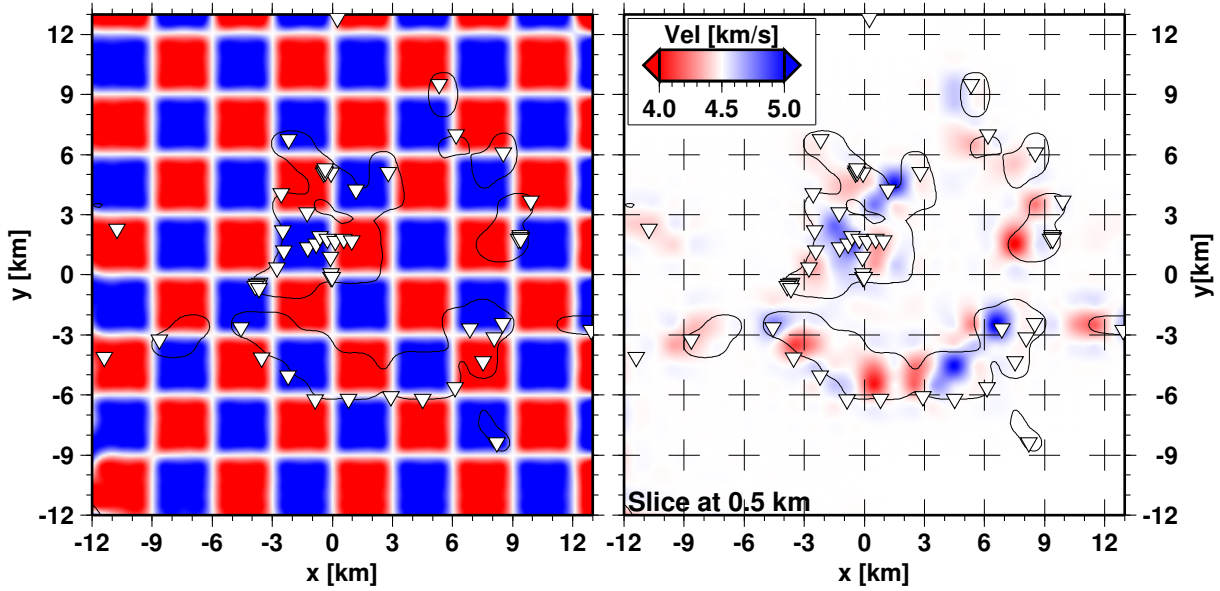


Figure B.36: Results from Synthetic inversion in horizontal slice at 0.5 km a.s.l.

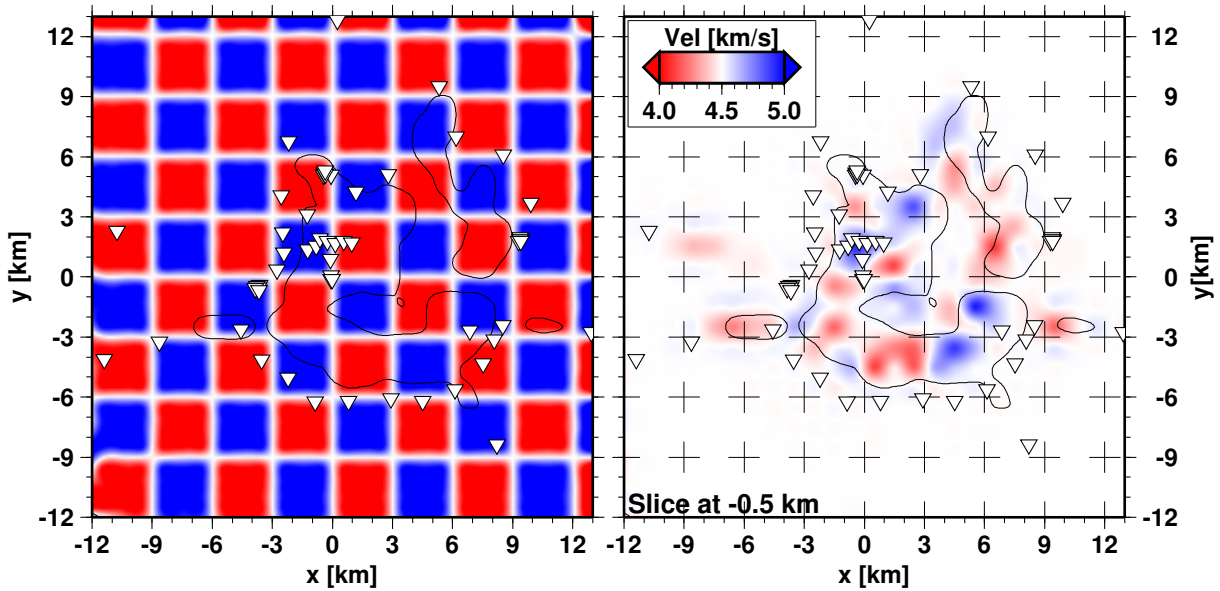


Figure B.37: Results from Synthetic inversion in horizontal slice at 0.5 km b.s.l.

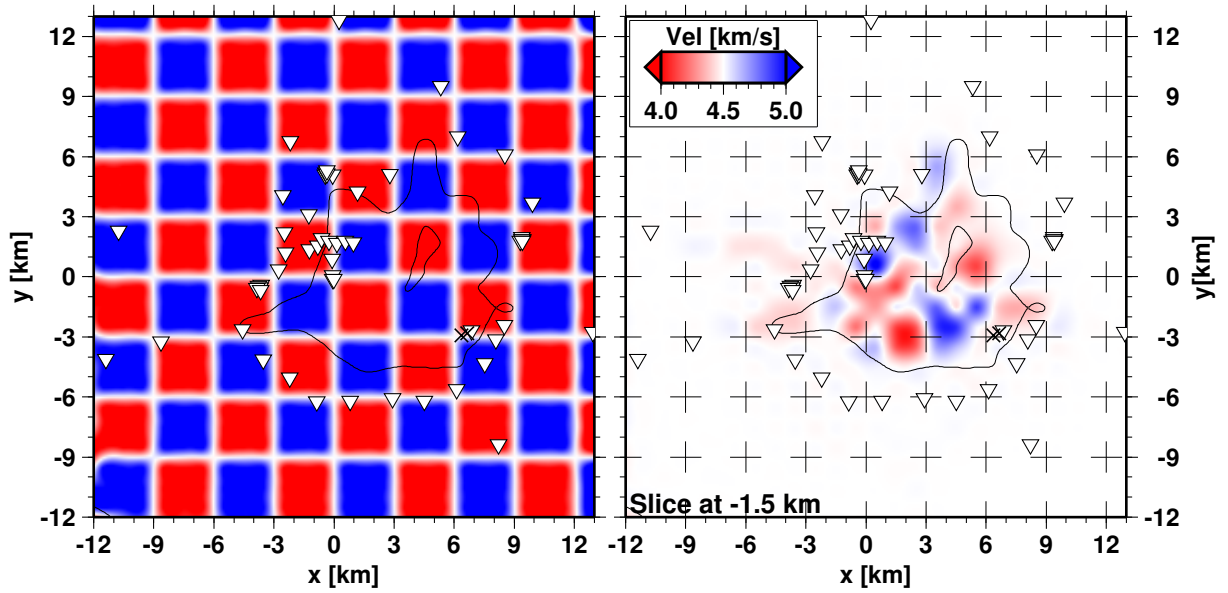


Figure B.38: Results from Synthetic inversion in horizontal slice at 1.5 km b.s.l.

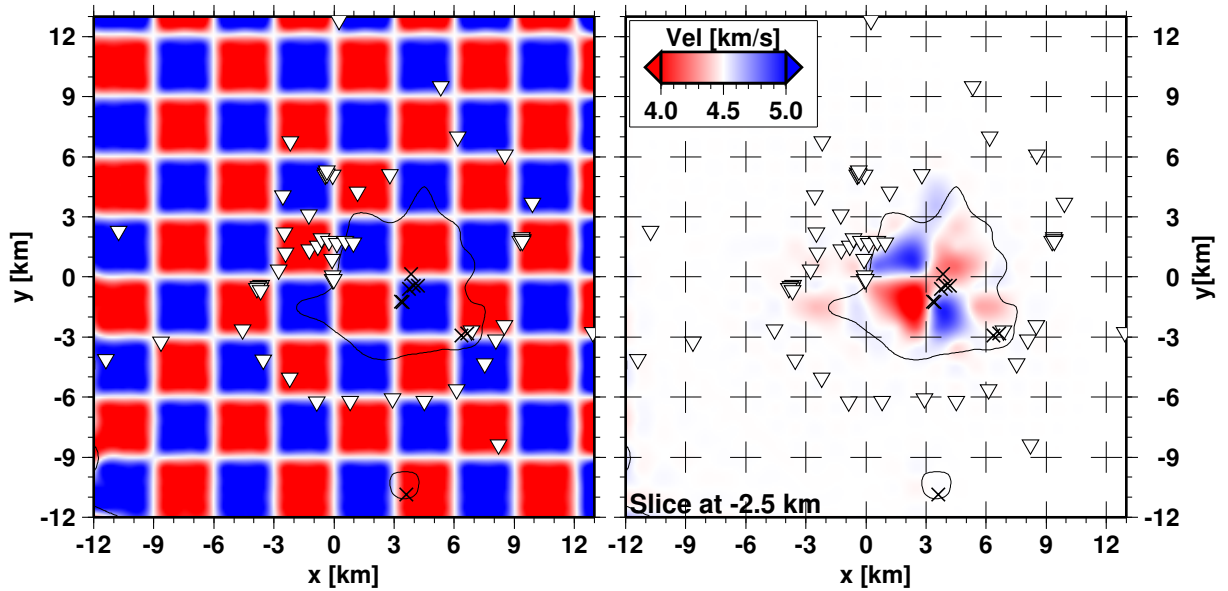


Figure B.39: Results from Synthetic inversion in horizontal slice at 2.5 km b.s.l.

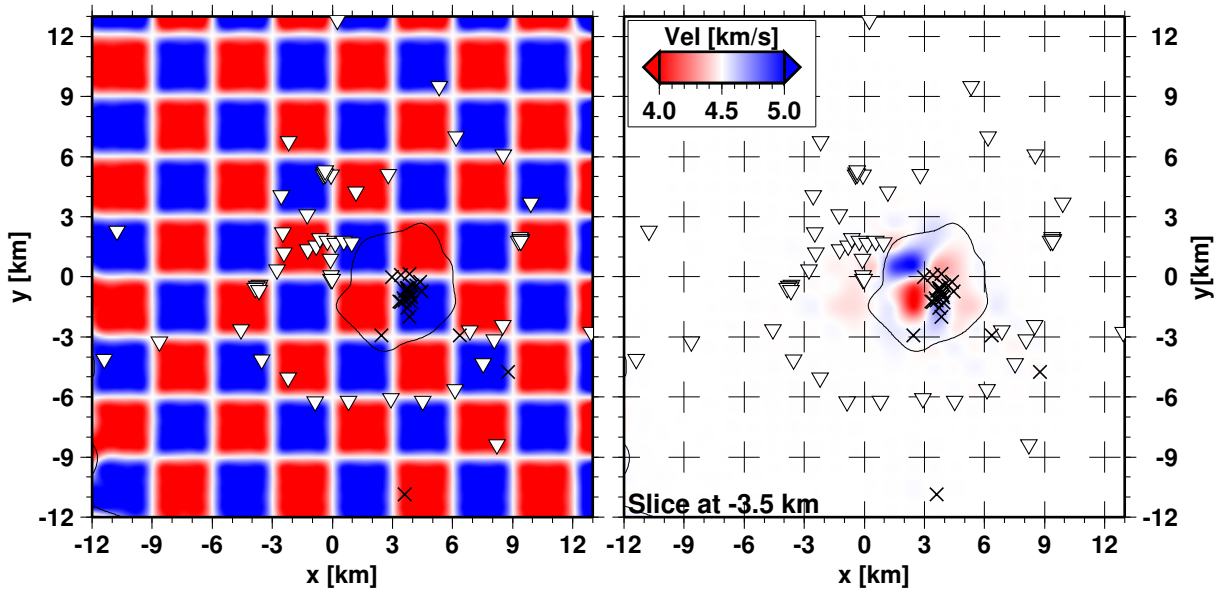


Figure B.40: Results from Synthetic inversion in horizontal slice at 3.5 km b.s.l.

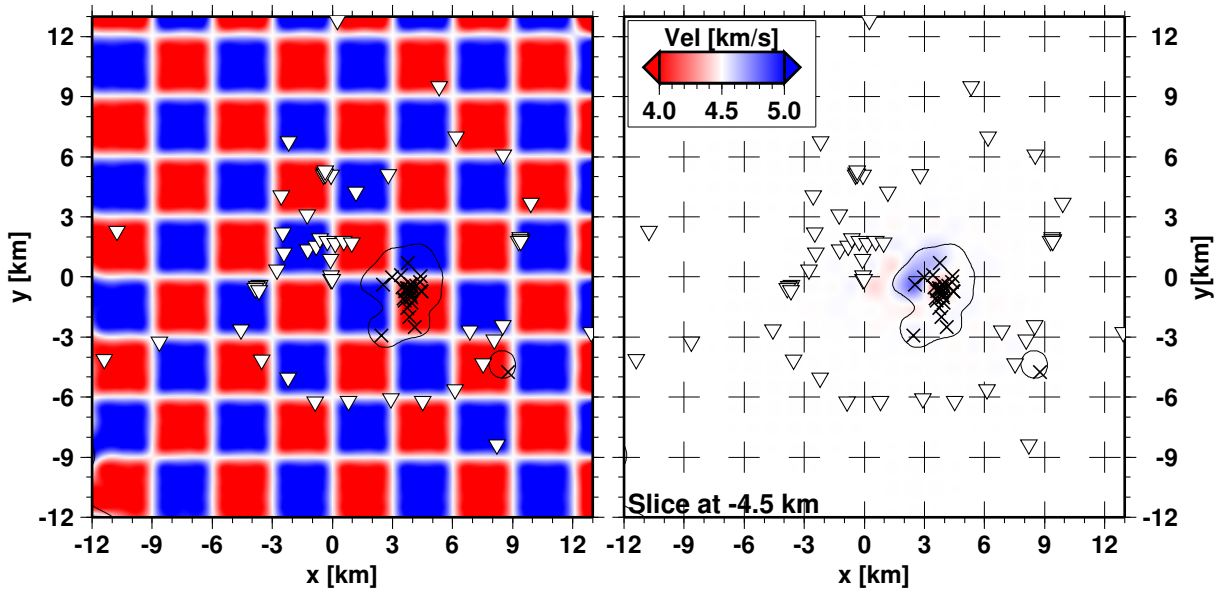


Figure B.41: Results from Synthetic inversion in horizontal slice at 4.5 km b.s.l.

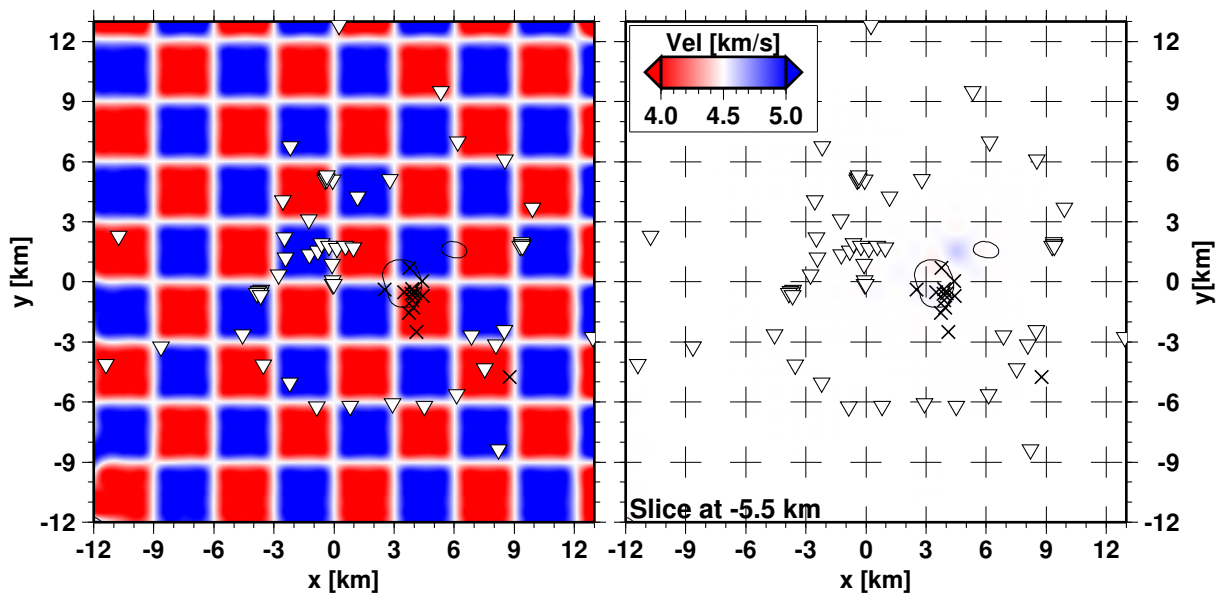


Figure B.42: Results from Synthetic inversion in horizontal slice at 5.5 km b.s.l.

B.4.2.2 Vertical Profiles East - West

From west (negative) to east (positive) centred at the crater.

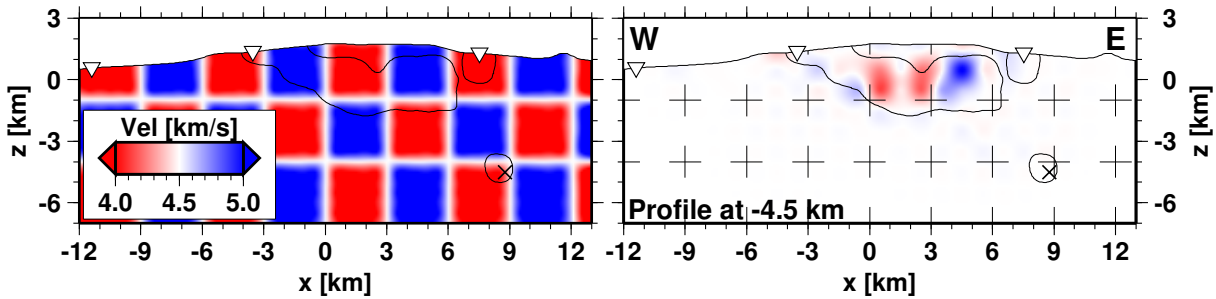


Figure B.43: Results from Synthetic inversion in vertical E-W profile at -4.5 km (west).

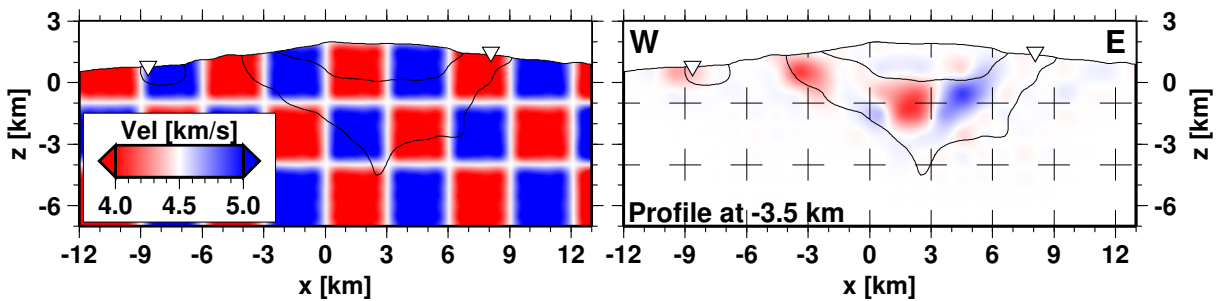


Figure B.44: Results from Synthetic inversion in vertical E-W profile at -3.5 km (west).

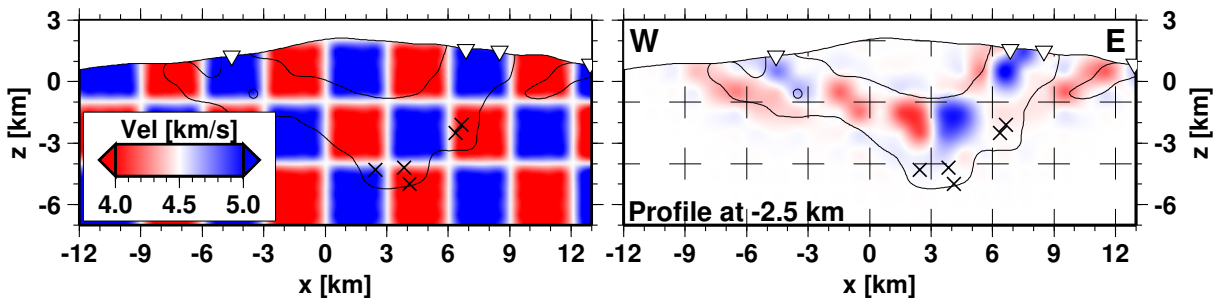


Figure B.45: Results from Synthetic inversion in vertical E-W profile at -2.5 km (west).

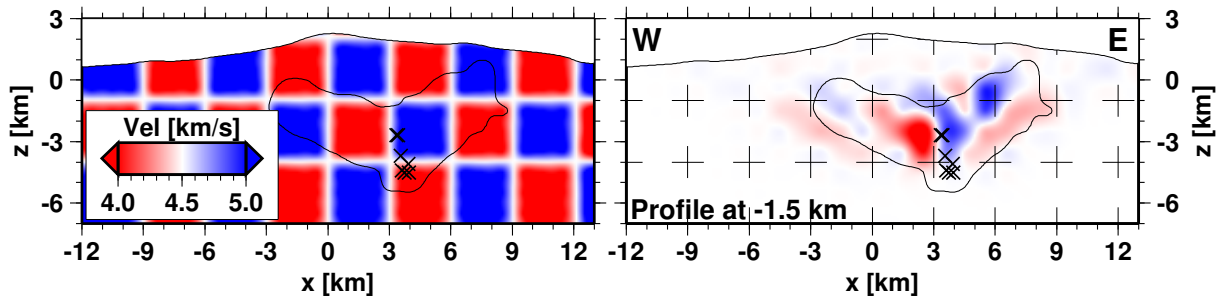


Figure B.46: Results from Synthetic inversion in vertical E-W profile at -1.5 km (west).

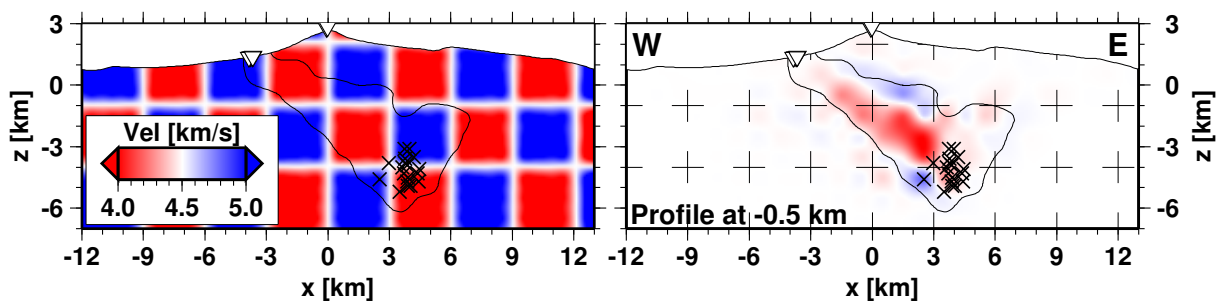


Figure B.47: Results from Synthetic inversion in vertical E-W profile at -0.5 km (west).

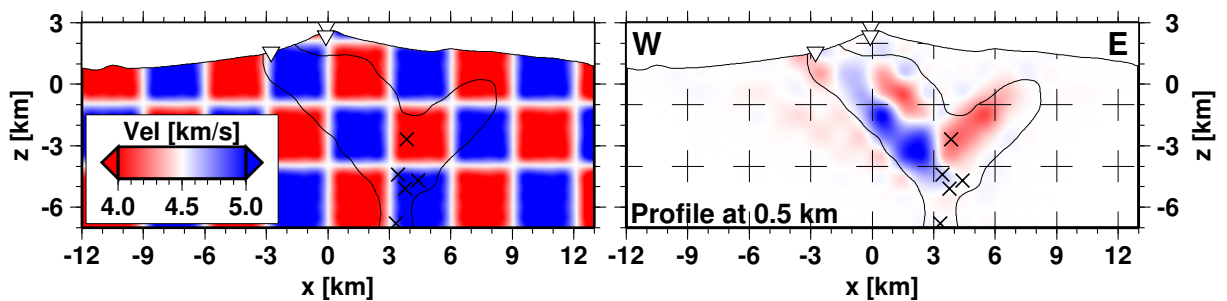


Figure B.48: Results from Synthetic inversion in vertical E-W profile at 0.5 km (east).

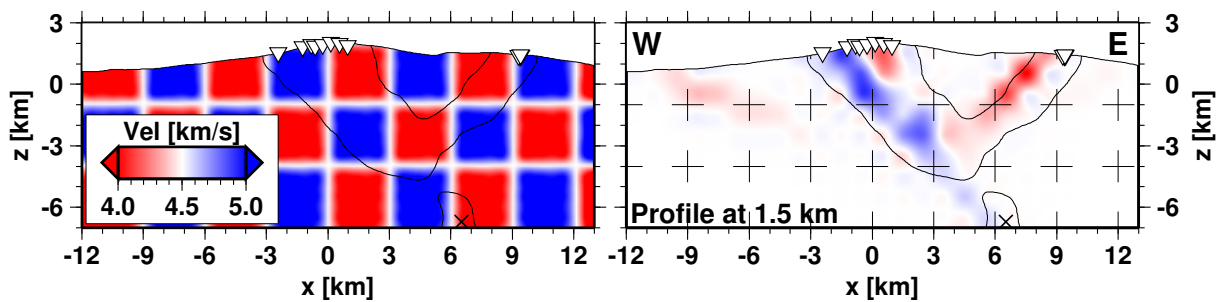


Figure B.49: Results from Synthetic inversion in vertical E-W profile at 1.5 km (east).

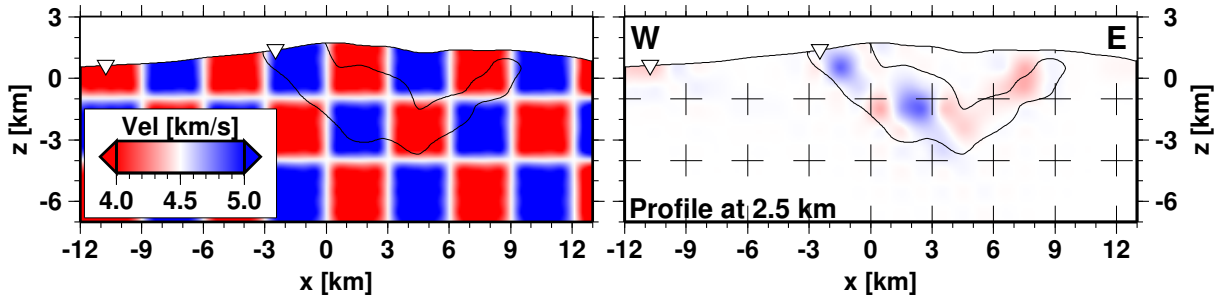


Figure B.50: Results from Synthetic inversion in vertical E-W profile at 2.5 km (east).

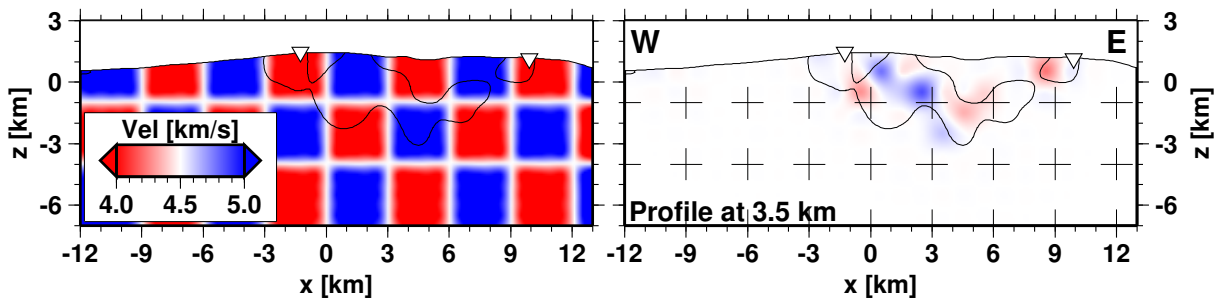


Figure B.51: Results from Synthetic inversion in vertical E-W profile at 3.5 km (east).

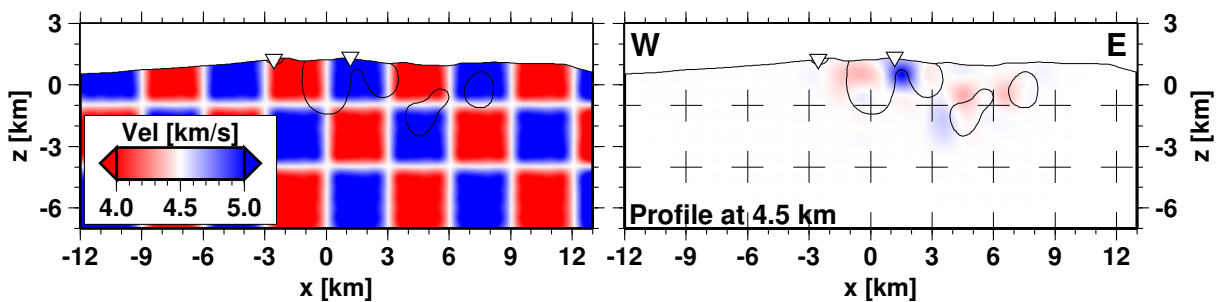


Figure B.52: Results from Synthetic inversion in vertical E-W profile at 4.5 km (east).

B.4.2.3 Vertical Profiles North - South

From North (positive) to South (negative) centred at the crater.

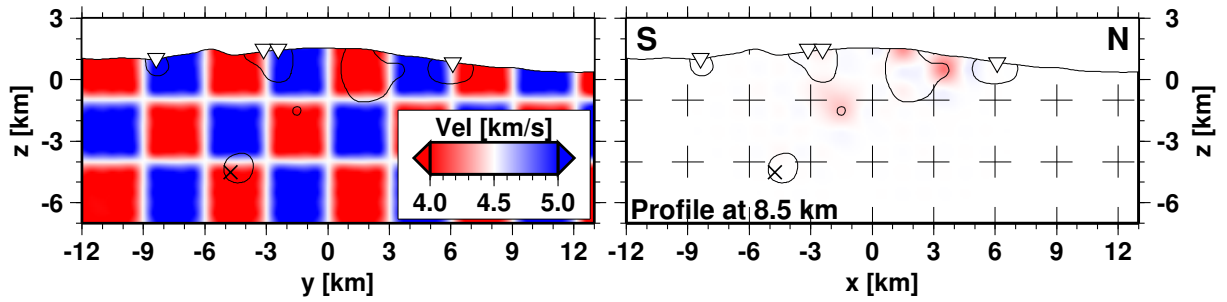


Figure B.53: Results from Synthetic inversion in vertical N-S profile at 8.5 km (north).

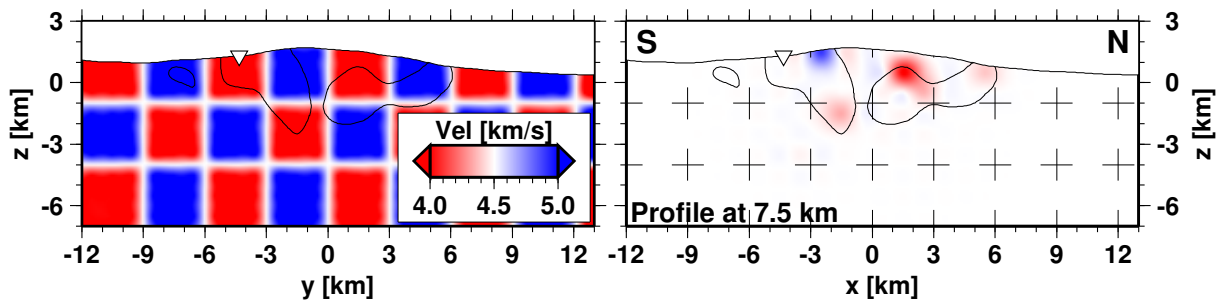


Figure B.54: Results from Synthetic inversion in vertical N-S profile at 7.5 km (north).

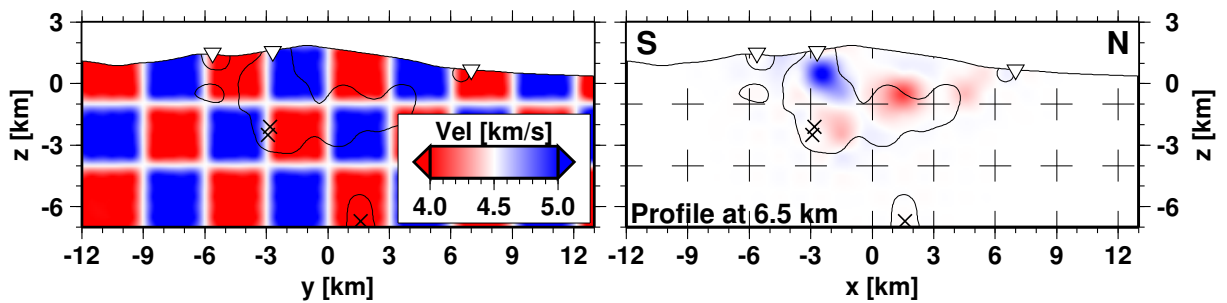


Figure B.55: Results from Synthetic inversion in vertical N-S profile at 6.5 km (north).

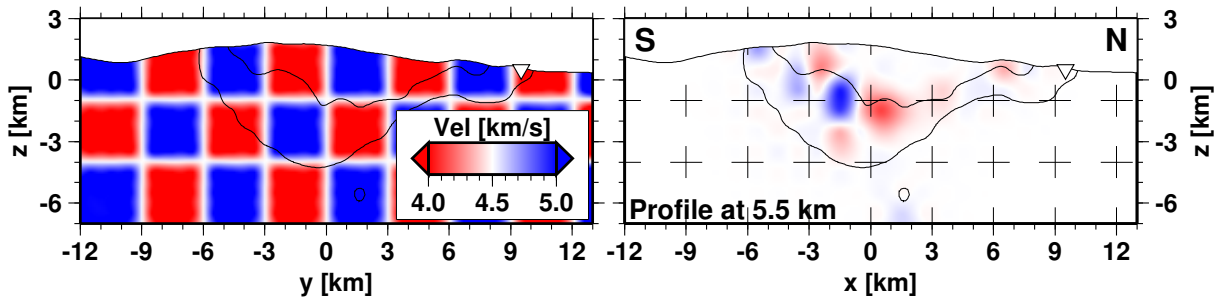


Figure B.56: Results from Synthetic inversion in vertical N-S profile at 5.5 km (north).

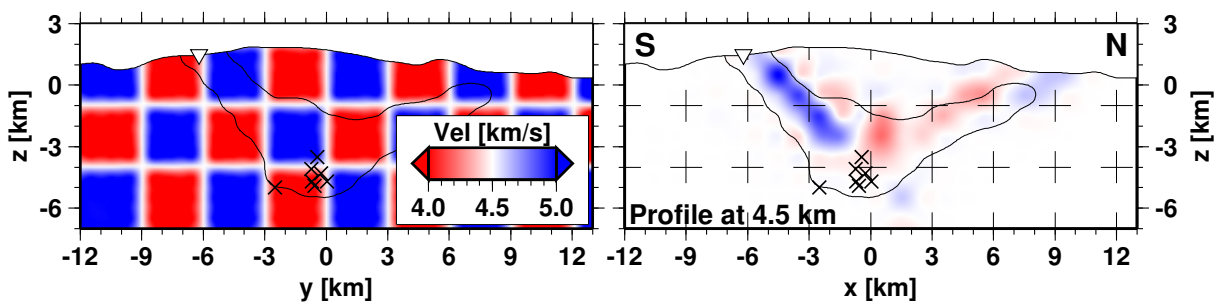


Figure B.57: Results from Synthetic inversion in vertical N-S profile at 4.5 km (north).

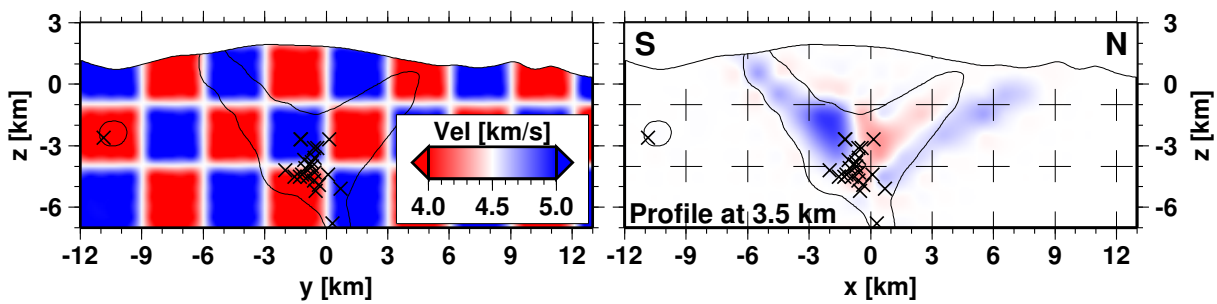


Figure B.58: Results from Synthetic inversion in vertical N-S profile at 3.5 km (north).

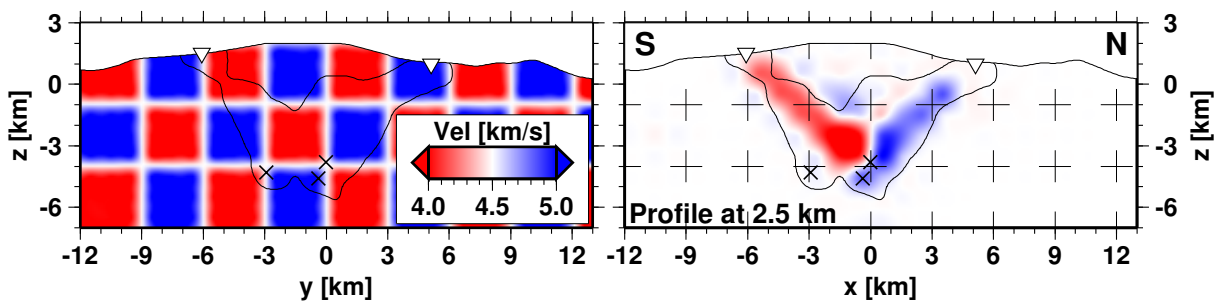


Figure B.59: Results from Synthetic inversion in vertical N-S profile at 2.5 km (north).

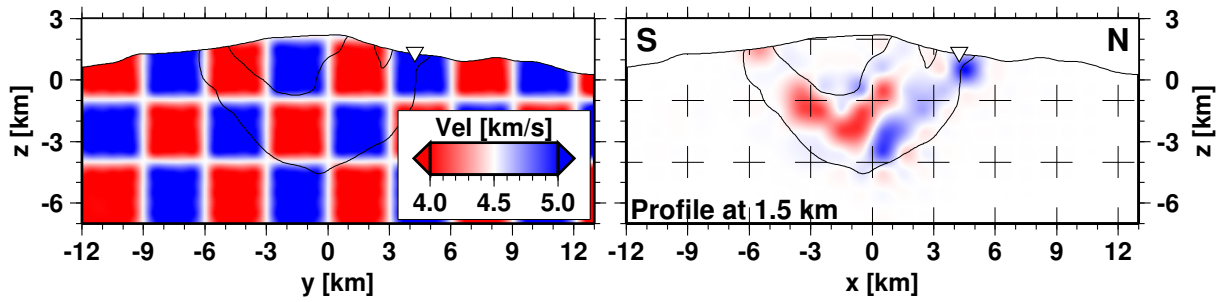


Figure B.60: Results from Synthetic inversion in vertical N-S profile at 1.5 km (north).

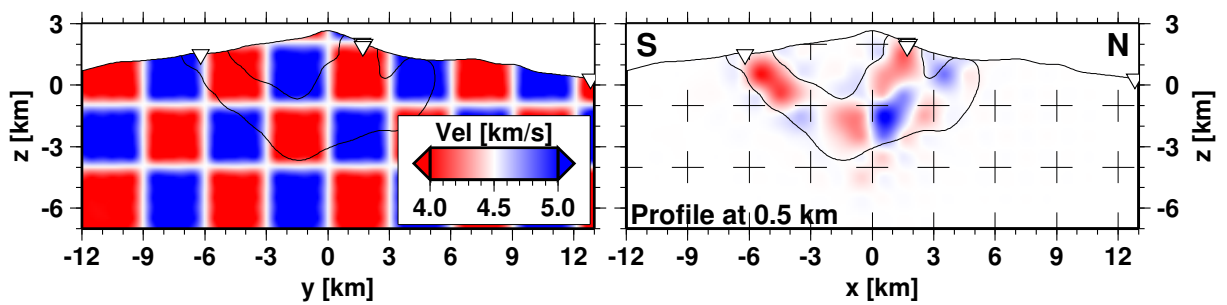


Figure B.61: Results from Synthetic inversion in vertical N-S profile at 0.5 km (north).

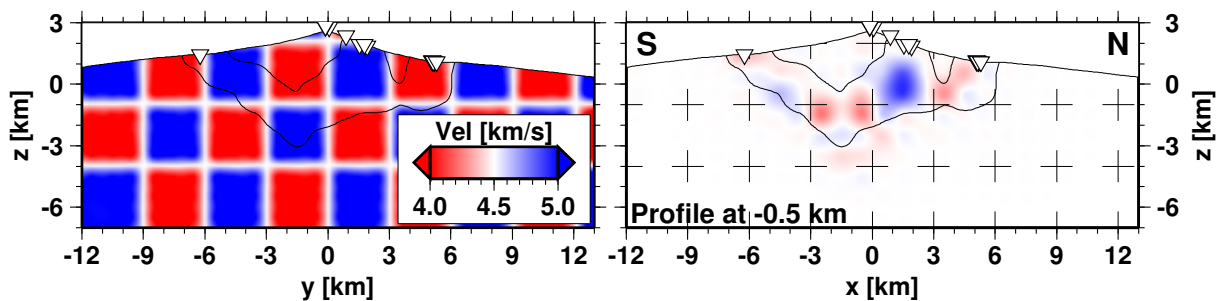


Figure B.62: Results from Synthetic inversion in vertical N-S profile at -0.5 km (south).

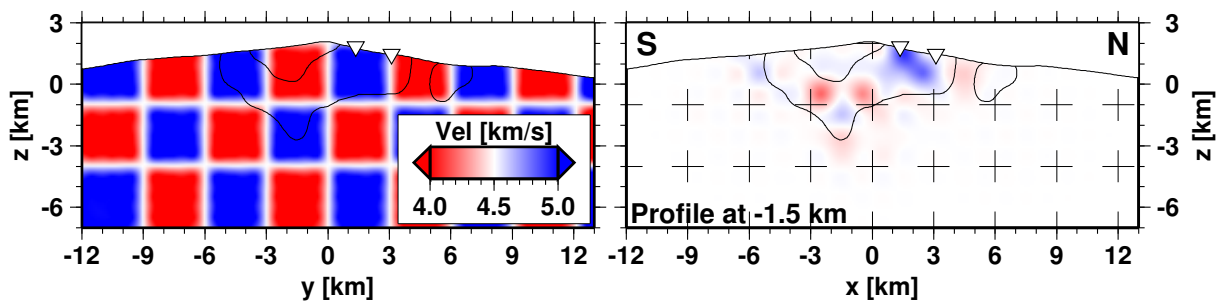


Figure B.63: Results from Synthetic inversion in vertical N-S profile at -1.5 km (south).

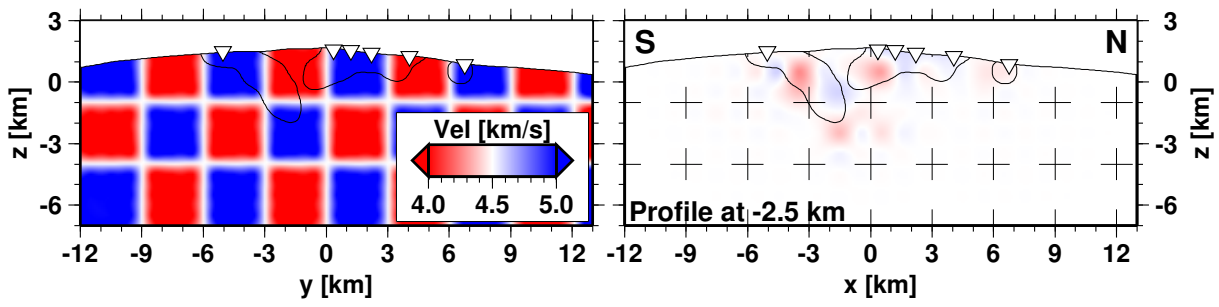


Figure B.64: Results from Synthetic inversion in vertical N-S profile at -2.5 km (south).

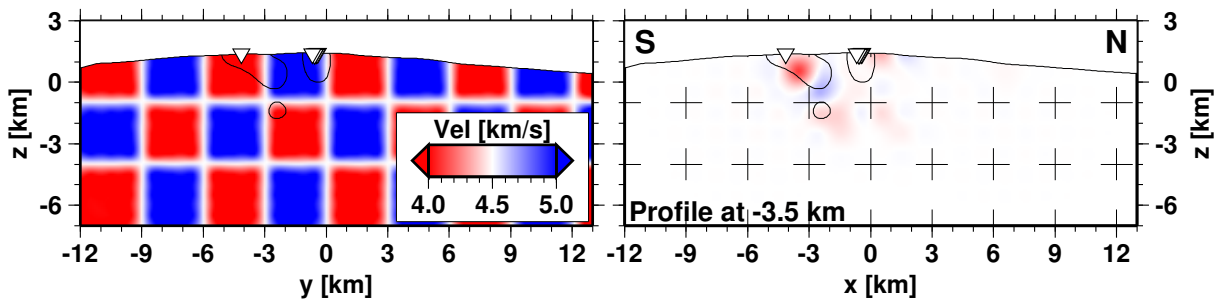


Figure B.65: Results from Synthetic inversion in vertical N-S profile at -3.5 km (south).

B.4.3 Bootstrap Results

Graphic results for the average of 100 runs are presented for average absolute velocity (top left), percentage of velocity variation (bottom left), number of rays per cube (bottom right), and standard deviation per cube (top right). Profiles are clipped, except “Number of Rays” showing only the area for cubes with 10 or more rays passing through.

B.4.3.1 Horizontal Slices

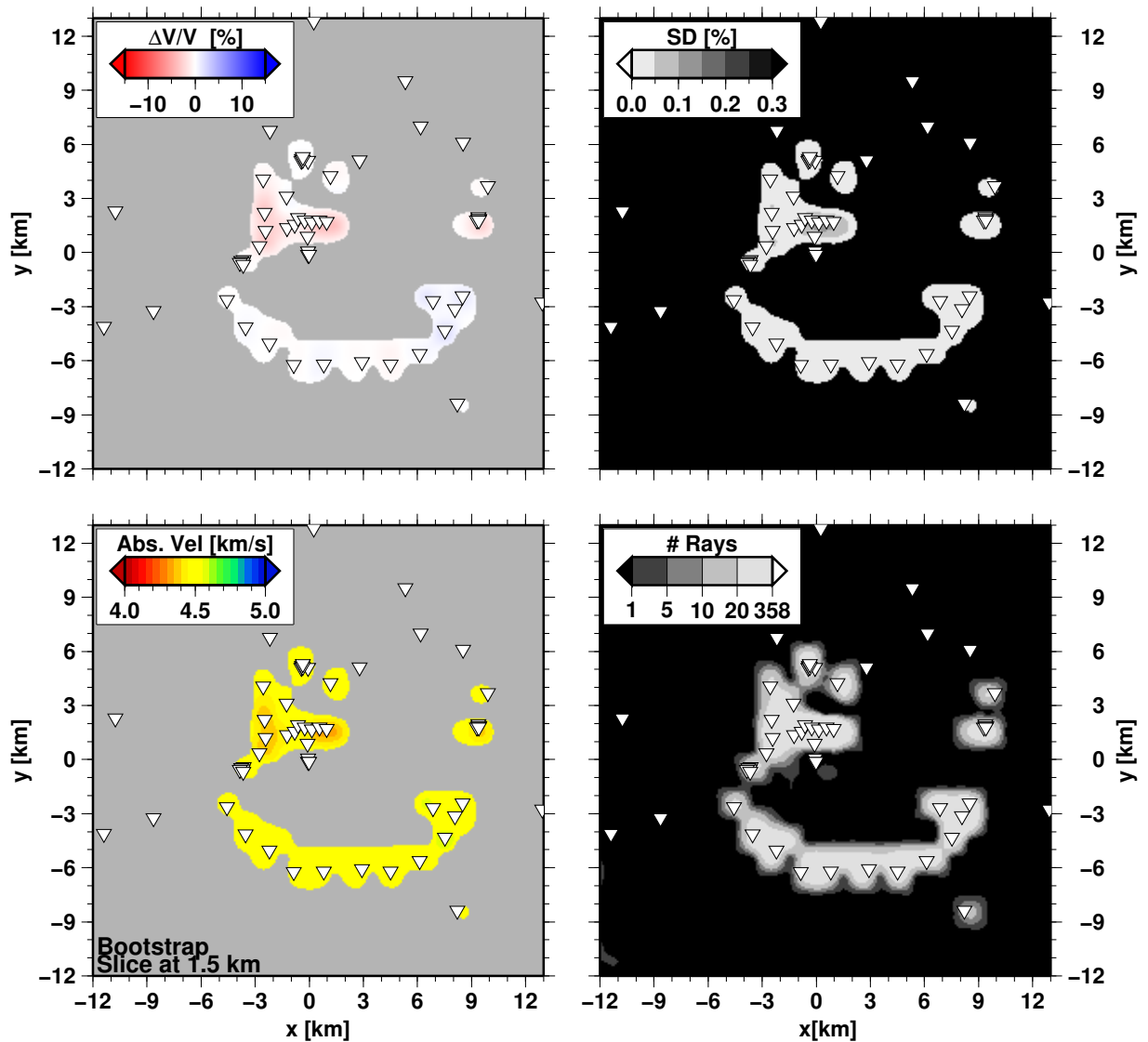


Figure B.66: Results from Bootstrapped tomography in horizontal slice at 1.5 km b.s.l.

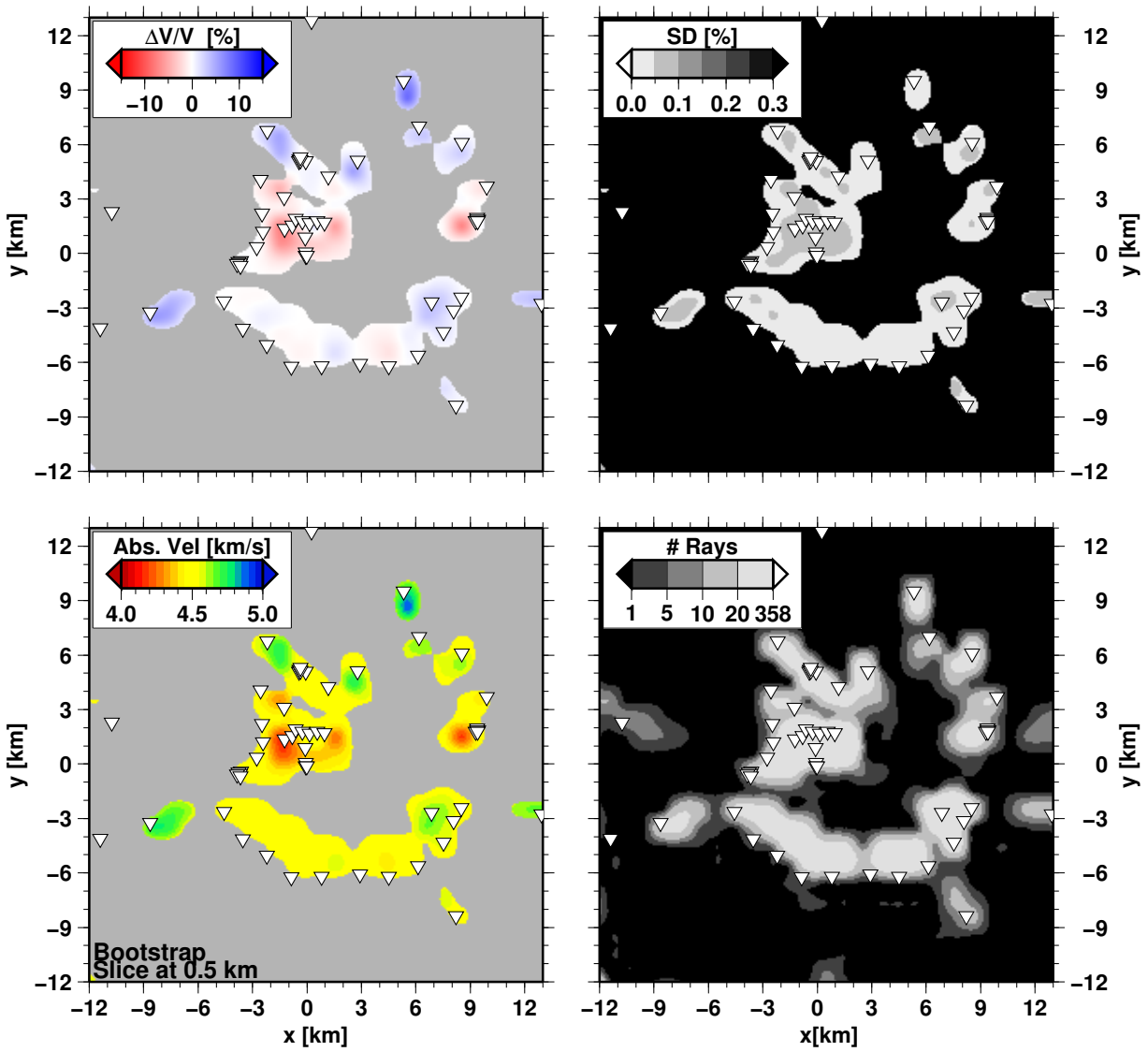


Figure B.67: Results from Bootstrapped tomography in horizontal slice at 0.5 km a.s.l.

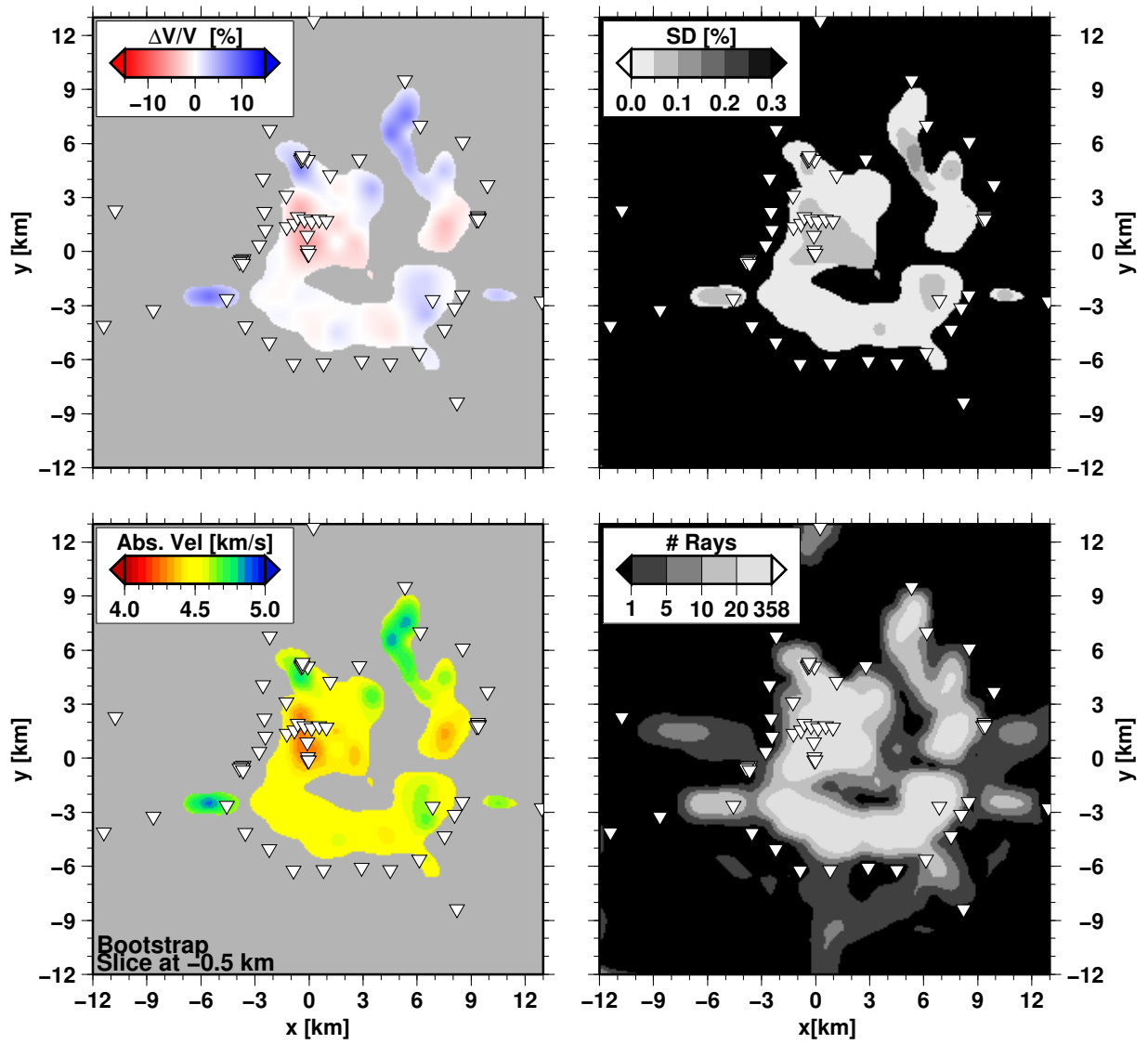


Figure B.68: Results from Bootstrapped tomography in horizontal slice at 0.5 km b.s.l.

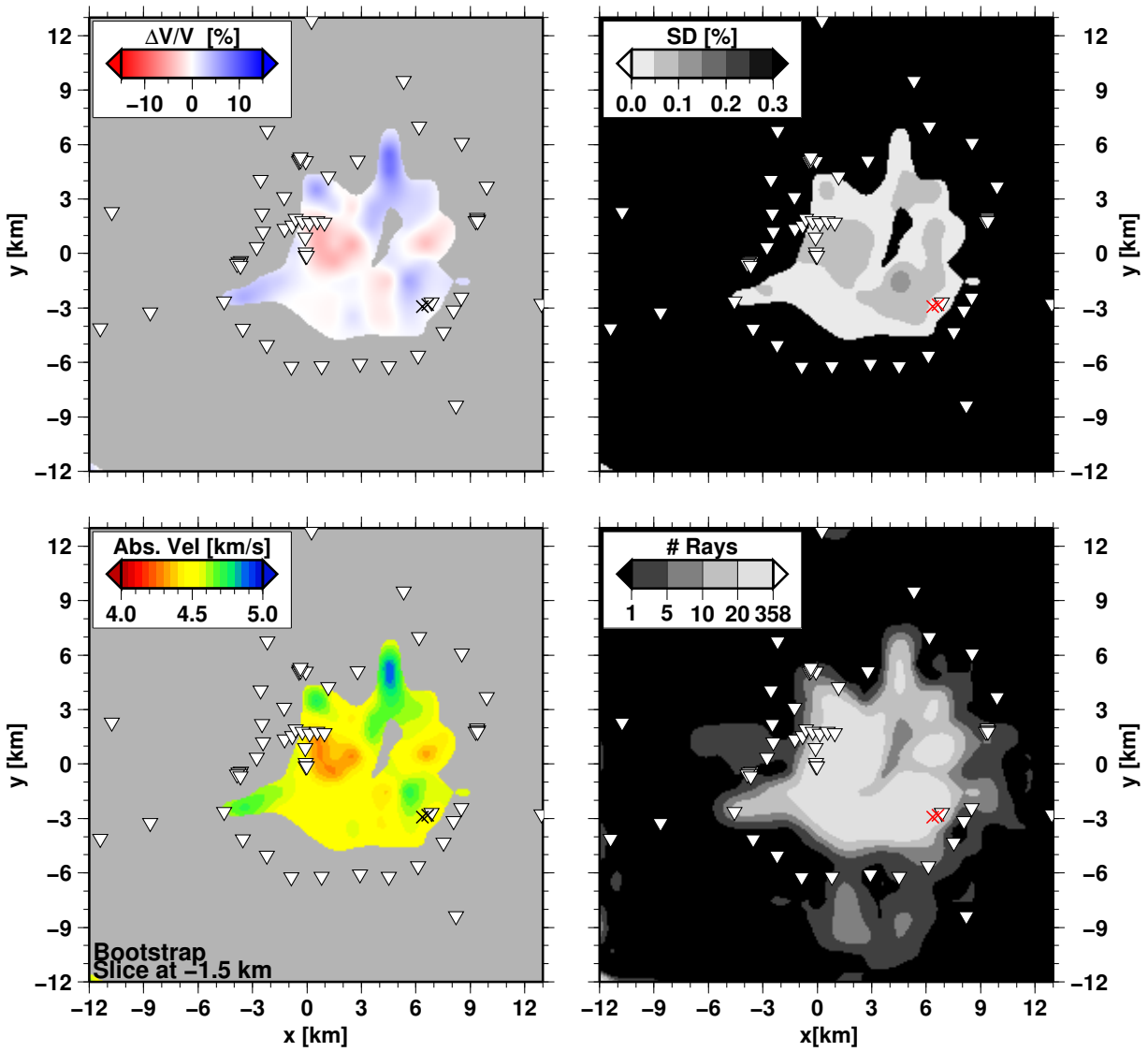


Figure B.69: Results from Bootstrapped tomography in horizontal slice at 1.5 km b.s.l.

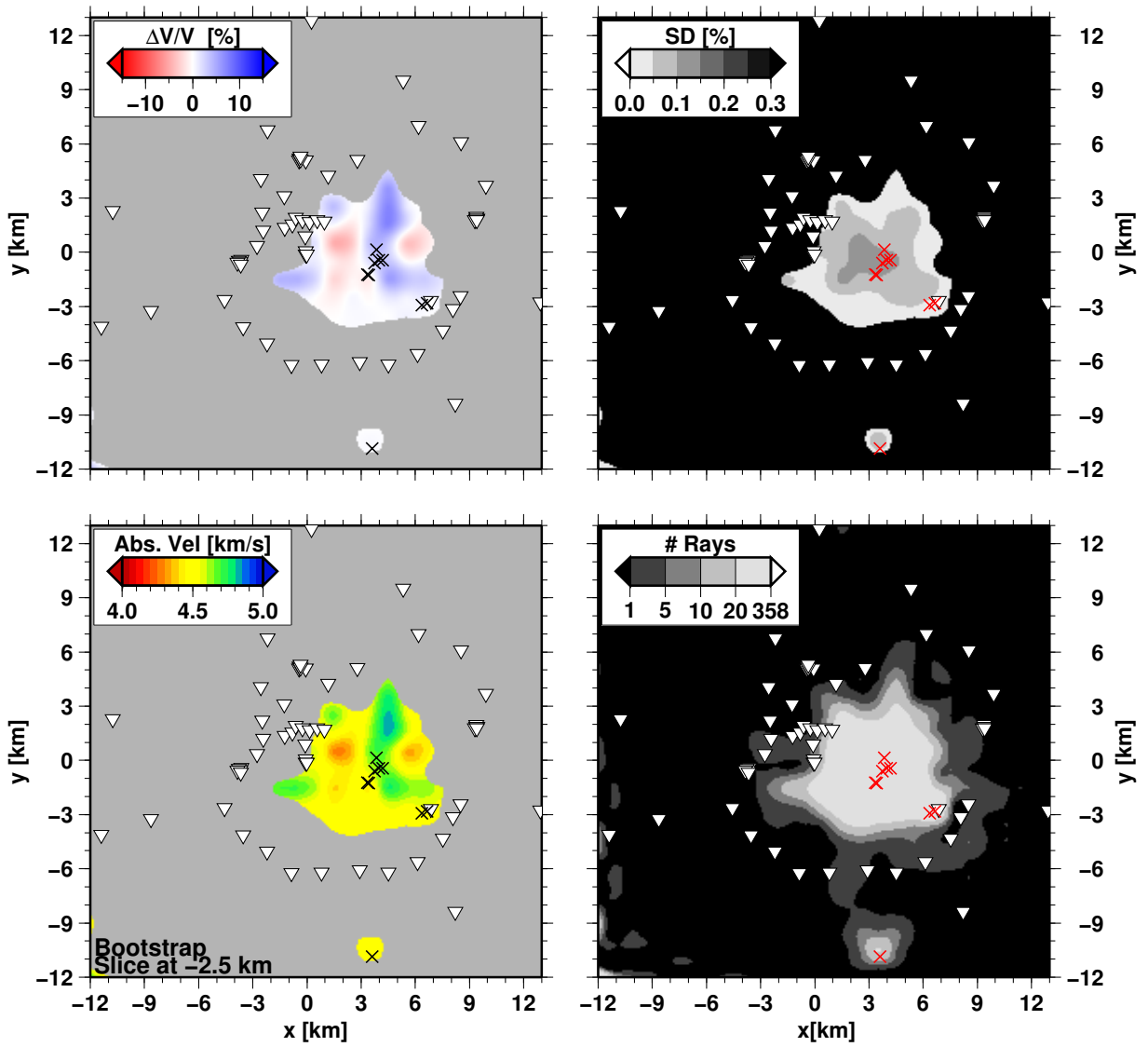


Figure B.70: Results from Bootstrapped tomography in horizontal slice at 2.5 km b.s.l.

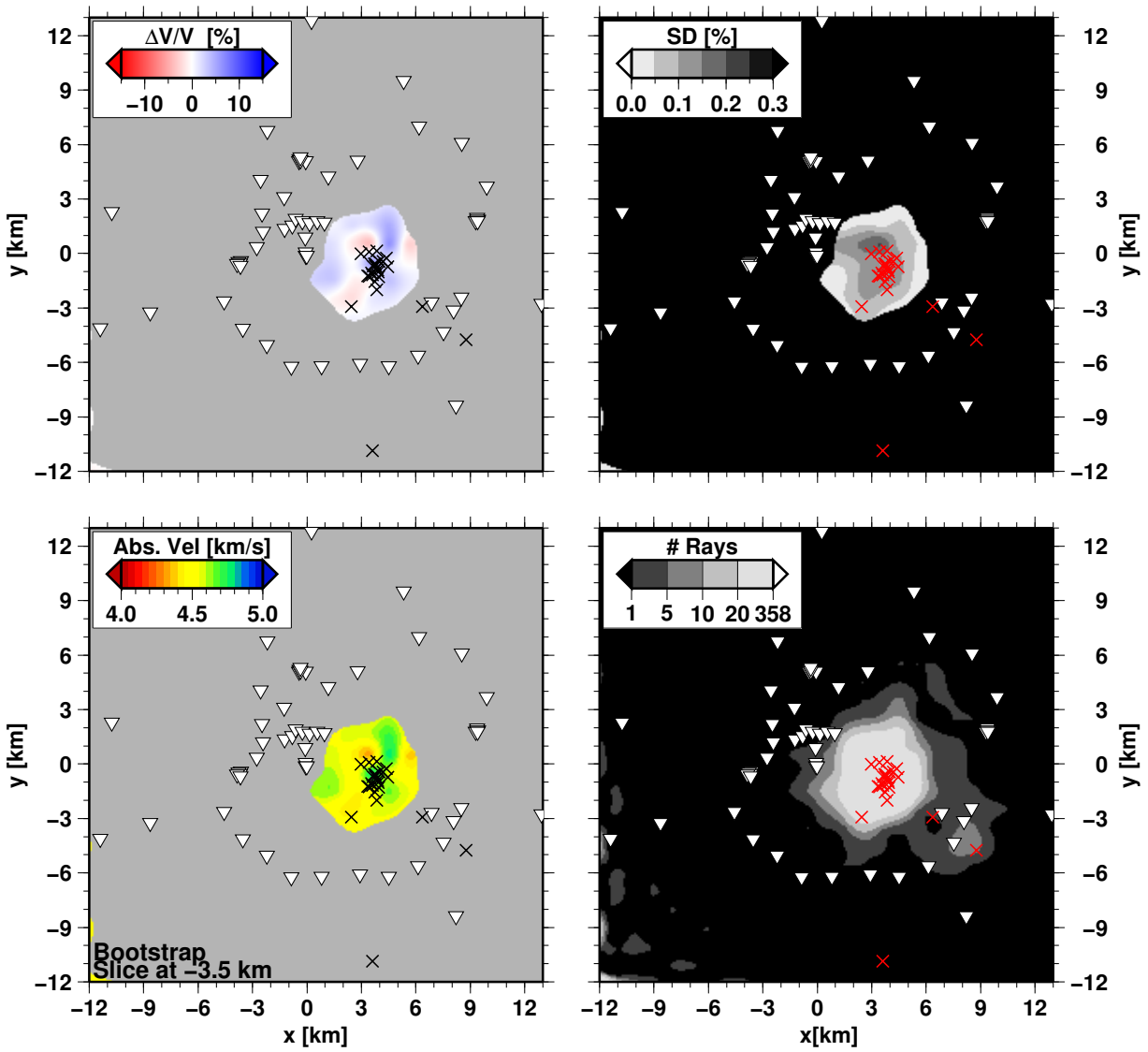


Figure B.71: Results from Bootstrapped tomography in horizontal slice at 3.5 km b.s.l.

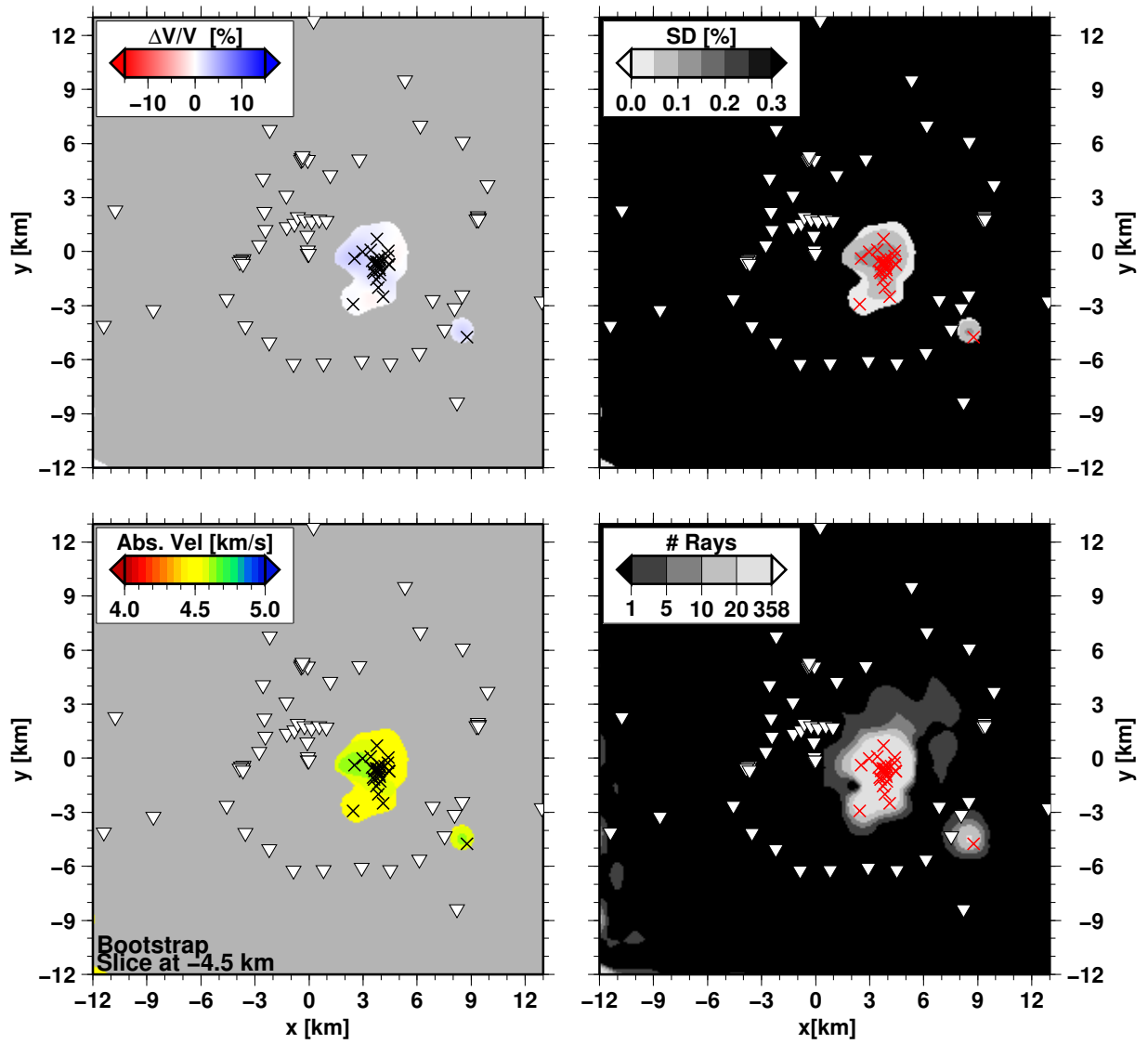


Figure B.72: Results from Bootstrapped tomography in horizontal slice at 4.5 km b.s.l.

B.4.3.2 Vertical Profiles

From West to East from the edifice.

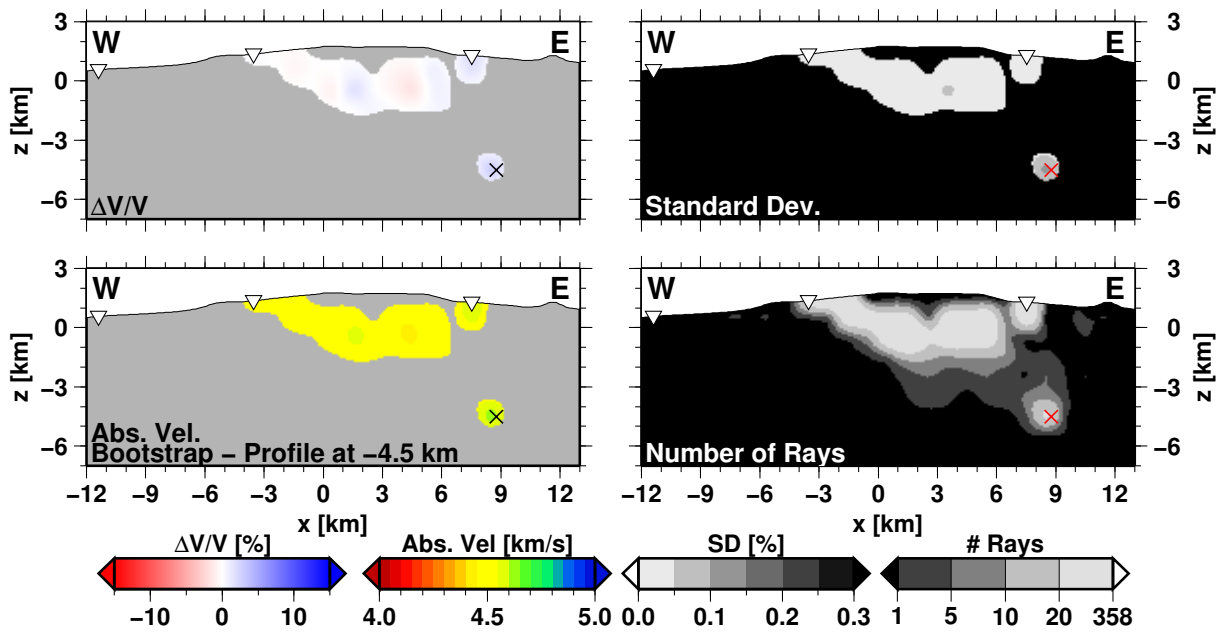


Figure B.73: Results from Bootstrapped tomography in vertical profile EW at -4.5 km (west)

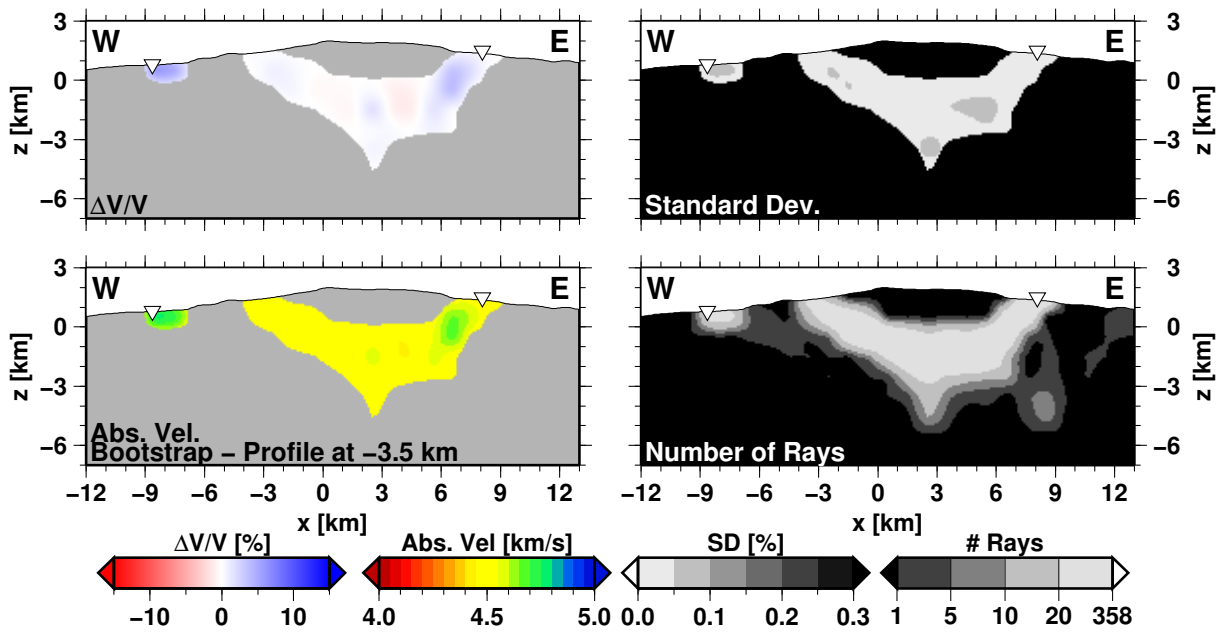


Figure B.74: Results from Bootstrapped tomography in vertical profile EW at -3.5 km (west)

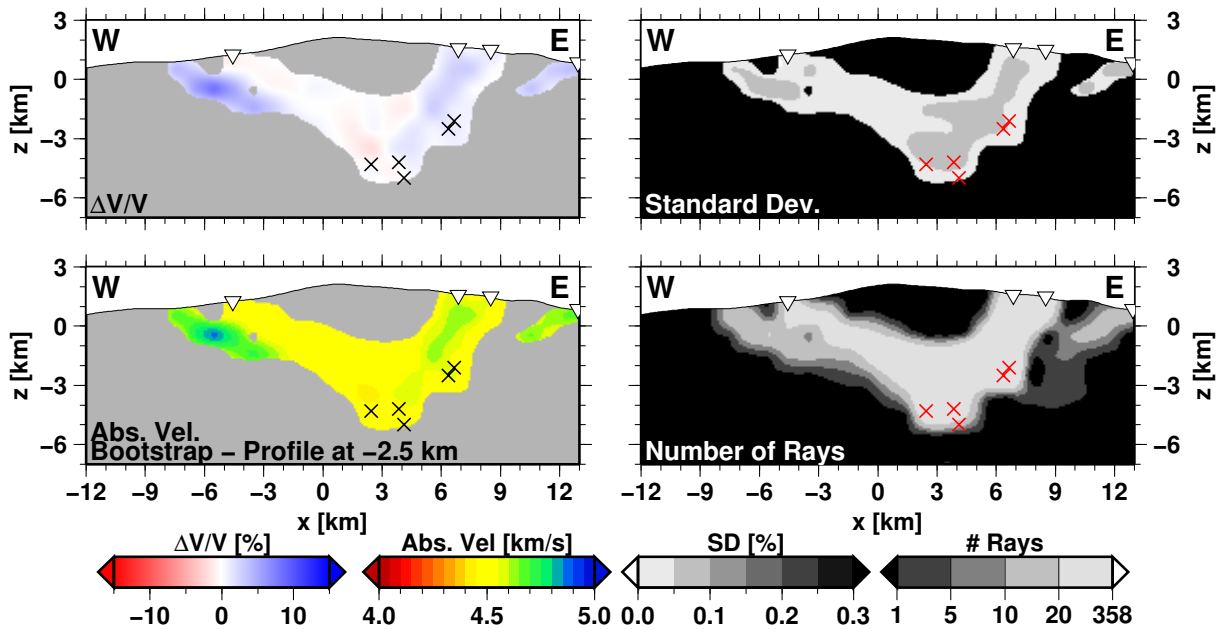


Figure B.75: Results from Bootstrapped tomography in vertical profile EW at -2.5 km (west)

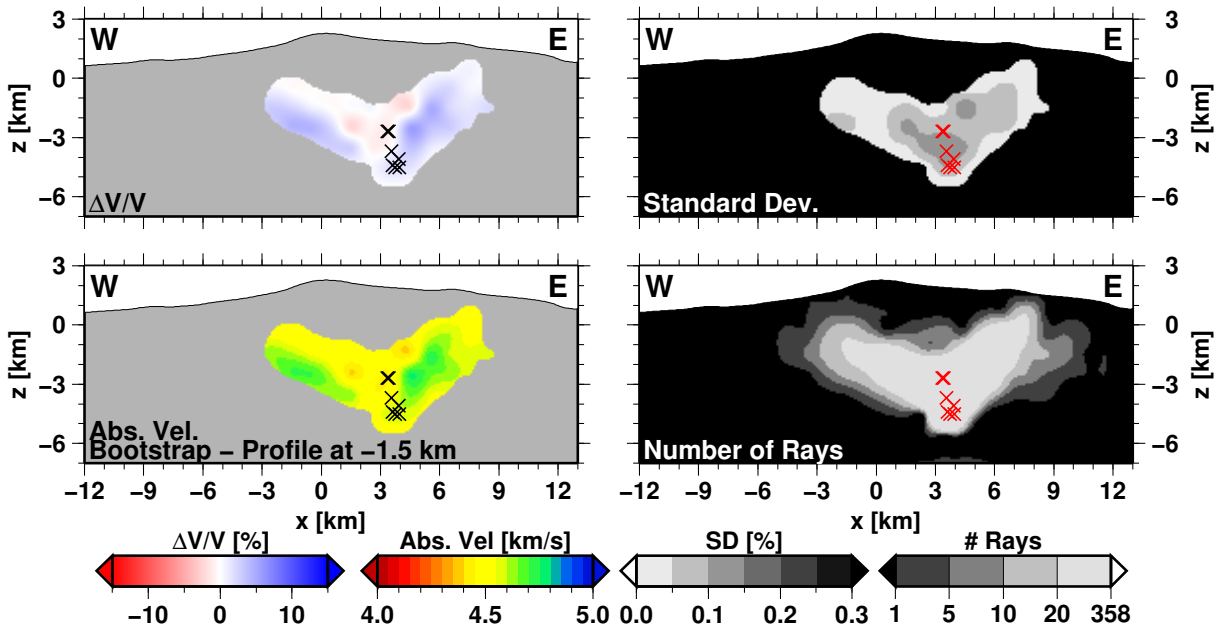


Figure B.76: Results from Bootstrapped tomography in vertical profile EW at -1.5 km (west)

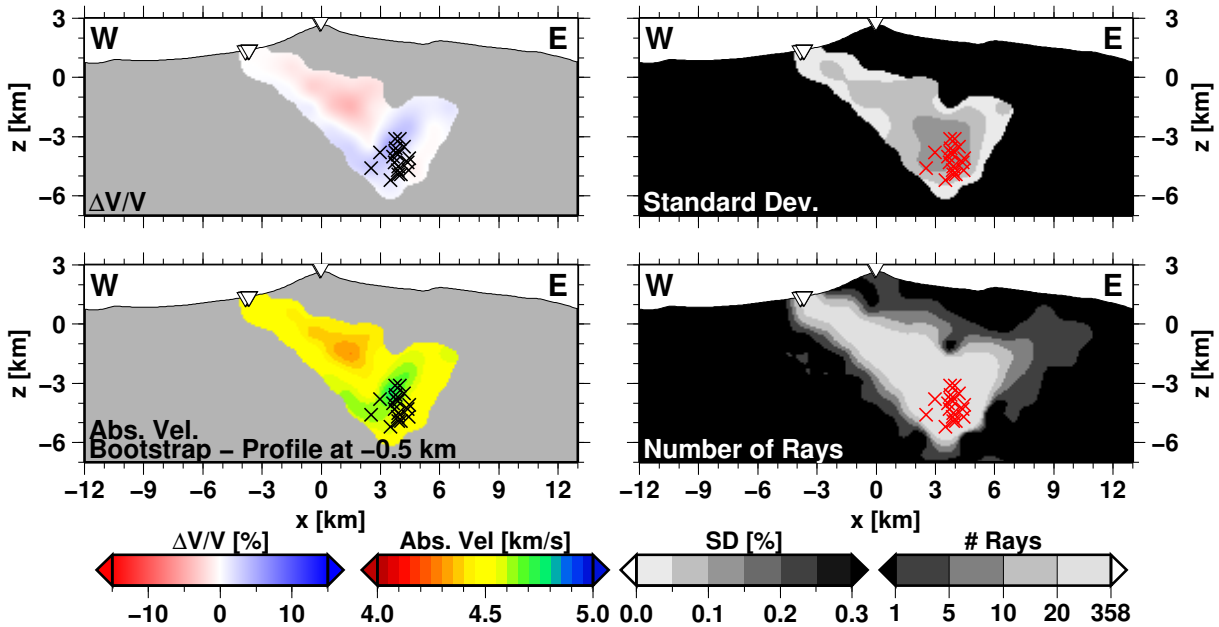


Figure B.77: Results from Bootstrapped tomography in vertical profile EW at -0.5 km (west)

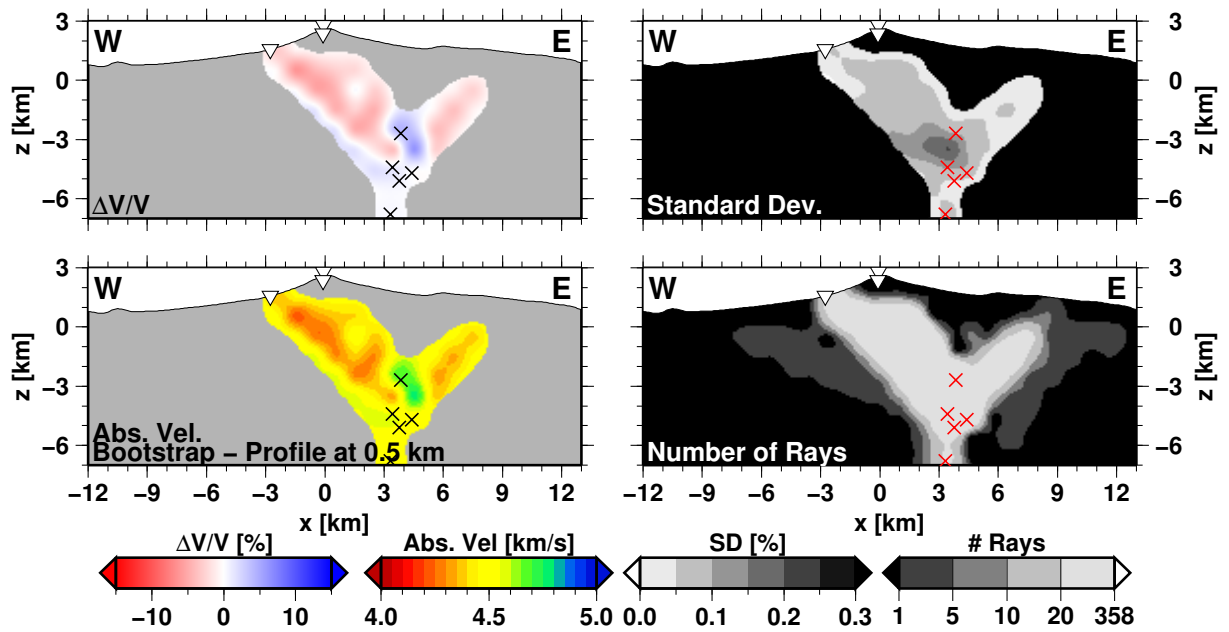


Figure B.78: Results from Bootstrapped tomography in vertical profile EW at 0.5 km (east)

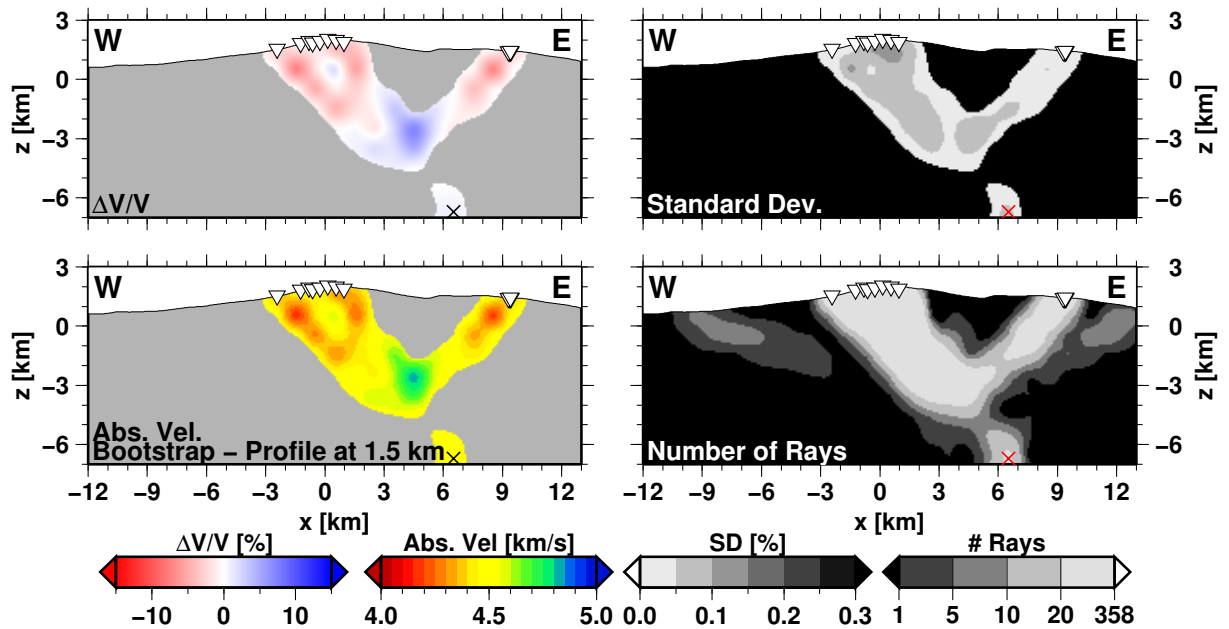


Figure B.79: Results from Bootstrapped tomography in vertical profile EW at 1.5 km (east)

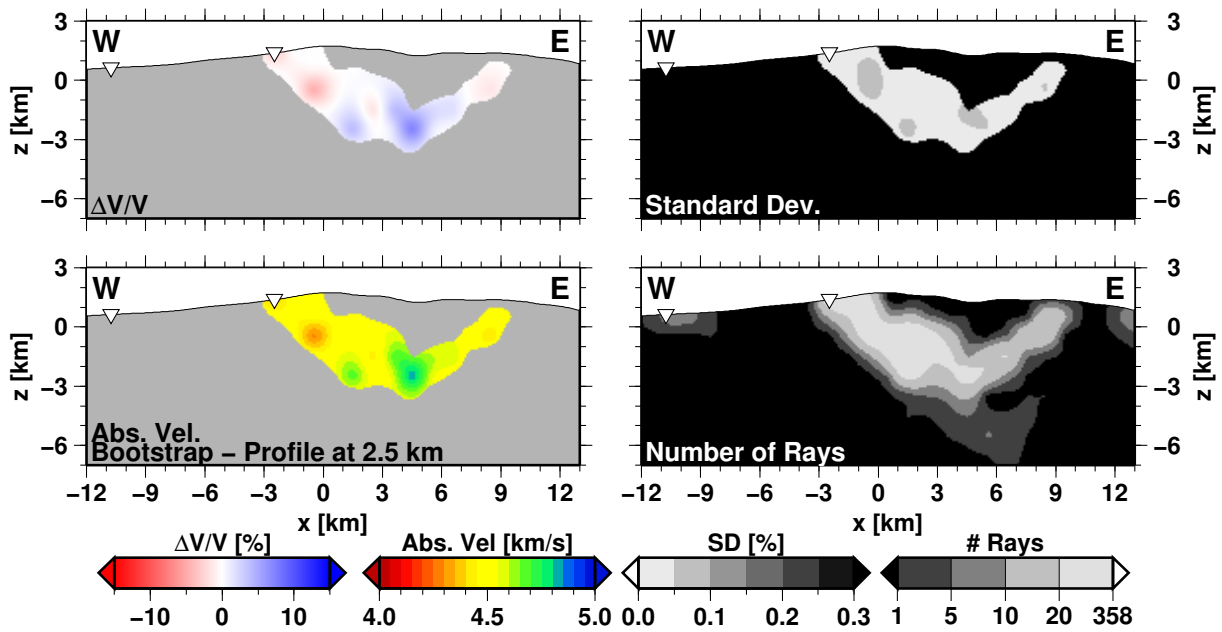


Figure B.80: Results from Bootstrapped tomography in vertical profile EW at 2.5 km (east)

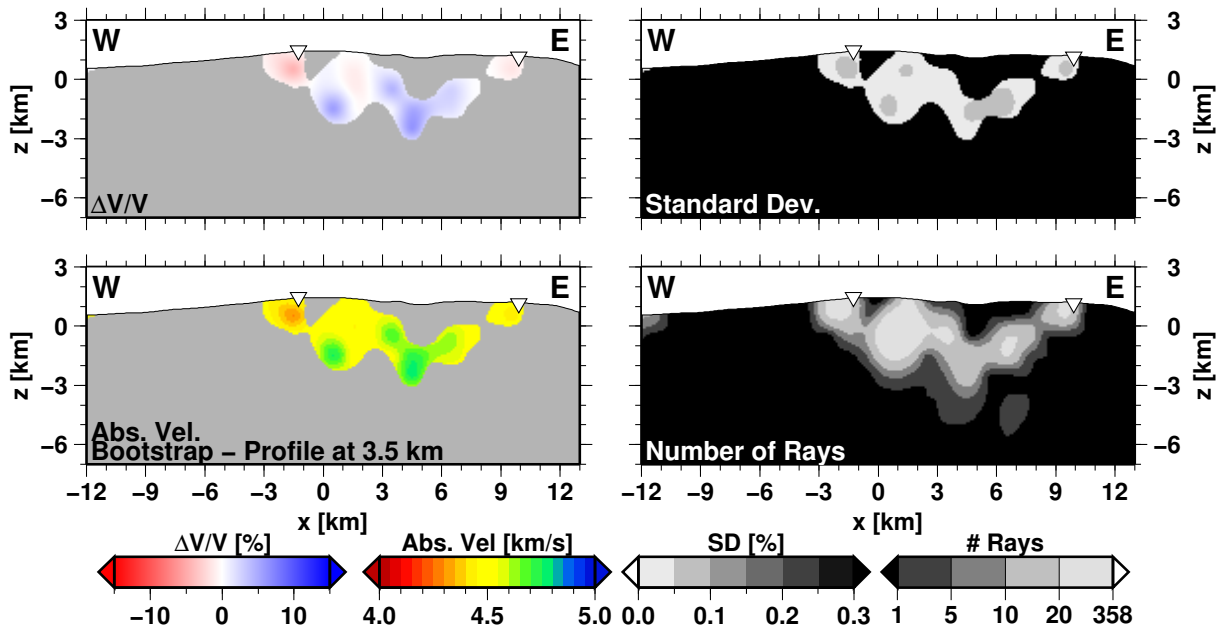


Figure B.81: Results from Bootstrapped tomography in vertical profile EW at 3.5 km (east)

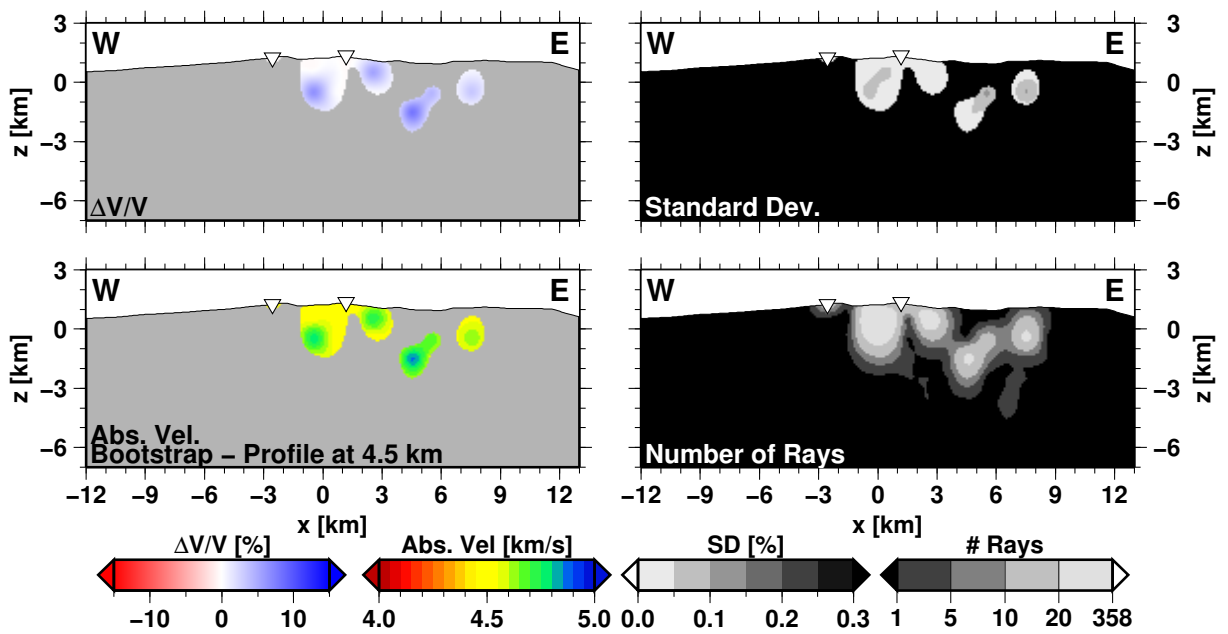


Figure B.82: Results from Bootstrapped tomography in vertical profile EW at 4.5 km (east)

Eidesstattliche Erklärung

Hiermit erkläre ich, daß die von mir für das Promotionsverfahren vorgelegte Abhandlung “Seismic Structure and Seismicity of Villarrica Volcano (Southern Central Chile)”, abgesehen von der Beratung der Betreuer nach Inhalt und Form, meine eigene Arbeit ist. Bisher ist die Arbeit noch nicht an anderer Stelle im Rahmen eines Prüfungsverfahrens vorgelegt worden.

Cindy Nathalie Mora Stock

Curriculum Vitae

CINDY NATHALIE MORA STOCK

Date of Birth: 24.05.1984
Place of Birth: Santiago, Chile
Nationality: Chilean

Education:
1990 - 2001 Colegio Maria Inmaculada,
Santiago - Chile

Higher Education:
2006 - 2009 Master of Sciences in Geophysics,
Universidad de Chile,
Santiago - Chile
2002 - 2006 Bachelor of Sciences in Geophysics,
Universidad de Chile,
Santiago - Chile

PhD Studies:
2010 - Doctor in Natural Sciences (Dr. rer. nat),
Christian - Albrechts - Universität,
Kiel - Germany